Tbx1: potential targets and interactors relevant to development of structures affected in DiGeorge Syndrome

Irinna Papangeli

Thesis submitted in fulfilment of the degree of Doctor of Philosophy

University College London

UCL - Institute of Child Health

December 2010

I, Irinna Papangeli, confirm that the work presented in this thesis is my own. Where information has been derived from other sources, I confirm that this has been indicated in the thesis.

To my family,

Acknowledgements

This work is the written report of my PhD, which would not have been possible without the following people. To them I am grateful.

First and foremost, I owe deep gratitude to my supervisor, Professor Peter Scambler, for his patient guidance, encouragement and advice throughout this research project. He has been a great mentor and a huge source of inspiration.

I would like to thank all the members of the Molecular Medicine Unit of the Institute of Child Health, past and present. I am most grateful to all of them for the long coffees, the Friday pubs and the overall warm and welcoming atmosphere they have created in the lab. Oh, and for teaching me everything.

A special thank you to Karen for the amazing baking at times of need and for proof reading this thesis. Karen, Anna, Victor, Amelie, Ariane and Jenifer you've all been excellent co-workers but most importantly great friends.

To all my friends in Greece for encouraging me, putting up with me and for being there throughout it.

A heartly thank you to my flatmates, who are now friends, Ioannis Gousias, Koralia Paschalaki, Theoni Leonidopoulou, Lydia Kyriazopoulou, Antonis Kaniadakis. Because helping with the little things sometimes makes all the difference.

Last but not least, to my family. My grand mum Rita, for being my role model, my aunt Rhoe, my uncle Stelios and my cousins, Theodore and Simon.

Mum and dad, for supporting me even if you don't always understand why, Alexandros and Nasos, for being the best brothers one could have,

μαζί θα τα καταφέρουμε.

ABSTRACT

22q11DS is the most common microdeletion syndrome in humans, causing a range of phenotypes associated with abnormal pharyngeal development. *TBX1* is considered the major genetic determinant of the syndrome. Deletion of *Tbx1* in animal models phenocopies the patient manifestations. In an effort to understand the pathways involved in these processes, potential *Tbx1* effectors previously determined by microarray screens were studied.

Smad7 is an inhibitor of the TGFβ/BMP pathways and to date several TGFβ/BMP signalling genes have been described in heart development. In this thesis *Smad7* was found expressed in pharyngeal and cardiovascular structures during mouse embryogenesis while a gene-trap mouse model displayed a partially penetrant 22q11DS-like phenotype. Furthermore, *Tbx1* and *Smad7* were found to interact synergistically towards arch artery morphogenesis.

Hes1 is a transcriptional repressor, part of the Notch signalling pathway, which produces craniofacial and cardiovascular anomalies when deactivated. Expression analysis undertaken demonstrated that Hes1 overlaps with Tbx1 in the embryonic pharynx and it is diminished in *Tbx1*$^{-/-}$ embryos. A conditional mutagenesis approach revealed non cell autonomous actions for *Hes1* in the ectoderm affecting great vessel and eye development, while *Hes1* was required in both the ectodermal and neural crest lineages for thymus morphogenesis.

Slit2 is a secreted protein that regulates axonal guidance, migration, outgrowth and branching. Recent evidence suggests a possible mechanism by which *Tbx1* may regulate neural crest patterning through the Slit/Robo pathway. *Slit1* and *Slit2* were here shown to share expression domains with *Tbx1* in the embryonic pharynx. Nevertheless, neither the *Slit2* nor the *Slit1;Slit2* mutation produced a 22q11DS-like phenotype while double mutation for *Tbx1;Slit2* did not enhance the *Tbx1* haploinsufficient phenotype.

Altogether, this thesis provides data clarifying a subset of *Tbx1* mechanisms important for cardiovascular development and identifies *Smad7* as a *Tbx1* regulated gene involved in great vessel morphogenesis.

ABBREVIATIONS

22q11DS, chromosome 22q11 deletion syndrome
AAo, ascending aorta
ALK, activin receptor-like kinase
AMH, anti-mullerian hormone
ANF, atrial natriuretic factor
AP, aorticopulmonary
A/S, antisense
ASD, atrial septal defect
AV, atrioventricular
AVC, atrioventricular canal
AVCD, atrioventricular canal defect
AVJ, atrioventricular junction
AVSD, atrioventricular septal defect
BAC, bacterial artificial chromosome
bHLH, basic helix-loop-helix
BMP, bone morphogenetic protein
BSA, bovine serum albumin
CADASIL, cerebral autosomal dominant arteriopathy with subcortical infarcts and leukoencephalopathy
CAFS, conotruncal anomaly face syndrome
CAMs cell adhesion molecules
Cas-L, Crk-associated substrate lymphocyte type
CAT, common arterial trunk
CHD, congenital heart disease
ChIP, chromatin immunoprecipitation
ChIP-Seq, ChIP with massively parallel sequencing
CIAP, calf intestinal alkaline phosphatase
CNS, central nervous system
CoA, coronary artery
COET, conditional over-expression of Tbx1
co-Smad, common mediator Smad

C-terminal, carboxyl-terminal

DA, ductus arteriosus

Dao, dorsal aorta

Dcc, deleted in colon cancer

del22q11, deletion of chromosome 22q11.2

DesAo, descending aorta

DMP, dorsal mesenchymal protrusion

DNA, deoxyribonucleic acid

DORV, double outlet right ventricle

E, day of embryonic development

ECE1, endothelin converting enzyme

ECM, extracellular matrix

EGF, epidermal growth factor

EGFR, epidermal growth factor receptor

EMSA, electromobility sift assay

EMT, epithelial-mesenchymal transition

En2, engrailed 2

ES, embryonic stem

EtOH, ethanol

FACS, fluorescence activated cell sorting

FDR, false discovery rate

FGF, fibroblast growth factor

FHF, first heart field

FN, fibronectin

GDF, growth and differentiation factor

GDNF, glial cell line-derived neurotrophic factor

HDAC, histone deacetylase

HES, hairy and enhancer of split

HEY, Hes-related transcription factor

HOS, Holt-Oram Syndrome

HUVEC, human umbilical vain endothelial cell

IAA, interrupted aortic arch

IAA-A, interrupted aortic arch type A

IAA-B, interrupted aortic arch type B

IAA-C, interrupted aortic arch type C

IF, immunofluorescence

IG, immunoglobulin

IP, intraperitoneal

IRES, internal ribosomal entry site

ISA, intersegmental artery

I-Smad, inhibitory Smad

L, left

LAP, latency-associated peptide

LCC, left common carotid

LCR, low copy repeat

LSCA, left subclavian artery

LTBP, latent TGFβ-binding protein

LV, left ventricle

m, milli

M, molar

MAML, mastermind-like

Mb, mega base

MEF, mouse embryonic fibroblast

MeOH, methanol

MES, midline epithelial seam

MH, mad-homology

MME, medial edge epithelia

MMP, matrix metalloproteinase protein

mRNA, messenger RNA

n, nano

Neo, neomycin

NICD, intracellular domain of Notch

NLS, nuclear localisation signal

NP, non patent

NRG, neuregulin

NTD, neural tube defect

N-terminal, amino-terminal

O/N, overnight

OCT, optimal cutting temperature double

OG, oral gavage

PAA, pharyngeal arch artery

PAC, P1 artificial chromosome

PBS, phosphate buffered saline

PCR, polymerase chain reaction

PDGF, platelet-derived growth factor

PFO, patent foramen ovale

PLB, passive lysis buffer

PT, pulmonary trunk

PTA, persistent truncus arteriosus

r, rhombomeric segment

R, right

RA, retinoic acid

RAA, right-sided aortic arch

RALDH2, retinaldehyde dehydrogenase 2

RBP-J, recombination signal binding protein for immunoglobulin kappa J region

RCC, right common carotid

RNA, ribonucleic acid

Robo, roundabout

RSCA, right subclavian artery

R-Smad, receptor activated smad

RT, reverse transcription

RV, right ventricle

S, sense

SA, splice acceptor

SAP, shrimp alkaline phosphatase

SARA, smad anchor for receptor activation

SDS, sodium dodecyl sulphate

SEMA3C, semaphorin 3C

SHF, second heart field

SHH, Sonic Hedgehog

SIK, salt-inducible kinase

SMC, smooth muscle cells

SMURF, smad ubiquitination regulatory factor

SNP, small nuclear polymorphism

SRF, serum response factor

TACE, tumor necrosis factor-α-converting enzyme

TAE, tris-acetate-EDTA

TBE, transcription binding element

TDR, typically deleted region

TE, Tris Base/HCl-EDTA

TESPA, 3-aminopropyl-triethoxysilane

TGA, transposition of the great arteries

TGFβ, transforming growth factor β

Th-P, thin patent

Tm, melting temperature

TOF, tetralogy of Fallot

UTR, untranslated region

UV, ultra violet

VEGF, vascular endothelial growth factor

VSD, ventricular septal defect

VSM, vascular smooth muscle

WB, western blotting

WT, wild type

YAP, yes-associated protein

μ, micro

GLOSSARY TERMS

Type I transmembrane receptors
Single pass transmembrane proteins, that have their C-terminus in the cytoplasm and their N-terminus oriented towards the lumen or extracellular space.
Type II transmembrane receptors
Single-pass transmembrane proteins that have their C-terminus on the cell surface and their N-terminus in the cytoplasm.

TABLE OF CONTENTS

LIST OF FIGURES

I. INTRODUCTION

III. SMAD7

LIST OF TABLES

I. INTRODUCTION

II. MATERIALS AND METHODS

III. SMAD7

I. INTRODUCTION

1. DiGeorge syndrome

DiGeorge is the most common microdeletion syndrome in humans, with an incidence of 1 in 4000-5000 live births (Emanuel, 2008; Wurdak et al., 2006; Yagi et al., 2003). Historically it was described separately as velocardiofacial syndrome (Shprintzen syndrome), conotruncal anomaly face syndrome (CAFS or Takao syndrome) and Sedlackova syndrome, however, in recent years all have been grouped under chromosome 22q11 deletion syndrome (22q11DS) (Epstein, 2001; Momma, 2010; Paylor and Lindsay, 2006; Saitta et al., 2004; Schwinger et al., 2010).

The clinical phenotype is very heterogeneous and includes congenital heart defects (approximately 70% of all cases), craniofacial dysmorphism and thymic and parathyroid aplasia/ hypoplasia (Shprintzen, 2008; Wurdak et al., 2006). Behavioural, learning and psychiatric complications have also been reported (Shprintzen, 2008; Wurdak et al., 2006). All these manifestations can be grouped in three categories: (1) the pharyngeal phenotype, representing abnormalities in the development of the pharyngeal apparatus, (2) the neurobehavioral phenotype, concerning learning and psychiatric disabilities and (3) a heterogeneous group of clinical symptoms, including kidney, non-craniofacial skeletal and vascular defects (Baldini, 2004). The majority of patients exhibit features of at least two of the three categories of phenotypes (Baldini, 2004). The cardiovascular phenotype of the 22q11DS includes both conotruncal and aortic arch defects, namely tetralogy of Fallot (TOF) (~30%), interrupted aortic arch type B (IAA-B) (~15%), ventricular septal defect (VSD) (~15%), common arterial trunk (CAT) (~10%) or others (~5%) (Yamagishi, 2002). Hemizygous deletion of chromosome 22q11.2 is the second most common genetic cause of congenital heart disease (CHD) and is present in approximately 60% of the patients with IAA-B, 35% of the patients with CAT and 15% of the patients with TOF (or 55% of the patients with TOF combined with pulmonary atresia and major aortopulmonary collateral arteries) (Yamagishi, 2002).

In over 85% of the cases the disease is caused by a 3 Mb hemizygous deletion of chromosome 22q11.2 (*del22q11)* (Emanuel, 2008; Wurdak et al., 2006; Yamagishi and Srivastava, 2003). This 3 Mb typically deleted region (TDR) that encompasses approximately 40 genes, is flanked by low copy repeat (LCR) sites near or at the break points of *del22q11* (Aggarwal and Morrow, 2008; Baldini, 2004; Paylor and Lindsay,

2006; Yamagishi and Srivastava, 2003). The sequence identity shared by these LCRs predisposes the respective regions to non-allelic homologous recombination, resulting in aberrant interchromosomal exchange and subsequent deletion (Baldini, 2004; Emanuel, 2008; Saitta et al., 2004). The remaining 7-8% of patients carry recurrent 1.5-2 Mb nested deletions, however there are cases of smaller atypical deletions, all of which have phenotypic manifestations consistent with the diagnosis of 22q11DS (Emanuel, 2008; Gong et al., 2001; Paylor and Lindsay, 2006; Scambler, 2010; Yagi et al., 2003). Correlations between the genotype and the phenotype of the syndrome are unlikely as there is no difference in the severity of the phenotype among the various deletions (Aggarwal and Morrow, 2008; Saitta et al., 2004). Even patients that share the same sized deletion exhibit significant clinical variability (Aggarwal and Morrow, 2008). Most of the deletions occur *de novo*, with 10% or less being inherited from an affected parent (Saitta et al., 2004). In a proportion of patients that do not carry the typical deletion there have been found point mutations in *TBX1*, a gene localising within the TDR (Paylor et al., 2006; Stoller and Epstein, 2005a; Torres-Juan et al., 2007; Yagi et al., 2003; Zweier et al., 2007).

2. The pharyngeal apparatus, derivative affected structures and embryology

2.1. The embryonic system

A large proportion of the phenotypes observed in 22q11DS patients are associated with incorrect patterning of the pharyngeal apparatus (Wurdak et al., 2006), a vertebrate-specific, transient structure that forms in the lateral side of the embryo (Graham, 2008; Grevellec and Tucker, 2010). It is constituted of five bilaterally symmetrical arches, formed successively in an anterior to posterior direction (Graham, 2008; Grevellec and Tucker, 2010; Wurdak et al., 2006). In mouse this occurs between the 8th and 11th day of embryonic development (E8.0-E11.0) while in humans it develops between the 2nd and 7th week of gestation (Wurdak et al., 2006). The arches are numbered from 1 to 6, omitting number 5 by convention (Wurdak et al., 2006). Within the pharyngeal arches five sets of arteries are initially formed (Wurdak et al., 2006). These undergo extensive remodelling throughout development to become the mature left-sided aortic arch (Gittenberger-de Groot et al., 2006; Kameda, 2009; Kellenberger, 2010; Molin et al., 2002; Snider et al., 2007).

Different cell types are recruited to form the apparatus, deriving from all the embryonic layers. Ectodermal and endodermal cells populate the external and internal surfaces respectively, while mesenchyme colonises the intermediate region (Figure 1.1) (Graham, 2003; Grevellec and Tucker, 2010). The boundaries of each arch are defined by the regions of contact of the ectoderm and the endoderm between the arches (Graham, 2003; Grevellec and Tucker, 2010). This is apparent externally as ectodermal clefts and internally as endodermal pouches (Graham, 2003; Grevellec and Tucker, 2010). Neural crest cells populate each arch and mesodermal cells are confined to the core of the mesenchyme surrounding each arch artery (Graham, 2003; Graham, 2008). The different cell populations produce distinct structures. The ectoderm generates the epidermal lining of the arches and the sensory neurons of the epibranchial ganglia (Graham, 2001; Graham, 2003; Graham, 2008; Grevellec and Tucker, 2010). The endoderm forms the epithelium of the pharynx, the taste buds and endocrine glands (Graham, 2001; Graham, 2003; Graham, 2008; Grevellec and Tucker, 2010). The neural crest develops into skeletal and connective tissues and part of the neurosensory ganglia of the head while the core mesoderm is responsible for the head and neck musculature,

skeletal elements and the endothelial lining of the arch arteries (Graham, 2001; Graham, 2003; Graham, 2008; Grevellec and Tucker, 2010).

Each pair of arches is populated by the same cell types and generates the same basic components; nevertheless, each pair also has an individual identity (Graham, 2001; Graham, 2003). The first arch shapes the jaw, the second forms the hyoid apparatus and the more caudal arches are incorporated into the throat (Graham, 2001; Graham, 2003). The caudal pouches are also regionalised and give rise to the thyroid, parathyroid and thymus glands (Graham, 2008; Grevellec and Tucker, 2010; Jerome and Papaioannou, 2001).

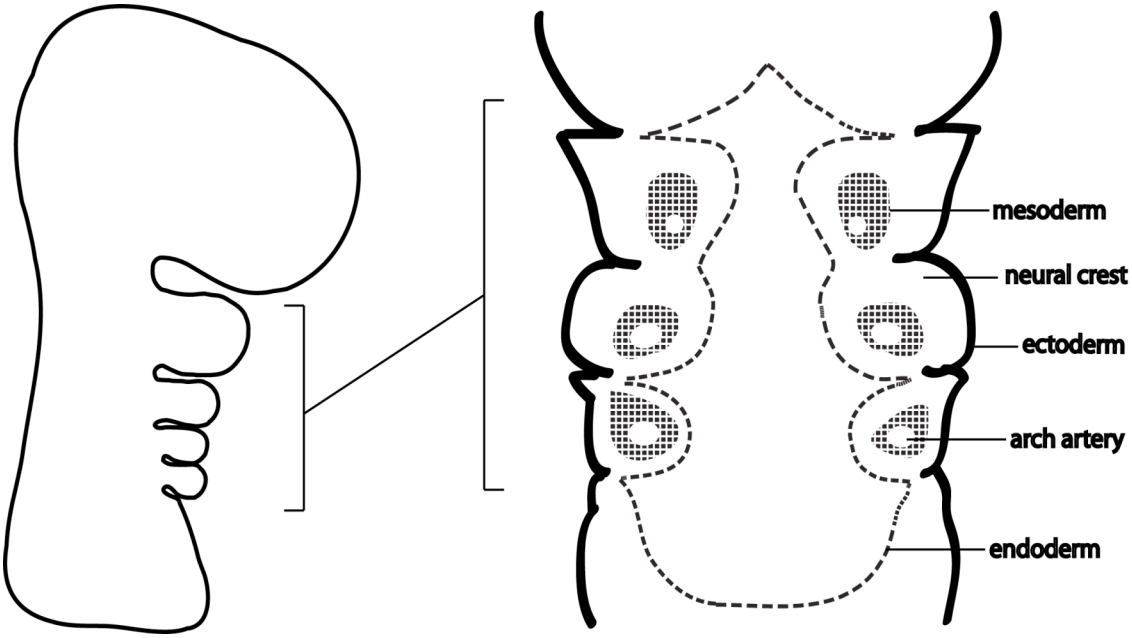

Figure 1. 1. The mammalian pharyngeal apparatus. Lateral and frontal views of the pharyngeal system consisting of a series of arches, which are covered by an ectodermal layer externally and an endodermal lining internally. Each arch surrounds an arch artery and is populated by mesoderm and neural crest cells.

2.2. Patterning roles of the different cell populations

2.2.1. The epithelia

Pharyngeal patterning requires reciprocal signalling between the constituent tissues, primarily between the pharyngeal epithelia, the ectoderm and the endoderm (Graham, 2003). The endoderm appears to drive pharyngeal segmentation (Graham, 2008). The endodermal pouches physically separate the branchial arches and by defining the anterior and posterior boundaries of each arch they provide distinct

identities for each (Graham, 2008; Grevellec and Tucker, 2010). Also, by being a segmentally organised tissue, the endoderm provides the necessary positional cues for the mesoderm and the invading neural crest of the arches (Graham, 2008). The pouches are first evident at the sites of contact between the endoderm and ectoderm of the pharyngeal apparatus (Graham, 2008; Grevellec and Tucker, 2010). Cells within the pouch endoderm have an organised network of actin cables required for pouch morphogenesis (Quinlan et al., 2004), so that throughout this process the endodermal tissue as a whole will expand in all directions while the pouches will mainly expand along the dorsoventral axis (Graham, 2008). Fibroblast growth factor (FGF) signalling is particularly important for pouch formation (Graham, 2008). The pharyngeal endoderm is required for the patterning of arch components, such as the epibranchial placodes, focal thickenings of the ectoderm that give rise to the epibranchial ganglia (Graham, 2008; Trainor and Krumlauf, 2001). In zebrafish and amphibia it has been shown that the chondrogenenic fate of the neural crest is promoted by the pharyngeal endoderm (Graham, 2008; Trainor and Krumlauf, 2001). The endoderm is also involved in the induction of neural crest-derived skeletal elements (Graham, 2008). The surface ectoderm, apart from its involvement in pharyngeal segmentation though clefting (Graham, 2008; Grevellec and Tucker, 2010), regulates the patterning of the neural crest of the first arch and consequently plays a key role in odontogenesis (Trainor and Krumlauf, 2001). Additionally, through *Fgf8*, which is expressed in the anterior ectoderm of the first arch, it determines the rostrocaudal polarity of the arch (Trainor and Krumlauf, 2001).

2.2.2. The mesoderm

It has been shown that the mesoderm provides maintenance signals for the neural crest cells of the second branchial arch, by permitting but not initiating *Hox* gene expression, thus regulating the identity of these cells (Trainor and Krumlauf, 2000). The cranial mesoderm, being primarily myogenic, is tightly linked to neural crest skeletal and connective tissue patterning (Trainor and Krumlauf, 2001). Maintaining an anterior-posterior register between the primordial tissues may be an important step in subsequent craniofacial morphogenesis (Trainor and Krumlauf, 2001).

2.2.3. The neural crest

The neural crest is not involved in pharyngeal metamerism (Graham, 2008). However, the gene expression pattern of each subpopulation of crest cells defines their response to endodermal cues and the generation of different derivatives (Graham, 2008). The neural crest cells are important for the final patterning of the arch arteries, although not required for the initial formation (Hutson and Kirby, 2007; Kameda, 2009). Neural crest cells migrate into the arches, surround the endothelial tubes that originally constitute the arch arteries and differentiate into the smooth muscle tunics of the future great arteries (Hutson and Kirby, 2007; Scholl and Kirby, 2009). Developmental anomalies that result in inability of the neural crest cells to colonise their final targets cause a large number of birth defects (Kulesa and Gammill, 2010; Tucker, 2004).

3. The neural crest in detail

The neural crest is a pluripotent, transient, migratory cell population originating from the dorsal aspect of the neural tube, at the junction between the neuroepithelium and the surface ectoderm, commonly known as the neural plate border (Aman and Piotrowski, 2010; Kalcheim and Burstyn-Cohen, 2005; Kulesa et al., 2004; Lallier et al., 1992; Sauka-Spengler and Bronner-Fraser, 2008; Tucker, 2004). Cues from the surrounding non-neural ectoderm and mesoderm induce the neural crest cells to undergo epithelial-mesenchymal transition (EMT), exit the neural tube and migrate extensively in a rostro-caudal progression throughout the body of the embryo (Aman and Piotrowski, 2010; Kalcheim and Burstyn-Cohen, 2005; Kulesa et al., 2004; Sauka-Spengler and Bronner-Fraser, 2008; Tucker, 2004). In mouse, migration commences at the five-somite stage (E8.25) (Kulesa et al., 2004). The neural crest cells differentiate at their sites of colonisation and eventually develop into several different cell types, tissues and organs (Aman and Piotrowski, 2010; Snider et al., 2007; Tucker, 2004). Along the neural axis four main subcategories of neural crest are identified: cranial, vagal, trunk and sacral (Jones and Trainor, 2005; Lallier et al., 1992), while the cranial crest includes a subpopulation known as the cardiac neural crest (Snarr et al., 2008; Snider et al., 2007). Each population has different migratory pathways and generates different sets of derivatives (Jones and Trainor, 2005; Lallier et al., 1992). The cranial neural crest cells, originating from pre-somitic levels, follow a cranial route through the mesenchyme and produce skeletal elements of the face, cranial parasympathetic and sensory ganglia (Jones and Trainor, 2005; Lallier et al., 1992), whilst contributing to the tunica media of the great arteries, the aorticopulmonary (AP) septum and the semilunar valves (Jones and Trainor, 2005; Nakamura et al., 2006; Snider et al., 2007). The vagal population, originating from the level of somites 1-7, migrates into the gut and populates the majority of the enteric ganglia, whilst trunk neural crest cells, originating from the level of somites 8-28, move between the somites and underneath the ectoderm and ultimately give rise to sensory and sympathetic ganglia, adrenal chromaffin cells and melanocytes (Jones and Trainor, 2005; Lallier et al., 1992). Last, the sacral neural crest population that originates below the level of somite 28, produces enteric ganglia and some parasympathetic and sensory ganglion cells (Jones and Trainor, 2005; Lallier et al., 1992).

3.1. Distinct phases of cranial neural crest migration

There are at least three phases of cranial neural crest cell migration. During the first phase the cells acquire the ability to migrate directionally, which involves cell contact and microenvironment interactions, followed by cell surface changes that promote migration (Kulesa et al., 2010; Kulesa and Gammill, 2010). In the second phase the neural crest cells move along the dorsolateral pathway towards the branchial arches, whilst remaining in loosely connected streams (Kulesa et al., 2010; Kulesa and Gammill, 2010). The cells proliferate at different rates and establish different trajectories, depending on the stream they follow, their position within the stream and their neighboring cells (Kulesa et al., 2010; Kulesa and Gammill, 2010). In the last phase the neural crest cells invade the branchial arches, a phase followed by repression of the cells' migratory ability upon arrival at the target site (Kulesa et al., 2010; Kulesa and Gammill, 2010). The different phases are regulated by a number of signalling cues with regard to targeted invasion, survival, proliferation and differentiation, with factors like Sonic hedgehog (SHH), Transforming growth factor β (TGFβ), Semaphorins/ Neuropilins and Slits/Robos (Kulesa et al., 2010).

3.2. Cranial neural crest migratory streams

The cranial neural crest cells migrate in three distinct, segregated streams, depending on the cranio-caudal origin of the migrating cells (Kulesa et al., 2004; Kulesa et al., 2010). The vertebrate hindbrain is segmented into seven rhombomeric segments (r) and provides a structural framework for the description of the cranial crest migratory streams (Kulesa et al., 2010; Trainor and Krumlauf, 2000). Neural crest cells from the first two rhombomeres (r1 and r2) migrate in a ventrolateral direction and along with midbrain-derived neural crest cells invade the first branchial arch (Kulesa et al., 2004). The second branchial arch is mainly populated by cells deriving from r4 (Kulesa et al., 2004). R3 produces fewer neural crest cells compared to r1 and r2, which migrate anteriorly following the r2 stream and posteriorly following the r4 stream (Kulesa et al., 2004; Trainor and Krumlauf, 2000). Similarly to r3, neural crest cells from r5 lack the ability to migrate laterally and move anteriorly and posteriorly, merging with the even-numbered streams from r4 and r6 (Kulesa et al., 2004; Trainor and Krumlauf, 2000). In comparison, more neural crest cells delaminate from r5 than r3, but still significantly less than from r4 (Kulesa et al., 2004). Neural crest cells migrating from r5 and r6

populate the third branchial arch while the fourth arch is populated by r7-derived and a minor r6-derived population of neural crest cells (Kulesa et al., 2004) (Figure 1.2). The neural crest free zones adjacent to r3 and r5 can be explained (prevailing theories) by limited neural crest cell production, increased apoptosis or compromised movement of the neural crest cells originating from the respective rhombomeres (Kulesa et al., 2010). *Hox* genes have a segment-restricted pattern of expression, suggestive of their role in patterning of the rhombomere identity and subsequently the vertebrate head (Trainor and Krumlauf, 2000; Trainor and Krumlauf, 2001).

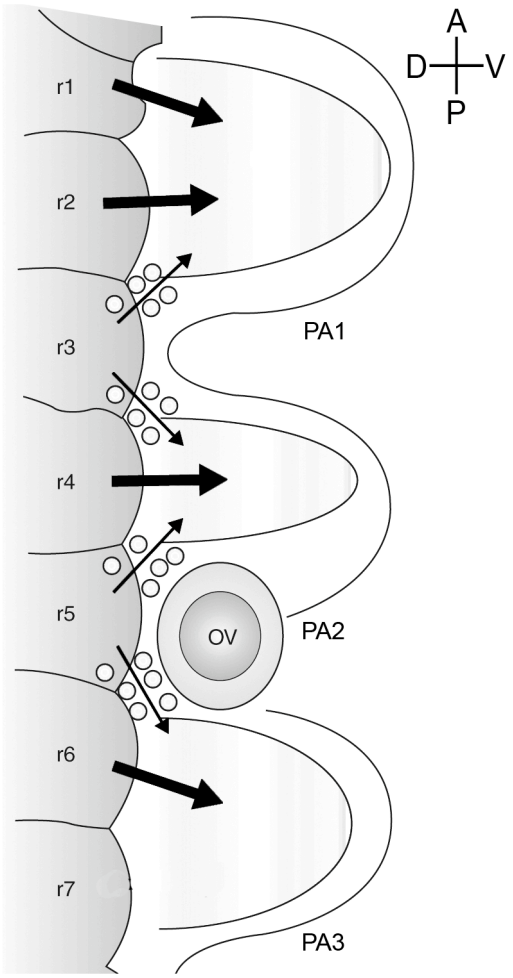

Figure 1. 2. Segmental organisation of the hindbrain and distinct pathways of cranial neural crest cell migration. The hindbrain is divided into seven rhombomeres (r1-7). The first arch is populated by neural crest cells originating from r1-2 and a minor r3-derived population. The second arch is invaded by neural crest cells originating from r4 and a small population from r3 and r5. The third arch is populated by r6 and a few r5-derived neural crest cells. PA, pharyngeal arch; ov, otic vesicle; r, rhombomere. Modified from Trainor and Krumlauf, 2001.

3.3. Cardiac neural crest

The cardiac neural crest is a subpopulation of the cranial neural crest that arises at the level between the otic placode and the fourth somite (Snarr et al., 2008; Snider et al., 2007). As it has common properties of both the cranial and trunk crest, it is thought to be a transitional region between the two (Hutson and Kirby, 2007; Scholl and Kirby, 2009). Similar to the more cranial crest it can give rise to ectomesenchyme while it cannot regenerate, which is a trunk crest property (Hutson and Kirby, 2007; Scholl and Kirby, 2009). The cardiac neural crest cells migrate through the caudal pharyngeal arches (arches 3, 4 and 6), where they form the vascular smooth muscle (VSM) cell lining of the arch arteries (Hutson and Kirby, 2007; Scholl and Kirby, 2009), into the outflow tract cushions and promote septation of the single great vessel of the primitive heart into the aorta and pulmonary arteries (Epstein et al., 2000; Scholl and Kirby, 2009; Snider et al., 2007; Stoller and Epstein, 2005b). After AP septation, the outflow tract cushions undergo remodelling and form the semilunar valve leaflets (Nakamura et al., 2006; Restivo et al., 2006). Cell lineage tracing experiments in the mouse have shown that the neural crest cells populate the ascending aorta, the right brachiocephalic artery, the left carotid artery, the ductus arteriosus, the pulmonary tract, the semilunar valves (Nakamura et al., 2006), generate all of the parasympathetic innervation of the heart (Hutson and Kirby, 2007) and are associated with the maturation of the proximal cardiac conduction system (Nakamura et al., 2006). The role of cardiac neural crest in normal patterning of the great arteries, cardiac outflow tract septation and myocardial function is supported by studies in avian models where ablation of the pre-migratory cardiac neural crest disrupts proper myocardial function and produces malformations of the outflow tract and the great vessels (Hutson and Kirby, 2007; Schafer et al., 2003). In the recent years, numerous models of heart disease have been described in the mouse, many of which recapitulate all or aspects of the neural crest ablation phenotype in the chick (Hutson and Kirby, 2007; Scholl and Kirby, 2009). In these models outflow tract and aortic arch artery abnormalities are commonly associated with cardiac neural crest defects, while impaired development and function of the myocardium have also been linked (Gittenberger-de Groot et al., 2006; Hutson and Kirby, 2007; Scholl and Kirby, 2009; Stoller and Epstein, 2005b).

3.4. Neural crest gene regulation

3.4.1. Induction

The events that govern initial specification and induction of the neural crest at the neural plate border are numerous and complex. A number of secreted signals is required from the surrounding epidermis, neural plate and underlying mesoderm involving factors like Wnts, Bone morphogenetic proteins (BMPs), FGFs and Retinoic acid (RA) signalling (Jones and Trainor, 2005; Kalcheim and Burstyn-Cohen, 2005; Kuriyama and Mayor, 2008; Scholl and Kirby, 2009). Prospective neural plate border cells then express *neural plate border specifier genes* (Kalcheim and Burstyn-Cohen, 2005). Notch/Delta signalling in the zebrafish neural plate border represses pro-neural gene expression, acting as a regulator of neural crest cell production (Kalcheim and Burstyn-Cohen, 2005). Eventually *neural crest survival* or *neural crest specifier genes* are expressed, signifying neural crest cell specification (Kuriyama and Mayor, 2008; Sauka-Spengler and Bronner-Fraser, 2008). Among others, these include *Snail* (*Snail* and *Slug*) family genes, *Sox9/10*, *FoxD3* and *Ap2α* (Kalcheim and Burstyn-Cohen, 2005; Sauka-Spengler and Bronner-Fraser, 2008; Scholl and Kirby, 2009). Subsequently, the neural crest cells express a third group of genes, the *neural crest effector genes* (or *migration/differentiation genes*) (Kuriyama and Mayor, 2008; Sauka-Spengler and Bronner-Fraser, 2008), proliferate, undergo EMT and proceed to delamination (Kuriyama and Mayor, 2008; Sauka-Spengler and Bronner-Fraser, 2008; Scholl and Kirby, 2009). EMT is accompanied by changes in neural crest cell *Cadherin*, *Connexin* and *Matrix Metalloproteinase* (MMPs, required for extracellular matrix digestion) expression patterns (Kuriyama and Mayor, 2008; Sauka-Spengler and Bronner-Fraser, 2008; Scholl and Kirby, 2009). The cardiac neural crest, as a subpopulation of the cranial neural crest, follows this initial sequence of inductive events but also possesses unique properties.

3.4.2. Cardiac neural crest migration

The definitive migration patterns and stereotypic destinations of the cardiac neural crest are tightly regulated. Depending on the cranio-caudal origin, the cranial neural crest cells express specific sets of *Hox* genes, nonetheless, they exhibit plasticity in this expression pattern, suggesting that environmental cues are important for establishing their regional identity (Trainor and Krumlauf, 2000). *Ephrin* and *Eph*-receptor genes are

also expressed in individual combinations by the neural crest and mesoderm of different arches, which restricts the intermingling of neural crest cells between different migratory streams (Kuriyama and Mayor, 2008; Scholl and Kirby, 2009). Permissive and restricted areas of migration determine these segmentally restricted streams (Christiansen et al., 2000; Kuriyama and Mayor, 2008). Extracellular matrix (ECM) proteins provide permissive signals, while Gdnf (glial cell line-derived neurotrophic factor) and Dcc (Deleted in Colon Cancer) are considered as possible attractants (Kuriyama and Mayor, 2008). However, no sound evidence exists in support of a definitive chemoattractant assisting neural crest migration (Kuriyama and Mayor, 2008). The Slit/Robo families of molecules were until recently thought to be involved only in trunk crest migration, acting in a ligand-receptor fashion as repellents of migrating neural crest, inhibiting the migration on the dorsal pathway (Kuriyama and Mayor, 2008). Calmont *et al.*, showed that *Robo1*-positive cardiac neural crest streams are detected as early as E9.0 in the mouse, while the ligand *Slit2* is expressed in the pharyngeal surface ectoderm at E8.75 and robustly in the pharyngeal endoderm by E9.5 (Calmont et al., 2009). Both genes appeared downregulated or misspatterned in a mouse model displaying cardiac neural crest migration defects, further supporting a role for Slit/Robo signalling in cardiac crest migration (Calmont et al., 2009).

Migrating neural crest cells do not only receive signals, but actively interact with their surrounding tissues during their journey and at the target sites (Scholl and Kirby, 2009). Cardiac crest cells modulate Fgf8 signalling in the pharyngeal epithelia (Hutson et al., 2009). Signalling in the caudal pharynx is important as it affects the splanchnic mesoderm, including progenitor cells that eventually populate the outflow tract (Kuriyama and Mayor, 2008; Scholl and Kirby, 2009). Cardiac neural crest ablation in avian models results in secondary failure in migration of second heart field (SHF)-derived myocardial progenitors into the outflow tract (Waldo et al., 2005). The cells undergo proliferation instead of initiating the process of migration to invade the outflow tract (Waldo et al., 2005). *Semaphorin 3C* (*Sema3C*), expressed by the outflow tract myocardium, and its receptor, *Plexin A2*, expressed by the cardiac crest cells, guide the final cardiac crest migration into the outflow tract (Kuriyama and Mayor, 2008; Scholl and Kirby, 2009). Other morphogens, like SHH signalling, shown to modulate responsiveness of enteric neural crest cells to Gdnf, and members of the BMP, FGF and RA signalling pathways shown through knock-out studies to affect proper cardiac

neural crest migration, are likely candidates in modulating this process (Jones and Trainor, 2005).

3.4.3. Differentiation

Upon arrival at their target sites, the neural crest cells respond to local signalling and differentiate *in situ* (Sauka-Spengler and Bronner-Fraser, 2008). The multipotency of the crest cells and the regulatory factors underlying it have been extensively studied. The Notch/Delta pathway favours glial over neuronal neural crest fates (Christiansen et al., 2000; Kalcheim and Burstyn-Cohen, 2005) in contrast with BMP signalling that promotes neurogenesis (Le Douarin and Dupin, 2003). Neural crest cells can give rise to autonomic or sensory neuronal types, a process controlled at least in part by *Neurogenins* (Christiansen et al., 2000). Endothelin signalling is involved in melanocyte and posterior enteric nerve plexus development (Le Douarin and Dupin, 2003). Other factors, like *Sox10* inhibit neural crest lineage commitment, thus maintaining the multipotency of the tissue (Kim et al., 2003). Apart from generating distinct derivatives, the neural crest acts on pharyngeal arch artery support (Hutson and Kirby, 2007; Scholl and Kirby, 2009) and subsequent re-patterning (Kameda, 2009; Snider et al., 2007) *Endothelin*, *Platelet-Derived Growth Factor* (*PDGF*) and *TGFβ* are considered mediators of these processes in the neural crest, studied in several animal models (Scholl and Kirby, 2009).

4. Pharyngeal arch arteries

4.1. Formation and remodelling

During normal cardiovascular development, five pairs of pharyngeal arch arteries connect the truncus arteriosus and the aortic sac at the distal end of the cardiac outflow with the paired dorsal aortae (DAo) (Gittenberger-de Groot et al., 2006; Kameda, 2009; Yanagisawa et al., 1998). Over the course of development this transient, symmetrical configuration remodels into the mature, unilateral, left-sided arterial system (Gittenberger-de Groot et al., 2006; Kameda, 2009; Kellenberger, 2010; Molin et al., 2002; Snider et al., 2007; Yanagisawa et al., 1998). After the initial construction of the endothelial network through vasculogenesis and angiogenesis, arteriogenesis takes place by differentiation of neural crest cells into a VSM layer, that provides support and stabilisation to the arch arteries (Gittenberger-de Groot et al., 2006). The remodelling process that follows involves programmed asymmetrical expansion, regression, persistence and change of relative position of the different vascular segments (Gittenberger-de Groot et al., 2006; Kameda, 2009; Yanagisawa et al., 1998). This extensive reconfiguration process occurs at around E11.5 in the mouse and by E13.5 it is completed for all branchial arch arteries and major vessels (Hiruma et al., 2002; Yanagisawa et al., 1998). Regression of the first two cranial sets of arch arteries occurs by E11.0 (Hiruma et al., 2002) and at E11.5 the remaining symmetrical pairs of arch arteries (pairs 3, 4 and 6) connect the two DAo with the ventrally located aortic sac, while the right sixth arch artery becomes slender commencing from its proximal part (Hiruma et al., 2002; Yanagisawa et al., 1998). The aortic sac begins to septate from its proximal part (Hiruma et al., 2002). At E12.0 the narrowing of the right sixth arch artery is followed by the narrowing of the left carotid duct (DAo segment connecting the third and fourth arch arteries, γ segment in Figure 1.3.A) (Yanagisawa et al., 1998). At E12.5 the aortic sac is separated into an ascending aorta and pulmonary trunk (Yanagisawa et al., 1998). The third arch arteries run parallel to the fourth pair, while they are being elongated in a cranial direction (Hiruma et al., 2002; Yanagisawa et al., 1998). Both carotid ducts are slender or completely absent (Hiruma et al., 2002; Yanagisawa et al., 1998). The caudal part of the right DAo (α segment in Figure 1.3.A) becomes thinner (Hiruma et al., 2002). By this stage the right sixth arch artery has completely regressed (Yanagisawa et al., 1998). At E13.0 the ascending aortic arch and

the proximal part of the brachiocephalic trunk (aortic sac-derived) continue to develop rostrally (Yanagisawa et al., 1998). The left fourth arch artery is enlarged and forms the arch of the aorta while the connection of the right DAo (α segment in Figure 1.3.A) to the abdominal DAo is very narrow (Yanagisawa et al., 1998). At E13.5 the third arch arteries are formed into the left and right common carotid arteries (LCC and RCC) and the right DAo is completely absent (Hiruma et al., 2002; Yanagisawa et al., 1998).

The regression process, that maintains the same pattern in all vascular segments programmed to regress, begins with a progressive decline in lumen diameter and a reduction in vessel wall thickness (Molin et al., 2002). This results in the formation of a characteristic smooth muscle strand, followed by the interruption of the vascular segment at its midpoint and finally the disappearance of the proximal and distal ends (Molin et al., 2002). Arteries of the same pair do not necessarily share a common remodelling program. For example the right fourth arch artery reduces in size before it becomes part of the right subclavian artery (RSCA) while the left fourth arch artery retains its size since it forms a segment of the mature aortic arch (Yanagisawa et al., 1998). The same stands for the sixth pair of arch arteries, whereby the right arch artery regresses completely while the left counterpart becomes the ductus arteriosus and supports circulation during the embryonic period (Yanagisawa et al., 1998).

Ultimately the first and second arch arteries become vasculature of the head (Hiruma et al., 2002; Kellenberger, 2010; Yanagisawa et al., 1998). The third pair forms the common carotid arteries, whilst the fourth arch arteries contribute to the distal part of the aortic arch (left arch artery) and the brachiocephalic artery and a proximal part of the RSCA (right arch artery) (Hiruma et al., 2002; Kellenberger, 2010; Yanagisawa et al., 1998). The right sixth arch artery regresses completely and the left sixth forms the ductus arteriosus (Hiruma et al., 2002; Kameda, 2009; Kellenberger, 2010; Yanagisawa et al., 1998) and the proximal parts of the pulmonary arteries (Kameda, 2009; Kellenberger, 2010). The seventh intersegmental arteries (ISA), caudal branches of the DAo, remodel into parts of the subclavian arteries (Kameda, 2009; Kellenberger, 2010). The aortic sac becomes part of the ascending aorta, proximal aortic arch and brachiocephalic artery (Kellenberger, 2010). By the end of the remodelling process an arch that lies to the left of the trachea, arches over the mainstream bronchus and continues as the DAo to the left of the spine is generated (Kellenberger, 2010). The first arterial branch passes to the right as the brachiocephalic artery, giving rise to the RCC

and RSCA arteries, followed in succession by the LCC and the left subclavian arteries (LSCA) (Kellenberger, 2010). The ductus arteriosus is positioned on the left and connects the proximal left pulmonary artery with the distal aortic arch (Figure1.3.D) (Kellenberger, 2010).

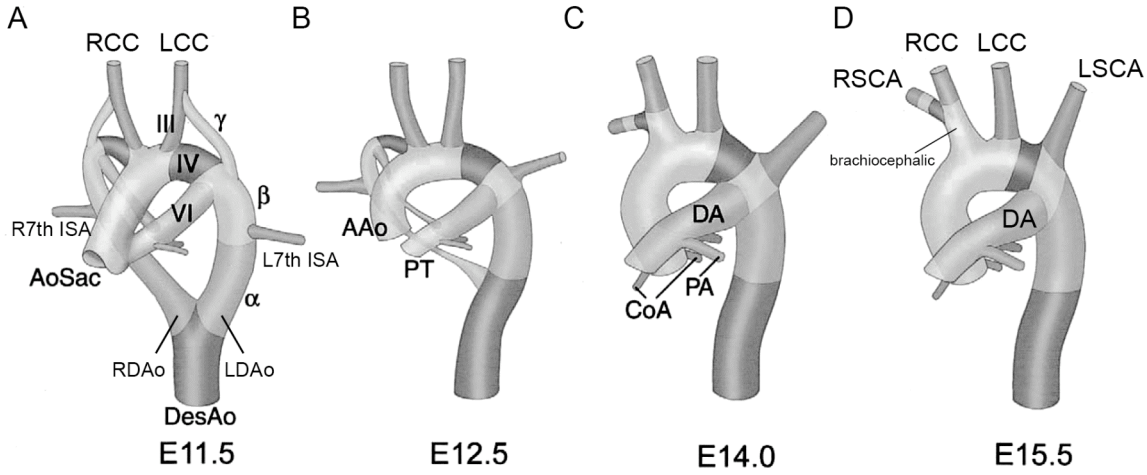

Figure 1. 3. Normal pharyngeal arch artery remodelling in the mouse. Remodelling commences at E11.5 with a symmetrical arterial system of paired aortic arches III, IV and VI, DAo segments α, β, and γ and seventh ISAs (A). By E12.5, the aortic sac (AoSac) has remodelled into a separate ascending aorta (AAo) and pulmonary trunk (PT) (B). After E14.0 the coronary arteries (CoA) connect to the AAo (C). By E15.5 the process has completed with the first arterial branch passing to the right as the brachiocephalic artery, which gives rise to the RCC and RSCA arteries, followed in succession by the LCC and LSCA. The ductus arteriosus is on the left connecting the proximal left pulmonary artery with the distal aortic arch (D). AAo, ascending aorta; CoA, coronary artery; DA, ductus arteriosus; DesAo, descending aorta; III, IV and VI, third, fourth and sixth aortic arches; PA, pulmonary artery; PT, pulmonary trunk; RCC/LCC, right/left common carotid artery; RSCA/LSCA, right/left subclavian artery; R7th ISA/L7th ISA, right/left seventh intersegmental artery. Modified from Molin et al., 2002.

4.2. Mechanisms of remodelling

The remodelling process of the pharyngeal arteries into their final arrangement and morphology, resulting in the mature great vessel configuration, is controlled by reciprocal signalling between the mesoderm-derived endothelial and neural crest-derived VSM lining of the arteries, as well as the surrounding mesenchyme and

endoderm of the arches (Snider et al., 2007). Interestingly, the fourth pair of arch arteries has a distinct vascular morphology (Molin et al., 2004). The smooth muscle cells (SMC) of the vessel walls have very low smooth muscle α-actin expression, prominent expression of neurofilament protein and the neural marker NCAM-1, while they present with an abundance of Smad2-positive nuclei (Molin et al., 2004). In *Tgfβ2*$^{-/-}$ mutants with fourth arch artery hypoplasia, atresia or aortic arch interruption, both markers appear miss-expressed while no Smad2-positive nuclei are detected (Molin et al., 2004). This characteristic pattern was not observed in the carotid ducts, third or sixth pairs of arch arteries nor in normally forming fourth arch arteries in *Tgfβ2*$^{-/-}$ mutants (Molin et al., 2004).

Aside from morphogenetic factors, the remodelling of the respective vascular segments is thought to be additionally regulated by blood flow haemodynamics (Gittenberger-de Groot et al., 2006; Molin et al., 2002; Yashiro et al., 2007). The significance of blood flow in cardiovascular development has been shown by means of mechanical obstruction of arterial or venus vessels or of heart segments (Hogers et al., 1997; Hogers et al., 1999). Such experiments produce several cardiac malformations like double outlet right ventricle (DORV), VSDs and arch artery defects in avian models (Hogers et al., 1997; Hogers et al., 1999). In the mouse model, regression of the right sixth arch artery appears to be controlled initially by mechanical and haemodynamic forces, which subsequently induce apoptotic cues (Yashiro et al., 2007). Yashiro *et al.*, demonstrated that the outflow tract movement between E11.5-E12.5, which occurs because of the rotation of the arterial pole, shifts the entry point of the right sixth arch artery towards the left, adjacent to the DAo (Yashiro et al., 2007). By ligating the left sixth arch artery, the authors induced abnormal regression of the vessel with concomitant persistence of its right counterpart, contrary to normal development (Yashiro et al., 2007). An *in vitro* experimental and computational study of normal and abnormal fetal aortic arch haemodynamics has shown differences in the blood flow between the normal and the disease settings (Pekkan et al., 2008). Moreover, flow modeling of the chicken embryonic pharyngeal system showed that spatial shear stress and velocity distributions change between stage 18 (arch arteries 2, 3 and 4 are present) and stage 24 (arch arteries 3, 4 and 6 are present) (Wang et al., 2009). The results correlate well with the shift of the three-pair arch artery configuration from an anterior to a posterior position and the increased cardiac output between the stages (Wang et al., 2009).

Selective apoptosis is also an important factor in the regression process (Molin et al., 2002). Apoptotic cells are initially preferentially seen in the mesenchyme surrounding the vascular segments that are programmed to regress (Molin et al., 2002). Eventually these cells grow in number and expand towards initially and later into the outer border of the smooth muscle tissue (Molin et al., 2002). A non-lumenised strip of SMCs is the last remainder of the vessel before complete regression (Molin et al., 2002).

The individual pairs of pharyngeal arches display distinct gene expression patterns, which may play a role in the remodelling process. *Hox(a-d)4* are exclusively expressed in the fourth pair of arches, while *Hoxb5* is detected in the sixth pair (Molin et al., 2002). *Hoxa3* is required for the morphogenesis of the third arch and pouch, while homozygous mutation of the gene results in, among others, anomalies of the carotid arch artery system due to compromised proliferation of the neural crest cells within the arch (Kameda, 2009). Similar misspatterning of the cellular component of each arch, in particular of the neural crest population that is responsible for the VSM layer of each arch artery, may result in several remodelling defects (Kameda, 2009; Molin et al., 2002). Other morphogenetic factors may be equally important. Blocking SHH in quail embryos results in abnormal formation of the arch arteries, shown by failure of vessel lumenisation and abnormal subsequent remodelling (Kolesova et al., 2008). TGFβ enhances the expression of SMC-specific proteins that are essential for vessel wall structure (Kumar and Owens, 2003). Consistent with that, *Tgfβ2* homozygous mutants exhibit great vessel defects as a result of abnormal regression of the fourth arch (Molin et al., 2002). Nevertheless, the precise mechanisms underlying the patterning of the great vessels remain elusive.

4.3. Types of great vessel defects and embryological origin

Abnormal formation and/or remodelling of the branchial arch arteries can cause a number of congenital anomalies of the aortic arch and the great vessels, commonly seen in cardiovascular disease (Bialowas et al., 2000; Davies and Guest, 2003; Dillman et al., 2008; Kellenberger, 2010; Kutsche and Van Mierop, 1984; McElhinney et al., 1999; Mishra, 2009; Morishima et al., 2003; Van Mierop and Kutsche, 1984; Van Praagh et al., 1971; Yang et al., 2008). Such aberrations can occur as isolated lesions, without serious clinical symptoms, or can correlate with defects in heart development and cyanotic lesions (Bialowas et al., 2000; Kellenberger, 2010). There are at least four

distinct categories of anatomic arch anomalies that deviate from the normal left-sided configuration (Kellenberger, 2010).

1. Double aortic arch

A double aortic arch is observed when the caudal part of the right DAo fails to follow the normal regression process and instead persists, leading in the formation of a vascular ring (Davies and Guest, 2003; Kellenberger, 2010). Most commonly, the DAo is located on the left side of the spine so the right arch runs behind the esophagus and the left arch in front of the trachea (Kellenberger, 2010). Usually the right arch is higher and wider than the left (Davies and Guest, 2003; Kellenberger, 2010). The common carotid and subclavian arteries arise independently from the respective aortic arches while the ductus arteriosus may be present on either or both sides connecting the pulmonary arteries with the distal arches (Figure 1.4) (Kellenberger, 2010). A double aortic arch is usually an isolated anomaly that does not associate with cardiac abnormalities (Kellenberger, 2010).

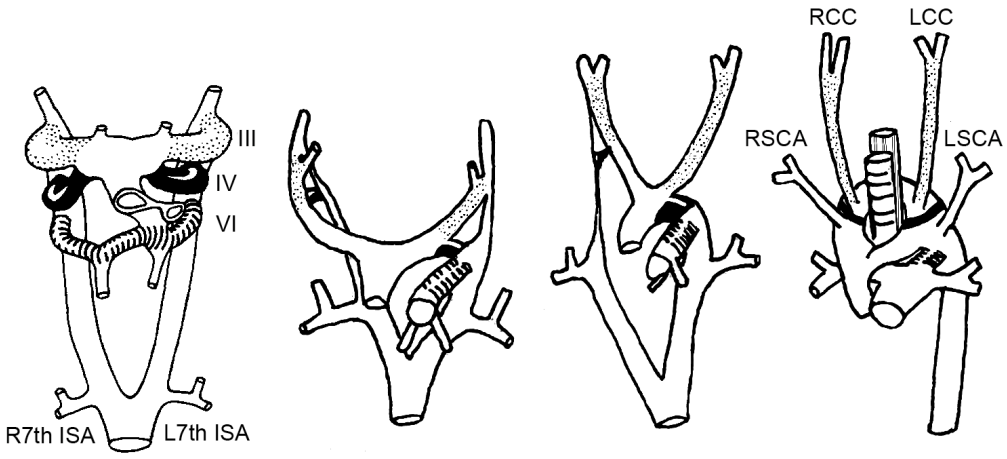

Figure 1. 4. Embryological origin of the double aortic arch. Persistence of the caudal part of the right DAo gives rise to a vascular ring. DAo, dorsal aorta; III, IV and VI, third, fourth and sixth aortic arches; RCC/LCC, right/left common carotid artery; RSCA/LSCA, right/left subclavian artery; R7th ISA/L7th ISA, right/left seventh intersegmental artery. Drawn after Van Mierop and Kutsche, 1984.

2. Right-sided aortic arch (RAA)

An RAA occurs when abnormal regression or failure of the left fourth arch artery to form is compensated by the enlargement of the right counterpart with concomitant persistence of the right DAo (Morishima et al., 2003). The entire right dorsal arch

persists resulting in a configuration where the mature arch lies on the right side of the trachea before descending on either the right or the left side of the spine (Bialowas et al., 2000; Davies and Guest, 2003; Kellenberger, 2010). Almost invariably this configuration is associated with cyanotic congenital heart lesions, most commonly TOF, pulmonary atresia with VSD or CAT (Bialowas et al., 2000; Kellenberger, 2010; McElhinney et al., 1999). There are two subcategories, RAA with mirror image branching (Figure 1.5.A, B) or RAA with abnormal branching (Figure 1.5.C, D) (Bialowas et al., 2000; Davies and Guest, 2003). In the first instance the arch has three branches, the left brachiocephalic trunk, which is the most proximal branch of the arch, the RCC and then the RSCA in succession (Davies and Guest, 2003; Kellenberger, 2010; McElhinney et al., 1999). The ductus arteriosus is often left-sided and connects the left brachiocephalic artery and the left pulmonary artery (Figure 1.5.A) (Kellenberger, 2010; McElhinney et al., 1999). If the ductus is right-sided and courses from the underside of the descending arch to the right pulmonary artery it forms a true mirror image arch (Figure 1.5.B) (Kellenberger, 2010; McElhinney et al., 1999). In the second instance, concurrent with the persistence of the right DAo is the complete regression of the left fourth branchial artery, thus producing an RAA that has four branches, beginning with the LCC proximal to the arch and followed in succession by the RCC, the RSCA and finally an aberrant LSCA (A-LSCA), that originates from the DAo and passes to the left, behind the oesophagus (Figure 1.5.C) (Davies and Guest, 2003; Kellenberger, 2010; McElhinney et al., 1999). If the ductus is left-sided a complete vascular ring is formed (Figure 1.5.D) (McElhinney et al., 1999). This configuration is less frequently associated with an intracardiac defect, but when it is, TOF is the most common lesion (McElhinney et al., 1999).

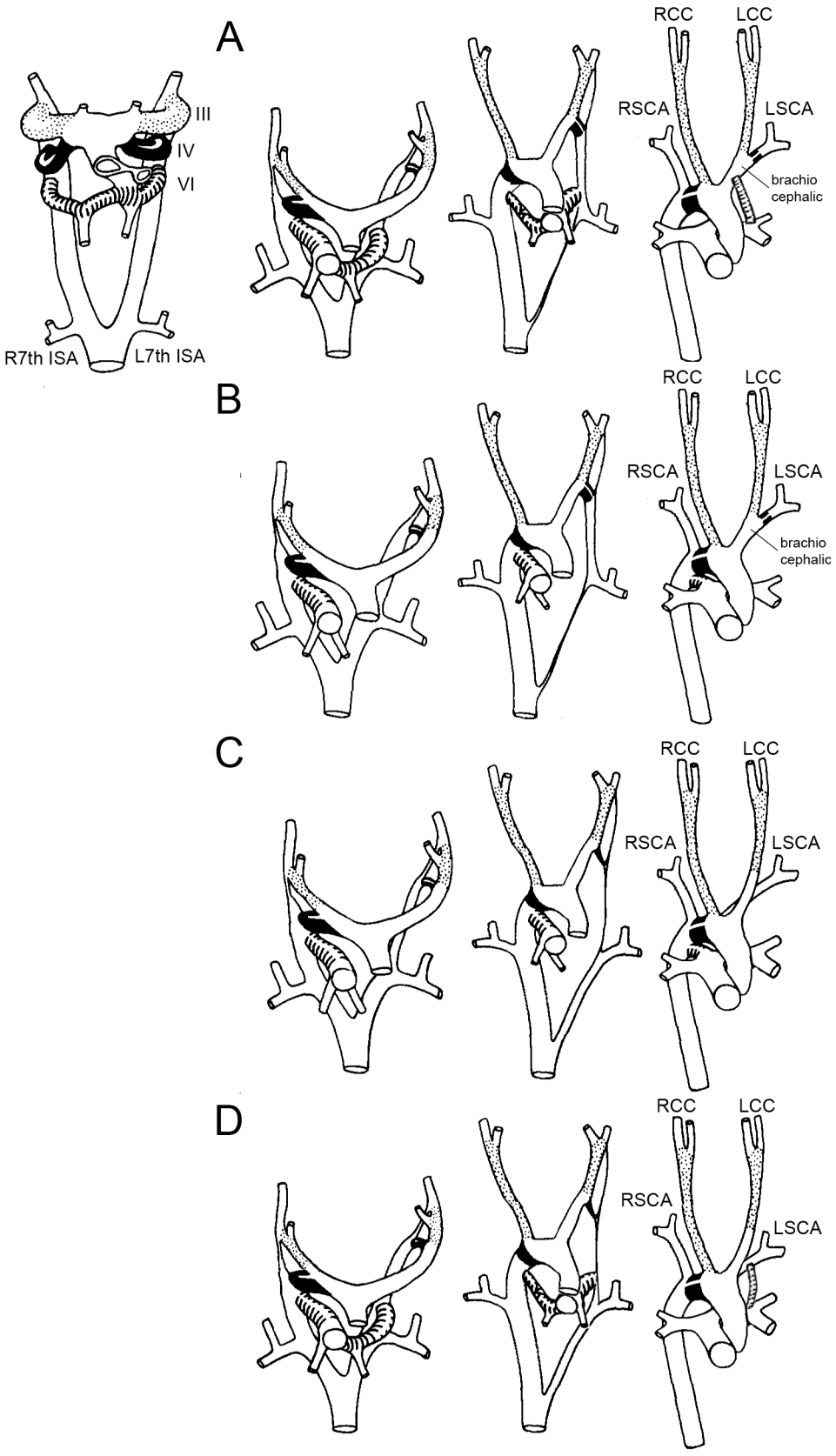

Figure 1. 5. Embryological origin of the RAA. Abnormal regression of the left fourth arch artery, enlargement of the right fourth arch artery and persistence of the right DAo

lead to a right-sided configuration (A-D). RAA with mirror image branching describes a right arch that has three branches, the left brachiocephalic trunk, the RCC and the RSCA in succession (A-B). If the ductus arteriosus is left-sided it connects the left brachiocephalic artery and the left pulmonary artery (A), while if it is right-sided it courses from the underside of the descending arch to the right pulmonary artery and forms a true mirror image arch (B). RAA with abnormal branching occurs after complete regression of the left fourth arch artery, which results in a right arch that has four branches, the LCC, the RCC, the RSCA and an A-LSCA that originates from the DAo and passes to the left, behind the oesophagus (C). If the ductus is left-sided a complete vascular ring is formed (D). DAo, dorsal aorta; III, IV and VI, third, fourth and sixth aortic arches; RCC/LCC, right/left common carotid artery; RSCA/LSCA, right/left subclavian artery; R7th ISA/L7th ISA, right/left seventh intersegmental artery. Drawn after Van Mierop and Kutsche, 1984.

3. Left-sided aortic arch, abnormal branching or interruptions

The normal aortic arch descends to the left; however, branching aberrations or missing segments produce abnormal anatomies (Bialowas et al., 2000; Davies and Guest, 2003; Kellenberger, 2010; Kutsche and Van Mierop, 1984).

Abnormal branching

A commonly affected vessel is the RSCA that forms aberrantly (A-RSCA) when the right fourth branchial artery is absent or involutes before the regression of the right DAo (Davies and Guest, 2003; Kutsche and Van Mierop, 1984; Morishima et al., 2003). Three different anatomies can arise (Kutsche and Van Mierop, 1984). If the caudal part of the right DAo persists it forms an A-RSCA with the right seventh ISA (Figure 1.6.A) (Davies and Guest, 2003; Kutsche and Van Mierop, 1984; Reardon et al., 1984). The A-RSCA originates from the DAo or a diverticulum and crosses to the right behind the oesophagus, constituting an incomplete vascular ring (retro-oesophageal RSCA) (Davies and Guest, 2003; Kellenberger, 2010; Morishima et al., 2003). If this is combined with the disappearance of the right third arch artery then the right brachiocephalic trunk leaves the aortic arch as the last branch and runs beyond the oesophagus (Bialowas et al., 2000). In rare cases where a right-sided ductus arteriosus is present connecting the right pulmonary artery and the right subclavian artery, the A-RSCA may originate from a retro-oesophageal diverticulum, forming a complete

vascular ring with the right-sided ductus connection (Kellenberger, 2010). In the second case, an A-RSCA can originate from the right pulmonary artery (Kutsche and Van Mierop, 1984). The dorsal segment of the right sixth arch artery persists and forms the A-RSCA with a segment of the right DAo and the right seventh ISA (Figure 1.6.B) (Kutsche and Van Mierop, 1984). The right sixth arch artery in this instance compensates for the absent fourth (Kutsche and Van Mierop, 1984). Alternatively, after regression of the right fourth arch artery an A-RSCA can arise from the persistence of the right carotid duct that remains connected to the brachiocephalic branch, thus giving rise to a cervically located RSCA (cervical RSCA) (Figure 1.6.C) (Kutsche and Van Mierop, 1984).

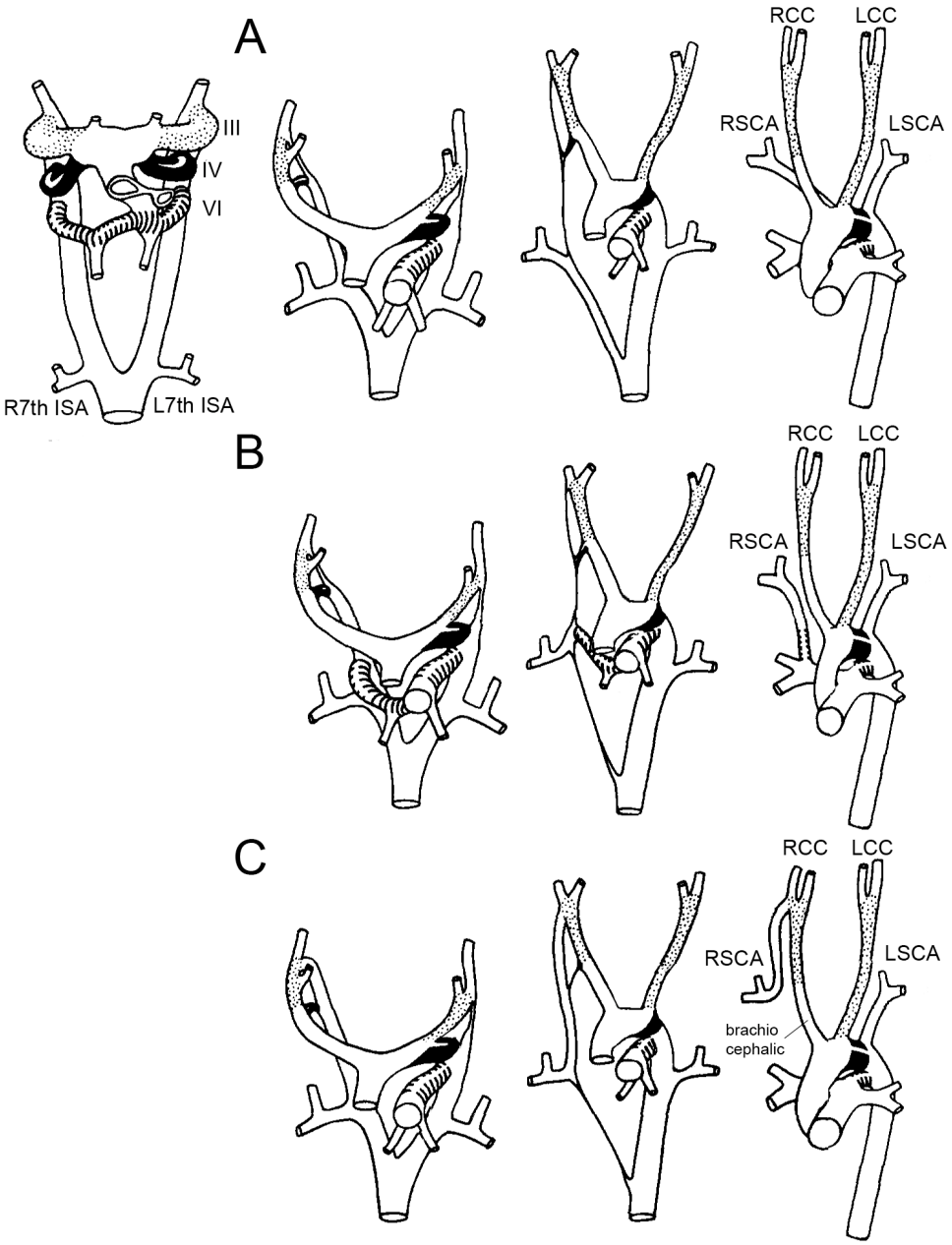

Figure 1. 6. Embryological origin of the left-sided arch with abnormal branching. Abnormal regression of the right fourth arch artery results in aberrant origin of the RSCA (A-C). If the caudal part of the right DAo persists it forms a retro-oesophageal RSCA with the right seventh ISA (A). If the dorsal segment of the right sixth arch artery persists it forms an A-RSCA with a segment of the right DAo and the right seventh ISA (B). If the right carotid duct persists it remains connected to the brachiocephalic trunk and gives rise to a cervically located A-RSCA (C). DAo, dorsal aorta; III, IV and VI, third, fourth and sixth aortic arches; RCC/LCC, right/left common

carotid artery; RSCA/LSCA, right/left subclavian artery; R7th ISA/L7th ISA, right/left seventh intersegmental artery. Drawn after Van Mierop and Kutsche, 1984.

Cervical aortic arch

In the case of a cervical aortic arch the apex of the arch extends beyond the sternum and into the neck (Davies and Guest, 2003; Kellenberger, 2010). The embryological basis of this anomaly is controversial, however, it is thought to be a result of abnormal formation or regression of the fourth branchial artery in combination with enlargement of the third arch artery and persistence of the respective carotid duct (Figure 1.7) (Morishima et al., 2003). This configuration provides an alternative route for the arch, via the carotid duct, raising it higher than normal (Morishima et al., 2003). It is another example of compensation for the abnormal formation or regression of the fourth arch artery (Morishima et al., 2003). More often it appears on the right side (cervical RAA) where the definitive arch is formed by the right third arch and right DAo (Davies and Guest, 2003; Kellenberger, 2010). The branches are variable, but the common carotid arteries and the RSCA often arise independently from the arch (Davies and Guest, 2003; Kellenberger, 2010).

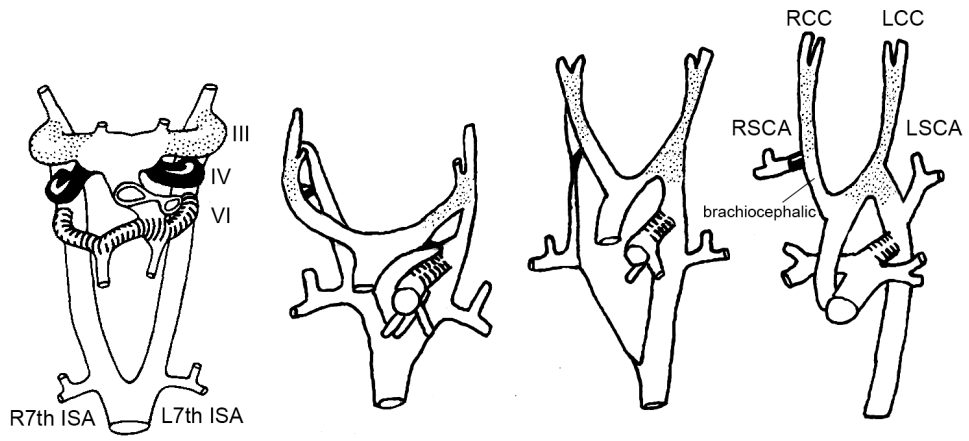

Figure 1. 7. Embryological origin of the cervical aortic arch. Abnormal regression of the fourth arch artery, enlargement of the third arch artery and persistence of the respective carotid duct lead to the formation of a cervically located aortic arch. DAo, dorsal aorta; III, IV and VI, third, fourth and sixth aortic arches; RCC/LCC, right/left common carotid artery; RSCA/LSCA, right/left subclavian artery; R7th ISA/L7th ISA, right/left seventh intersegmental artery. Drawn after Van Mierop and Kutsche, 1984.

4. Interruptions

An interrupted aortic arch (IAA) describes the luminal discontinuity or the presence of a fibrous strand between the ascending and descending aorta (Dillman et al., 2008; Mishra, 2009; Reardon et al., 1984; Van Mierop and Kutsche, 1984; Yang et al., 2008). Based on the site of the interruption the lesion is classified as three types (Dillman et al., 2008; Kellenberger, 2010; Mishra, 2009; Reardon et al., 1984; Van Mierop and Kutsche, 1984; Yang et al., 2008). Type A describes an interruption of the aortic arch distal to the left subclavian artery, in type B the defect is found between the LCC and left subclavian arteries and in type C the discontinuity exists between the brachiocephalic and the LCC arteries (Dillman et al., 2008; Kellenberger, 2010; Mishra, 2009; Reardon et al., 1984; Van Mierop and Kutsche, 1984; Yang et al., 2008). Each affected segment of the aortic arch has a different embryological origin, the junction of the fourth and sixth arches, the left fourth branchial arch and the aortic sac, respectively (Yang et al., 2008). Coarctation of the aorta, a partial involution of the left dorsal aortic arch (Davies and Guest, 2003), between the LSCA and the ductus arteriosus, is considered responsible for the pathogenesis of IAA-A (Figure 1.8.A) (Van Mierop and Kutsche, 1984). Abnormal formation or regression of the left fourth arch artery results in IAA-B (Figure 1.8.B) (Dillman et al., 2008; Kutsche and Van Mierop, 1984; Reardon et al., 1984; Van Mierop and Kutsche, 1984). The last type, IAA-C, is suggested to result after involution of the left limb of the aortic sac and its derivatives, the ventral portions of the left third and left fourth arches, with concomitant persistence of the left carotid duct (Figure 1.8.C) (Reardon et al., 1984; Van Praagh et al., 1971). All interruptions can coexist with an A-RSCA (Kellenberger, 2010; Kutsche and Van Mierop, 1984; Reardon et al., 1984; Van Mierop and Kutsche, 1984; Yang et al., 2008) and although a rare condition, 50-80% of all IAA cases are linked to 22q11DS, commonly in conjunction with an RAA (Dillman et al., 2008; Kellenberger, 2010; Mishra, 2009; Yang et al., 2008). Often patients also exhibit VSD, CAT and/or transposition of the great arteries (TGA) in association with an interruption (Dillman et al., 2008; Kellenberger, 2010; Mishra, 2009; Yang et al., 2008).

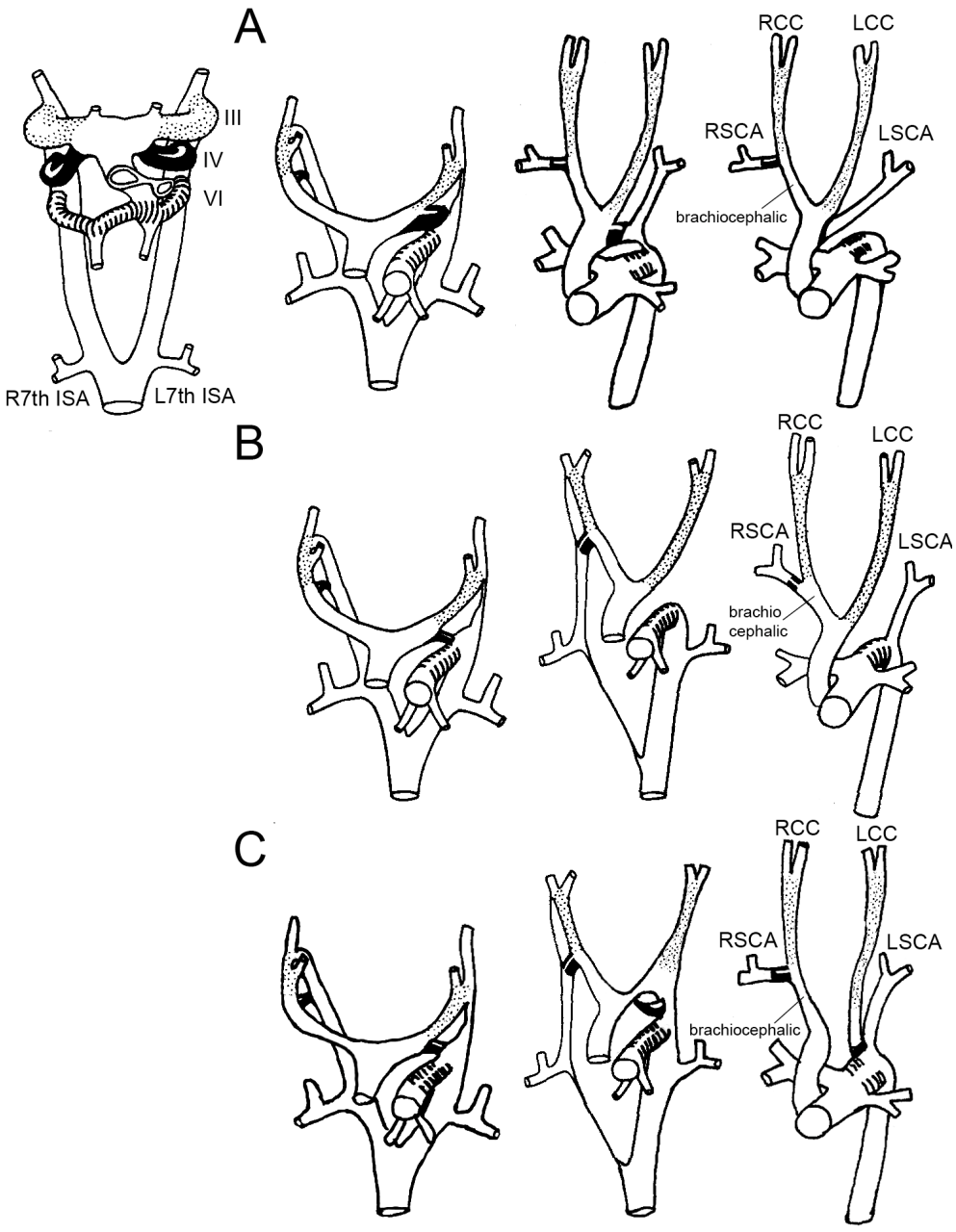

Figure 1. 8. Embryological origin of the IAA. An IAA-A can occur after an aortic coarctation between the LSCA and the ductus arteriosus (A), an IAA-B can result after abnormal formation or regression of the left fourth arch artery (B) while an IAA-C can arise after involution of the left limb of the aortic sac and the ventral segments of the left third and left fourth arches, with concomitant persistence of the left carotid duct (C). DAo, dorsal aorta; III, IV and VI, third, fourth and sixth aortic arches; RCC/LCC, right/left common carotid artery; RSCA/LSCA, right/left subclavian artery; R7th ISA/L7th ISA, right/left seventh intersegmental artery. Drawn after Van Mierop and Kutsche, 1984.

Other vascular malformations exist, like defects in the pulmonary vascular system (Davies and Guest, 2003), which will not be discussed in this thesis.

In some cases, like RAA or the cervical arch discussed above, failure of a vascular segment, in these cases the fourth arch arteries, results in compensatory arterial rearrangements, so that the end configuration is compatible with postnatal life. These rearrangements do not always occur and the underlying mechanisms of this plasticity are not known. The genetic background, haemodynamic forces, the type and time of occurrence of the primary defect, as well as stochastic events are all possible interplaying factors (Morishima et al., 2003).

5. Endocrine glands - pharyngeal pouch derivatives

The thymus, thyroid, parathyroid, and ultimobranchial bodies, endocrine glands that derive from the third and fourth pharyngeal pouches (Graham, 2008; Grevellec and Tucker, 2010; Jerome and Papaioannou, 2001; Manley and Capecchi, 1998), develop in parallel and subsequently migrate to their final destinations (Manley and Capecchi, 1998). For the purposes of this thesis, only the thymus gland will be further discussed.

The vertebrate thymus is a complex epithelial organ that forms in the caudal-ventral region of the third pouch and is responsible for the production of mature T-cells that are released in the systemic circulation (Manley, 2000). Thymic organogenesis requires reciprocal interactions between adjacent tissues of all three embryonic germ layers (Hollander et al., 2006; Manley, 2000). Initiating signals at E9.5 induce cells from the endoderm of the third pharyngeal pouch to proliferate, undergo EMT and delaminate from the inner layer of the foregut into the neural crest-derived underlying mesenchyme (Boehm, 2008; Manley, 2000). Although the thymic epithelium itself is of endodermal origin (Gordon et al., 2004), the surrounding neural crest-derived connective tissues affect its development (Gill et al., 2003; Manley, 2000; Muller et al., 2008) and give rise to the perivascular mesenchyme of the adult organ (Muller et al., 2008). Pre-migratory neural crest ablation experiments result in thymus dysplasia or aplasia (Gill et al., 2003; Grevellec and Tucker, 2010; Manley, 2000). Between E11.5-E12.0 primarily proliferative events take place so that the common thymus/parathyroid primordia increase significantly in size, while the thymus starts to expand caudally (Grevellec and Tucker, 2010). By then the thymic primordia express markers that promote endothelial cell differentiation, a process essential for the specification of the organ and the subsequent colonisation by thymocyte progenitor cells (Boehm, 2008; Gill et al., 2003; Grevellec and Tucker, 2010; Hollander et al., 2006; Manley, 2000). From E12.5 to E13.5 these bilateral primordia separate from the endoderm of the pharynx and move caudally, ventrally and medially, towards the anterior thoracic cavity (Grevellec and Tucker, 2010; Hollander et al., 2006). At the same time lymphoid precursors migrate into the thymic epithelium, where they become committed to the T-cell lineage (Gill et al., 2003; Hollander et al., 2006). At E15.5 each primordium still descends caudally and medially before reaching its final position above the heart and joining its symmetric thymic lobe (Grevellec and Tucker, 2010).

Defective thymic development may reflect abnormalities in either the specification of the endodermal cells of the third pouch, mainly controlled by the expression of *Foxn1* and upstream factors (Boehm, 2008), or the formation of the third pouch itself. In *Hoxa3* and *Eya1* mutants there is loss of third pouch identity and subsequent loss of the gland primordia (Grevellec and Tucker, 2010). *Tbx1* and *Pax9* mutants present with thymic hypo/aplasia as a result of arrested development of the thymic primordium (Boehm, 2008; Grevellec and Tucker, 2010; Hollander et al., 2006). *Pbx1* and *Six1* genes also have a reported role in pharyngeal pouch formation (Boehm, 2008). Wnt and BMP signalling are postulated to initiate or maintain *Foxn1* expression in the thymic epithelium, respectively (Boehm, 2008). In addition to *Pax* and *Hox* factors, FGFs appear to be required for pharyngeal gland relocation, and indeed *Fgf10* and *Fgf7* are expressed in the mouse thymus during organ migration to the midline (Grevellec and Tucker, 2010). SHH signalling is involved in controlling the size of the thymic field, while the overall size of the gland is probably regulated by p63 and FGF signalling (Boehm, 2008).

6. Palate - pharyngeal arch derivative

Facial clefting, a common characteristic of the 22q11DS phenotype (Shprintzen, 2008; Wurdak et al., 2006), has three main categories: isolated cleft lip and/or alveolus, isolated cleft palate and combined cleft lip, alveolus and palate (Meng et al., 2009). The clefts can be complete or incomplete and unilateral or bilateral (Meng et al., 2009). Developmentally, the five facial primordia that give rise to the maxillo-mandibular complex are two pairs of mandibular and maxillary prominences and the frontonasal prominence (Figure 1.9) (Jugessur et al., 2009). These prominences consist of epithelial outgrowths of mesoderm and neural crest cells deriving from the midbrain and hindbrain (Jugessur et al., 2009). Mandibular clefts are extremely rare, possibly indicating that the early fusion of the mandibular prominences is very robust (Jugessur et al., 2009). The generation of the maxilla, primary and secondary palate however, requires a more complex sequence of fusion events (Jugessur et al., 2009).

The maxillary prominence is a first pharyngeal arch derivative and gives rise to the zygomatic complex, the lateral maxilla and the secondary palate (Jugessur et al., 2009). The latter forms as an outgrowth of the maxillary prominence (Gritli-Linde, 2007; Jugessur et al., 2009). The frontonasal prominence extends caudally and gives rise to the midfacial structures including the medial part of the nose, the philtrum, the intermaxillary segment and the primary palate (Jugessur et al., 2009). Fusion of the left and right maxillary prominences with the intermaxillary segment results in the continuous upper jaw that includes the primary palate (Gritli-Linde, 2007; Jugessur et al., 2009). The secondary palate is formed from the palatal shelves that initially grow vertically from the maxillary prominence but eventually elevate and oppose each other as the tongue flattens and the overall oral volume increases (Gritli-Linde, 2007; Jugessur et al., 2009; Meng et al., 2009). The subsequent contact and fusion of the shelves results in the formation of the secondary palate (Gritli-Linde, 2007; Jugessur et al., 2009; Meng et al., 2009). The primary and secondary palates must also fuse at their contacting sites, a process that requires interplay between different transcription factors, growth factors and signalling molecules (Gritli-Linde, 2007; Jugessur et al., 2009; Meng et al., 2009). Facial clefts can result from abnormal progression of either of these processes, although the most frequent mechanisms are deficient mesenchymal cell proliferation or failure of epithelial fusion (Nie et al., 2006).

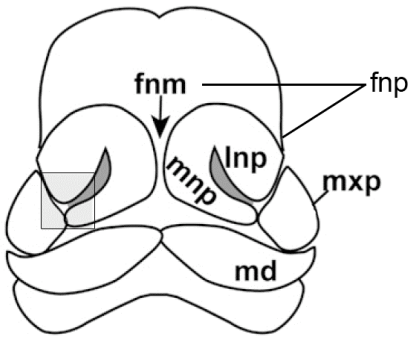

Figure 1. 9. The mouse facial primordia. The facial prominences surround the stomodeal opening. Fusion of the lip will take place at the intersection of the tissues in the grey box. fnm, frontonasal mass; fnp, frontonasal prominence; lnp, lateral nasal prominence; mnp, medial nasal prominence; md, mandibular prominence; mxp, maxillary prominence. Modified from Szabo-Rogers et al., 2010.

The development of the secondary palate requires complex interactions among epithelial cells, mesenchymal cells and the ECM in an ordered sequence (Meng et al., 2009). It is a multi-step process that includes palatal shelf growth, elevation, medial elongation, fusion and the disappearance of the midline epithelial seam (MES) (Nie et al., 2006; Okano et al., 2006). In mouse, the palatal primordia first appear between E11.5-E12.5 at the lateral edges of the maxillary process (Gritli-Linde, 2007; Meng et al., 2009; Okano et al., 2006). The shelves extend vertically along the sides of the tongue and elongate by E14.5 (Gritli-Linde, 2007; Meng et al., 2009; Okano et al., 2006). The opposing edges of the palatal shelves contact each other and adhere by the glycoprotein coat and desmosomal junctions of the medial edge epithelia (MME) (Meng et al., 2009; Okano et al., 2006). During this fusion process the MME form the MES (Gritli-Linde, 2007; Meng et al., 2009; Okano et al., 2006). Although the mechanism of disappearance of the epithelia in the MES is unclear, apoptosis, migration towards the periphery of the midline and EMT have been suggested (Gritli-Linde, 2007; Meng et al., 2009; Okano et al., 2006). The MES has disappeared by E16.0 when the palatal fusion is completed and then ossification takes place to form the hard palate (Gritli-Linde, 2007; Meng et al., 2009). The posterior end of the palate remains unossified and constitutes the soft palate (Gritli-Linde, 2007; Meng et al., 2009).

The mechanisms that regulate palate development have been extensively studied and most studies revolve around the TGFβ family. TGFβ factors, including BMPs and Activins, are involved in proliferation, apoptosis, ECM synthesis and deposition, cell migration, EMT and degradation of basement membranes, all processes that occur during palatogenesis (Meng et al., 2009). Different factors have been shown responsible for different processes, for example, *Tgfβ3* is required for palatal shelf fusion whilst *Tgfβ1*, *Tgfβ2* and the BMPs play a role in mesenchymal proliferation (Meng et al., 2009). Individual transcription factors like *Msx1*, *Lhx8*, *Shox2* and *Osr2* are expressed in the developing palatal shelves and are indispensable for palatogenesis, acting on tissue patterning, growth or differentiation (Gritli-Linde, 2007). Other factors that have a role in palate development are the *epidermal growth factor receptor* (*Egfr*), FGFs and *Pdgfc* as well as the SHH and Wnt pathways (Gritli-Linde, 2007; Jugessur et al., 2009; Meng et al., 2009). Cell adhesion molecules, like integrins, cadherins, nectins and desmosomal components, and ECM components such as collagens, glycoproteins and proteoglycans are also important (Gritli-Linde, 2007; Meng et al., 2009).

7. The heart

7.1. Heart and outflow tract formation

The vertebrate heart originates mainly from mesodermal cell populations (Dunwoodie, 2007; Moorman et al., 2003; Perez-Pomares et al., 2009; Snarr et al., 2008; Wagner and Siddiqui, 2007a). During gastrulation, cardiac precursors lying in the rostral half of the primitive streak in an anterior-posterior sequence migrate laterally towards the anterior part of the embryo to form two bilateral heart-forming regions (anterior lateral plate mesoderm) (Nakajima, 2010; Snarr et al., 2008; Wagner and Siddiqui, 2007a). Cells from this pre-cardiac mesoderm undergo differentiation into endocardial and myocardial lineages, which combined are known as the first heart field (FHF) (Snarr et al., 2008). The bilateral heart fields converge medially to form a crescent shaped domain (E7.0) (Perez-Pomares et al., 2009; Snarr et al., 2008; Wagner and Siddiqui, 2007a). This is followed by fusion of the paired primordia at the embryonic midline and establishment of the primitive heart tube (E8.0) (Nakajima, 2010; Perez-Pomares et al., 2009; Snarr et al., 2008; Wagner and Siddiqui, 2007a). At the same time the heartbeat is initiated and the blood streams through the tube in a caudal (venous inflow) to cranial (arterial outflow) direction (Dunwoodie, 2007). The linear heart tube consists of an outer myocardial layer, an intermediate layer of acellular matrix, the cardiac jelly, and an inner endocardial layer (Dunwoodie, 2007; Snarr et al., 2008; Wagner and Siddiqui, 2007b). Developmentally the primitive tube develops into the left ventricle (LV), part of the atrioventricular (AV) region and the atria (Nakajima, 2010; Perez-Pomares et al., 2009) and has a small cellular contribution to the right ventricle (RV) (Nakajima, 2010). The growth of the tube is facilitated by both myocardial cell proliferation and cell addition processes (Dunwoodie, 2007; Nakajima, 2010). Cells are recruited into the outflow tract from two distinct cell populations, the cardiac neural crest (Dunwoodie, 2007; Kaartinen et al., 2004; Kirby, 2002; Nakajima, 2010; Perez-Pomares et al., 2009; Snider et al., 2007) and the SHF, a second cardiogenic domain that provides myocardial progenitors (Dunwoodie, 2007; Kirby, 2002; Moorman et al., 2003; Nakajima, 2010; Perez-Pomares et al., 2009; Snider et al., 2007; Wagner and Siddiqui, 2007a). During the looping stage of the heart tube the outflow region shifts to the right, followed by dorsal-anterior relocation of the inflow complex such that the inflow and outflow complexes converge (Dunwoodie, 2007).

Differential growth in the anterior-posterior and dorsoventral axes of the heart tube create inner and outer curvatures, while the cardiac chambers are starting to form, indicated by the development of trabeculae, a sponge-like layer of myocytes (by E13.5) (Wagner and Siddiqui, 2007b). Furthermore, the cardiac jelly that was initially uniformly distributed in the heart tube, condenses locally in the atrioventricular junction (AVJ) and the outflow tract, producing swellings known as endocardial cushion primordia (Snarr et al., 2008). At the end of the looping stage the primitive heart undergoes remodelling, including the formation of the interventricular septum that will divide the ventricles, and the cardiac conduction system (Dunwoodie, 2007). The chamber walls thicken and form the "compact layer" by increasing the proliferation rate of the outer ventricular walls (Dunwoodie, 2007). The endocardial cushion primordia are colonised by different populations of mesenchymal cells (Wagner and Siddiqui, 2007b) and eventually form the scaffold for the AP septum in the outflow tract region and the aortic and pulmonary valves (Dunwoodie, 2007). In the atrioventricular canal (AVC, the boundary between the atrial and ventricular regions) the endocardial cushions develop into the tricuspid and mitral valves (Dunwoodie, 2007). The principal stages of cardiac development are summarised in Figure 1.10.

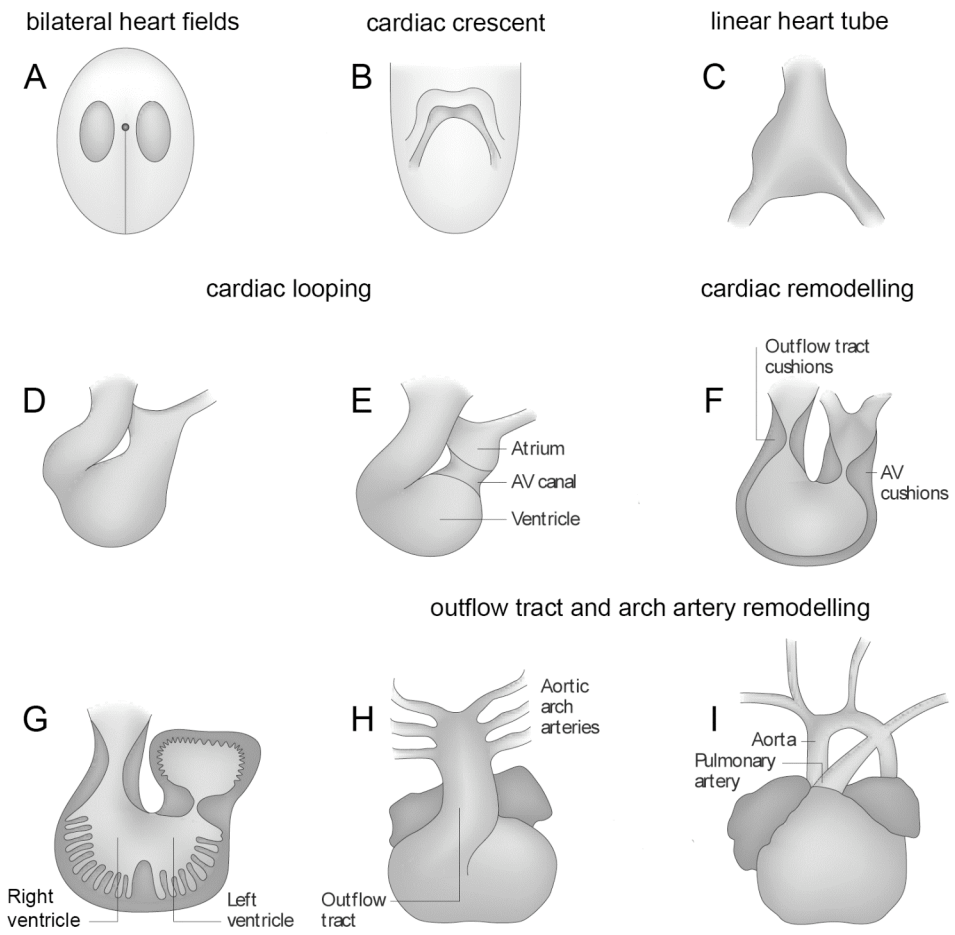

Figure 1. 10. Stages of heart development. The bilateral heart fields (A) converge at the midline and form the cardiac crescent (B) and subsequently the linear heart tube (C). The tube elongates and undergoes a rightward looping (D). Further remodelling includes AVC formation that forms a boundary between the presumptive atrial and ventricular regions of the heart (E), endocardial cushion formation, which will act as the precursors of the four major heart valves (F), chamber trabeculation (G), chamber septation and remodelling of the outflow tract into the aorta and the pulmonary artery (H). Finally, an organ with four distinct chambers is produced (I). AV, atrioventricular. Modified from High and Epstein, 2008.

7.2. Heart and outflow tract septation and remodelling

7.2.1. Heart

The septation process of the heart tube into the four-chambered mature configuration occurs at three levels, the atrium, the ventricle and the arterial pole (Gittenberger-de Groot et al., 2005), although the latter is described separately in this

thesis. Following the looping stage of the heart, endocardial cells in the outflow tract and AV segments undergo EMT and populate the cardiac jelly, producing the endocardial cushions (Nakajima, 2010). Atrioventricular septation is facilitated by the AV cushions at the AVJ (Anderson et al., 2003b; Snarr et al., 2008). Initially two major cushions (superior and inferior) arise, followed by a pair of lateral cushions (Snarr et al., 2008). Fusion of the superior and inferior cushions, with contribution from the outflow tract cushions, promotes closure of the primary interventricular septum (Gittenberger-de Groot et al., 2005). The cushions are also adjoined to the muscular ventricular septum, which forms between the growing apical regions of the right and left ventricles (Anderson et al., 2003b). In that respect, the membranous part of the interventricular septum is formed from the proximal parts of the outflow tract cushions that fuse with the already completed AV component (Figure 1.11.A) (Anderson et al., 2003b; Gittenberger-de Groot et al., 2005). The primary atrial septum is considered to form from different components in addition to the AV cushions (Snarr et al., 2008; Webb et al., 1999). The muscular primary atrial septum (septum primum), also known as the mesenchymal cap, develops on the dorso-cranial wall of the primary atrium, elongates, descends into the atrial cavity and fuses with the superior endocardial cushion, thus separating the left from the right atrium (Figure 1.11.B) (Anderson et al., 2003b; Snarr et al., 2008; Webb et al., 1999). A more caudally located, second mesenchymal mass, the dorsal mesenchymal protrusion (DMP) that was originally described as the spina vestibuli, arises at the venous pole of the heart, grows into the atrium and fuses with the inferior endocardial cushion (Anderson et al., 2003b; Snarr et al., 2008). A muscular infolding of the atrial wall into the right of the primary atrial septum, the septum secundum, also contributes to the closure of the ostium secundum (secondary atrial foramen) (Kirby, 2002; Webb et al., 1999). Essentially, it is the fusion of several different mesenchymal components that leads to the closure of the primary atrial foramen (Anderson et al., 2003b). By the end of the septation process the superior cushion forms the aortic leaflet of the mitral valve and the inferior cushion forms the septal leaflet of the tricuspid valve, while the DMP mesenchyme forms the myocardial base of the primary atrial septum (Snarr et al., 2008).

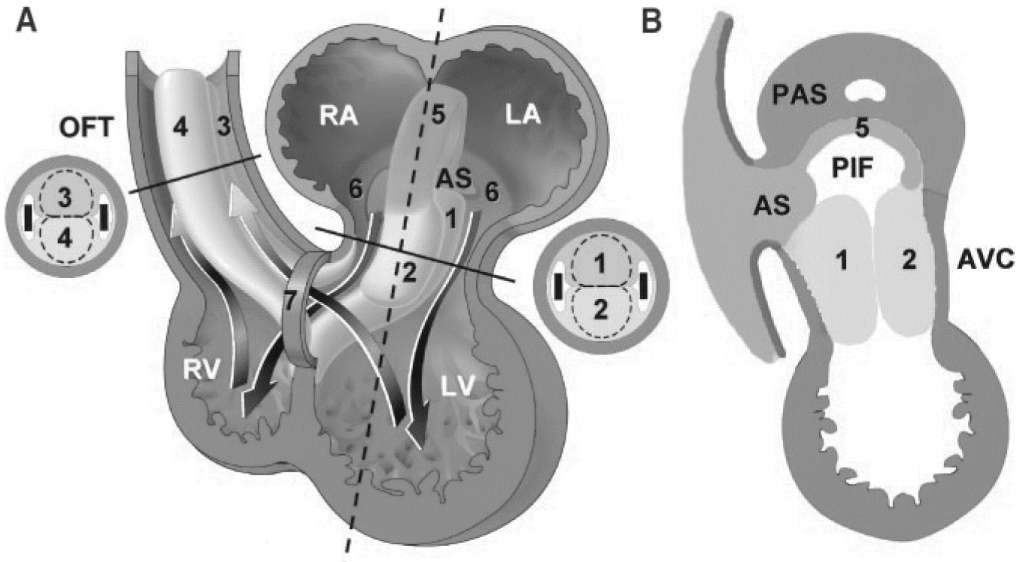

Figure 1. 11. Cardiac septation. Four chamber view of the embryonic heart before septation (A). The outflow tract is deviated rightward to visualise the AVC. The developing embryonic atria (RA, LA) and ventricles (RV, LV) have formed as "balloons" on the outer curvature of the heart tube while their interconnecting structures retain a tubular shape. Transverse section through the AVC and outflow tract indicate the position of the endocardial cushions. Sagittal section through the primary atrial septum (PAS), AVC, and the LV (following the dashed line in A) shows the relation between the AV cushions and the atrial spine (B). 1, inferior AV cushion; 2, superior AV cushion; 3,4, outflow tract cushions; AVC, atrioventricular canal; AS, atrial spine with spur (5) on the leading edge of the PAS; 6, body of atrium; 7, interventricular septation; PAS, primary atrial septum; OFT, outflow tract; R/LA, right/ left atrium; R/LV, right/left ventricle (Lamers and Moorman, 2002).

Reciprocal interaction between the overlaying myocardium and the endocardium promotes the EMT process required for the formation of the AV cushions (Nakajima, 2010; Wagner and Siddiqui, 2007b). TGFβ/BMP factors are crucial for the induction of the EMT process (Kirby, 2002; Nakajima, 2010). In the chick TGFβ2 mediates endothelial cell-cell separation while TGFβ3 promotes morphological cell changes required for the migration into the ECM (Kirby, 2002). *Hyalouronic acid* (Ha) *synthase 2* (*Has2*)/*ErbB2*, *ErbB3*/*Ras* (Jiao et al., 2003), *Vascular endothelial growth factor* (*VEGF*), Wnt and Notch pathways are also involved in the formation of the AV cushions (Wagner and Siddiqui, 2007b). *VEGF* appears to inhibit EMT and thus cushion formation and is found upregulated in the AVC after initiation of cushion

formation, probably limiting the cells undergoing EMT (Kirby, 2002). *BMP2* and *Tbx2* are required for AVC development by specifying the boundary between the canal and the chamber myocardium (Niessen and Karsan, 2008).

7.2.2. Outflow tract

During the course of development the cardiac outflow tract, the single outflow vessel located on the arterial pole of the primitive heart tube, remodels into separate aortic and pulmonary arteries (Restivo, 2006). The outflow tract, also known as the conotruncus, consists of two myocardial regions, the conus on the proximal (connection with the ventricles) and the truncus on the distal (connection with the aortic sac) side (Lamers and Moorman, 2002; Restivo et al., 2006) which give rise to different structures of the definitive heart (Restivo et al., 2006). Septation of the truncus arteriosus divides the common outflow orifice into the arterial valve orifices, whereas septation and rotational remodelling of the conus produces the subpulmonary infundibulum (a muscular tube supporting the leaflets of the pulmonary valve, (Anderson, 2000)) (Restivo et al., 2006). Both segments contain a pair of cushions (conal and truncal) (Gittenberger-de Groot et al., 2005; Restivo et al., 2006; Snarr et al., 2008) that in a proximal to distal direction follow a rightward spiraling course (Lamers and Moorman, 2002). The septation process is mediated by the truncal and conal endocardial cushions (Restivo et al., 2006). Initially the opposing cushions fuse across the lumen of the outflow tract in a distal to proximal direction (Gittenberger-de Groot et al., 2005; Webb et al., 2003). The truncal septum that forms divides the outflow tract into the aortic and pulmonary outlet components (Webb et al., 2003) so that the aortic channel connects to the third and fourth and the pulmonary channel to the sixth arch arteries (Figure 1.12) (Lamers and Moorman, 2002). Apart form the AP septum, the truncal cushions also contribute to the formation of the semilunar valves (Snarr et al., 2008). These cushions are originally heavily populated by neural crest-derived cells (Snarr et al., 2008). The same sequence of events takes place in the proximal part of the outflow tract (Webb et al., 2003), where a septum separating the outlets of the left and right ventricles is formed after fusion of the conal cushions (Snarr et al., 2008). Endocardial cells compose the proximal part of the conal septum while the distal part is predominantely of neural crest origin, including a minor SHF-derived population (Snarr et al., 2008). Remodelling of the conal cushions ultimately forms the leaflets and supporting sinusal walls of the aortic and pulmonary valves (Webb et al., 2003). The

spiral path of the endocardial cushions within the outflow tract results, after septation, in the positioning of the root of the ascending aorta caudal to that of the pulmonary trunk, while the fourth pair of arch arteries remains cranial to the sixth pair (Webb et al., 2003).

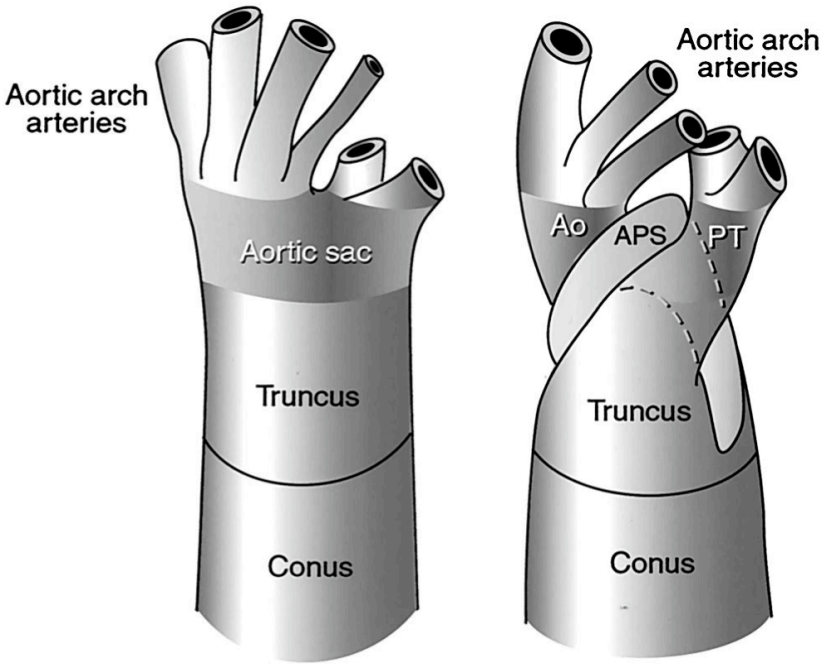

Figure 1. 12. Conotruncal septation. The division of the outflow tract by the aorticopulmonary septum (APS) begins in the aortic sac between the fourth (systemic) and sixth (pulmonary) aortic arch arteries to form the base of the aorta (Ao) and pulmonary trunk (PT), which proceeds into the truncus and conus. Ao, aorta; APS, aorticopulmonary septum; PT, pulmonary trunk (Kirby, 2002).

The outflow tract remodelling process requires complex interactions between the myocardium, endocardium and neural crest cells (Bajolle et al., 2006). Signals from the overlaying myocardium induce endocardial cells to undergo EMT and form the conotruncal cushions (Bajolle et al., 2006). Neural crest cells are required in normal heart septation as they invade the ECM of the cushions and participate in AP septation (Bajolle et al., 2006). Cardiac neural crest ablation in the chick produces outflow tract defects including TOF, CAT, DORV (Bajolle et al., 2006). TGFβ, BMP and RA signalling factors play an important role in EMT and the subsequent morphological cell changes that will allow cell migration into the underlying ECM, while *VEGF* appears to have inhibitory roles in the EMT process (Kirby, 2002).

7.3. Heart fields and signalling factors

7.3.1. Induction

The cardiac fate of pre-cardiac mesoderm is determined very early in embryogenesis by interplay of positive and negative regulatory signals between the surrounding tissues and the pre-cardiac mesoderm (Dunwoodie, 2007). The lateral mesoderm interacts with the anterior endoderm and non-neural ectoderm that promote cardiac specification, while the axial tissues and the neural plate repress the formation of heart tissue in the head mesoderm (Dunwoodie, 2007). SHH, BMP, FGF and Wnt-JNK (non canonical) signalling are positive cues towards a cardiogenic fate, while Wnt-β-catenin (canonical) signalling and Wnt ligands like Wnt-1 and Wnt-3a, anti-BMPs, Chordin, Noggin and Serrate are repressing it (Dunwoodie, 2007; Wagner and Siddiqui, 2007a). The negative signals are possibly required to restrict the cardiogenic induction to a specific population of mesodermal cells (Wagner and Siddiqui, 2007a). The FHF, initially defined as a "region of mesoderm that gives rise to differentiated cardiomyocytes", describes a population of myocardial and endocardial progenitors that derive from pre-cardiac mesodermal cells and give rise to the future LV, the atria, the sinus venosus and have a small contribution to the future RV (Dunwoodie, 2007; Nakajima, 2010). The SHF is a population of undifferentiated myocardial progenitor cells (Dunwoodie, 2007; Nakajima, 2010; Perez-Pomares et al., 2009; Rochais et al., 2009a), located medially and caudally to the cardiac crescent (Dunwoodie, 2007; Nakajima, 2010). These cells contribute to the outflow tract, RV and parts of the LV and inflow region (Dunwoodie, 2007). Although there was initial debate concerning the term used to describe this cell population, a consensus has now been met in regarding the anterior or secondary heart field as a subpopulation of the SHF (Perez-Pomares et al., 2009). The anterior or secondary heart field was identified with the use of cell labelling and genetic markers including *Fgf10* and enhancer elements of *Mef2c* (Dunwoodie, 2007). The SHF cells possess distinct molecular and spatio-temporal properties, like elevated proliferation and differentiation delay as compared to FHF cells and are distinguished by the expression of *Isl1*, *Tbx1 Fgf8* and *Fgf10* genes (although FHF cells transiently express certain SHF genes like *Isl1* and *Fgf8*) (Rochais et al., 2009a). Mommersteg *et al.* recently provided evidence that the splanchnic mesoderm divides into subpopulations corresponding to the heart fields from E7.5 progressively,

indicating that before that stage the cardiac progenitors constitute a common population (Mommersteeg et al., 2010).

7.3.2. Induction of FHF and SHF lineages

Most cardiac induction studies fail to discriminate between the induction of the different heart fields, and although similar inductive processes are involved, there are characteristic differences (Dunwoodie, 2007). Indeed, FGF signalling, along with TGFβ-like factors (Dunwoodie, 2007; Kirby, 2002; Perez-Pomares et al., 2009; Wagner and Siddiqui, 2007a) and SHH signalling are required by both heart fields for subsequent expression of *Nkx2.5* and *Mef2c* (Dunwoodie, 2007). *Tbx5* however is specifically restricted in the FHF, and interacts with *Nkx2.5* and *Gata4* to stimulate chamber-specific genes later in development (Dunwoodie, 2007). *Hand1* and *Hand2* are amongst the earliest cardiac transcription factors identified, restricted in the FHF and SHF respectively (Dunwoodie, 2007). *Tbx20* is expressed in the FHF at the cardiac crescent stage while at the linear heart tube stage an extension of its expression is observed into the SHF (Dunwoodie, 2007). *Isl1* is the gene that defined the SHF and is expressed from the cardiac crescent stage to at least E9.75, while it is switched off as cells enter the heart tube (Dunwoodie, 2007). *Foxh1*, which is restricted in the SHF but not in its derivatives (Dunwoodie, 2007), is hypothesised to regulate *Fgf8* and *Fgf10*-related induction of *Isl1* and *Tbx1*-positive progenitors into activating myocardial factors including *Gata4* and *Mef2c* (Perez-Pomares et al., 2009). In terms of transcriptional regulation, *Nkx*, *GATA*, *Mef2c*, *T-box* and *Hand* family genes are amongst the most important ones, all characteristic of a myogenic cell program (Kirby, 2002; Perez-Pomares et al., 2009; Wagner and Siddiqui, 2007a). Cardiomyogenesis is inhibited by Notch signalling by promotion of non-muscle pericardial cell fates (High and Epstein, 2008). While cells from the SHF are being added into the linear heart tube, SHH, FGF and canonical Wnt signalling regulate the survival, proliferation and migration of these myocardial progenitors (Rochais et al., 2009a). BMP signalling is suggested to downregulate *Isl1* expression in the SHF-derived cells that have entered the outflow tract, thus promoting cell differentiation instead of expansion (Rochais et al., 2009a).

7.3.3. Remodelling

As development proceeds, RA signalling is required for the cranio-caudal polarity of the heart tube (Kirby, 2002). The myocardial identity for subsequent chamber formation is determined at various stages during heart development (Kirby, 2002). The rightward looping of the heart tube is important for chamber formation and is governed by asymmetric gene expression patterns established early in development through embryonic laterality (Wagner and Siddiqui, 2007a). The ventricles are initially specified along the anterior-posterior axis but acquire distinct identities after the looping stage and their left-right juxtaposition (Wagner and Siddiqui, 2007a). Conversely, left and right atria formation is a result of differences in left and right progenitor pools of lateral plate mesoderm (Wagner and Siddiqui, 2007a). The heart is partitioned into chamber and non-chamber myocardium, which is crucial for further heart remodelling (Dunwoodie, 2007). Transcription factors involved in chamber specification are *Hand1*, *Cited1*, *Irx1*/*Irx3*/*Irx5*, members of the *T-box* family, the vasoactive hormone atrial natriuretic factor (ANF, encoded by the *Nppa* gene), conduction proteins of the connexin family, and the muscle-specific cytoskeletal protein Chisel (encoded by the *Smpx* gene) (Dunwoodie, 2007). Subsequent ventricular trabeculation is implemented through RA, *neuregulin*/*ErBb* and *Bmp10* signalling (Wagner and Siddiqui, 2007b). Notch signalling is suggested to act in the endocardium as an upstream regulator of both the latter pathways, in terms of proliferation and differentiation of trabecular myocytes (High and Epstein, 2008). Furthermore, studies have shown that *Hey* genes, which are Notch targets, are involved in the AVC formation while *Notch1* and *RBP-J* take part in the EMT that precedes endocardial cushion formation (High and Epstein, 2008).

7.4. Types of heart defects

As cardiac remodelling progresses, the AP (truncal), outflow (conal), AV, interventricular and primary atrial septa align and fuse with each other, thus producing the four-chambered mature organ (Nakajima, 2010). Aberrations in either of the processes can result in various types of cardiac malformations (Nakajima, 2010).

1. Alignment defects

This category includes the malformations of the inflow or outflow of the heart, resulting from aberrant alignment or the atria with the ventricles or aberrant alignment of the aorta and pulmonary trunk with the right and left ventricles (Kirby, 2002). Inflow

malalignment results in defects like double inlet left ventricle and straddling tricuspid valve, while malalignment of the outflow is always associated with a dextroposed aorta, whereby the aorta overrides and receives blood from the right ventricle (Kirby, 2002). Dextroposed aorta occurs in DORV and TOF (Kirby, 2002).

In DORV both the great arteries arise from the RV (Figure 1.13.B) (Johnson, 2010) and there is loss of fibrous continuity between the AV and semilunar valves (Johnson, 2010; Kirby, 2002). The only outlet from the LV is through a VSD (Johnson, 2010; Kirby, 2002). Depending on the type of VSD present a DORV can be subaortic, subpulmonic, doubly committed, or remote (Johnson, 2010). The great arteries may be normally related, side-by-side, or malposed (Johnson, 2010).

Tetralogy of Fallot is the concomitant existence of interventricular communication (VSD), obstruction of the right ventricular outflow tract, overriding aorta and secondary hypertrophy of the RV (Figure 1.13.C) (Bailliard and Anderson, 2009; Carotti et al., 2008). Pulmonary atresia with VSD (or TOF with pulmonary atresia or PA-VSD) constitutes the extreme spectrum of a TOF where the blood to the pulmonary arteries flows through the patent arterial duct or through multiple aortopulmonary collateral arteries (Bailliard and Anderson, 2009; Carotti et al., 2008; Johnson, 2010).

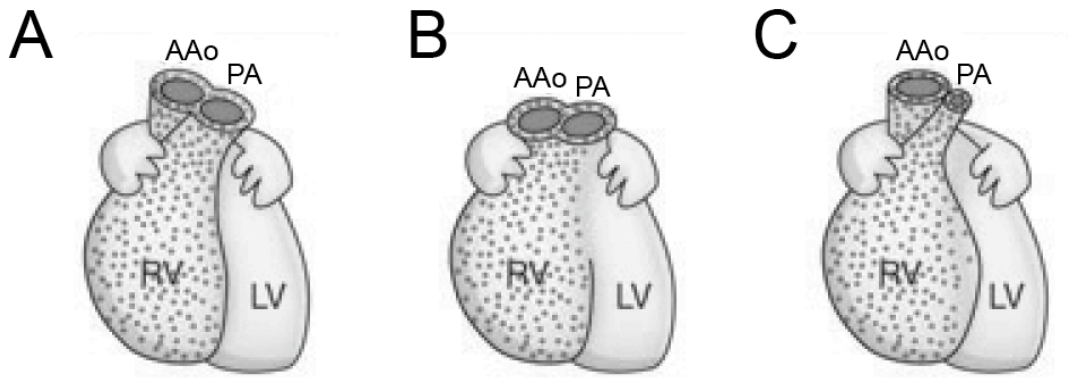

Figure 1. 13. Cardiac alignment defects. Normal alignment of the pulmonary artery (PA) with the RV and the ascending aorta (AAo) with the LV (A). In a DORV both the PA and AAo originate from the RV (B). In TOF, apart from VSD (not shown here) there is obstruction of the right ventricular outflow tract, overriding aorta and secondary hypertrophy of the RV (C). AAo, ascending aorta; DORV, double outlet right ventricle; PA, pulmonary artery; R/LV, right/left ventricle; TOF, tetralogy of Fallot; VSD, ventricular septal defect. Modified from Nakajima, 2010.

2. Septation defects

Atrioventricular canal defects (AVCD) cover a spectrum of abnormalities, from the partial form with defects in the lower part of the primary arterial septum to the complete form in which absence of the AV septum results in a single common AVC (Jiao et al., 2003). VSDs are openings in the ventricular septum classified according to their location as membranous or muscular (Figure 1.14.A) (Minette and Sahn, 2006). The muscular septum can be further divided into inlet, trabecular, and infundibular components (Minette and Sahn, 2006). Atrial septal defects (ASD) describe similar malformations in the primary atrial foramen (Figure 1.14.B) (Hein et al., 2005). A patent foramen ovale (PFO) is a defect in the septum secundum itself, or non-adherence of the septum primun and secundum (Hein et al., 2005). Last, in an atrioventricular septal defect (AVSD), where the atrial septum fails to meet the ventricular septum, there is a common AVJ instead of the figure-of-eight normal configuration (Adachi et al., 2008).

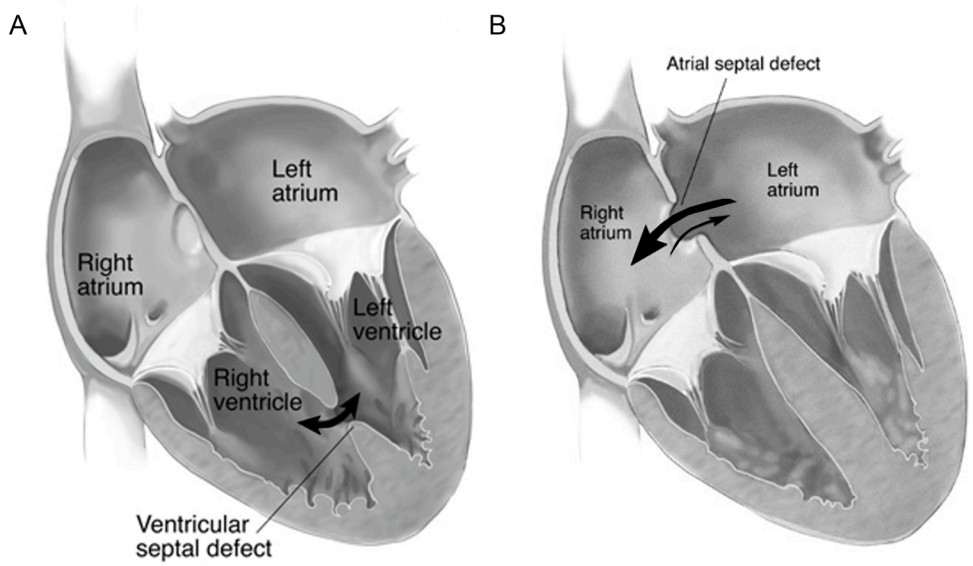

Figure 1. 14. Cardiac septation defects. In a VSD there is interventricular communication resulting from abnormal ventricular septation (A), while in an ASD there is similarly communication between the atria, caused by malformations in the primary atrial foramen (B). ASD, atrial septal defect; VSD, ventricular septal defect.

7.5. Types of outflow tract defects (conotruncal malformations)

During normal conotruncal development, the outflow tract elongates and rotates to a final position with the pulmonary trunk arising from the right ventricle being

positioned on the left ventral side of the left ventricle-originating aorta (Nakajima, 2010). Aberrations in the correct development, for example by compromised addition of neural crest cells (Jia et al., 2007; Nie et al., 2008) or myocardial progenitors from the SHF (Xu et al., 2004), and/or remodelling of the conotruncus can cause a range of congenital malformations (Carotti et al., 2008; Johnson, 2010; Nakajima, 2010; Restivo et al., 2006).

1. Common arterial trunk

CAT describes a malformation in which a single outlet from the heart, the common arterial trunk, often dilated, supplies the systemic, coronary and pulmonary circulations (Figure 1.15.B) (Carotti et al., 2008; Johnson, 2010; Restivo et al., 2006). The single truncal valve that forms is usually abnormal, with two to five cusps with different degree of stenosis and/or regurgitation (Johnson, 2010). The defect occurs due to incorrect development and lack of fusion of the truncal cushions that fail to produce a truncal septum (Restivo, 2006). The pulmonary arteries originate together or independently from the truncal root (Johnson, 2010).

2. Transposition of the great arteries

TGA describes a defect in which the RV is connected to the right ventrally malpositioned aorta and the LV is connected to the left dorsal pulmonary trunk (Figure 1.15.C) (Nakajima, 2010). It is thought to be caused by shortening and reduced rotation of the outflow tract, straight conotruncal septation and ventriculo-arterial misconnections (Nakajima, 2010).

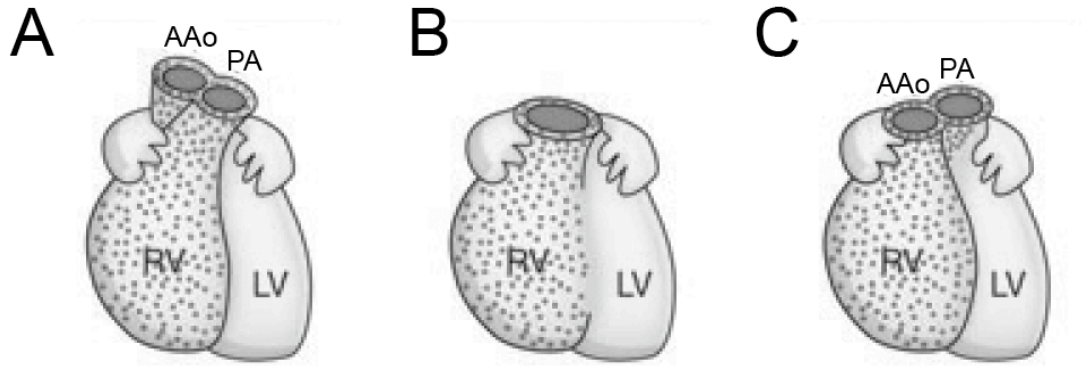

Figure 1. 15. Outflow tract defects. Normal alignment of the pulmonary artery (PA) with the RV and the ascending aorta (AAo) with the LV (A). In CAT there is a single great vessel arising from the heart (B), while in TGA the RV is connected to the right

ventrally malpositioned aorta and the LV is connected to the left dorsal pulmonary trunk (C). AAo, ascending aorta; CAT, common arterial trunk; PA, pulmonary artery; R/LV, right/left ventricle; TGA, transposition of the great arteries. Modified from Nakajima, 2010.

7.6. Mechanisms and models of great vessel and outflow tract defects

7.6.1. Mechanisms

The great vessel and outflow tract defects described earlier can be a result of abnormal formation and/or remodelling of the primitive structures. A considerable number of underlying causes has been suggested for these events, although there are still mechanisms that remain unclear. Cardiac neural crest cells provide the mesenchymal support and subsequent VSM layer to the pharyngeal arch arteries (Hutson and Kirby, 2007; Scholl and Kirby, 2009), while also contributing to the AP septum (Epstein et al., 2000; Nakamura et al., 2006). Aberrations in crest migration, proliferation or *in situ* differentiation, described in several animal models below, result in such cardiovascular defects. Moreover, single gene mutations, like the *Tbx1* mutation, that directly affects the formation of the fourth arch arteries (Lindsay et al., 2001) and the SHF myocardial contribution to the outflow tract (Xu et al., 2004), or the *Tgfβ2* mutation, that affects the remodelling of the fourth arch arteries (Molin et al., 2002), lead to a range of great vessel and outflow tract defects. Other factors like blood flow haemodynamics are likely to play a role too. Studies have shown that the hydrodynamic conditions in the developing outflow tract favour laminar blood flow from the RV through the left ductus arteriosus and into the left DAo, leading to predominance of a left-sided configuration (McElhinney et al., 1999). If the pulmonary outflow is decreased in the developing heart, then the right-to-left ductal flow is lost or at least decreased, thereby abolishing the flow-related impetus for persistence of the left ductus and dorsal aorta (McElhinney et al., 1999). This may allow for a more stochastic distribution of right and left arch predominance (McElhinney et al., 1999). Although this theory has not been proven, empirical evidence are lesions with right ventricular outflow obstruction (TOF, pulmonary atresia, and CAT) which are frequently accompanied by an RAA (McElhinney et al., 1999). The combination of multiple factors is more likely responsible for the congenital anomalies of the aortic arch. In recent years a vast array of mouse models presenting with great vessel and outflow tract

defects have been used towards understanding all these mechanisms. In most cases perturbation of a pathway results in a combination of outflow tract and great vessel malformations, although the formation and remodelling of these structures depend on distinct and independent processes. Interestingly, most of the mutants described with aberrant remodelling of the vessels involve elements of the TGFβ pathway.

7.6.2. Animal models

Endothelin (*ET_A, ECE-1*) mutants form their pharyngeal arch arteries in anatomically correct positions and at the expected time, while these are populated by neural crest cells and form the VSM layer (Yanagisawa et al., 1998). At term however mutants present with multiple great vessel and outflow tract defects including IAA-B, DORV and persistent truncus arteriosus (PTA) (Yanagisawa et al., 1998). The authors discuss possible incorrect differentiation and proliferation of the post-migratory crest in the absence of endothelin signalling, although these were not further tested (Yanagisawa et al., 1998). The same was observed in the *PdgfRα/β* neural crest conditional mutants, which exhibited retro-oesophageal A-RSCA and PTA phenotypes with 100% penetrance at term (Richarte et al., 2007). Neural crest migration into the arches and subsequent differentiation into VSM were normal (Richarte et al., 2007). Fewer cells were scored migrating through the conotruncal region and into the heart, while the neural crest cell proliferation and apoptosis rates were normal (Richarte et al., 2007). Reduced cellularity was considered the primary cause of the defects, and it may indeed be for the PTA and VSD phenotypes, but it does not directly explain the A-RSCA, since all arch arteries were normally populated with crest cells that efficiently differentiated into VSM (Richarte et al., 2007).

In *TβRII* neural crest conditional mutants (at term phenotypes include PTA, VSD and IAA-B with complete penetrance) the pharyngeal arch artery formation, neural crest migration into the arches and the conotruncal region, and VSM support of the arch arteries occurred normally (Choudhary et al., 2006). The neural crest proliferation and apoptosis rates in the AP septum were also normal (Choudhary et al., 2006). The authors rationalised that the neural crest cells that migrated had lost their ability to signal to the surrounding tissues, due to lack of the receptor (TβRII), leading to an arrest of development of the respective structures (Choudhary et al., 2006). The only perturbation found was inappropriate apoptosis of cells surrounding the right fourth arch artery, but this may be secondary to signalling disturbances (Choudhary et al.,

2006). Similarly, null mutants for the *latent TGFβ binding protein 1* (*Ltbp1*, which belongs to a family of large extracellular glycoproteins) had unaffected neural crest migration, correct invasion of the outflow tract and normal proliferation and apoptosis rates of the post migratory neural crest cells (Todorovic et al., 2007). The absence of an AP septum, leading to PTA, VSD and ASD at term, was attributed to a functional defect of post migratory neural crest while the enhanced apoptosis observed in the VSM cells surrounding the fourth arch artery explained the development of IAA-B (Todorovic et al., 2007). It did not however provide a genetic mechanism for it. From a cellular marker point of view, the neural crest cells in the null animals did not express *Plexin A2* or *FoxC1*, two cardiac neural crest markers, although the VSM layer appeared normal in the arch arteries (Todorovic et al., 2007). In the septating outflow tract, decreased TGFβ signalling was detected but no further associations were made (Todorovic et al., 2007).

Bmp4 is suggested to be required for the recruitment or differentiation of SMCs in both the arch arteries and the outflow tract (Liu et al., 2004). Conditional mutants for *Bmp4* in the branchial arch mesenchyme and outflow tract myocardium (*Nkx2.5Cre*) exhibit among others IAA-B, VSD and PTA (Liu et al., 2004). In the mutants cellular apoptosis in the endoderm in the proximity of the outflow was modestly upregulated, while cell proliferation was severely reduced in the outflow tract cushions (Liu et al., 2004). Additionally, the pharyngeal arch arteries were well formed but the VSM component was comprised of fewer cells, in comparison to wild types, while fewer SMCs were also found invading the outflow tract at the same stage (Liu et al., 2004). Conditional deletion of the gene in the cardiomyocyte lineage induced AV septation defects, although the endocardial cushion formation was normal, suggesting *Bmp4* plays a role in the septation process after the formation of the cushions (Jiao et al., 2003). Other members of the BMP pathway like *Alk6* or *Alk2*, when conditionally ablated in the neural crest produce outflow tract septation defects, frequently leading to PTA. In *Alk6* conditional mutants, the crest cells migrated normally into the arches and some into the outflow tract, and although great vessel morphogenesis was unaffected, the outflow septum failed to form (Stottmann et al., 2004). The authors suggested that *Alk6* is required in the neural crest for successful colonisation of the outflow tract, while it is also probably involved in regulatory signalling to the surrounding tissues (Stottmann et al., 2004). *Alk2* conditional mutants presented with bilateral third or sixth arch artery regression and failure to complete AP septation, although an initial septum was formed (Kaartinen et al., 2004). PTA was scored with complete penetrance, while hyperplastic

RV and pharyngeal arch artery defects were also observed (Kaartinen et al., 2004). Although neural crest cells populated the pharyngeal arches normally, differentiation into VSM was proven defective around the third and sixth arch arteries (Kaartinen et al., 2004). The neural crest cell outflow tract invasion was also defective, so the authors concluded that *Alk2* might be essential for migration and/or maintenance of the neural crest cells in the outflow tract (Kaartinen et al., 2004). A different theory suggests that a minimum population may be required in the arches before allowing further migration of cells into the outflow tract (Scholl and Kirby, 2009). This would mean that *Alk2* has primarily a pharyngeal role and secondary to that regulates neural crest invasion of the outflow tract (Scholl and Kirby, 2009).

Another similar example is the conditional ablation of *Smad4* in the neural crest, which affects outflow tract septation and causes delay in pharyngeal arch artery remodelling (Nie et al., 2008). While neural crest migration occurred normally towards the arches in these mutants, large clumps of dying cells were observed, so the neural crest contribution to the outflow tract was dramatically reduced (Nie et al., 2008).

Null mutation of the *Crkl* locus produced a 22q11DS-like phenotype including IAA, cervical RSCA, DORV, overriding aorta and VSD (Guris et al., 2001). There was no notable abnormality in the development of the arch arteries at E11.5, while neural crest migration was normal in the $Crkl^{-/-}$ embryos between E9.5-E10.5 (Guris et al., 2001). The authors did not elaborate on the causes of abnormal arch artery remodelling.

Conditional deletion of *β-catenin* in the pharyngeal mesenchyme from E10.5 onwards induced pharyngeal arch artery remodelling defects by inhibiting normal regression of the carotid ducts between E11.5-E13.5 (Huh and Ornitz, 2010). This was associated with a range of great vessel defects, including A-RSCA, increased spacing between the right brachiocephalic and LCC arteries and lower positioning of the LSCA on the DAo, compared to wild type controls (Huh and Ornitz, 2010). Neural crest patterning did not appear disturbed in these mutants, and the causative mechanism was reasoned to be lack of apoptosis in the pharyngeal mesenchyme surrounding the carotid ducts (Huh and Ornitz, 2010). As with the *Crkl* mutation (Guris et al., 2001), the *β-catenin* conditional mutants recapitulated the 22q11DS-like phenotype, while the Wnt-β-catenin signalling was also shown required to repress *Tbx1* and FGF signalling in the pharyngeal apparatus (Huh and Ornitz, 2010).

In conclusion, although many mouse models have been described so far with defects in great vessel and outflow tract remodelling, very few provide links to individual processes, like selective apoptosis (Molin et al., 2002), failed differentiation of post migratory crest (Liu et al., 2004) or reduced cellularisation of various structures (Kaartinen et al., 2004; Richarte et al., 2007). For the majority of the models the underlying causes are unknown, and even in the few, the individual processes are usually not sufficient to explain the complete phenotype. It is now clear that remodelling of the outflow tract and great vessels requires the combination of multiple, tightly regulated mechanisms, involving different sets of genes and pathways. The neural crest cells are important not only for the support of the primitive arch arteries, through the VSM lining, but probably also for the future persistence or regression of each vascular segment, while cellular contribution to the AP septum is more straightforward in outflow tract development. The importance of the other embryonic tissues should not be understated either, since the mesoderm provides the endothelial layer of the arch arteries and the myocardial component of the heart and outflow tract, whereas the ectoderm is a distant regulator of several developmental process via molecular signalling.

8. Mouse models of DiGeorge syndrome and candidate genes

The common 3 Mb deletion carried by the majority of the 22q11DS patients harbors over 35 genes (Momma, 2010) and, although in different genomic organisation, they are conserved and localise in a relatively compact genomic region of the mouse chromosome 16 (Baldini, 2002). This is with the exception of *CLTCL* and the LCRs, that do not appear to be conserved in the mouse (Baldini, 2002). With the use of mouse chromosome engineering technologies several of the 22q11DS phenotypes have been successfully modeled in the mouse and there are now both single-gene and multi-gene deletions for most of the genes within *del22q11* (Baldini, 2002; Lindsay, 2001; Paylor and Lindsay, 2006). The first hemizygous deletion, generated by Lindsay *et al.*, was named *Df1* and encompassed mouse homologues of 18 out of the 24 genes that are deleted in patients carrying the 1.5 Mb deletion (Lindsay et al., 1999). Heterozygous mice (*Df1*/+) exhibited aortic arch defects (Lindsay et al., 1999) while the homozygotes displayed early embryonic lethality (Lindsay et al., 2001). The aortic arch phenotype was rescued in mice that carried the *Df1* deletion on one chromosome 16 and a reciprocal duplication on the other, which essentially restored normal gene dosage (Lindsay et al., 1999). Deletions of the proximal or distal region of the TDR did not produce a 22q11DS phenotype (Kimber et al., 1999; Lindsay et al., 2001; Puech et al., 2000). Merscher *et al.* generated mice carrying a hemizygous deletion spanning from *Idd* to *Hira* genes, named *Lgdel*/+ (Merscher et al., 2001). This deletion contained the *Df1* region and another 5 genes, and the mice displayed aortic arch anomalies similar to the *Df1*/+ mice, with additional parathyroid aplasia (Merscher et al., 2001). In an effort to localise the haploinsufficient gene, independently two groups, Lindsay *et al.* and Merscher *et al.* used chromosomal engineering and transgenic complementation and both concluded that the critical gene responsible for the aortic arch phenotype seen in *Df1*/+ and *Lgdel*/+ mice was *Tbx1* (Lindsay et al., 2001; Merscher et al., 2001).

9. *TBX1*

9.1. General

TBX1 localises within chromosome 22q11.2 and is an important regulator of pharyngeal development in mammals (Arnold et al., 2006; Baldini, 2002; Lindsay et al., 2001; Merscher et al., 2001; Zhang et al., 2005). It is a member of the T-box family of genes, coding for transcription factors characterised by a highly conserved DNA binding domain, the T-box (Naiche et al., 2005; Plageman and Yutzey, 2005). Five distinct *T-box* gene subfamilies have been reported in mammals that include at least 17 different genes (Naiche et al., 2005). Some of these genes have been associated with human genetic disorders, such as *TBX5* with Holt-Oram Syndrome (HOS) and *TBX3* with Ulnar mammary syndrome (Hoogaars et al., 2007; Naiche et al., 2005; Plageman and Yutzey, 2005), while *TBX1* is considered to be the main determinant of 22q11DS (Paylor et al., 2006; Stoller and Epstein, 2005a; Torres-Juan et al., 2007; Yagi et al., 2003; Zweier et al., 2007).

Binding site selection experiments have identified a palindromic sequence that has the highest affinity for Brachyury, the first T-Box protein identified in Drosophila (Conlon et al., 2001; Wilson and Conlon, 2002). Brachyury binds to the sequence as a dimer, with each monomer binding half of the sequence or T-half site (Conlon et al., 2001; Wilson and Conlon, 2002). All the T-box proteins that have been examined so far, including the human TBX1A (Sinha et al., 2000), can bind to the site as monomers or dimers, while some bind sequences containing two or more T-half sites, arranged in various orientations (Sinha et al., 2000; Wilson and Conlon, 2002).

9.2. *Tbx1* mouse models and expression pattern

Aside from the deletions of chromosome 16 that include *Tbx1*, there are several mouse mutants carrying *Tbx1* mutations (Table 1.1) (Arnold et al., 2006; Jerome and Papaioannou, 2001; Lindsay et al., 2001; Merscher et al., 2001; Xu et al., 2004; Zhang et al., 2005; Zhang et al., 2006). The typical knock-out displays hypoplasia and defective segmentation the pharynx with complete loss of the caudal pharyngeal arch arteries (3rd, 4th and 6th pairs) (Lindsay et al., 2001), PTA, complete aplasia of the thymus and parathyroid glands, microtia and craniofacial malformations (Jerome and Papaioannou, 2001). Death occurs at birth due to cardiovascular insufficiency (Jerome

and Papaioannou, 2001). *Tbx1*$^{+/-}$ animals are indistinguishable to the *Df1*/+ and *Lgdel*/+ models, exhibiting fourth arch artery hypo/aplasia with complete penetrance, which produces a 10% incidence of neonatal lethality (Jerome and Papaioannou, 2001; Lindsay et al., 2001). A smaller percentage (30-50%) of the heterozygous embryos display fourth arch artery-derived defects at term, including IAA-B, A-RSCA and RAA (Jerome and Papaioannou, 2001; Lindsay et al., 2001; Zhang et al., 2005). *Tbx1* is expressed from as early as E7.5 in the head and splanchnic mesoderm, located dorsally to the cardiac crescent (Chapman et al., 1996; Huynh et al., 2007). Half a day later, at E8, it is expressed in the pharyngeal epithelia and mesoderm (Huynh et al., 2007; Vitelli et al., 2002a) as well as the head mesenchyme, while by E9 surface ectoderm expression is observed at the level of the presumptive caudal arches (Huynh et al., 2007). At E9.5 *Tbx1* is found in the head mesenchyme, pharyngeal ectoderm, endoderm (Chapman et al., 1996; Huynh et al., 2007; Lindsay et al., 2001), core and splanchnic mesoderm including the SHF (Huynh et al., 2007). However, at no given developmental stage is *Tbx1* ever expressed in the neural crest-derived mesenchyme (Chapman et al., 1996; Huynh et al., 2007; Lindsay et al., 2001; Merscher et al., 2001; Vitelli et al., 2002a). Later on in development *Tbx1* expression is detected in several cardiac tissues including the RV, atria, conal region, ascending aorta and pulmonary trunk (Huynh et al., 2007). In non cardiac tissues, *Tbx1* is found in the tongue, otic vesicle (Chapman et al., 1996), sclerotome, lung buds, regions of the surface ectoderm that correspond approximately to the nuchal region and part of the face, follicles and vibrissae, tooth buds and muscle segments of the limbs (Huynh et al., 2007).

Other animal models - xenopus, fish

Both the sequence and the expression of *Tbx1* are well conserved throughout species, so models of the syndrome have also been developed in organisms other than the mouse (Scambler, 2010). In zebrafish, the *vgo* mutation, generated in a large scale mutagenesis screen, represents a null allele of the *tbx1* gene (Piotrowski et al., 2003). The *vgo/vgo* fish display lack of segmentation of the posterior pharyngeal arches, small otic vesicles and neural crest-derived craniofacial abnormalities (Piotrowski et al., 2003). The mutants exhibit aortic arch and thymic defects closely phenocopying 22q11DS (Piotrowski et al., 2003). Nonetheless, in zebrafish the mutation is recessive and the heterozygotes are normal, in contrast with the human and mouse deletions, which are haploinsufficient (Piotrowski et al., 2003). *Tbx1* knock-down in zebrafish

through a morpholino approach induced otic vesicle, thymus, posterior pharyngeal arch, arch artery and pharyngeal cartilage abnormalities (Zhang et al., 2010). Heart looping disturbances, associated with reduced heart rate were also observed (Zhang et al., 2010). Similar to the mouse model, the neural crest cells that populate the arches of the morphant fish were greatly reduced (Zhang et al., 2010).

In *Xenopus* embryos, repression of *XTbx1* produced a range of dosage-sensitive abnormalities during embryogenesis (Ataliotis et al., 2005). The defects included severely hypoplastic pharyngeal apparatus, abnormally looped heart, pericardial edema and disorganised or absent head cartilage structures (Ataliotis et al., 2005). Co-expression of the repressor with *XTbx1* mRNA could improve the severity of the phenotypes, although not completely rescue them (Ataliotis et al., 2005).

Name	Synonyms	Category	Mutation	Reference
$Tbx1^{tm1Pa}$ targeted mutation 1, Virginia Papaioannou		targeted (Knock-out)	Insertion, intragenic deletion. A loxP-flanked neomycin selection cassette replaced most of the coding region of the gene.	Jerome *et al.*, 2001
$Tbx1^{tm1Rak}$ targeted mutation 1, Raju Kucherlapati	$Tbx1^{-}$	targeted (Knock-out)	Insertion, intragenic deletion. A hygromycin resistance cassette was inserted into exons 1 and 2.	Merscher *et al.*, 2001
$Tbx1^{tm1Bld}$ targeted mutation 1, Antonio Baldini	$Tbx1^{-}$, $Tbx1^{lacZ}$	targeted (Reporter)	Insertion. An IRES-lacZ reporter gene followed by a loxP-flanked neomycin resistance cassette was inserted into exon 5, resulting in a functionally null allele.	Lindsay *et al.*, 2001
$Tbx1^{tm1Dsr}$ targeted mutation 1, Deepak Srivastava	$Tbx1^{neo}$	targeted (Floxed/Frt)	Insertion. A hypomorphic allele created by the insertion of an FRT-flanked neomycin resistance gene into intron 3, and loxP sites flanking exons 4-8.	Hu *et al.*, 2004
$Tbx1^{tm1.1Dsr}$ targeted mutation 1.1, Deepak Srivastava	$Tbx1^{null}$	targeted (Knock-out)	Intragenic deletion. The FRT-flanked neomycin cassette and exons 4-8 were removed by *Cre*-mediated excision in $Tbx1^{tm1Dsr}$ mice.	Hu *et al.*, 2004
$Tbx1^{tm2Bld}$ targeted mutation 2, Antonio Baldini	$Tbx1^{neo}$	targeted (Floxed/Frt)	Insertion. A hypomorphic allele created by the insertion of a floxed PGK-neo cassette and a third loxP site such that cre-mediated recombination may excise exon 5 and/or the neo cassette.	Xu *et al.*, 2004
$Tbx1^{tm3Bld}$ targeted mutation 3, Antonio Baldini	$Tbx1^{flox}$	targeted (Floxed/Frt)	Insertion. Exon 5 was flanked by loxP sites by cre-mediated recombination of $Tbx1^{tm2Bld}$ in ES cells that removed the neomycin cassette.	Xu *et al.*, 2004

Tbx1$^{tm4(cre/Esr1)Bld}$ targeted mutation 4, Antonio Baldini	Tbx1^{mcm}	targeted (Knock-in)	Insertion. An IRES and a Mer*Cre*Mer fusion gene were inserted into exon 5 via homologous recombination, resulting in tamoxifen inducible cre expression under the control of the endogenous Tbx1 promoter.	Xu *et al.*, 2004
Tg$^{(Tbx1\text{-}Cre)1Joe}$ transgene insertion 1, Jonathan A Epstein	Tbx1^{-Cre}	transgenic (*Cre*/Flp)	Insertion. *Cre* recombinase gene was adjoined to mouse Tbx1 promoter sequence that extended 16 kb from the start codon and included the proximal promoter and three conserved enhancer regions.	Brown *et al.*, 2004
Tbx1$^{tm1(Fgf8)Vite}$ targeted mutation 1, Francesca Vitelli	Tbx1^{Fgf8}	targeted (Knock-in)	Insertion. A 0.8 kb Fgf8 cDNA encoding isoform 8b was inserted into exon 5.	Vitelli *et al.*, 2006
Tbx1^{tm1Bern} targeted mutation 1, Bernice E Morrow	Tbx1^{hygro}	targeted (Floxed/Frt)	Insertion. A hygromycin resistance cassette flanked by loxP sites was inserted between exons 3 and 4 along with a single loxP site between exons 1 and 2.	Arnold *et al.*, 2006
Tbx1$^{tm1.1Brn}$ targeted mutation 1.1, Bernice E Morrow	Tbx1^{flox}	targeted (Floxed/Frt)	Insertion. Exons 2 and 3 were flanked with loxP sites by cre-mediated recombination that removed the hygromycin cassette of Tbx1^{hygro} mice.	Arnold *et al.*, 2006
Tbx1$^{tm1.2Brn}$ targeted mutation 1.2, Bernice E Morrow	Tbx1^{-}	targeted (Knock-out)	Intragenic deletion. Exons 2 and 3 were removed by cre-mediated excision in Tbx1^{flox} mice.	Arnold *et al.*, 2006
Tbx1^{tm5Bld} targeted mutation 5, Antonio Baldini	Tbx1^{neo2}	targeted (Knock-out)	Insertion. A hypomorphic allele that can revert to a functional allele upon cre recombination, created by insertion of a floxed neomycin cassette into intron 5.	Zhang *et al.*, 2006
Tbx1$^{tm6(cre)Bld}$ targeted mutation 6, Antonio Baldini	Tbx1*Cre*	targeted (Knock-in)	Insertion. An IRES-*Cre* cassette was inserted into exon 5. Author states that this is a null allele.	Huynh *et al.*, 2007
Tg$^{(COET)1Bld}$ transgene insertion 1, Antonio Baldini	Tbx1^{-COET}	transgenic (*Cre*/Flp)	Insertion. A chicken β-actin promoter drives the expression of a loxP-flanked neomycin resistance cassette and triple polyadenylation signal, followed by a mouse *Tbx1* cDNA.	Vitelli *et al.*, 2009
Tbx1^{m1Jlk} spontaneous mutation 1, John Klingensmith	Tbx1^{GtoT}	spontaneous	Single point mutation. A G to T transversion in the boundary region between exon 2 and intron 2 at the 5th base into intron 2. This mutation results in splicing irregularities including exon skipping and intron retention.	Choi *et al.*, 2009
Chromosome 16 deletions and human BAC transgene that incorporates *Tbx1*				
Del(16Es2el-Ufd1l)217Bld deletion, Chr 16, Antonio Baldini	del(16) (Es2-Ufd1l), Del217Bld, Df1	targeted (Knock-out)	Intergenic deletion. Deletion on chromosome 16, including 19 genes, spanning from Es2el to Ufd1l	Lindsay *et al.*, 2001

Del(16Dgcr2-Hira)1Rak deletion 1, Chr 16, Raju Kucherlapati	Del1Rak, Lgdel	targeted (other)	Intergenic deletion. Deletion on chromosome 16, including 24 genes, spanning from Idd to Hira	Merscher *et al.*, 2001
$Tg^{(GNB1L, TBX1, GP1BB, SEPT5)23Rak}$ transgene insertion 23, Raju Kucherlapati	316.23, BAC316.23, Tg316	transgenic	Insertion.	Merscher *et al.*, 2001
Tbx1 localises on chromosome 16, comprises of 9 exons and the initiator is in exon 2. Information is collated at: http://www.informatics.jax.org/searches/allele_report.cgi?_Marker_key=13762				

Table 1. 1. Genetic mutations of *Tbx1* in mouse models.

9.3. *Tbx1* is required in different tissues, dosages and time-points

Tbx1 in mice is important in early heart and pharyngeal development (Jerome and Papaioannou, 2001; Lindsay et al., 2001; Merscher et al., 2001) in a tissue-specific (Arnold et al., 2006; Xu et al., 2004; Zhang et al., 2005; Zhang et al., 2006), time (Xu et al., 2005) and dosage (Vitelli et al., 2009; Zhang and Baldini, 2008) dependent fashion. A multitude of studies have been undertaken in order to establish the different roles of the gene in these developmental processes.

Tissue-specific roles

Hemizygous deletion of *Tbx1* in the mesoderm, with the use of the *Mesp1* or *Nkx2.5 Cre* drivers ($Tbx1^{Fl/+}$;*Mesp1Cre* or $Tbx1^{Fl/+}$;*Nkx2.5Cre*), did not produce the fourth arch artery phenotype seen in the $Tbx1^{+/-}$ animals, concluding that the mesodermal expression of *Tbx1* is unrelated to fourth arch artery development (Zhang et al., 2005). Hemizygous deletion of *Tbx1* in the mesoderm on an already heterozygous background ($Tbx1^{Fl/-}$;*Mesp1Cre* or $Tbx1^{Fl/-}$;*Nkx2.5Cre*) recapitulated most of the null phenotype, with the exception of no evidence of palatal defects and the aortic arch phenotype being milder (Xu et al., 2004; Zhang et al., 2006). Nevertheless, consistently with the single allele conditional deletion experiments, reactivation of the gene in the mesoderm was sufficient to completely rescue the severe outflow tract phenotype, together with the second, third, and sixth arch artery phenotype and the external ear hypoplasia, but not the thymic hypoplasia or the fourth arch artery defects (Zhang et al., 2006).

Epithelial hemizygous excision of *Tbx1* using a more general *Cre* driver initially (*Foxg1Cre*, shown by reporter expression to induce recombination in the pharyngeal epithelia as well as the pharyngeal mesoderm) and a more specific one later (*TgFgf15Cre* or *TgFgf15HspCre*, shown by reporter expression to induce recombination in the pharyngeal epithelia) was sufficient to cause fourth arch artery defects, although with reduced penetrance (Zhang et al., 2005). The authors rationalised that the reduced penetrance was a result of the time of activation of the *Cre* drivers (approximately E9), or, at least in part, due to the different genetic backgrounds between this and previous studies (Zhang et al., 2005). A second study used the same *Cre* driver (*Foxg1Cre*) to hemizygously delete *Tbx1* in the endoderm on a heterozygous background, but in this case all mice were maintained on the same genetic background (Arnold et al., 2006). The tissue-specific inactivation was tested by *in situ* hybridisation, which proved intact *Tbx1* expression and absent *Cre* expression in the mesoderm (Arnold et al., 2006), although there was no mention regarding the ectodermal domain. All conditional null embryos recapitulated the null phenotype in full and it was concluded that *Tbx1* is required in the pharyngeal endoderm for the patterning of the apparatus, and secondary to that it affects the development of the derivative structures (Arnold et al., 2006). The authors suggested that lack of segmentation indirectly affects outflow tract development by compromising neural crest migration into the AP septum and SHF cell addition to the elongating outflow tract, recognising however the existence of cell-autonomous roles of the mesodermal *Tbx1* in outflow tract development (Arnold et al., 2006).

The early, haploinsufficient role of *Tbx1* in fourth arch artery development has been proven pivotal in the subsequent development of the cardiovascular phenotype (Jerome and Papaioannou, 2001; Lindsay et al., 2001; Merscher et al., 2001). In an effort to clarify the tissue-specific requirements of the gene in the development of the fourth arch artery, fate mapping experiments were undertaken, showing that *Tbx1*-expressing cells contribute to the endothelial lining of the fourth arch artery, but not to the VSM layer, which is of neural crest origin (Zhang et al., 2005). However, conditional deletion of *Tbx1* in endothelial precursors (*Tie2Cre* or *Mesp1Cre*) did not reproduce the $Tbx1^{+/-}$ haploinsufficiency phenotype (Zhang et al., 2005). This suggests that *Tbx1* may have earlier roles (before the endothelial progenitor stage) in fourth arch artery development or that other tissue-specific *Tbx1* actions are involved. Deleting *Tbx1* in the endothelial cell lineage using the *Tie2Cre* promoter affected the

lymphangiogenesis of E18.5 embryos, while *TBX1* regulated the transcription of growth factors and angiogenic markers in human umbilical vain endothelial cells (HUVECs) *in vitro* (Chen et al., 2010).

The fourth arch artery defect has complete penetrance in both *Df1*, and *Tbx1* heterozygous lines and is attributed to failure of growth, rather than formation of the vessel (Lindsay and Baldini, 2001; Vitelli et al., 2002a). One reason the fourth arch artery collapses in these mutants is considered the deficiency the *Df1* and *Lgdel* heterozygous animals present in neural crest cell differentiation into VSM of the fourth and sixth arch arteries (Kochilas et al., 2002; Lindsay and Baldini, 2001). Defects have also been seen in the neural crest cell migratory pathways of *Tbx1* homozygotes (Moraes et al., 2005; Vitelli et al., 2002a), which until recently was believed to be secondary to the absence of pouches and normal signalling in the pharyngeal region (Arnold et al., 2006; Vitelli et al., 2002a). Similar defects have not been observed in *Df1*/+ (Lindsay and Baldini, 2001) or *Lgdel*/+ (Kochilas et al., 2002) animals, however, the cardiac neural crest cell migration pattern was recently shown to be compromised in *Tbx1* heterozygous and *Tbx1* hypomorphic embryos that have no pharyngeal segmentation defects (Calmont et al., 2009). The progressive reduction in *Tbx1* mRNA levels correlated well with increased penetrance of fourth arch artery defects and with increased incidence of cardiac neural crest cell defects in the hypomorph mutants (Calmont et al., 2009). This showed that *Tbx1* has non-cell autonomous roles in neural crest cell migration and that additional to defective *in situ* differentiation, migration is also associated with fourth arch artery defects (Calmont et al., 2009). Moreover, the same study provided evidence linking the ectodermal expression of *Tbx1*, via *Gbx2*, to fourth arch artery development (Calmont et al., 2009).

To conclude, epithelial *Tbx1* expression in the pharynx is suggested to regulate segmentation of the apparatus, and secondary to that thymus, parathyroid, cardiovascular and craniofacial morphogenesis (Arnold et al., 2006; Zhang et al., 2005) while mesodermal expression is required mainly for outflow tract development, but also contributes to arch artery, craniofacial and glandular formation (Zhang et al., 2006). The ectodermal expression of *Tbx1* is directly associated with the development of the fourth arch artery (Calmont et al., 2009) whereas endothelial *Tbx1* is involved in lymphangiogenesis (Chen et al., 2010).

Time-dependent roles

Xu *et al.* used a tamoxifen inducible *CaggsCre* driver to produce a time course of *Tbx1* inactivation and assess the time-dependent requirements of the gene in the development of the different structures and organs (Xu et al., 2005). The genomic *Tbx1* locus was completely recombined by 24 hrs after drug injection, thus causing ubiquitous deletion (Xu et al., 2005). In summary, tamoxifen injection at E7.5 (full excision by E8.5) recapitulated the germ line homozygous mutant phenotype, although not with complete penetrance, at E8.5 (full excision by E9.5) produced outflow tract and thymic defects along with cleft palate, at E9.5 or E10.5 (full excision by E10.5 or E11.5) thymic and palate defects and at E11.5 (full excision by E12.5) only palate defects (Table 1.2) (Xu et al., 2005). Also, with induction at E7.5 the embryos lacked the caudal pharyngeal arches (arches 3, 4 and 6) while with induction at E8.5 the embryos lacked arches 4 and 6 (Xu et al., 2005). A defect in proliferation of the endodermal cells in these mutants was further shown (Xu et al., 2005). In the same respect, a tamoxifen inducible allele that drives *Cre* expression under the control of the *Tbx1* gene was used to map the fate of *Tbx1*-expressing cells at different time-points (Xu et al., 2005). Following induction at E7.5, among other tissues, the pharyngeal ectoderm and the endothelium of the fourth arch arteries were labelled, which was not observed after induction at E8.5 or E9.5 (Xu et al., 2005). Induction at E8.5 however, revealed a strong contribution of labeled cells to the outflow tract, which was very weak with induction at E9.5 (Xu et al., 2005). The authors concluded that *Tbx1* is important for expansion of the endodermal tissue during the formation of the 3rd pouch (between E9.0-9.5) that directly affects pharyngeal segmentation (Xu et al., 2005). Moreover, they postulated that the fourth arch artery haploinsufficiency phenotype is due to an early requirement for *Tbx1*, that precedes the morphological appearance of the arteries, at E9.5 (Xu et al., 2005). It was also suggested that the crucial time point *Tbx1* is required at for the development of the outflow tract was between E8.5 and E9.5, through an outflow tract-specific subpopulation of cardiomyocyte precursors (Xu et al., 2005). Thymus development was controlled by *Tbx1* in the same interval and there was a strong contribution of labeled cells to the thymic primordia after induction at E8.5 (Xu et al., 2005). However, there was an additional, although limited, contribution of labeled cells to the thymus, after induction at E9.5 and E10.5, indicating different mechanisms for formation and morphogenesis (Xu et al., 2005).

tamoxifen / phenotype	E7.5	E8.5	E9.5	E10.5	E11.6
aortic arch (haploinsufficiency)	abnormal (44%)	normal	normal	normal	normal
external ears	hypoplastic	normal	normal	normal	normal
outflow tract	PTA	PTA	normal	normal	normal
thymus	absent	absent	small	small	normal
secondary palate	cleft	cleft	cleft	cleft	cleft (45%)

Table 1. 2. The *Tbx1* time-dependent phenotype. Phenotypes scored in E18.5 conditional homozygous (*Tbx1*$^{Fl/-}$;*CaggsCre*) or heterozygous (*Tbx1*$^{Fl/+}$;*CaggsCre*, aortic arch defects only) embryos after in utero exposure to tamoxifen at the stages indicated. The penetrance of the defects was complete, unless indicated otherwise. PTA, persistent truncus arteriosus (Xu et al., 2005).

Dosage-dependent roles

Zhang *et al.* generated a series of mouse mutants with near-continuous variation of the *Tbx1* mRNA dosage by combining different *Tbx1* alleles (Zhang and Baldini, 2008). The levels of *Tbx1* mRNA were measured by quantitative real time PCR (Zhang and Baldini, 2008). They showed that the levels gradually decreased from wild type (100%) to null (*Tbx1*$^{-/-}$, 0%) embryos, with the intermediate levels being *Tbx1*$^{+/Neo2}$ (70.5%), *Tbx1*$^{+/Neo}$ (53.3%), *Tbx1*$^{+/-}$ (49.9%), *Tbx1*$^{Neo2/Neo2}$ (34%) and *Tbx1*$^{Neo/Neo}$ (4.1%) (Zhang and Baldini, 2008). They also included *Dp1*/*Dp1* embryos (179%), that carry a chromosomal duplication encompassing *Tbx1* (Zhang and Baldini, 2008). The phenotypic analysis demonstrated that *Tbx1*$^{Neo/Neo}$ embryos were nearly identical to *Tbx1*$^{-/-}$ embryos with the exception of normal palatogenesis and a milder outflow tract alignment phenotype in some embryos (Zhang and Baldini, 2008). All heterozygous mutants had high viability in contrast with all the homozygous and double heterozygous mutants (except for *Dp1*/*Dp1*), which had a 100% incidence of neonatal lethality (Zhang and Baldini, 2008). *Tbx1*$^{+/Neo2}$, *Tbx1*$^{+/Neo}$ and *Tbx1*$^{+/-}$ had hypoplastic thymus and aortic arch artery abnormalities of fourth arch origin (Zhang and Baldini, 2008).

The penetrance of the defects was variable and increased with reduced *Tbx1* dosage (Zhang and Baldini, 2008). In $Tbx1^{Neo2/Neo2}$ the thymic hypoplasia was more severe, and the aortic arch artery defects had complete penetrance (Zhang and Baldini, 2008). Further reduction of *Tbx1* dosage in the $Tbx1^{Neo/Neo}$ embryos caused outflow tract defects additionally to the thymus and aortic arch artery defects (Zhang and Baldini, 2008). Pharyngeal patterning defects were also associated with *Tbx1* mRNA levels (Zhang and Baldini, 2008). At E10.5 $Tbx1^{Neo2/Neo2}$ embryos had hypoplastic fourth pharyngeal arches and absent fourth arch arteries, while $Tbx1^{Neo2/-}$ embryos had a pharyngeal segmentation phenotype similar to that of $Tbx1^{-/-}$ embryos, although in some cases one of the two sixth arch arteries was present and there were rudimentary fourth pouches (Zhang and Baldini, 2008). The $Tbx1^{Neo/Neo}$ pharyngeal phenotype was indistinguishable to the $Tbx1^{-/-}$ phenotype (Zhang and Baldini, 2008). The authors concluded that there is a linear correlation between aortic arch artery defects and *Tbx1* mRNA levels within the range of 75-25% mRNA levels, while for the outflow tract defects the range is much narrower (Zhang and Baldini, 2008). Moreover, it was noted that there was very limited variability, with regard to the type of outflow tract defects seen, in animals with the same genotype, with the exception of the $Tbx1^{Neo2/Neo}$ that included the entire range of defects scored, as well as individuals with normal outflow tract (Zhang and Baldini, 2008). This suggests that phenotypic variability is also associated with the mRNA dosage (Zhang and Baldini, 2008). The results of this study are summarised in Table 1.3.

Tbx1 genotype	*Tbx1* dosage*	lethality	AoA	thymus	outflow tract (s)	outflow tract (a)	cleft palate
Neo2/+	70.5%	low	x	m. hypo			
Neo/+	53.3%	low	x	m. hypo			
+/-	49.9%	low	x	m. hypo			
Neo2/Neo2	34%	complete	x	s. hypo			
Neo2/Neo	18.5%	complete	x	aplasia	x		
Neo2/-	15.4%	complete	x	aplasia	x	x	
Neo/Neo	4.1%	complete	x	aplasia	x	x	
-/-	0.2%	complete	x	aplasia	x	x	x

Table 1. 3. The *Tbx1* dosage-dependent phenotype. *Tbx1* mRNA levels in the different genotypes measured by quantitative real time PCR and the phenotypic characteristics of each mutation. AoA, aortic arch; s, septation defect; a, alignment defect; m. hypo, mild hypoplasia; s. hypo, severe hypoplasia; x, indicates the presence of a defect. * relative to the wild type levels (Zhang and Baldini, 2008).

Similar to the *Dp1* line that was used by Zhang *et al.* as a *Tbx1* over-expression construct (Zhang and Baldini, 2008), another transgenic model was generated that expresses *Tbx1* cDNA upon *Cre* recombination (Vitelli et al., 2009). Vitelli *et al.* used this line (*COET*, *conditional over-expression of Tbx1*) to rescue the *Tbx1* heterozygous phenotype by employing the $Tbx1^{+/Cre}$ line (Vitelli et al., 2009). This model has an IRES-*Cre* cassette inserted in exon 5, in the same respect as the $Tbx1^{tm1Bld}$ mutation, so it is essentially a null allele (Vitelli et al., 2009). By quantitative real time PCR it was shown that the *COET* allele is comparable to the level of expression of two wild type alleles (Vitelli et al., 2009). Nonetheless, the *COET*;$Tbx1^{+/Cre}$ animals died perinatally, while 95% of term embryos exhibited aortic arch and intracardiac defects and 79% exhibited thymic defects (Vitelli et al., 2009). Interestingly, the *COET* allele seemed to rescue the early fourth arch artery phenotype (33%, n=12, in *COET*;$Tbx1^{+/Cre}$ as opposed to 80%, n=5, in $Tbx1^{+/Cre}$ embryos) (Vitelli et al., 2009), although this result was not statistically significant. Next, the authors examined the *COET*;$Tbx1^{-/Cre}$ mutation, and showed that in this setting *Tbx1* levels were comparable to wild type at

E10.5, whereas the *Tbx1* expression pattern was somewhat expanded, compared to wild type (Vitelli et al., 2009). It was rationalised that the *COET* allele is irreversibly activated after *Cre* recombination, thus *Tbx1* remains active and functions in tissues it is normally shut down (Vitelli et al., 2009). For this reason the *COET* allele did not rescue the haploinsufficient $Tbx1^{+/Cre}$ phenotype, although it was sufficient to rescue most aspects of the *Tbx1* loss of function phenotype, with the exception of the fourth arch and associated artery which remained hypoplastic in the rescued embryos (Vitelli et al., 2009). Overall, early stage pharyngeal patterning as well as outflow tract septation, ear and palate defects were ameliorated or rescued in the *COET*;$Tbx1^{-/Cre}$ mutants (Vitelli et al., 2009). The fact that the *COET* allele could rescue most of the *Tbx1* loss of function ($Tbx1^{-/Cre}$) phenotypes but only some of the *Tbx1* haploinsufficiency ($Tbx1^{+/Cre}$) phenotypes led the authors to conclude that some organs are sensitive not only to the *Tbx1* dosage but also to dysregulation of the expression of the gene, and that the *COET*;$Tbx1^{+/Cre}$ was essentially a gain of function mutation (Vitelli et al., 2009).

Fourth arch phenotype penetrance and genetic rescue

Over the last ten years there has been extensive study of *Tbx1* and its roles in cardiovascular development. Different groups have generated a multitude of *Tbx1* alleles (Table 1.1) and have described the same general phenotypic characteristics for all. However, the penetrance of each phenotype varies greatly, especially considering the fourth arch artery defect. Such differences may be due to the different genetic backgrounds used or they could reflect small sample sizes, nevertheless it remains an issue that should be accounted for. The *Df1* mutation in heterozygosity results in 100% penetrance of fourth arch artery defects at E10.5 (Lindsay et al., 2001), while the penetrance of the same defect in $Tbx1^{+/tm1Bld}$ embryos has been reported as complete (100%, n=14, Lindsay et al., 2001) or incomplete (93%, n=14, Vitelli et al., 2002b and 46%, n=11, Calmont et al., 2009) by three different studies. Similarly 45% of $Tbx1^{+/tm1Pa}$ embryos show a fourth arch artery defect on an inbred background, which is reduced to 19% on a mixed background (Jerome and Papaioannou, 2001).

Linsday *et al.* first described the phenomenon of genetic rescue of the fourth arch artery phenotype of the *Df1* mutants (Lindsay and Baldini, 2001). This line in heterozygosity exhibits complete penetrance of fourth arch artery defects at E10.5, which is however reduced to 65.5% in E11.5 embryos and to 32% in term embryos (Lindsay and Baldini, 2001). The same stands for the $Tbx1^{tm1Bld}$ mutation that has

complete penetrance of fourth arch defects in heterozygosity at E10.5 (Lindsay et al., 2001), which is reduced to 26-38% in term embryos (Calmont et al., 2009; Vitelli et al., 2002b Vitelli et al., 2006; Zhang and Baldini, 2008). Furthermore, although the *Lgdel*/+ embryos were not examined at the early stage, given that they carry a deletion that includes the *Df1* region, the penetrance of the E10.5 fourth arch artery defects is expected to be high, nonetheless, defects were scored in 46% of term embryos (Merscher et al., 2001). Similarly the penetrance of the defect in term $Tbx1^{+/tm1Rak}$ embryos is 50% (Merscher et al., 2001), in term $Tbx1^{+/tm1Dsr}$ embryos is 22% (Hu et al., 2004), in term $Tbx1^{+/tm3Bld}$;*CaggsCre* embryos is 44% (tamoxifen injection at E7.5) (Xu et al., 2005) and in term $Tbx1^{+/tm1(Fgf8)Vite}$ embryos is 75% (Vitelli et al., 2006). The genetic recovery of the fourth arch artery defects has also been associated with the genetic background (Taddei et al., 2001). Taddei *et al*. demonstrated that in term 129SvEv *Df1*/+ embryos the incidence of the defect was 16.1%, while the same mutation on a mixed background produced an approximately 32% penetrant phenotype (Taddei et al., 2001). C57BL/6J *Df1*/+ embryos had a much higher penetrance, of 50% (Taddei et al., 2001). Differences were not observed with regard to the types of defects seen in the different strains (Taddei et al., 2001). Of particular note is the finding that irrespective of the different genetic background, the fourth arch artery defect presented with complete penetrance in all groups of E10.5 *Df1*/+ embryos (Taddei et al., 2001). The authors concluded that the phenotypic variability of the 22q11DS-like phenotype of the *Df1* mutation is genetically controlled and postulated that there are genetic modifiers unrelated to allelic variation at the haploid locus but more likely located elsewhere in the genome (Taddei et al., 2001).

The genetic background of a mouse strain refers to the genetic make-up of the strain that involves all alleles in all loci, apart from the mutated gene of interest (JAX®, 2006). Different genetic modifiers can affect the phenotype expressivity, penetrance and dominance of each gene (Nadeau, 2001). Since each strain has unique background alleles, a mixed background can influence the phenotype of a mutation, transgene, or other genetic insert (JAX®, 2006). This explains why normal development and physiology may vary significantly among inbred strains (JAX®, 2006). In light of the above studies, certain general considerations should be regarded when the effects of the genetic background are being discussed. There is no ideal genetic background for every class of phenotypes (Montagutelli, 2000). Nonetheless, the phenotypic differences seen in different backgrounds can assist the generation of mouse models that resemble

aspects of human diseases more closely (Montagutelli, 2000). Genetic heterogeneity exists in most human genetic diseases and the human phenotypes can present great ranges, while mouse mutants in an inbred background exhibit more homogeneous phenotypes (Montagutelli, 2000). These can be compared with only a subset of human patients (Montagutelli, 2000). By assessing the mutation on a different genetic background the range of phenotypes can widen (Montagutelli, 2000). In summary, a mutation should be considered to induce a phenotype in a specific genomic context (Montagutelli, 2000). Consequently, great caution is needed when comparing data between different experiments and studies, as the background genetic modifiers can play an important role in the resulting phenotype.

9.4. *Tbx1* interactors and modifiers of 22q11DS

As discussed previously, the vast majority of 22q11DS patients carry an identical 3 Mb deletion (Emanuel, 2008; Wurdak et al., 2006; Yamagishi and Srivastava, 2003). They present however with considerable phenotypic variability, with phenotypes ranging from life threatening heart defects to developmental delay and mild craniofacial abnormalities (Shprintzen, 2008; Vitelli and Baldini, 2003; Wurdak et al., 2006; Yamagishi and Srivastava, 2003). Genetic background modifiers affect the penetrance of the cardiovascular phenotype in a *del22q11* mouse model, suggesting that a complex network of interactions is taking place from the genotype towards the end phenotype (Taddei et al., 2001). Initial studies focused around genes that affect the development and morphogenesis of pharyngeal arch and pouch derivatives and are co-expressed with *Tbx1*. *Fgf8*, *retinaldehyde dehydrogenase 2* (*Raldh2*) and *Vegf* are three of the several genes that have been studied in this respect (Scambler, 2010; Taddei et al., 2001; Vitelli and Baldini, 2003).

Fgf8 is strongly expressed in the pharyngeal clefts and pouches and the ectoderm of the first pharyngeal arch (Vitelli and Baldini, 2003). Hypomorphic mutants exhibit cardiovascular defects similar to the *Tbx1* mutation phenotype, including fourth arch related aortic arch, outflow tract septation, alignment and rotation defects (Vitelli and Baldini, 2003). In addition, pharyngeal segmentation of the caudal arches appears compromised (arches 3, 4 and 6) and *Fgf8* mRNA is completely lost in the pharyngeal endoderm of $Tbx1^{-/-}$ mutants (Vitelli and Baldini, 2003). Double heterozygous animals present with higher incidence of aortic arch and thymic defects, supporting a genetic interaction between the two genes, placing *Tbx1* upstream of *Fgf8* in the endoderm

(Vitelli and Baldini, 2003). However, *Fgf8* expression off a *Tbx1* promoter is not sufficient to rescue the fourth arch artery phenotype seen in $Tbx1^{+/-}$ embryos (Vitelli et al., 2006). The same allele, which is effectively a *Tbx1* null allele, was used in combination with $Tbx1^{Neo2}$ that expresses minimal levels of *Tbx1* (Vitelli et al., 2010). $Tbx1^{Neo2/Fgf8}$ animals presented with an improved outflow tract phenotype, including PTA, DORV and TGA, as compared to the $Tbx1^{Neo2/-}$ embryos that displayed 95% penetrance of PTA (Vitelli et al., 2010). It was further shown that $Tbx1^{-/-}$ mouse embryonic fibroblasts (MEFs) did not respond normally to Fgf8, which was improved in $Tbx1^{Neo2/-}$ MEFs (Vitelli et al., 2010). The authors concluded that reduced *Fgf8* expression in Tbx1 null embryos contributes to the outflow tract septation phenotype and that *Tbx1* is required for tissue-specific response to Fgf8 (Vitelli et al., 2010).

RA and its receptors play a crucial role in pharyngeal development, while a hypomorph mutant for *Raldh2* (converts retinaldehyde to RA) displays aortic arch anomalies, as well as outflow tract septation, thymic and parathyroid malformations (Vermot et al., 2003). *Raldh2* was found greatly upregulated in the pharyngeal region of *Tbx1* null embryos, due to a cranial expansion of the expression domain (Ryckebusch et al., 2010), although after E8.5 this is attributed at least in part to pharyngeal hypoplasia (Ivins et al., 2005). Evidence from *in vivo* systems as well as proteomic analyses support a mutually repressive regulatory interaction between RA signalling and *Tbx1* (Caterino et al., 2009; Guris et al., 2001; Ivins et al., 2005; Roberts et al., 2005; Ryckebusch et al., 2010).

Vegf is required for vasculogenesis and angiogenesis, while mice lacking one of the isoforms exhibit aortic arch, craniofacial, and glandular defects, as well as reduced vascular densities of the affected organs (Stalmans et al., 2003). *Tbx1* appears reduced in the *Vegf* mutants and morpholino knock-down experiments in zebrafish support a genetic interaction between the two genes (Stalmans et al., 2003). Small nuclear polymorphism (SNP) variants of *VEGF* have been found more frequent in 22q11DS patients with cardiovascular defects than in normal controls (Stalmans et al., 2003). TBX1 is also shown to regulate *VEGFR3* expression by binding onto a conserved transcription binding element (TBE) found in the regulatory region of *VEGFR3*, a result validated by chromatin immunoprecipitation (ChIP) analysis (Chen et al., 2010).

Homozygous deletion of *Crkl* recapitulates the 22q11DS phenotype displaying craniofacial, arch artery, outflow tract, thymic and parathyroid defects, although the

heterozygous deletion does not produce a phenotype (Guris et al., 2001). *Crkl* was one of the four genes included in the P1 artificial chromosome (PAC) that was used to genetically rescue the *Df1* 22q11DS-like phenotype (Lindsay et al., 2001). As with previous studies, the genetic interaction between *Crkl* and *Tbx1* was studied through double mutagenesis, which showed increased frequency and severity in the aortic arch, thymic and parathyroid defects, as compared to $Tbx1^{+/-}$ mice (Guris et al., 2006). The defects were at least in part a result of aberrant development of caudal pharyngeal arch formation as well as abnormal regional patterning of the apparatus, maybe a result of locally aberrant RA signalling (Guris et al., 2006).

The pathway seems very complex, since *Fgf8* and *Crkl* genetically interact too towards the formation and possibly subsequent remodelling of the fourth arch and the outflow tract (Moon et al., 2006). Double heterozygotes as well as $Fgf8^{+/-}$;$Crkl^{-/-}$ embryos present with increased penetrance and severity of cardiovascular defects (Moon et al., 2006). The pharyngeal epithelia, neural crest and SMC populations located near or migrating into the arches showed a marked increase in apoptosis (Moon et al., 2006). Additionally, FGF receptors bound directly to the SH2 domain of Crkl *in vitro* (Moon et al., 2006). Taken together, these results suggest that *Fgf8*, *Crkl* and *Tbx1* may operate in common pathways during cardiovascular and pharyngeal development.

Huh *et al.*, recently demonstrated that the Wnt-β-catenin signalling is a repressor of *Tbx1* and the *Tbx1*-related FGF downstream signalling in the pharyngeal apparatus of mouse embryos (Huh and Ornitz, 2010). Moreover, conditional inactivation of *β-catenin* in the pharyngeal mesenchyme induced a range of 22q11DS-like phenotypes, including craniofacial, cardiovascular, ear, thymic and parathyroid defects, while diminishing the *Fgf8* dosage in these mutants could partially rescue the arch artery remodelling phenotype (Huh and Ornitz, 2010).

More recent studies have employed microarray hybridisations and mouse models in order to establish *Tbx1*-associated genes. As mentioned earlier, *Gbx2* interacts with *Tbx1* in the surface ectoderm, regulating fourth arch artery morphogenesis (Calmont et al., 2009). Null mutation of *Gbx2* produces a cardiovascular phenotype reminiscent of the *Tbx1* heterozygous and null phenotype (Calmont et al., 2009). *Hes1*, a Notch regulated repressor gene, is also suggested as a potential *Tbx1* interactor (van Bueren et al., 2010). During early embryogenesis *Hes1* shares expression domains with *Tbx1*

while the *Hes1* null phenotype is reminiscent of the *Tbx1* heterozygous and null phenotypes with incomplete penetrance (van Bueren et al., 2010).

Regulatory elements of the *Tbx1* gene have also been characterised. One such enhancer includes a conserved Fox-binding site and can drive expression of a reporter gene in the pharyngeal endoderm and head mesenchyme in transgenic experiments, while Foxc1, Foxc2 and Foxa2 can bind to it (Vitelli and Baldini, 2003). SHH signalling regulates *Foxa2* and *Foxc2* and it is important for aortic arch and outflow tract development (Vitelli and Baldini, 2003). While *Tbx1* is reduced in *Shh* mutants, the pharyngeal phenotype of these animals is less severe than in *Tbx1* mutants, suggesting either that loss of *Shh* only partially diminishes *Tbx1* expression or that other regulatory mechanisms might be important for expression of *Tbx1* (Vitelli and Baldini, 2003).

Tbx1 has been shown to bind serum response factor (Srf), a master regulator of muscle differentiation, and negatively regulate its protein levels but not *Srf* mRNA, indicating regulation is not occurring at the transcriptional level (Chen et al., 2009). Affinity purification experiments have also identified Smad1 as a potential Tbx1 interactor, which was validated by co-immunoprecipitation assays (Fulcoli et al., 2009). This protein interaction interfered with the Smad1-Smad4 complex and inhibited the activation of a Smad-responsive reporter gene (Fulcoli et al., 2009).

It is now evident that multiple genes, through different pathways, act as genetic modifiers of the phenotype of *del22q11*, some studied more extensively than others. Understanding which mechanisms underlie the resulting set of phenotypes is of great importance. Nevertheless, caution is needed when interpreting the results of such studies, since a more severe phenotype observed in double mutants may be a result of additive effects, due to interfering of independent and parallel pathways that are required in normal development.

9.5. *TBX1* human mutations

Further evidence supporting the role of *TBX1* as a major genetic determinant in the etiology of 22q11DS are mutations of the gene, reported in human patients that do not carry the common chromosome 22q11.2 deletion. Yagi *et al.* first reported two missense (F148Y, G310S) and one frameshift (1223delC) mutations in *TBX1* in a study of 13 patients without *del22q11* (Yagi et al., 2003). The frameshift mutation led to a

premature stop codon and the truncated TBX1 protein lacked the C-terminal domain including the nuclear localisation signal (NLS) and a putative transactivation domain (Yagi et al., 2003). *In vitro* experiments by Stoller *et al.* subsequently showed that the truncated protein localised predominantly to the cytoplasm, in contrast with the wild type form found exclusively in the nucleus (Stoller and Epstein, 2005a). Additionally, even after forced nuclear localisation with fusion of the mutated construct with the SV40 NLS, the mutant protein failed to promote transcriptional activation (Stoller and Epstein, 2005a). The other two mutations had no effect on the protein (Stoller and Epstein, 2005a). All the patients in this study had the typical facies of CAFS, while the patient carrying the 1223delC mutation displayed TOF, RAA and hypoplastic thymus (Yagi et al., 2003). More recently, Paylor *et al.*, in a screen for genes implicated in the neurobehavioural manifestations of 22q11DS identified *Tbx1* and *Gnb1l* as potential factors (Paylor et al., 2006). Sequencing of those genes in a small cohort of patients with 22q11DS-like phenotype but without the typical 22q11.2 deletion, revealed in all three family members a frameshift mutation in *TBX1* (1320-1342del23bp) that disrupts the central domain of a highly conserved NLS (Paylor et al., 2006). Further *in vitro* experiments demonstrated that the mutant protein could in fact translocate to the nucleus like the wild type form, but it could not activate the reporter construct (Paylor et al., 2006). Therefore, the authors concluded that the 1320-1342del23bp is a null mutation causing *TBX1* haploinsufficiency in the carriers (Paylor et al., 2006). Zweier *et al.*, examined 10 patients exhibiting the 22q11DS phenotype but without carrying any typical or atypical 22q11.2 deletions (Zweier et al., 2007). A heterozygous missense mutation (H194Q) in *TBX1* was identified in one of the patients that did not however exhibit cardiac defects (Zweier et al., 2007). The mutation was located within the T-box domain and *in vitro* assays demonstrated that it induces overactivation of the reporter (Zweier et al., 2007). The previously described F148Y and G310S missense mutations (Yagi et al., 2003) were tested too, and showed a statistically significant increase in activation as well (Zweier et al., 2007). *In vitro* assays suggested that there was no increase in the expression levels between the mutant and wild type proteins, implying a gain of function effect of the mutations (Zweier et al., 2007). Modelling of the mutant proteins revealed that both the F148Y and H194Q are expected to increase the protein stability by additional hydrogen bonds (Zweier et al., 2007). Torres-Juan *et al.* screened 38 patients that have some of the features of 22q11DS and do not carry any typical or atypical deletions or duplications of chromosome 22q11.2 (Torres-Juan et al., 2007).

Apart from previously described polymorphisms, two novel rare variants of the *TBX1* gene were reported in heterozygosity (L411P, −39C → T) (Torres-Juan et al., 2007). The L411P change was located nine nucleotides downstream of the 1223delC frameshift mutation but it was not situated within the identified NLS (Torres-Juan et al., 2007). The second variant was a −39C → T nucleotide change in the second exon of the gene, within the 5'UTR (Torres-Juan et al., 2007). Computer modelling of the −39C → T variant predicted decreased stability of the secondary structure of the mRNA at the 5'UTR and differential folding (Torres-Juan et al., 2007). Subsequent *in vitro* translation experiments showed increase of protein reporter levels, indicating that the mutation may increase the endogenous TBX1 levels (Torres-Juan et al., 2007). The patient that carried the L411P mutation among other defects had TOF (Torres-Juan et al., 2007). The −39C → T variant was found in two brothers also exhibiting TOF (Torres-Juan et al., 2007). The healthy mother carried the familial mutation. (Torres-Juan et al., 2007). To date, no *TBX1* mutations have been associated with non-syndromic congenital heart defects (Scambler, 2010) and there is no evidence suggesting that variants of the remaining *TBX1* copy of 22q11DS patients affect the phenotypic variability (Rauch et al., 2004).

All in all, two frameshift mutations, affecting the NLS of the protein (Paylor et al., 2006; Stoller and Epstein, 2005a; Yagi et al., 2003), three missense mutations, possibly attributing gain of function properties (Yagi et al., 2003; Zweier et al., 2007), and a rare variant that increases the translational efficiency of the gene (Torres-Juan et al., 2007) suggest that haploinsufficiency of *TBX1* may cause 22q11DS.

10. Research project outline - *Tbx1* targets and pathways

TBX1 has proven to be an important regulator in the development of several embryonic structures (Arnold et al., 2006; Lindsay et al., 2001; Merscher et al., 2001; Xu et al., 2004; Zhang et al., 2005), and is now considered the major determinant of 22q11DS (Paylor et al., 2006; Stoller and Epstein, 2005a; Torres-Juan et al., 2007; Yagi et al., 2003; Zweier et al., 2007). Extensive research in mouse models has illuminated the distinct tissue-specific and time and dosage-dependent requirements for *Tbx1* in heart and pharyngeal development, the main structures affected in 22q11DS (Arnold et al., 2006; Vitelli et al., 2009; Xu et al., 2005; Xu et al., 2004; Zhang and Baldini, 2008; Zhang et al., 2005; Zhang et al., 2006). However, although it has been the focus of research for over ten years, since it was mapped within *del22q11* (Chieffo et al., 1997), the genetic pathways and downstream effectors are only partially characterised. Microarray experiments performed by us and others have established a list of potential Tbx1 target genes (Ivins et al., 2005; Liao et al., 2008; van Bueren et al., 2010). A large number of those genes have been validated by means of real time quantitative PCR and/or whole mount *in situ* hybridisation (Ivins et al., 2005; Liao et al., 2008; van Bueren et al., 2010). We recently undertook a refined approach towards identifying *Tbx1* targets by comparing the genetic profiles of *Tbx1*-expressing cells from heterozygous ($Tbx1^{+/lacZ}$) and null ($Df1/Tbx1^{lacZ}$) embryos on microarray chips, using Fluorescence activated cell sorting (FACS)-Gal to isolate the cells (van Bueren et al., 2010). On the basis of their expression profiles, association with known pathways and involvement in pharyngeal and/or heart development, *Smad7*, *Hes1* and *Slit2* were selected for further analysis, in the context of 22q11DS. The aim of this project was to characterise putative *Tbx1* downstream effectors and to link the pathways with the pathogenesis of the different 22q11DS phenotypes.

Smad7 is an inhibitor of the TGFβ pathway, shown to be expressed in cardiac tissues throughout mouse embryonic development (Liu et al., 2007; Luukko et al., 2001; Zwijsen et al., 2000). The TGFβ signalling is involved in heart development and has been studied primarily through knock-out models targeting genes of the pathway. Most are embryonic lethal and induce a range of cardiovascular phenotypes such as great vessel, valve and outflow tract defects, as well as cardiac hypertrophy and fibrosis (Person et al., 2005). Interestingly, *Smad6*, the only other inhibitory *Smad*, has a reported role in heart development and has a restricted expression pattern in the

cardiovasculature (Galvin et al., 2000). The standard *Smad6* knock-out exhibits cardiac valve hyperplasia and outflow tract septation defects (Galvin et al., 2000). Recently, a cardiovascular phenotype was also reported for the *Smad7* mutant mice, including VSD and outflow tract defects (Chen et al., 2009). During this project, a *Smad7* gene-trap model was used to study the knock-out phenotype in the context of 22q11DS. The complexity of biological systems has lately turned the focus of research from individual genes to the interactions between genes (Wang et al., 2010). Examining such functional relationships can be a useful tool in understanding the basic principles of the underlying genetic networks (Hartman et al., 2001; Wong et al., 2004). Genetic interactions are involved in many complex phenotypes and are the defining basis of multigenic genetic human disease (Wong et al., 2004). As part of this thesis the possible genetic interaction between *Tbx1* and *Smad7* was assessed, while further analysis involved efforts dissecting the genetic pathway *Tbx1* acts in, via *Smad7*, to regulate pharyngeal arch artery remodelling.

Hes1 is an effector of the Notch pathway and presented a good candidate, since other Notch target genes have a reported role in cardiovascular development (High and Epstein, 2008; Niessen and Karsan, 2008). Notch signalling is involved in many steps of cardiac development, namely cardiomyocyte differentiation, AVC and valve development, ventricular trabeculation and outflow tract remodelling (Niessen and Karsan, 2008). Animal models modulating the Notch pathway functions exhibit a range of cardiac defects such as VSD, ASD, TOF, cardiomyopathy, pulmonary artery stenosis, valve defects, abnormal heart looping and trabeculation defects (High and Epstein, 2008). We have shown that *Hes1* null mutants present with a range of defects including cardiovascular malformations (van Bueren et al., 2010). The tissue-specific requirements, however, for *Hes1* are not known. To that end conditional mutagenesis was employed, while the expression of Notch and FGF effectors was studied in the respective mutants, to elucidate the pathway through which *Hes1* acts towards great vessel morphogenesis.

Last, Slit2 is a secreted protein that binds to its receptor and regulates axon guidance and migration as well as outgrowth and branching (Andrews et al., 2008). Slit/Robo signalling is required for trunk neural crest migration in the chicken embryo (De Bellard et al., 2003; Jia et al., 2005). Several studies have discussed the neural crest migration defects in *Tbx1* null embryos (Baldini, 2002; Kelly et al., 2004; Moraes et al.,

2005; Vitelli et al., 2002a), but none has suggested a possible mechanism so far, apart from attributing it to the pharyngeal malformation defect (Arnold et al., 2006; Vitelli et al., 2002a). We recently showed that the cardiac neural crest migration pattern is altered in *Tbx1* heterozygous and hypomorph embryos too, while *Slit2* and *Tbx1* share common domains of expression during early embryogenesis (Calmont et al., 2009). *Slit2* was downregulated in *Tbx1* homozygous mutants (Calmont et al., 2009). For the purposes of this project, the phenotype of the *Slit2* and *Slit1;Slit2* null mutations, as well as the potential genetic interaction between *Slit2* and *Tbx1* in the development of structures affected in 22q11DS were assessed.

II. MATERIALS AND METHODS

All reagents were of AnalaR grade and supplied by Sigma Aldrich or BDH unless otherwise stated. Solutions were made using milliQ H_2O and autoclaved where appropriate. All stock solutions used are detailed in APPENDIX I.

1. Mouse strains, breeding, genotyping

1.1. Mouse strains

Tbx1$^{+/lacZ}$ mice were obtained from Antonio Baldini, Baylor College of Medicine, Houston, Texas, USA. They contain a non-functional *Tbx1* allele, which was generated by inserting an Internal Ribosomal Entry Site (IRES)-*β-galactosidase* reporter gene followed by a loxP-flanked neomycin resistance cassette into exon 5 (Lindsay et al., 2001). The mice were maintained on a C57BL/6J background.

Tbx1$^{+/mcm}$ mice were obtained from Antonio Baldini, Baylor College of Medicine, Houston, Texas, USA. They contain a non-functional *Tbx1* allele which was generated by insertion of a targeting cassette containing an IRES followed by the mER;*Cre*;mER encoding sequence into exon 5 via homologous recombination, resulting in tamoxifen inducible Cre expression under the control of the endogenous Tbx1 promoter (Xu et al., 2004). The mice were maintained on a C57BL/6J background.

Tbx1$^{+/Neo2}$ mice were obtained from Antonio Baldini, Baylor College of Medicine, Houston, Texas, USA. They contain a hypomorphic *Tbx1* allele that can revert to a functional allele upon Cre recombination and were generated by insertion of a floxed neomycin resistance cassette into intron 5 (Zhang et al., 2006). The mice were maintained on a C57BL/6J background.

Smad7 gene-trap mice were obtained from BayGenomics, University of California, San Francisco, USA. The pGT0Lxf vector is integrated within intron 3 of Smad7 and consists of the first intron of the *Engrailed 2* (*En2*) gene followed in succession by the mouse *En2* exon 2 splice acceptor, the *β-galactosidase* gene and the SV40 polyadenylation site. The splice acceptor is flanked by two lox sites (http://baygenomics.ucsf.edu/). The mice were maintained on a C57BL/6J background.

Hes1$^{+/-}$ mice were obtained from Francois Guillemot, National Institute for Medical Research, London, UK. The *Hes1* mouse was generated by replacing the first three

exons of the gene with a PGK-neomycin resistance cassette (Ishibashi et al., 1995). The mice were maintained on an MF1 or C57BL/6J background.

Hes1^{Fl} mice were obtained from Ryoichiro Kageyama, Institute for Virus Research, Kyoto University, Kyoto, Japan. They were generated by insertion of a targeting cassette containing loxP sites flanking the last three exons of the gene (Imayoshi et al., 2008). The mice were maintained on a C57BL/6J background.

Wnt1Cre mice were obtained from Andrew Copp, Neural Development Unit, Institute of Child Health, University College London, London, UK. They were generated by insertion of a cassette containing the Cre recombinase coding sequence between the *Wnt1* promoter and the *Wnt1* enhancer (Danielian et al., 1998). The mice were maintained on a C57BL/6J background.

Ap2αCre mice were obtained from Anne Moon, University of Utah School of Medicine, Salt Lake City, Utah, USA. They were generated by insertion of an IRES-Cre cassette in the 3' untranslated region (UTR) of the Ap2α locus (Macatee et al., 2003). The mice were maintained on a C57BL/6J background.

Mef2c-AHF-Cre mice were obtained from Brian Black, University of California, San Francisco, California, USA. They were generated by cloning the *Mef2c* anterior heart field promoter and enhancer into a Cre recombinase expression plasmid also containing the SV40 splice acceptor and polyadenylation sequence (Verzi et al., 2005). The mice were maintained on a C57BL/6J background.

Foxa2mcm mice were obtained from Anne Moon, University of Utah, Salt Lake City, Utah, USA. They were generated by insertion of a targeting cassette containing an IRES followed by the mER;Cre;mER encoding sequence into the Foxa2 locus (Park et al., 2008). The mice were maintained on a C57BL/6J background.

Sox17-2A-iCre mice were obtained from Heiko Lickert, Helmholtz Zentrum Munchen, Institute of Stem Cell Research, Neuherberg, Germany. They were generated by replacing the Sox17 translational stop codon in exon 5 by a T2A (Thosea asigna virus, TaV) self-cleaving peptide followed by the improved Cre (iCre) for the efficient and equimolar translation of Sox17 and iCre (Engert et al., 2009). Sox17 and iCre are posttranslationally cleaved by a 2A-mediated ribosome-skipping mechanism (Engert et al., 2009). The mice were maintained on a C57BL/6J background.

Slit2$^{+/-}$ mice were obtained from Marc Tessier-Lavigne, Departments of Anatomy and of Biochemistry and Biophysics, Howard Hughes Medical Institute, University of California, Berkeley, California, USA. The mice were generated by replacing the first two exons with a PGK-neomycin resistance cassette that includes a tauGFP fusion protein (Plump et al., 2002). They were maintained on a C57BL/6J background.

ROSA26 reporter mice were obtained from Philippe Soriano, Department of Developmental and Regenerative Biology, Mount Sinai School of Medicine, New York University, New York, USA. The mice were generated by insertion of a targeting vector that includes a splice acceptor, a loxP-flanked PGK-neomycin resistance cassette followed by a *β-galactosidase* reporter gene and a polyadenylation sequence (Soriano, 1999). They were maintained on a C57BL/6J background.

CD1 mice were used as wild type controls for expression profile analysis.

1.2. Breeding

Embryos were collected from timed matings. At midday, females with a copulation plug were considered to be at embryonic day 0.5. Pregnant females were killed by cervical dislocation and the uterus was placed in Phosphate Buffered Saline (PBS) for further dissection.

1.3. Tamoxifen administration

Pregnant females were treated with tamoxifen (T5648 or H6278, Sigma Aldrich) at different time points of embryonic development, by intraperitoneal (IP) injection or oral gavage (OG). It was prepared by dilution to 100mg/ml in 100% EtOH at 37 °C and then 1:10 in autoclaved peanut or sesame oil.

1.4. Genotyping

Genotyping of mice and embryos was carried out by polymerase chain reaction (PCR) analysis of yolk sac or tail tip genomic DNA. An aliquot of each sample was checked by agarose gel electrophoresis. The primer sequences and cycling conditions used are detailed in APPENDIX II.

2. DNA extraction

2.1. Lysis Buffer extraction

DNA extraction from yolk sacs (embryo genotyping) or tail tip biopsies (pup or adult mouse genotyping) by incubation in Tail Lysis Buffer and 100μg/ml Proteinase K (Roche, UK) at 55 °C, overnight (O/N). The enzyme was heat inactivated at 95-100 °C for 5 minutes. The DNA was precipitated in an equal volume of isopropanol, washed in 70% ice-cold ethanol (EtOH), air dried and resuspended in Tris Base/HCl-EDTA (TE), pH 8.

2.2. Phenol-Chloroform extraction

DNA purification from enzymatic reactions was performed as follows. Dilution in DEPC H_2O and equal volume of phenol (pH 8) and chloroform (49:1 $CHCL_3$:IAA), centrifugation at 12,000 x g for 20 minutes, collection of the aqueous phase, dilution in equal volume of chloroform, centrifugation at 12,000 x g for 15 minutes and collection of the aqueous phase, precipitation on ice in 1/10 volume RNAase-free 3M sodium acetate (pH 5.2) and 2.5 volumes of ice-cold RNAase-free 100% EtOH for 30 minutes, followed by centrifugation for 20 minutes, washing of the pellet in ice-cold RNAase-free 70% EtOH, air-drying and resuspending in DEPC H_2O.

3. Polymerase Chain Reaction

3.1. Primer design

Primers were designed manually or by using the Primer3 program (http://primer3.sourceforge.net/) and obtained from Sigma Aldrich or Operon. Forward and reverse PCR primers were designed with 50-60% GC content, at a 20-30 bp oligonucleotide length, with absence of repeat sequences and with similar melting temperatures (Tm).

3.2. PCR conditions

The reactions were carried out in sterile, distilled H_2O in a final volume of 25μl in PCR tubes as follows:

20-50ng genomic DNA

1X NB buffer

200µM each dNTP

1.5mM $MgCl_2$

0.8µM forward and reverse primer

1u Taq Polymerase (Bioline)

For amplification of large DNA fragments, Expand Long Template PCR System (Roche, UK) was used according to the supplier's instructions.

For amplification of DNA fragments that would be used for cloning reactions, Expand High Fidelity^{Plus} PCR System (Roche, UK) was used according to the supplier's instructions, to reduce the chance of mutations being introduced in the amplified products.

4. Gel electrophoresis

DNA was separated on a 1-2% agarose gel containing 0.5µg/ml ethidium bromide in 1X TAE. An appropriate 100 bp or 1 kb DNA ladder (Invitrogen) was also loaded. Samples were run in a 1/6 volume of loading buffer and gels were electrophoresed at 50-150V until the fragments had separated sufficiently. DNA was visualised by UV illumination.

5. Sequencing

Cycle sequencing reactions were performed with BigDye Terminator v3.1 (Applied Biosystems) and run on the MegaBACE (Amersham Biosciences), which uses the dideoxynucleotide chain termination method for sequencing. Sequencing reactions were carried out in 20 µl reaction volumes as follows: 3 µl miniprep plasmid DNA or PCR product, 5 pmol forward or reverse primer and sterile H_2O were heated to 95 °C for 5 minutes then 2 µl dilution buffer and 1 µl BigDye premix were added. The sequencing program used consisted of a denaturation step at 95 °C for 5 minutes followed by 36 cycles at 95 °C for 20 seconds, 50 °C for 10 seconds and 60 °C for 3 minutes.

Samples were sequenced by an in house sequencing facility. Files from the MegaBACE were downloaded in ABD format and analysed using the Sequencher v4.2 program.

6. RNA extraction

6.1. Trizol (Invitrogen)

RNA was extracted from cells using Trizol reagent (Invitrogen). The cells were scraped off the well surface using a cell scraper and were homogenised by passing the sample through a pipette tip several times. Whole embryos were collected in cold PBS, transferred immediately in Trizol and homogenised by passing the sample through a syringe needle several times. The sample was left at room temperature for 5 minutes to allow complete dissociation of nucleoprotein complexes. Chloroform was added at one fifth of the initial Trizol volume to each sample and shaken by hand. The samples were then left for 3 minutes at room temperature before centrifuged at 12,000 x g for 15 minutes at 4 °C to separate the aqueous, RNA-containing phase from the organic phase. The aqueous phase was collected into a new tube and isopropanol was added at half the original Trizol volume. The samples were incubated for 10 minutes at room temperature and were then centrifuged at 12,000 x g for 10 minutes at 4 °C to pellet the RNA. The pellet was washed with 75% ethanol at the original Trizol volume and centrifuged again at 7,500 x g for 5 minutes. Finally, the RNA pellet was air dried, resuspended in RNAase-free H_2O and incubated at 55-60 °C to help dissolve the pellet.

6.2. RNAeasy (Qiagen)

Whole embryos were collected in buffer RLT, homogenised by passing the sample through a syringe needle several times and processed according to the supplier's instructions.

7. Reverse transcription (RT)

cDNA was synthesised using 1μg total RNA with Superscript reverse transcriptase II (Invitrogen), according to the supplier's instructions. The samples were kept at -20 °C.

8. Quantitative real time PCR

Quantitative real time PCR primers were designed to span one or more exons. Some primer sequences were obtained from Primerbank (http://pga.mgh.harvard.edu/primerbank/index.html), a public database of PCR primers specifically designed for use in quantitative real time PCR (Wang and Seed, 2003).

Primers were synthesised by Sigma Aldrich or Operon. All the oligonucleotides and cycling conditions used are detailed in APPENDIX II.

The reactions were carried out in MicroAmp^{TM} (Applied Biosystems) optical plates and adhesive covers. SYBR green PCR master mix (Qiagen) was used, according to the supplier's instructions. All reactions were performed in triplicate on an ABI Fast Real Time PCR system 7900 HT (Applied Biosystems). Product specificity was determined by analysing the dissociation curves. These curves highlight the melting temperature of the double-stranded product and the presence of primer dimers. Expression values were determined as previously reported, from the data collected from the SDS2.2.1 software (Bookout and Mangelsdorf, 2003). Expression values for each gene were normalised to *Gapdh* expression. Relative changes in gene expression were calculated by comparing the normalised expression values in the control samples with the normalised expression values in the other samples. The values are reported as the mean fold change relative to the controls, which were designated the value of one.

9. Protein extraction

9.1. Embryo collection

Embryos for protein extraction were collected in cold PBS, transferred immediately into RIPA buffer, homogenised by passing the sample through a syringe needle several times and incubated for 1.5 hours at 4 °C rocking. Protease (Complete, Roche, UK) or phosphatase (PhosSTOP, Roche, UK) inhibitors were added to the buffer and the samples were centrifuged at maximum speed for 10 minutes, the supernatant was collected and stored at -80 °C.

9.2. Protein quantification - Bradford

Protein samples were quantified using the Bradford method, by creating a standard curve. The following Bovine serum albumin (BSA) (Biorad) dilutions were prepared. One µl of each protein sample was diluted in 800µl distilled H_2O.

Sample	BSA	H_2O	Final BSA concentration
1	0µl	800µl	0µg/ml
2	10µl	790µl	1.5µg/ml

3	20µl	780µl	3µg/ml
4	40µl	760µl	6µg/ml
5	80µl	720µl	12µg/ml
6	120µl	680µl	18µg/ml

In each tube 200µl of Bradford solution (Biorad) was added, the samples were incubated for 5 minutes at room temperature and an absorbance reading at 595nm was taken for each.

9.3. Western Blotting

9.3.1. Protein denaturation

The protein samples were mixed with 6X in laemmli buffer containing 10% 2-mercaptoethanol, denatured by incubation for 10 minutes at 100 °C, cooled on ice, centrifuged and used for electrophoresis.

9.3.2. SDS - Polyacrylamide gel electrophoresis (PAGE)

The gels were prepared with a 10-15% acrylamide resolving gel (ProtoGel acrylamide mix, National Diagnostics, 0.375M Tris pH 8.8, 0.1% SDS, 0.1% APS, 1% TEMED, in distilled H_2O) and a 10% acrylamide stacking gel (ProtoGel acrylamide mix, National Diagnostics, 0.13M Tris pH 6.8, 0.1% SDS, 0.1% APS, 1% TEMED, in distilled H_2O). A colour protein ladder (Precision Plus Protein™ Kaleidoscope™, Biorad) was also loaded. The denatured protein samples were electrophoresed in 1X Running buffer at 100-150V at room temperature until the ladder bands had separated sufficiently.

9.3.3. Western Blotting

The electrophoresed proteins were transferred onto an Immuno-Blot™ PVDF membrane (Biorad) by wet transfer for 2 hours at 150mA at 4 °C in 1X Transfer buffer. The PDVF membrane was equilibrated in 100% MeOH for 10 minutes prior to use.

9.3.4. Immunodetection

The membrane was rinsed once in 1X TBS and blocked for 1-2 hours at room temperature in blocking buffer (5% non-fat milk in 1X TBS/0.05%Tween or 5% BSA in 1X TBS/0.1%Tween for phosphorylated proteins), rocking. The membrane was

washed briefly in 1X TBS/0.05%Tween and incubated with the primary antibody diluted in blocking buffer O/N at 4 °C, rocking. The next day the membrane was washed four times in 1X TBS/0.5%Tween for 10 minutes at room temperature, rocking and incubated with the appropriate 1/2,500 HPR-linked secondary antibody, diluted in blocking buffer for 1 hour at room temperature, rocking, followed by four washes in 1X TBS/0.5%Tween for 10 minutes at room temperature, rocking. The signal was detected using the ECL Western Blotting detection Reagents (GE Healthcare), performed according to the supplier's instructions, followed by overlaying an X-Ray film on the membrane and film developing. All antibodies used are detailed in APPENDIX I.

9.3.5. Membrane stripping

The membrane was stripped for 30 minutes at room temperature, rocking, in Restore™ PLUS Western Blot Stripping Buffer (Thermo Scientific), and was used for further immunodetection.

10. Whole mount in situ hybridisation

The digoxygenin-labeled RNA probes were created in the laboratory by IMAGE clones obtained from Geneservice Limited (UK) or imaGenes (Germany), except for *Smad7* (Christine Mummery), *Hes1* (Francois Guillemot), *Tbx1* (Albert Basson), *Fgf8* (Gail Martin), *Fgf10* (Albert Basson), *Etv4*, *Slit1* (Marc Tessier-Lavigne) and *Slit2* (David Ornitz) that were kindly offered by other groups.

All the plasmids acquired from Geneservice Limited (UK) and were used for RNA probe transcription were verified through sequencing using BigDye® Terminator v3.1 Cycle Sequencing Kit (Applied Biosystems, USA). All the plasmids acquired from imaGenes (Germany) were provided EST sequence verified.

10.1. Ribophore labeling and purification

10.1.1. Plasmid linearisation

Five μg of plasmid DNA was linearised with an appropriate enzyme to create a 5' overhang. The enzymes and RNA polymerases used for each vector are detailed in APPENDIXIII. The linear DNA was purified by phenol-chloroform extraction.

10.1.2. Labelling

The *in vitro* transcription reaction was performed by combining the following: 4µl 5X transcription buffer (Promega), 2µl 0.1M DTT, 2µl DIG-labeled NTPs, 10.5µl (1µg) linearised plasmid, 0.5µl Ribonuclease inhibitor (40u/µl) and 2µl SP6, T7 or T3 RNA polymerase (10u/µl) (Promega). The mixture was incubated at 37 °C for 2 hours (or 40 °C for SP6). 1µl of the probe was electrophoresed on a 1% agarose gel to check synthesis. An RNA band of approximately 10-fold greater intensity than the plasmid band indicated that approximately 10µg of probe had been synthesised.

10.1.3. Purification

The RNA probe was purified by dilution of the reaction in DEPC H_2O and precipitation on ice by adding 1/10 volume of RNAase-free 3M sodium acetate (pH 5.2) and 2.5 volumes of ice-cold RNAase-free 100% EtOH for 1.5 hours. This was followed by centrifugation for 15-20 minutes at 12,000 x g. The pellet was washed in ice-cold RNAase-free 70% EtOH, centrifuged for 10 minutes at 12,000 x g and finally resuspended in DEPC H_2O.

10.2. Embryo collection

Embryos for whole mount *in situ* hybridisation were collected in cold PBS, fixed in 4% paraformaldehyde in PBS O/N, dehydrated in a gradient series of methanol (MeOH)/PBT (PBS, 0.1% Tween-20) and kept in 100% MeOH at -20 °C.

10.3. Embryo pretreatment

The embryos were rehydrated in a gradient series of methanol/PBT for 5 minutes and two washes in PBT for 5 minutes. The embryos were then bleached by incubating for 1 hour in fresh 6% H_2O_2 (1/5) in PBT. This was followed by three washes in PBT for 5 minutes and incubation in 10µg/ml Proteinase K (Roche, UK) in PBT for 4-15 minutes depending on the embryo stage (Table 2.1). The embryos were washed three times in PBT for 5 minutes and refixed for 20 minutes in 4% paraformaldehyde/0.2% glutaraldehyde in PBT. They were then washed twice in PBT for 5 minutes, once in 1:1 mixture of PBT/Hybridisation solution for 10 minutes and once in Hybridisation solution for 10 minutes. The embryos were subsequently incubated, rocking, at 70 °C for over two hours.

embryo age (embryonic day)	duration of incubation (minutes)
6.5	4
7.5	4-5
8.5	6
9.5	7
10.5	8-10
11.5	12
12.5	15

Table 2. 1. Embryo stage and incubation times in 10µg/ml Proteinase K in PBT for whole mount *in situ* hybridisation.

10.4. Embryo hybridisation

The embryos were incubated in 0.3mg/ml DIG-labeled RNA in Hybridisation solution at 70 °C, O/N.

10.5. Post hybridisation washes, blocking and antibody incubation

The embryos were washed once in Hybridisation solution for 5 minutes at 70 °C and twice in Solution I for 30 minutes at 70 °C, rocking. This was followed by one wash in Solution I and three washes in Solution II for 30 minutes at 65 °C, rocking. The embryos were cooled down to room temperature in the final solution and washed three times in MAB for 5 minutes at room temperature, rocking. The embryos were then blocked in MAB/2% BBR/10% heat inactivated sheep serum (GIBCO, Invitrogen) for 60-90 minutes at room temperature, rocking. The Anti-Digoxigenin-AP Fab fragments (Roche, UK) antibody was pre-absorbed while embryos were blocking (3mg embryo powder was weighed in an eppendorf tube with 0.5ml MAB/2% BBR, which was incubated at 70 °C for 30 minutes, rocking. This was vortexed thoroughly, cooled on ice, 5µl heat inactivated sheep serum and 1µl of antibody was added, and the mix was incubated for 60-90 minutes at 4 °C, rocking. This was centrifuged at maximum speed for 10 minutes and the supernatant was collected. The embryos were incubated in

1/2,000 pre-absorbed antibody (the 0.5ml supernatant collected was diluted in 1.5ml MAB/2% BBR/1% heat inactivated sheep serum) O/N at 4 °C, rocking.

10.6. Post antibody washes

The antibody solution was removed and the embryos were washed three times in MAB for 5 minutes at room temperature, rocking, followed by at least five washes in MAB for 60-90 minutes at room temperature, rocking, while the last wash was performed O/N at 4 °C, rocking.

10.7. Colour development

The embryos were washed three times in NTMT for 10 minutes at room temperature, rocking and then incubated in BM Purple staining solution in the dark, at room temperature, rocking, for as long as each probe required for developing to the desired extent. The colour reaction was stopped rinsing the embryos in 2mM EDTA/PBT. The embryos were then postfixed in 4% paraformaldehyde in PBS for 1 hour at room temperature or O/N at 4 °C, rocking. The embryos were washed twice in PBS for 10 minutes at room temperature, rocking and stored in PBS at 4 °C.

10.8. Viewing/Imaging

The imaging was conducted by a Zeiss SteREOLumar.V12 stereomicroscope equipped with AxioCam HRc digital camera and AxioVis40 v4.41.0 digital imaging software. The images were processed with Adobe Photoshop CS.

11. Embryo powder

Embryos at E13.5-E15.5 (approx. 5 litters) were collected in cold PBS, and the heads were removed. The embryos were homogenised in 3ml ice-cold PBS, using a glass tissue homogeniser. Four volumes of ice-cold acetone were added (12ml), the homogenate was mixed vigorously and left on ice for 30 minutes, while mixed every 5-10 minutes. The homogenate was centrifuged at 10,000 rpm for 10 minutes at 4 °C, the pellet was resuspended in ice-cold acetone by vigorous mixing and left on ice for 10 minutes. This was centrifuged at 10,000 rpm for 10 minutes at 4 °C, the pellet was transferred to a clean filter paper and was spread and dispersed repeatedly with a

spatula. It was let to air dry O/N at room temperature and the next day it was collected in an eppendorf tube and stored at 4 °C.

12. X-gal staining

Embryos were collected in cold $MgCl_2$/PBS, fixed in 1% paraformaldehyde/0.2% glutaraldehyde in 2mM $MgCl_2$/PBS for 20-30 minutes at room temperature, washed three times in 2mM $MgCl_2$/PBS for 5 minutes at room temperature and used immediately for X-gal staining. The embryos were then incubated in X-gal buffer containing 1mg/ml X-gal (Promega) at 37 °C until the staining developed to the desired extent. The embryos were rinsed in PBS and fixed O/N in 4% paraformaldehyde in PBS.

13. Intracardiac ink injection

Embryos were collected in cold PBS, fixed in 4% paraformaldehyde in PBS O/N at 4 °C, washed three times in PBS and stored in PBS at 4 °C. Indian Ink (Pelikan) was injected into the outflow tract or aorta of embryos using a microinjection needle to visualise the pharyngeal arch arteries or great vessels of the heart.

14. Embedding and sectioning

14.1. Paraffin embedding

The embryos were dehydrated in 1:1 PBS/EtOH, followed by a gradient series of EtOH washes (70%-100%), at room temperature for at least 30 minutes. This was followed by two washes in Histoclear (National Diagnostics, UK) at room temperature for 30 minutes, one wash in a 1:1 Histoclear/ Paraffin solution at 60 °C for 20 minutes and three washes in paraffin at 60 °C for 30-60 minutes. The embryos were placed in the appropriate molds and left to set at least O/N before sectioning.

The embedded embryos were sectioned at 5-10μm thickness in coronal, transverse or parasagittal planes. The sections were flattened on water at 42 °C, set on TESPA coated slides (2% 3-aminopropyl-triethoxysilane in acetone) and air dried O/N. Rehydration of the sections was performed through incubation at 60 °C for 10 minutes two washes in Histoclear for 10 minutes, followed by a gradient series of EtOH washes (100%-30%) and two washes in distilled H_2O, for 2 minutes, at room temperature. Counterstaining

was performed in hematoxylin (Raymond A Lamb, UK) for 3 minutes followed by eosin (Raymond A. Lamb, UK) for 1 minute. The sections were air-dried O/N and mounted with DPX mountant (Merck, UK).

14.2. OCT embedding

Embryos were collected in cold PBS, fixed in 4% paraformaldehyde for 2-3 hours at 4 °C, rinsed in PBS once and left to equilibrate in 30% sucrose in PBS O/N at 4 °C. They were then transferred in 1:1 sucrose/Optimal Cutting Temperature double (OCT) and frozen in 100% OCT on dry ice. OCT-embedded embryos were sectioned in coronal, transverse or parasagittal planes. Sections were cut at 10μm, collected onto Superfrost+ glass slides, allowed to dry and stored at -80 °C.

15. Immunohistochemistry

Slides were allowed to reach room temperature and were rinsed once in PBS to remove OCT before being permeabilised with 0.5% Triton X-100/PBS for 5 minutes at room temperature. They were rinsed twice in PBS, allowed to dry to enable use of Immedge pen to draw around the sections and were then blocked for 1 hour in blocking buffer (1% BSA, 10% serum). The slides were subsequently incubated with the primary antibody diluted in blocking buffer, O/N at 4 ^{0}C. The next day the slides were washed three times in 0.1% Triton X-100/PBS and rinsed twice in PBS. They were then incubated with the secondary antibody diluted in blocking buffer 1/500 for 1 hour at room temperature and washed three times in PBS for 5 minutes. DAPI (1/25,000 in PBS) was added onto the slides for 20 seconds to visualise the nuclei and the slides were washed three times in PBS for 5 minutes before mounting with CitiFluor^{TM} (Citifluor Ltd). All antibodies used are detailed in APPENDIX I.

16. Viewing/Imaging

Imaging for counterstained sections was conducted by a Zeiss Axiophot 2 microscope, equipped with a Kontron Prog/Res/3012 digital camera, using Adobe Photoshop 6 as the image importing software. The images were subsequently processed with Adobe Photoshop CS. For sections processed for immunofluorescence a Zeiss Imager Z.1 microscope equipped with AxioCam MRm digital camera and AxioVis40 v4.7.1 digital imaging software was used. The images were processed with Adobe Photoshop CS.

17. Cloning

17.1. Plasmid mini-midi-maxi preps

IMAGE clone plasmid DNA and Bacterial artificial chromosomes (BACs) were received as stab cultures (Geneservice Limited, UK or imaGenes, Germany). On arrival, bacteria were streaked out onto LB plates containing the appropriate antibiotic and left to grow O/N at 37 °C. A culture of LB broth containing the appropriate antibiotic was inoculated with one colony and incubated O/N at 37 °C, shaking. 20% glycerol stocks were prepared and stored at -80°C. Purified plasmid DNA was isolated using Qiagen plasmid purification kits (Qiagen) according to the supplier's instructions. Plasmid DNA was eluted in either distilled H_2O or EB buffer.

17.2. Digests

Digests of plasmid DNA were carried out in a total volume of 50µl using 1-5µg plasmid DNA, 5µl 10X enzyme buffer, 0.5µl 100X BSA, 1-2u of enzyme in distilled H_2O. The plasmids were digested at the appropriate temperature for optimal enzyme activity for 2 hours and then electrophoresed on an agarose gel for analysis.

17.3. Gel extraction

Gel extraction was carried out to isolate and purify DNA fragments from agarose gels. The QIAquick gel extraction kit (Qiagen) was used following the manufacturer's instructions and DNA was eluted in 30µl distilled H_2O.

17.4. TA cloning

Purified PCR products were cloned directly into plasmids using TOPO XL PCR Cloning Kit (Invitrogen, UK) or pGEM-T Easy Vector System (Promega, UK), according to manufacturer's instructions.

17.5. Ligation

For each ligation of a linear plasmid vector and a corresponding DNA fragment three different insert/vector molar ratios (3:1, 1:1, 1:3) as well as a vector only control were used. The quantity (ng) of the insert was calculated each time by the formula (Promega):

$$\frac{\text{ng vector x size (kb) of insert}}{\text{size (kb) of vector}} \text{ x insert/vector molar ratio = ng of insert}$$

Essentially, 100ng plasmid vector, ng of insert accordingly, 1µl 10X ligation buffer (Promega), 1µl T4 DNA ligase (Promega) and distilled H_2O to a total volume of 10µl were mixed together. The ligation reaction was incubated O/N at 16 °C, according to the supplier's instruction.

17.6. De-phosphorylation of plasmids

The TKGL2 plasmids were de-phosphorylated to remove the phosphate groups from the 5'-ends to prevent self-ligation of the vector. Shrimp alkaline phosphatase (SAP) (USB) was used following the supplier's instructions. The firefly luciferase vector TKGL2 was obtained from the Anita Rauch (Institute of Human Genetics, Schwabachanglage, Germany). It was digested at 37ºC overnight using Acc65I simultaneously with calf intestinal alkaline phosphatase (CIAP) in the Acc65I buffer to prevent self ligation.

17.7. Transformation

Transformation of plasmid, BAC DNA or ligation product into JM109 competent cells (Promega) by thawing the cells on ice, adding the DNA into the cells and incubating for 20 minutes on ice, performing a heat shock for 45 seconds in a 42 ºC water bath and growing in 1ml LB broth for 1 hour at 37ºC, shaking. Finally, 200µl was plated on an LB agar plate with the appropriate antibiotic and incubated O/N at 37 ºC.

18. Mammalian cell culture

Jeg3 cells were obtained from Anita Rauch, (Institute of Human Genetics, Schwabachanlage, Erlangen, Germany). They were cultured in RPMI 1640 + Glutamax medium (GIBCO, Invitrogen) supplemented with 10% fetal bovine serum (FBS) and 1% penicillin/streptomycin (GIBCO, Invitrogen). Cells were maintained at 37 °C, 5% CO_2 in a humidified chamber.

19. Cell transfections

Lipofectamine 2000 (Invitrogen) was used for cell transfections, according to the supplier's instructions.

20. Luciferase assay

Transfected cells were lysed 24 hours post transfection and the luciferase activity was measured.

20.1. β-galactosidase Luciferase Assay

The cells were washed in PBS and lysed in 200µl 1X Reporter Lysis Buffer (Promega) for 15 minutes at room temperature. The cells were then scraped using the end of a pipette tip and the lysate was transferred to eppendorf tubes. The tubes were centrifuged at maximum speed for 2 minutes and the supernatant was collected.

For the luciferase reading, 20µl of each lysate was transferred to a round bottom tube and 100µl of luciferase buffer (Promega) was added to each tube individually and immediately before taking a reading using the TD-20/20 Luminometer (Turner Designs, USA) set at a 3 second delay followed by a 15 second reading. For β-galactosidase activity measurement, 75µl of each cell lysate was added to 75µl of 1X Reporter Lysis Buffer and 150µl β-galactosidase assay buffer (0.2M Na phosphate, 2mM $MgCl_2$, 0.1M 2-mercaptoethanol, 1.5mg/mL *ortho*-Nitrophenyl-β-galactoside). A blank tube was also prepared. The tubes were vortexed and incubated at 37 ºC until a yellow colour developed. The reaction was stopped with 500µl 2M Na_2CO_3 and the tubes were centrifuged for 2 minutes. An absorbance reading at 420nm was taken using the Nanodrop ND-1000.

20.2. Dual Luciferase Assay

This assay was performed using the Dual Luciferase Assay Kit (Promega). The cells were washed in PBS and lysed using 250µl 1X Passive Lysis Buffer (PLB) for 15 minutes. The PLB does not require cell scraping afterwards. 20µl of each lysate was transferred to round bottom tubes and the luciferase assay and normalisation was performed according to the manufacturer's protocol. Essentially, two readings are obtained – one for firefly luciferase activity and the other for renilla luciferase activity (for normalisation).

21. Bone and cartilage staining

Embryos were collected in cold PBS and processed immediately for bone and cartilage staining. This was performed by fixing the embryonic heads in 95% EtOH for 3 days

and then placing them in acetone for at least two days, at room temperature. The heads were stained for at least 3 days in fresh bone and cartilage staining solution at 37 ºC. The heads were washed in distilled H_2O and cleaned in 1% KOH for several days, until the skeleton was visible through the tissue. Then they were cleaned through 20%, 50% and 80% glycerol 1:1 with KOH and stored in 100% glycerol.

22. Bioinformatics

Genome sequences were acquired from the UCSC Genome Bioinformatics Site (http://genome.cse.ucsc.edu/). The sequences were aligned using the Multiple sequence local alignment and visualisation tool (MULAN, http://mulan.dcode.org/). The user defined consensus sequence search for the T-half site was performed using the TCACAM sequence, whereby M = A or C.

23. Statistics

Chi square, Fisher's exact test (one tailed), t-test (two tailed) or Mann-Whitney U test were used for statistical analysis of the data collected in this thesis. The significance level was set at $p<0.05$. The Mann-Whitney U test, which uses a system of rankings and assigned values, was performed by hand.

24. Gel band quantification

ImageJ was use to quantify western blot and agarose gel electrophoresed samples.

III. SMAD7

1. Introduction – Literature review

1.1. TGFβ pathway

1.1.1. Biological functions

TGFβ family cytokines have many and diverse roles in embryonic development, being involved in processes like embryonic asymmetry, stem cell self renewal and differentiation, growth, cell proliferation and differentiation, ECM remodelling, immune response, organogenesis and wound healing (Guo and Wang, 2009; Javelaud and Mauviel, 2004; Moustakas and Heldin, 2009; Park, 2005; Yan et al., 2009). Aberrations in the TGFβ signalling are often linked to human disease, including cancer, tissue fibrosis and autoimmune disorders (Guo and Wang, 2009; Javelaud and Mauviel, 2004; Kamiya et al., 2010; Moustakas and Heldin, 2009; Park, 2005; Yan et al., 2009).

1.1.2. Protein interactions

The TGFβ superfamily is divided into two subfamilies, the TGF-β/activin/nodal/myostatin/inhibin consisting group and the BMP/anti-mullerian hormone (AMH) and growth and differentiation factors (GDFs) group (Moustakas and Heldin, 2009; Yan et al., 2009). All TGFβ ligands are synthesised as precursor proteins, with a longer N-terminal pro-peptide, known as the latency-associated peptide (LAP), followed by a shorter C-terminal mature polypeptide (Javelaud and Mauviel, 2004; Moustakas and Heldin, 2009). Proteases cleave the TGFβ LAP from the mature peptide, which however remain in association, with the LAP enveloping the smaller mature peptide within its core (Javelaud and Mauviel, 2004; Moustakas and Heldin, 2009). ECM components, the latent TGFβ-binding proteins (LTBPs), associate with this complex and regulate the secretion and storage of TGFβ (Javelaud and Mauviel, 2004; Moustakas and Heldin, 2009; Yan et al., 2009). Several of the TGFβ family members have this TGFβ LAP ability of maintaining the ligand in an inactive state, but not all (Moustakas and Heldin, 2009). Most tissues are abundant in latent TGFβ, although activation of minimal amounts of it are enough to generate maximal cellular response (Bujak and Frangogiannis, 2007). The TGFβ ligands transduce their signal through serine/threonine kinase transmembrane type I and type II receptors and their downstream effectors, the Smads (Moustakas and Heldin, 2009; Ross and Hill, 2008).

Five type II and seven type I receptors of the TGFβ superfamily have been identified in mammals and each TGFβ/BMP pathway ligand binds to a characteristic combination of type I and type II receptors (Table 3.1) (Ikushima and Miyazono, 2010; Moustakas and Heldin, 2009; Ross and Hill, 2008; ten Dijke and Hill, 2004). The receptors form hetero-tetrameric complexes in the presence of the dimeric ligand (Ikushima and Miyazono, 2010; Moustakas and Heldin, 2009). Upon activation, TGFβ ligands bind to type II receptors and the complex activates the type I receptors, also known as activin receptor-like kinases (ALKs), by phosphorylation in the juxtamembrare region (Javelaud and Mauviel, 2004; Ikushima and Miyazono, 2010; Moustakas and Heldin, 2009; Ross and Hill, 2008; ten Dijke and Hill, 2004; Wrana, 2000). This leads to subsequent downstream signals through activation of the receptor activated Smads (R-Smads, Smad1, Smad2, Smad3, Smad5 and Smad8) that form complexes with the common mediator Smad4 (co-Smad), translocate to the nucleus and together with other transcription factors, regulate gene expression (Bujak and Frangogiannis, 2007; Javelaud and Mauviel, 2004; Ikushima and Miyazono, 2010; Moustakas and Heldin, 2009; Park, 2005; ten Dijke and Hill, 2004; Wrana, 2000). The TGFβ/nodal/activin pathways signal via Smad2 and Smad3, while the BMP/GDF pathways via Smad1, Smad5 and Smad8 (Figure 3.1) (Moustakas and Heldin, 2009; Yan et al., 2009). In the case of Smad2/3 the interaction between the type I receptor and the R-Smads is facilitated by the membrane-bound scaffold protein Smad anchor for receptor activation (SARA) and the adaptor molecule Dab2 (Ross and Hill, 2008). Although the pathway is otherwise very conserved, in endothelial cells TGFβ ligands can induce phosphorylation of Smad1, Smad5 and Smad8 through a receptor complex that contains the tissue-specific Alk1 type I receptor (Ross and Hill, 2008). Inhibitory Smads (I-Smads, Smad6-7) are negative regulators of the TGFβ/BMP signalling and are induced by TGFβ, BMP or activin signals through activated R-Smad complexes, thus establishing a negative feedback loop (Park, 2005; Yan et al., 2009). Smad7 is a general antagonist of both the TGFβ and BMP pathways, whereas Smad6 preferentially inhibits the latter (Moustakas and Heldin, 2009; Park, 2005; Ross and Hill, 2008; Yan et al., 2009). Both I-Smads act by stably binding to type I receptors, competitively preventing R-Smad binding and phosphorylation (Park, 2005; Ross and Hill, 2008; ten Dijke and Hill, 2004; Yan et al., 2009). Subsequently the I-Smads recruit phosphatases and E3-ubiquitin ligases, known as Smad ubiquitination regulatory factors (Smurfs, Smurf1 and Smurf2), to the

activated type I receptor leading to proteasomal degradation of the receptor and termination of the signalling (Ross and Hill, 2008; ten Dijke and Hill, 2004; Yan et al., 2009). During this process Smad7 itself is degraded (Yan et al., 2009). I-Smads can additionally inhibit co-activator recruitment by the R-Smads, interfere with the formation of the R-Smad/co-Smad complexes, (Moustakas and Heldin, 2009; Park, 2005; Ross and Hill, 2008), or bind to and disrupt Smad-DNA complexes in the nucleus, thereby inhibiting their transcriptional activity (Moustakas and Heldin, 2009; Ross and Hill, 2008; Yan et al., 2009). Smad7 also negatively regulates the pathway by promoting dephosphorylation and hence deactivation of TGFβ type I receptors through recruitment of a complex of GADD34 and the catalytic subunit of protein phosphatase 1 (Shi et al., 2004).

PATHWAY	TFGβ	BMP	GDF	Activin	AMH
Ligand	TFGβ1	BMP2,4	GDF5,6,7	Inhibin βA	AMH
	TFGβ2	BMP5,6,7	GDF9b	Inhibin βB	
	TFGβ3	BMP8A,8B	GDF10,11	Nodal	
		BMP9,10	GDF15		
			GDF1,3		
			GDF8		
			GDF9		
RII	TβRII	BMPRII	BMPRII	ActRIIA	AMHRII
		ActRIIA, ActRIIB	ActRIIA, ActRIIB	ActRIIB	
RI	TβRI (ALK5)	BMPRIA (ALK3)	BMPRIA (ALK3)	ActRIB (ALK4)	BMPRIA (ALK3)
	ALK1	BMPRIB (ALK6)	BMPRIB (ALK6)	ALK7	BMPRIB (ALK6)
	ALK2	ALK2	ALK2		ALK2
	BMPRIA (ALK3)	ALK1	ActRIB (ALK4)		
			ALK7		
			TβRI (ALK5)		
R-Smad	SMAD2,3	SMAD1,5,8	SMAD1,5,8	SMAD2,3	SMAD1,5,8
	SMAD1,5,8		SMAD2,3		
Co-Smad	SMAD4	SMAD4	SMAD4	SMAD4	SMAD4
I-Smad	SMAD7	SMAD6,7	SMAD7	SMAD7	SMAD6,7

Table 3. 1. TGFβ superfamily signalling factors in human. Receptors are listed as type II (RII), and type I (RI). Ligands, type I receptors and R-Smads are color-coded: blue, BMP-like pathways; red, TGF/activin-like pathways. Modified from Moustakas and Heldin, 2009.

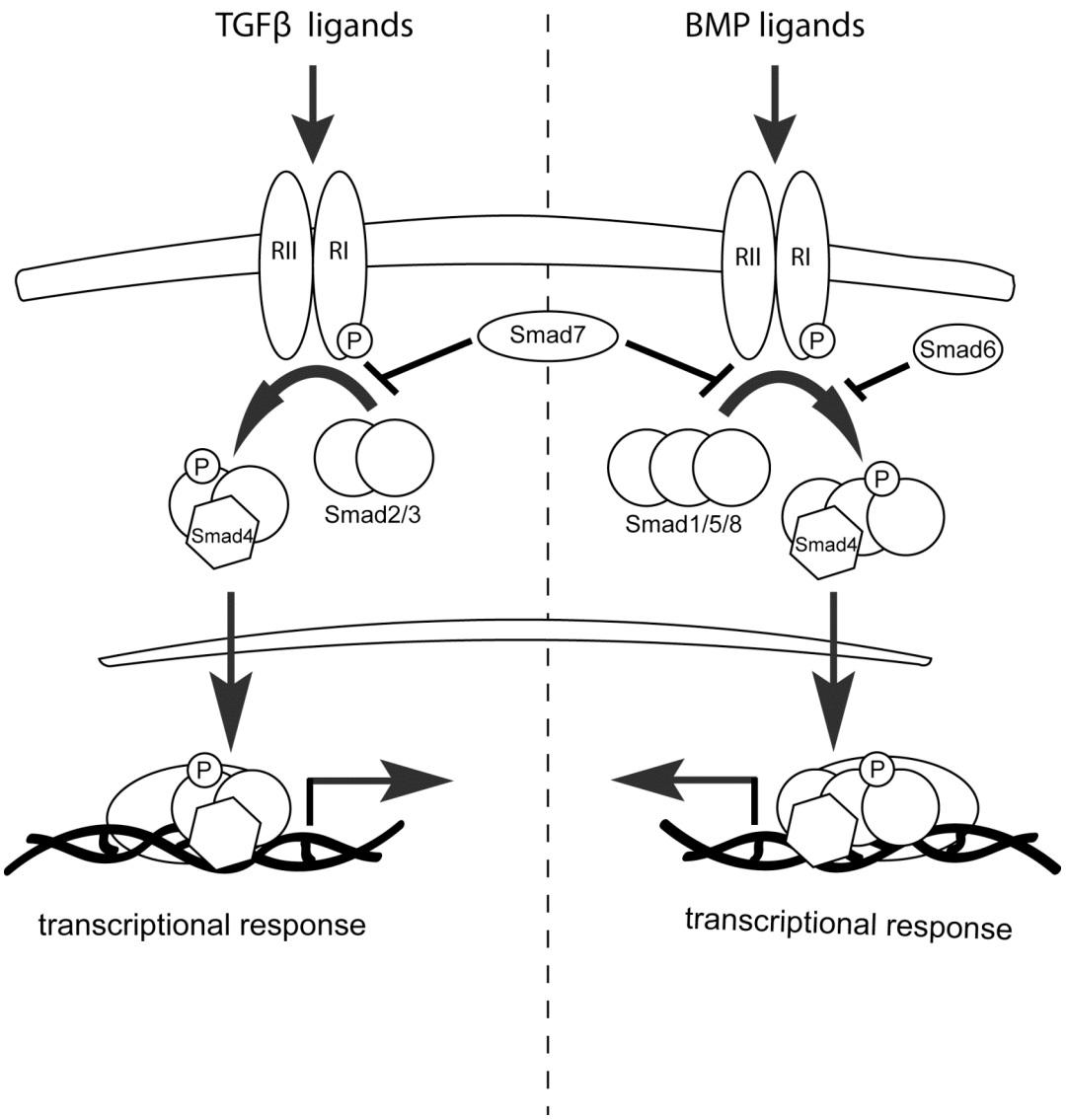

Figure 3. 1. Simplified schematic representation of the TGFβ/BMP pathways. Upon ligand binding receptor activated Smad complexes (Smad2/3 or Smad1/5/8) become phosphorylated and associate with the common mediator Smad4, translocate to the nucleus and together with other transcription factors, regulate gene expression. Smad7 inhibits both branches of the pathway, while Smad6 selectively inhibits the BMP branch.

1.1.3. Smad proteins

Smad proteins are characterised by two highly conserved regions, the Mad-homology 1 (MH1) domain at the N-terminus and the MH2 domain at the C-terminus, which are joined together by an intermediate linker domain (Ross and Hill, 2008; Yan et al., 2009). The MH1 domain carries NLSs and a DNA-binding domain and is important

for cytoplasmic anchoring, nuclear import and gene transcription regulation (Ross and Hill, 2008; Yan et al., 2009). The MH2 domain binds to type I receptors, can interact with other proteins, mediates Smad homo- and hetero-complex formation as well as cytoplasmic anchoring and transactivation of target genes (Ross and Hill, 2008; Yan et al., 2009). The linker domain is rich in prolines and phosphorylatable serines or threonines and interacts with prolyl-isomerases and ubiquitin ligases (Moustakas and Heldin, 2009). Both Smad6 and Smad7 have the conserved C-terminal MH2 domain, but not the N-terminal MH1 domain or the phosphorylation site by the type I receptors at the C-terminal tail (Figure 3.2) (Park, 2005; Yan et al., 2009). The two I-Smads are similar in only 36.7% of their N-terminus (Yan et al., 2009). Smad7 facilitates specific inhibition of the TGFβ/activin signalling through both its N-terminus and MH2 domains (Yan et al., 2009).

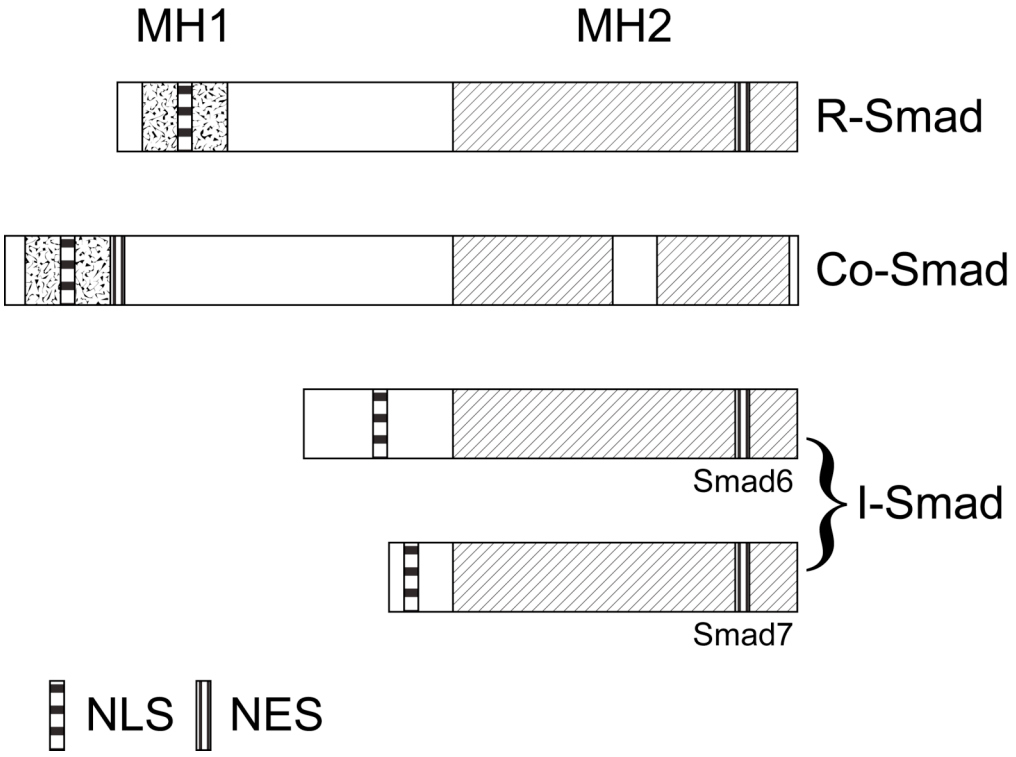

Figure 3. 2. Smad protein structure. Simplified structures of the mammalian Smad proteins divided into receptor-activated Smads (R-Smad), common-mediator Smad (Co-Smad) and inhibitory Smads (I-Smad). The conserved N-terminal Mad-homology 1 (MH1) (speckled shading) and C-terminal MH2 (angled-stripped box) domains are shown as well as the nuclear localisation signal (NLS, horizontal-striped box) and the nuclear export signal (NES, vertical-striped box). Co-Smad, common-mediator Smad; I-Smad, inhibitory Smad; MH, mad homology; NLS, nuclear localisation signal; NES;

nuclear export signal; R-Smad, receptor-activated Smad. Drawn after Moustakas and Heldin, 2009.

1.1.4. Cross-talk with other pathways

Several elements of the TGFβ/BMP pathways, and primarily the Smad proteins, make direct and dynamic contacts with numerous other proteins (Guo and Wang, 2009). Moreover, TGFβ signalling has multiple targets, both transcriptional and non-transcriptional, that all combined provide interconnections with other cellular signalling pathways (Guo and Wang, 2009). This cross-talk includes pathways such as the MAPK, P13/Akt, Wnt, SHH, Notch, IL, TNFβ and IFN-γ (Guo and Wang, 2009; Park, 2005). In that respect, I-Smads are also induced by other extracellular stimuli, apart from the TGFβ/BMP regulation (Park, 2005).

1.1.5. Smad7 interactors/regulators

I-Smad expression and duration are essentially regulated at the transcriptional level or by post-translational degradation at the protein level in cells (Park, 2005). The TGFβ/activin pathway controls *Smad7* expression through direct binding of Smad3 and Smad4 to the *Smad7* promoter (Nagarajan et al., 1999). Also, the Ski protein with co-operation of Smad4 inhibits the *Smad7* promoter basal activity (Park, 2005). Degradation of Smad7 by Arkadia, promotes TGFβ/BMP signalling (Yan et al., 2009). Jab1/CSN5, a protein complex that is part of the COP9 signalosome complex, regulates the stability of Smad7 and thus effects TGFβ/BMP signalling (Yan et al., 2009). Smad7 binding partners like Hic-5/ARA55, Yes-associated protein (YAP65), the salt-inducible kinase (SIK), and Crk-associated substrate lymphocyte type (Cas-L) contribute in the regulation of the pathway (Yan et al., 2009). Smad7 can be acetylated by the coactivator protein p300 and deacetylated by histone deacetylases (HDACs) or SIRT1 (Yan et al., 2009). Smad7 acetylation inhibits its ubiquitination and subsequent degradation, so Smad7 degradation is regulated by the balance between acetylation, deacetylation, and ubiquitination (Yan et al., 2009). Smad7 is also known to stabilise β-catenin by protecting it from degradation by inhibiting its phosphorylation by Gsk3-β and by inhibiting recruitment of the ubiquitin ligase Smurf2, *in vitro* (Tang et al., 2008). A β-catenin/E-cadherin complex is thus favoured over a β-catenin degradation in the cytoplasm, promoting cell adhesion (Tang et al., 2008).

1.2. *TGFβ*/*BMP*/*Smad* gene mutations

Members of the *TGFβ* superfamily have been studied by means of gene knock-out or conditional mutagenesis in the mouse, which display a range of phenotypes including cardiovascular defects (Chen et al., 2004; Chen et al., 2009; Choudhary et al., 2006; Galvin et al., 2000; Gaussin et al., 2005; Gaussin et al., 2002; He et al., 2002; Jia et al., 2007; Jiao et al., 2003; Kaartinen et al., 2004; Kim et al., 2001; Li et al., 2006; Liu et al., 2004; Ma et al., 2005; Molin et al., 2002; Nie et al., 2008; Sanford et al., 1997; Solloway and Robertson, 1999; Song et al., 2007; Stottmann et al., 2004; Tang et al., 2010; Todorovic et al., 2007; Wang et al., 2006; Wurdak et al., 2005; Zhang and Bradley, 1996). The majority of the knock-outs are embryonic lethal and induce cardiovascular phenotypes including great vessel, valve and outflow tract defects, as well as cardiac hypertrophy and fibrosis (Chen et al., 2004; Chen et al., 2009; Choudhary et al., 2006; Galvin et al., 2000; Gaussin et al., 2005; Gaussin et al., 2002; He et al., 2002; Jia et al., 2007; Jiao et al., 2003; Kaartinen et al., 2004; Kim et al., 2001; Li et al., 2006; Liu et al., 2004; Ma et al., 2005; Molin et al., 2002; Nie et al., 2008; Sanford et al., 1997; Solloway and Robertson, 1999; Song et al., 2007; Stottmann et al., 2004; Tang et al., 2010; Todorovic et al., 2007; Wang et al., 2006; Wurdak et al., 2005; Zhang and Bradley, 1996). TGFβ signalling plays an important role in the development of tissue fibrosis, since stimulation of the pathway promotes the conversion of fibroblasts into myofibroblasts and enhances ECM protein synthesis whilst repressing ECM degradation (Bujak and Frangogiannis, 2007).

1.2.1. *TGFβ* mutants

The different phenotypes of the *Tgfβ1*, *Tgfβ2* and *Tgfβ3* knock-out models reflect the non-compensated functions of the three TGFβ isoforms (Bujak and Frangogiannis, 2007). The *Tgfβ1* null mutation is embryonic lethal with a penetrance of 50%, while all surviving mice eventually die within five weeks due to a wasting syndrome associated with multifocal inflammation and massive lymphocyte and macrophage infiltration in multiple organs (Bujak and Frangogiannis, 2007). Mice deficient for *Tgfβ2* exhibit perinatal mortality and a range of malformations including fourth arch artery, outflow tract and intracardiac septation defects (Bartram et al., 2001; Sanford et al., 1997). The fourth arch artery defect was further associated with a marked reduction in Smad2 expression, confined in the specific vascular segment (Molin et al., 2004). Interestingly,

the mutants display craniofacial and ear defects too (Sanford et al., 1997), resembling the *Tbx1* mutant phenotype (Jerome and Papaioannou, 2001). *Tgfβ3* nulls present with cleft palate and abnormal lung development due to defective EMT interactions (Bujak and Frangogiannis, 2007). It has also been suggested that TGFβ signalling mediates processes of the inflammatory response in cardiac infarction, like monocyte recruitment at the wound site and promotion of granulation tissue formation (Bujak and Frangogiannis, 2007).

Conditional deletion of *TβRI* (*Alk5*) in the neural crest led to abnormal pharyngeal arch artery remodelling and outflow tract septation, secondary to increased apoptosis of the crest cells (Wang et al., 2006). Neural crest ablation of *TβRII* produced craniofacial malformations, thymus and parathyroid gland hypo/aplasia, and cardiovascular defects, all reminiscent of the 22q11DS phenotype (Choudhary et al., 2006; Wurdak et al., 2005). The phenotypes were attributed to loss of neural crest differentiation properties (Wurdak et al., 2005), or defective signalling to the surrounding tissues (Choudhary et al., 2006). Null mutants for *Ltbp1* displayed pharyngeal arch artery, outflow tract and intracardiac septation defects (Todorovic et al., 2007). The absence of the AP septum was explained in this case too by functional defects of post migratory neural crest cells (Todorovic et al., 2007).

1.2.2. *BMP* mutants

Complete inactivation of *Bmp2* resulted in delayed formation of the heart tube, which was found outside the amniotic cavity and eventually progressed into severe cardiac dysmorphogenesis (Zhang and Bradley, 1996). Conditional deletion of the gene in the AV myocardium led to early embryonic lethality and defects in AV cushion morphogenesis (Ma et al., 2005). Conditional deletion of *Bmp4* in the cardiomyocyte lineage induced AV septation defects, although the endocardial cushion formation was normal (Jiao et al., 2003). *Bmp4* conditional mutants in the branchial arch mesenchyme and outflow tract myocardium exhibited a range of cardiovascular defects including pharyngeal outflow tract and ventricular septation anomalies, due to abnormal differentiation into or recruitment of SMCs (Liu et al., 2004). Null mutation of *Bmp10* induced arrest of cardiogenesis at E9.0-E9.5 (Chen et al., 2004). The mutant embryos presented with hypoplastic ventricular walls and absence of ventricular trabeculae, while the endocardial cushion development arrested at the acellular stage (Chen et al.,

2004). It was shown that *Bmp10* deficient cardiomyocytes fail to proliferate and generate the ventricular trabeculae (Chen et al., 2004). Double knock-outs for *Bmp6* and *Bmp7* exhibited defective outflow tract cushion formation (Kim et al., 2001), while double knock-outs for *Bmp5* and *Bmp7* died by E10.5 from abnormal cardiogenesis (Solloway and Robertson, 1999). The phenotype was first noticed at the linear heart tube stage that progressed to disorganised cardiac morphology and absent endocardial cushions of the surviving embryos at E10.5 (Solloway and Robertson, 1999). Neural crest deletion of the BMP type I receptors *Alk2* (Kaartinen et al., 2004) and *Alk6* (Stottmann et al., 2004) resulted in abnormal or absent AP septum, while cardiac-specific deletion of *Alk3* resulted in AV cushion, trabeculae and interventricular septum defects, but not outflow tract defects (Gaussin et al., 2002). It was also shown that *Alk3* is required in cardiomyocytes for *Tgfβ2* expression (Gaussin et al., 2002). Consistently, conditional deletion of *Alk3* specifically in the AV cardiomyocyte lineage resulted in AV valve defects (Gaussin et al., 2005). Additionally, inactivation of *Alk3* in the endocardium with a *Tie2Cre* driver resulted in failure of AV endocardial cushion formation with incomplete penetrance (Ma et al., 2005).

1.2.3. *Smad* mutants

Smad4 is the common mediator Smad, required by all branches of the pathway to promote Smad-dependent response (Bujak and Frangogiannis, 2007; Javelaud and Mauviel, 2004; Ikushima and Miyazono, 2010; Moustakas and Heldin, 2009; Park, 2005; ten Dijke and Hill, 2004). Ablation of the gene in the neural crest led to outflow tract cushion hypoplasia and subsequent outflow tract septation defects (Jia et al., 2007; Nie et al., 2008), hypoplastic ventricular septa, thin ventricular wall and delayed remodelling of the pharyngeal arch arteries (Nie et al., 2008). The neural crest cells followed a normal migration pattern into the caudal arches (Jia et al., 2007; Nie et al., 2008) but failed to invade the outflow tract (Jia et al., 2007). Abnormal apoptosis of neural crest cells within the arches (Jia et al., 2007; Nie et al., 2008) led to a diminished cardiac crest cell contribution into the outflow tract (Jia et al., 2007). Inactivation of the gene in the myocardium induced an initially incorrect alignment of the AV cushions, which did not however affect AV septation, while the myocardial walls exhibited reduced cellularity, suggested as the primary cause of embryonic lethality for these mutants (Song et al., 2007). *Smad6*, the only other I-Smad apart from *Smad7*, is also

involved in heart development and displays a restricted expression pattern in the cardiovasculature (Galvin et al., 2000). The standard knock-out exhibited cardiac valve hyperplasia and outflow tract septation defects (Galvin et al., 2000). Mutations of the rest of the Smad genes, apart from *Smad7*, produce early embryonic lethality and a spectrum of defects not directly associated with the cardiovasculature (from the MGI website, http://www.informatics.jax.org/).

Smad7 is shown to be expressed in cardiac lineages throughout embryonic development (Liu et al., 2007; Luukko et al., 2001; Zwijsen et al., 2000) while a recently reported systemic conditional knock-out for *Smad7* displayed perinatal lethality and a cardiovascular phenotype including VSD, thin ventricular wall, ventricular non-compaction and malalignment of the pulmonary and aortic arteries (Chen et al., 2009). Interestingly, deletion of the first exon of the gene in mice had a mild effect on the B cells of the immune system but did not induce any other gross abnormalities (Li et al., 2006). Furthermore, overexpression of *Smad7* in the neural crest lineage that essentially abrogates TGFβ/BMP signalling in this tissue resulted in impaired craniofacial, pharyngeal and cardiovascular development, including outflow tract and ventricular septation defects and retro-oesophageal localisation of the RSCA (Tang et al., 2010). Overexpression of the gene in epithelial tissues under a keratin K5 promoter that targets the epidermis, hair follicles, other stratified and squamous epithelia and the thymic epithelia, resulted in defects in multiple organs, including severe thymic hypoplasia (He et al., 2002). In the chick model, overexpression of SMAD7 induced vessel enlargement with compromised connectivity to the rest of the plexus, although this was independent to VSM cell recruitment (Vargesson and Laufer, 2001).

The genetic mutations of components of the TGFβ/BMP pathways described to date produce a similar group of cardiovascular phenotypes. It is apparent that neural crest is affected in the majority of the models, which directly associates with compromised cellular contribution into the outflow tract and deficient differentiation into SMCs (Choudhary et al., 2006; Jia et al., 2007; Kaartinen et al., 2004; Nie et al., 2008; Stottmann et al., 2004; Todorovic et al., 2007; Wang et al., 2006; Wurdak et al., 2005). Such aberrations lead to outflow tract and cardiac septation abnormalities, related with endocardial cushion formation defects or failure in the septation process itself (Bartram et al., 2001; Choudhary et al., 2006; Jia et al., 2007; Kaartinen et al., 2004; Nie et al., 2008; Sanford et al., 1997; Stottmann et al., 2004; Todorovic et al.,

2007; Wang et al., 2006; Wurdak et al., 2005). Nonetheless, mutations of *TGFβ* superfamily genes also induce a different set of cardiovascular phenotypes that are related to defects in the pharyngeal arch artery remodelling or formation processes (Bartram et al., 2001; Choudhary et al., 2006; Nie et al., 2008; Todorovic et al., 2007; Wang et al., 2006; Wurdak et al., 2005). Often, these defects are described together with outflow tract or intracardiac defects, although their embryological origin is different (see introduction: 4.3, 7.4, 7.5). The first group of phenotypes, with regard to outflow tract and cardiac septation, along with the causative mechanisms have been more extensively studied than the great vessel defects. Of particular note is the fact that mutations targeting genes of the BMP pathway almost exclusively produce heart and/or outflow tract septation anomalies (Chen et al., 2004; Gaussin et al., 2005; Gaussin et al., 2002; Jiao et al., 2003; Kaartinen et al., 2004; Kim et al., 2001; Liu et al., 2004; Ma et al., 2005; Solloway and Robertson, 1999; Stottmann et al., 2004) while *TGFβ* gene mutations are additionally linked to great vessel malformations (Bartram et al., 2001; Choudhary et al., 2006; Todorovic et al., 2007; Wang et al., 2006; Wurdak et al., 2005).

2. Project overview

Our microarray data that identified *Smad7* as a putative Tbx1 target gene (van Bueren et al., 2010), the previously published *Smad7* expression pattern in the cardiovasculature (Liu et al., 2007; Luukko et al., 2001; Zwijsen et al., 2000) and the extensive implication of the TGFβ/BMP pathways in heart development, led us to further investigate this gene. Expression analysis was undertaken to establish the *Smad7* expression domains during early embryogenesis. *Smad7* gene-trap heterozygous intercrosses provided embryos for the assessment of cardiovascular, thymic and secondary palate phenotypes, in the context of the *Tbx1*/22q11DS phenotype. Double heterozygous embryos for *Tbx1* and *Smad7* were used to examine a potential genetic interaction between the two genes in great vessel development. Biochemical assays were employed to investigate direct TBX1 binding onto the *Smad7* promoter, assess the Smad7 actions on the two branches of the TGFβ/BMP pathways and also examine any shear stress involvement in the cardiovascular phenotype of the *Smad7* mutants through *Klf* factors. Finally, a model of *Smad7* gene restoration in a time-controlled fashion during embryogenesis was standarised to the extent time allowed for this thesis.

3. Results

3.1. *Smad7* in *Tbx1* mutant embryos

Whole mount *in situ* hybridisation was used to show that *Smad7* mRNA is downregulated in E9.5 $Tbx1^{lacZ/lacZ}$ embryos in the pharyngeal endoderm and mesenchyme but not ectoderm, compared to littermate stage-matched wild type controls (Figure 3.3.C, C', D, D'). This result corroborates the original microarray data (van Bueren et al., 2010) and supports the hypothesis that *Smad7* could be a Tbx1 downstream target. To overcome the problem of the physical malformation of the pharyngeal apparatus of the $Tbx1^{lacZ/lacZ}$ embryos, hypomorphs were used to examine *Smad7* mRNA levels. $Tbx1^{Neo2/Neo2}$ embryos express 34% of the wild type *Tbx1* mRNA dosage and lack the pharyngeal segmentation defect (Zhang and Baldini, 2008). By whole mount *in situ* hybridisation it was shown that *Smad7* mRNA was not affected in the $Tbx1^{Neo2/Neo2}$ embryos, compared to littermate stage-matched wild type controls (Figure 3.3E, E', F, F').

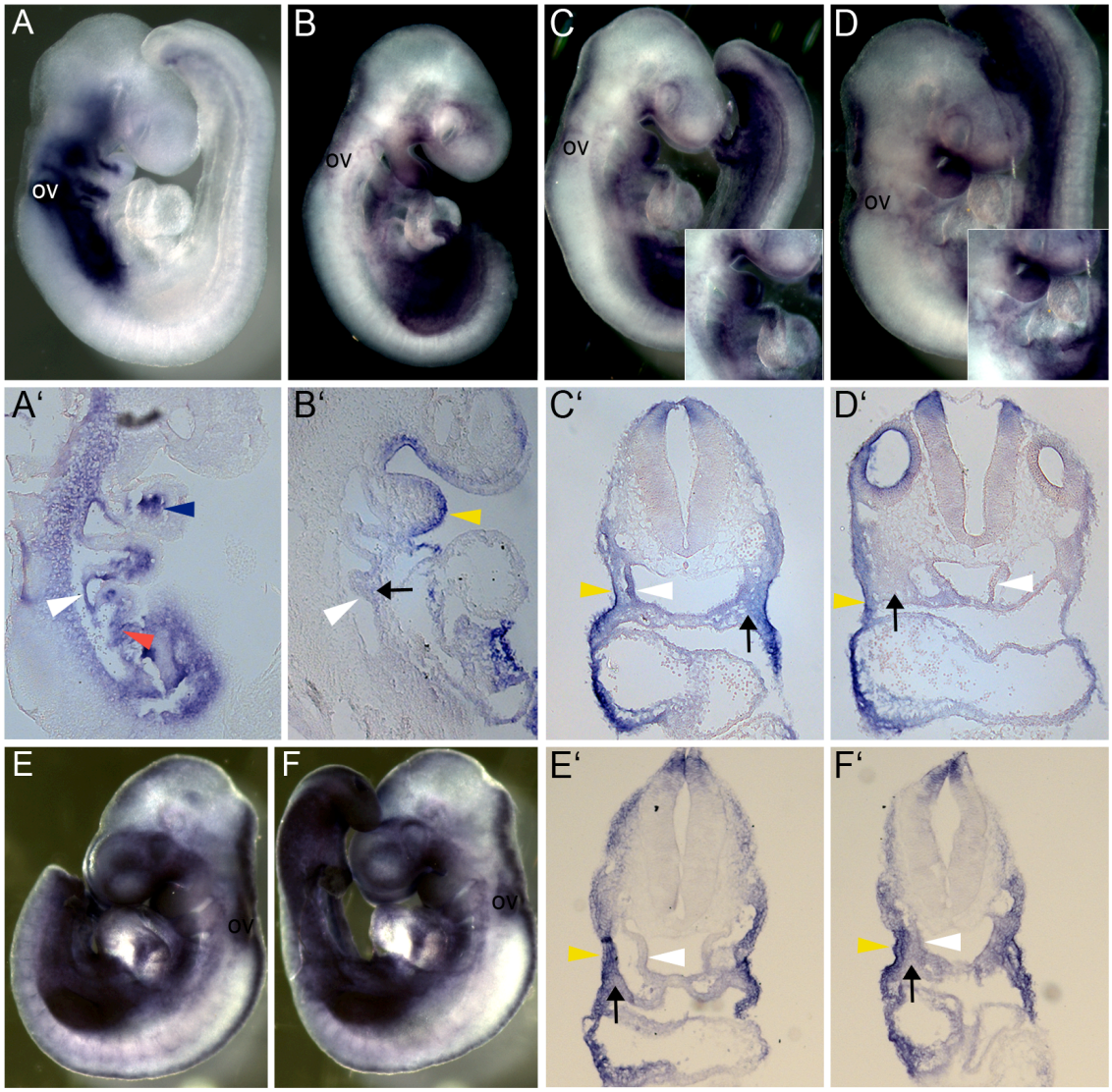

Figure 3. 3. *Tbx1* and *Smad7* mRNA expression detected by *in situ* hybridisation at E9.5. (A, A') Wild type *Tbx1* mRNA expression in whole mount (A) and parasagittal section (A'). (B, B') Wild type *Smad7* mRNA expression in whole mount (B) and parasagittal section (B'). (C, C', D, D') *Smad7* mRNA expression in wild type control embryo in whole mount (C) and transverse section at the caudal pharyngeal level (C') and in $Tbx1^{lacZ/lacZ}$ embryo in whole mount (D) and transverse section at the caudal pharyngeal level (D'). (E, E', F, F') *Smad7* mRNA expression in wild type control embryo in whole mount (E) and transverse section at the caudal pharyngeal level (E') and in $Tbx1^{Neo2/Neo2}$ embryo in whole mount (F) and transverse section at the caudal pharyngeal level (F'). Black arrow, pharyngeal mesenchyme; yellow arrowhead, pharyngeal ectoderm; blue arrowhead, core mesoderm; red arrowhead, SHF mesoderm; white arrowhead, pharyngeal endoderm; ov, otic vesicle; SHF, second heart field.

Irinna Papangeli

3.2. Tbx1 binding onto the *Smad7* promoter

To test whether *Smad7* is a Tbx1 target a bioinformatics approach was initially undertaken, to identify putative Tbx1 and other cardiac transcription factor binding elements, conserved throughout species, on the *Smad7* regulatory region. MULtiple sequence Local Alignment and visualisation tool (http://mulan.dcode.org/) was used to align the genomic sequences of the different species and highlight the conserved domains. The T-half site TCACACCT (Conlon et al., 2001; Wilson and Conlon, 2002) was used as a putative Tbx1 binding site search term. In a genomic region including the *Smad7* gene and 25 kb upstream and downstream sequence, several cardiac transcription factor binding sites were found conserved, across four species, human, mouse, rat and dog. There was a single putative Tbx1 binding site conserved, located approximately 13 kb upstream the 5'UTR (Figure 3.4).

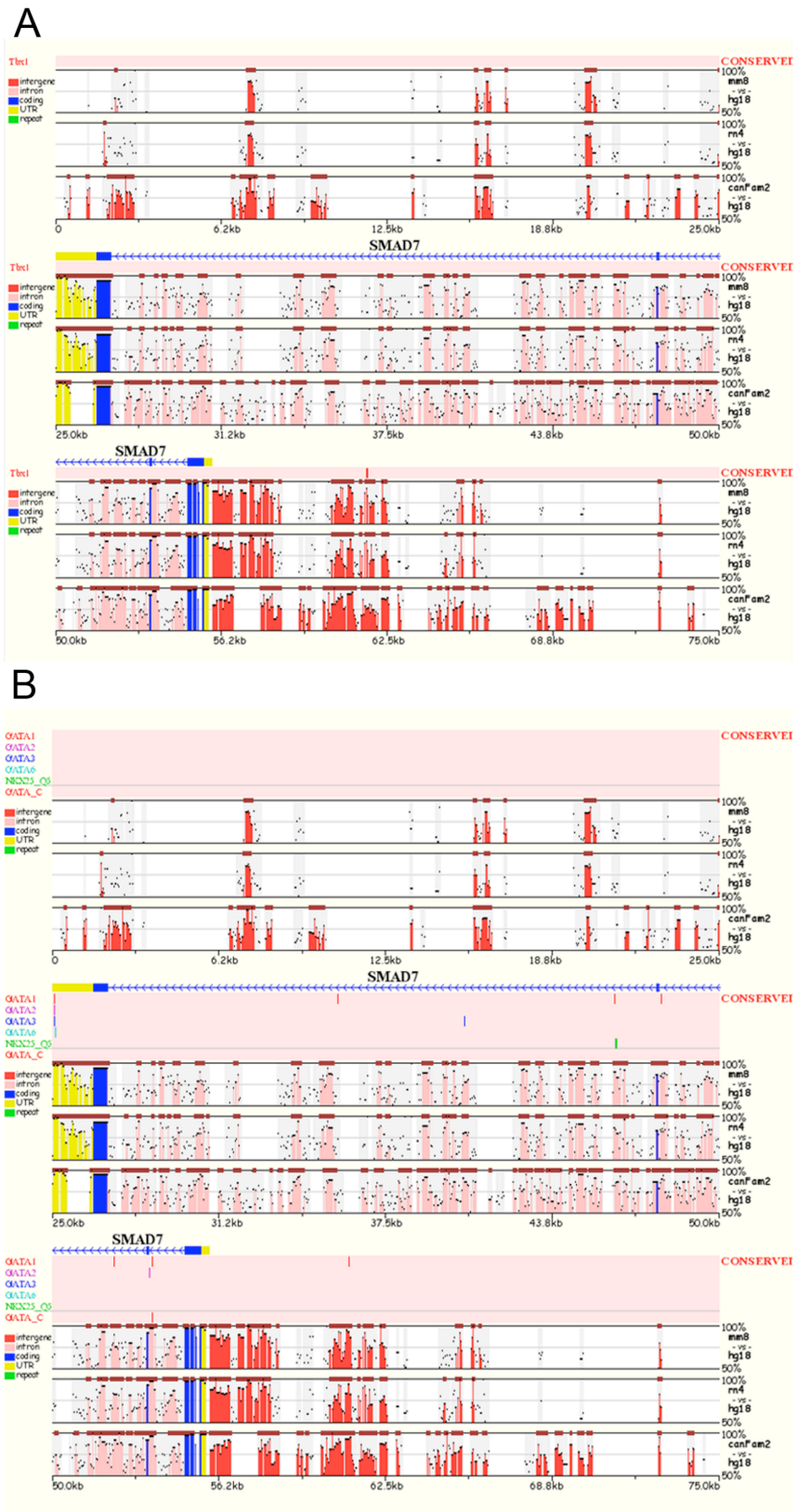

Figure 3. 4. Conserved TBEs on the *Smad7* gene and upstream/downstream regulatory regions among human, mouse rat and dog genomes. A putative Tbx1 binding site (A). Gata and Nkx factor binding sites (B).

To investigate this further, luciferase promoter assays were used to assess *in vitro* binding between TBX1 and *Smad7*, as previously described (Zweier et al., 2007). Around 2 kb of the upstream regulatory region of *Smad7*, relative to the transcription initiation site, was subdivided into overlapping sections of about 500 bp each. The putative Tbx1 binding site was not included since it was outside the 4.3 kb *Smad7* promoter that was shown to recapitulate gene-specific expression in the mouse embryo (Liu et al., 2007). Additionally, the conserved site was single and not in form of a palindrome, thought to be required for TBX1 binding (Sinha et al., 2000). The fragments were subcloned into the *luciferase* vector TKGL2 and transfected into cells together with either an empty vector or a *TBX1C* expressing construct. An empty TKGL2 vector was used as a negative control while the 2T-TKGL2 vector, which contains two palindromic T-box binding sites, was used as a positive control. A renilla *luciferase* or *β-galactosidase* expressing vector were used to assess the transfection efficiency and normalise the results within experiments. One of the four sequences tested, *Smad7.4*, showed a statistically significant increase in reporter expression ($p<0.05$, Mann-Whitney U test) (Figure 3.5.B), while *Smad7.2* showed a marked decrease, statistically significant when using the dual luciferase method ($p<0.05$, Mann-Whitney U test) (Figure 3.5.A). Although informative, these data do not provide conclusive results, as they need to be repeated for validation. Furthermore, the activation of the luciferase reporter measured from positive controls was much higher than the activation seen with the *Smad7*;*luciferase* plasmids. Also, despite the fact a proof reading Taq polymerase was used during the PCR amplification step, sequencing of all subcloned fragments is required to exclude the presence of randomly integrated mutations.

The promoter cloning and luciferase assay experiments were carried out by a member of the lab, Jennifer Huang. These results were generated during her master's course in which I helped to design the research project and supervised the experiments.

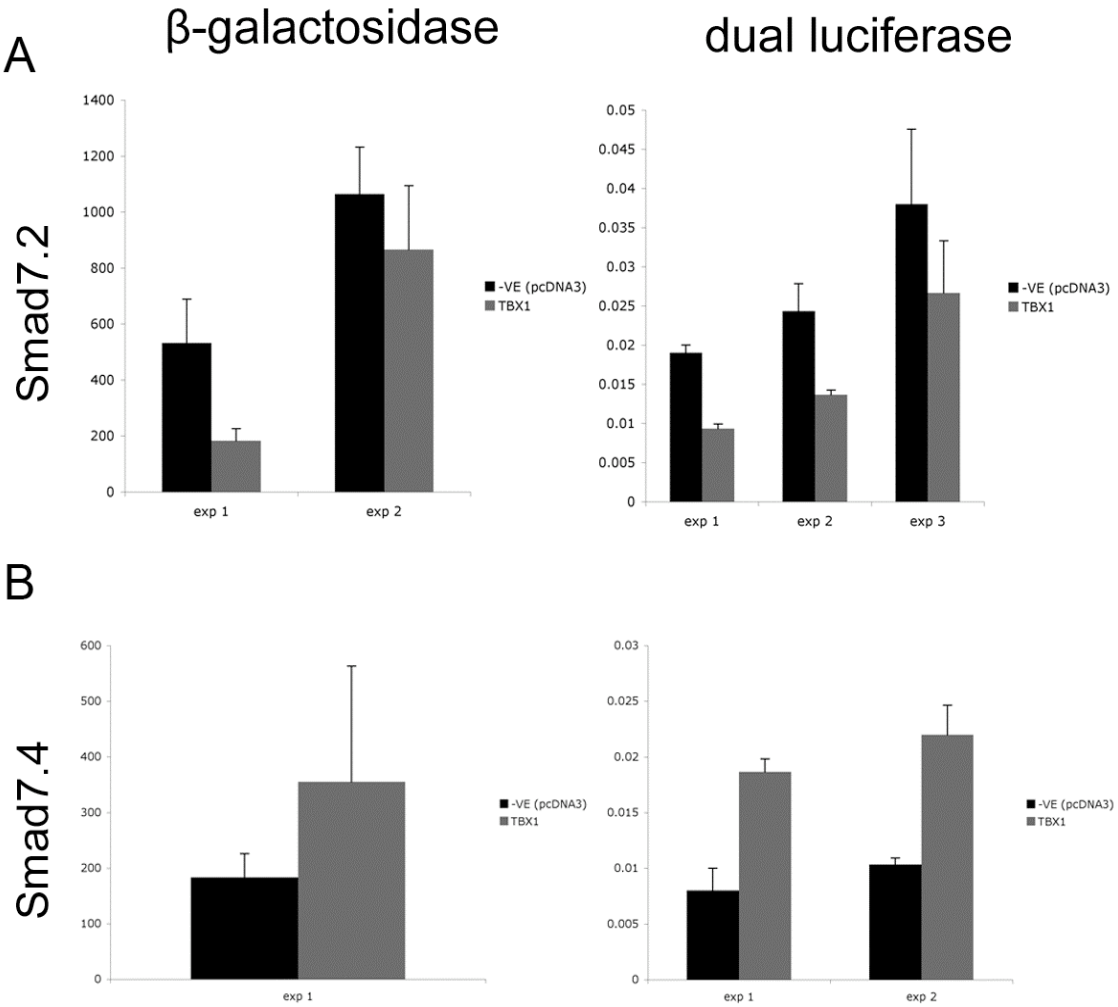

Figure 3. 5. *Smad7* promoter activation by TBX1. Graphical representation of luciferase activation after TBX1C or pcDNA3 co-expression with *Smad7.2*;TKGL2 (A) or *Smad7.4*;TKGL2 (B). The experiments are grouped based on the method used for normalisation within experiments; β-galactosidase or renilla luciferase expression. exp, independent experiments.

3.3. *Smad7* gene-trap validation

Smad7 gene-trap mice (hereafter $Smad7^{GT/GT}$) were obtained from BayGenomics, University of California, San Francisco, USA. They derived from the YHCO53 embryonic stem cell line in which the pGT0Lxf vector had integrated within intron 3 of *Smad7*, as verified by Bay Genomics. The vector consists of the first intron of the *Engrailed 2* (*En2*) gene followed in succession by a splice acceptor, the *β-galactosidase* gene and an SV40 polyadenylation site. The splice acceptor is flanked by two lox sites (Figure 3.6.C) (http://baygenomics.ucsf.edu/).

Heterozygous mice and embryos were initially distinguished by PCR amplification of an *En2* vector sequence. The embryo genotype was also verified by β-galactosidase expression through X-gal staining. To be able to identify the $Smad7^{GT/GT}$ from the $Smad7^{+/GT}$ mutants it was necessary to locate the exact insertion site of the vector. Primers were designed in 500 bp intervals, corresponding to forward sequences of the *Smad7* intron 3, and were used in combination with a reverse primer within the *En2* intron sequence in the gene-trap vector to amplify and hence locate the insertion site. Wild type DNA (negative for the *En2* intron PCR) was used as a negative control. The amplified products were sequenced, which resulted in the identification of the insertion site at +11,546 bp relative to the starting site of intron 3. Specific genotyping primers were subsequently designed (Figure 3.6.A).

Efficient knock-down of the *Smad7* gene by the gene-trap was verified using quantitative real time PCR comparing whole embryo RNA at E9.5 from $Smad7^{+/+}$, $Smad7^{+/GT}$ and $Smad7^{GT/GT}$ embryos (Figure 3.6.B). Two different sets of primers were used, one spanning exons 3 and 4 and one within exon 4 of Smad7. One copy of the gene-trap vector resulted in less than half the dosage of the *Smad7* gene, which was significantly different to the wild type levels when using *Smad7* exons 3-4 primers ($p<0.05$, t-test). Two copies of the gene-trap vector completely inhibited *Smad7* mRNA transcription, which was significantly different to the wild type levels with either primer pair ($p<0.01$, t-test, *Smad7* exons 3-4 primers, $p<0.05$, t-test, *Smad7* exon 4 primers) (Table 3.2). All efforts to measure the Smad7 protein levels in the different genotypes using the commercially available antibodies did not give a result, which has been a problem for other similar studies of Smad7 (Li et al., 2006; Tang et al., 2010).

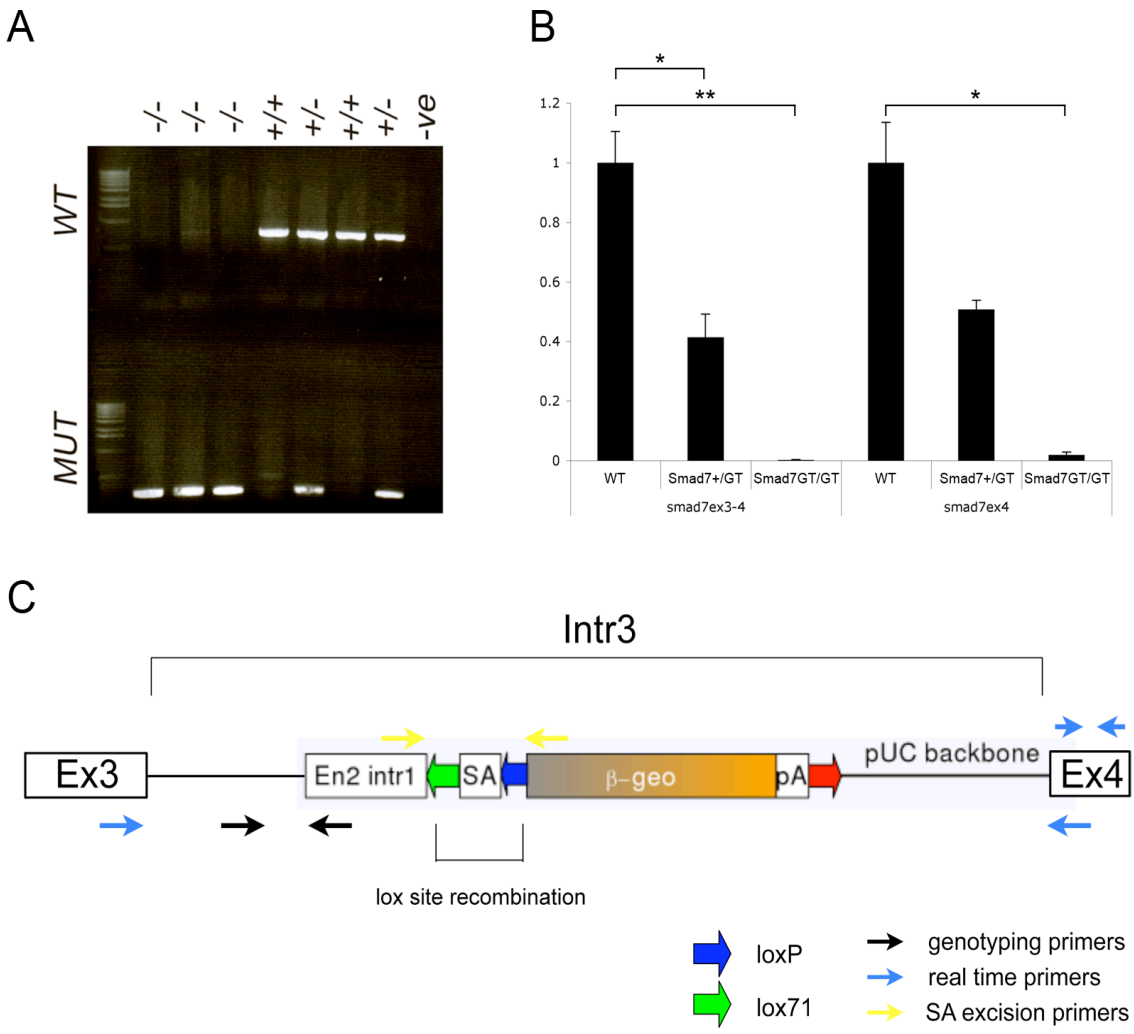

Figure 3. 6. *Smad7* gene-trap model characterisation. Genotyping PCR for the *Smad7* gene-trap allele (A). Quantitative real time PCR for amplicons spanning *Smad7* exon 3-4 or within exon 4 in the different genotypes, in single embryos (B). Schematic representation of the gene-trap vector inserted into *Smad7* intron 3, including the PCR primer site locations and lox sites (C). Ex, exon; Intr, intron; MUT, mutant; PA, polyadenylation; SA, splice acceptor; WT, wild type; β-geo, β-galactosidase/neomycin cassette.

Primer pair	Genotype	Average	SD
Smad7 ex4	WT	1	-
	Smad7$^{+/GT}$	0.442	0.092
	Smad7$^{GT/GT}$	0.016	0.005
Smad7 ex3-4	WT	1	-
	Smad7$^{+/GT}$	0.380	0.040
	Smad7$^{GT/GT}$	0.002	0.001

Table 3. 2. *Smad7* gene-trap validation by quantitative real time PCR. Quantitative real time PCR results showing the average levels of *Smad7* transcripts in the different genotypes normalised to the wild type. ex, exon; WT, wild type.

Through heterozygous intercrosses it was observed that the gene-trap homozygous animals were underrepresented at P10 according to Mendelian rations, but the values did not reach statistical significance ($p>0.05$, Chi-square test) (Table 3.3). This partial embryonic lethality could be due to several different causes, including cardiovascular insufficiency.

Genotype	n observed	n expected
WT	11	9.5
Smad7$^{+/GT}$	22	19
Smad7$^{GT/GT}$	5	9.5
Total	**38**	

$p>0.05$

Table 3. 3. Frequency of P10 genotypes observed from *Smad7*$^{+/GT}$ (x) *Smad7*$^{+/GT}$ matings. P value from Chi square test between the wild type and *Smad7*$^{GT/GT}$ groups. WT, wild type.

The gene-trap vector introduces a *β-galactosidase* gene that is essentially expressed instead of *Smad7*; therefore *β-galactosidase* expression should recapitulate the *Smad7* expression pattern in a tissue-specific manner. Characterisation of the expression of the trapped vector was performed by X-gal staining and was compared to the *Smad7* expression pattern as identified by whole mount *in situ* hybridisation. During the embryonic stages E7.5-E12.5 it was confirmed that the reporter expression matched the *Smad7* mRNA pattern (Figure 3.7).

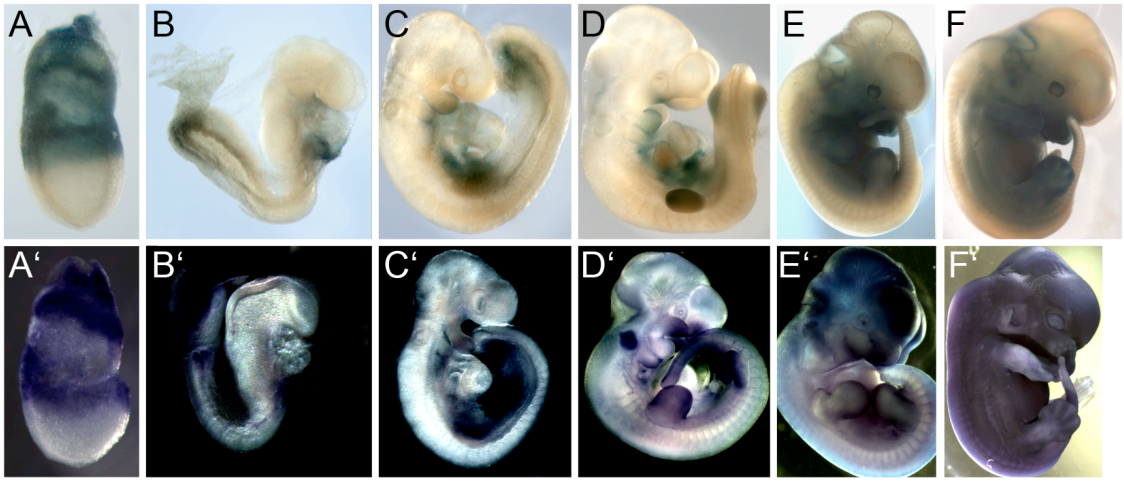

Figure 3. 7. *Smad7* expression during embryogenesis. *Smad7* expression detected by X-gal staining of *Smad7*$^{+/GT}$ embryos (A-F) or whole mount *in situ* hybridisation on wild type embryos (A'-F') from E7.5 to E12.5.

3.4. *Smad7* in the mouse embryo

Smad7 mRNA transcripts were detected by whole mount *in situ* hybridisation in extraembryonic tissues at E7.5. A day later, at E8.5, weak expression was identified in the pharyngeal ectoderm and endocardial and myocardial lining of the primitive heart tube (Figure 3.8.A-A''). During this stage strong staining was only observed in the distal part of the tail (Figure 3.8.B). At E9.0, the *Smad7* expression domains included the pharyngeal mesenchyme, endoderm and predominantly ectoderm, while transcripts were also identified in the endocardial lining and the myocardial wall of the common ventricular chamber of the heart. Half a day later, at E9.5, *Smad7* was strongly expressed in the pharyngeal ectoderm of the first arch, while weaker expression was detected in the pharyngeal endoderm and splanchnic mesenchyme (Figure 3.8.C-C''). *Smad7* mRNA transcripts were also detected in the endocardial and myocardial lining of the heart (Figure 3.8.C''). At E10.5 *Smad7* expression was maintained in the pharyngeal ectoderm throughout the apparatus, while it was detected strong in the endothelial lining of the anterior and posterior pairs of cardinal veins and in small clusters of cells scattered within the first two pairs of pharyngeal arches (Figure 3.8.D-D''). During the same stage expression in the outflow tract and AV cushions as well as in the endocardial and myocardial layers of the heart was observed (Figure 3.8.D''). At E11.5, as identified by X-gal staining, *Smad7* was expressed in the endothelium of the pharyngeal arteries, the outflow tract and AV cushions and the cardiac trabeculae. The

Smad7 expression profile in pharyngeal and cardiac tissues in the wild type embryo as identified through this thesis is summarised in Table 3.4.

E8.5	**E9.5**	**E10.5**	**E11.5***
P ectoderm	P ectoderm P endoderm P mesenchyme	P ectoderm	
Heart tube endocardial lining	Heart tube endocardial lining	Heart tube endocardial lining	
Heart tube myocardial lining	Heart tube myocardial lining	Heart tube myocardial lining	Heart trabeculae
	OFT	OFT cushions	OFT septa
		AV cushions	AV septa
		Cardinal vein endothelium	P artery endothelium

Table 3. 4. *Smad7* expression in pharyngeal and cardiac structures. Expression of *Smad7* in the mouse embryo from E8.5 to E11.5, as identified by X-gal and whole mount *in situ* hybridisation. AV, atrioventricular; OFT, outflow tract; P, pharyngeal. * by X-gal only.

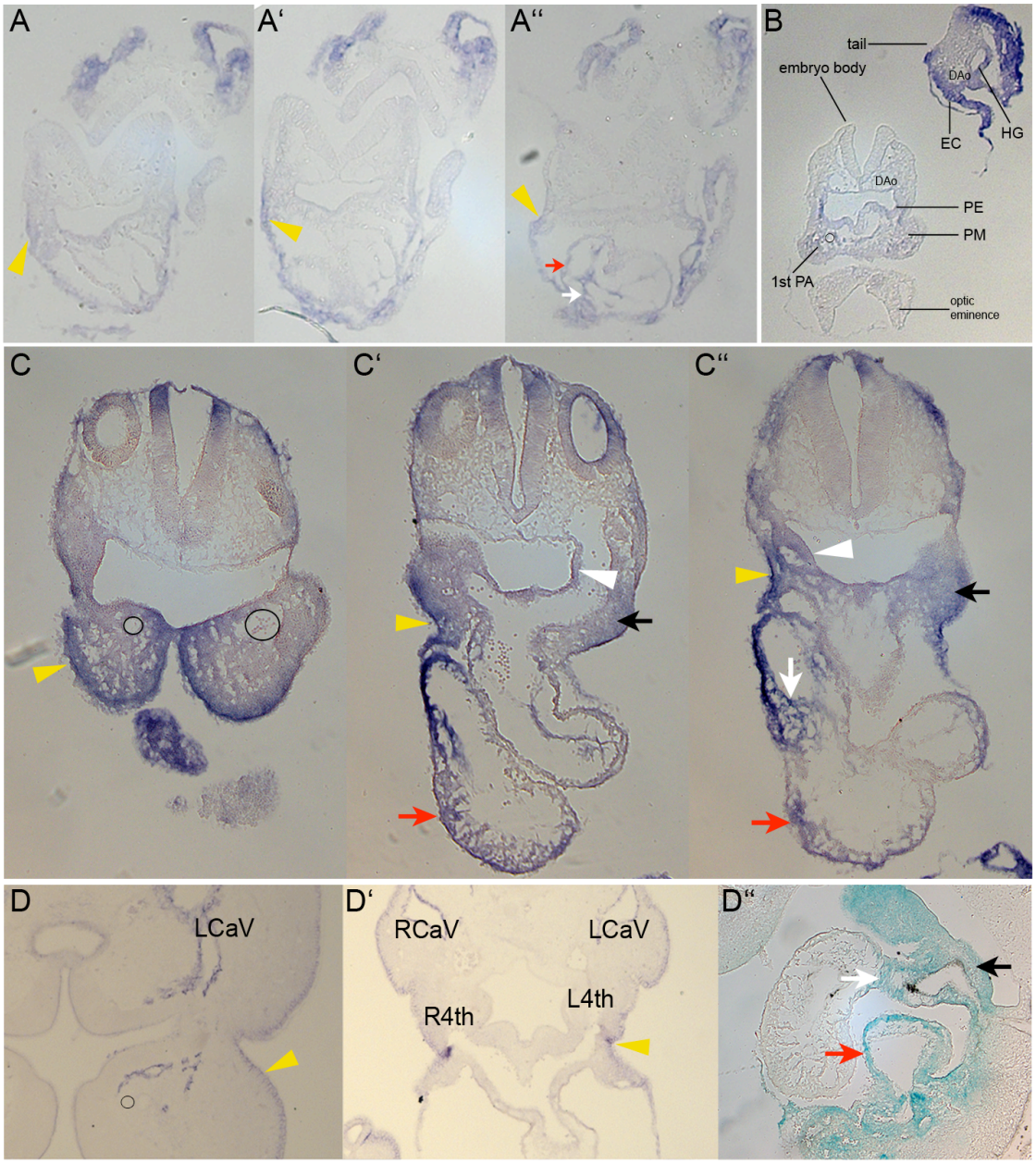

Figure 3. 8. *Smad7* expression in pharyngeal and cardiac structures. (A-D') Consecutive transverse sections of wild type mouse embryos showing *Smad7* mRNA expression after whole mount *in situ* hybridisation at E8.5 (A-A'', B), E9.5 (C-C'') and E10.5 (D-D'). Parasagittal section of a $Smad7^{+/GT}$ embryo at E10.5 after X-gal staining (D''). At E8.5, *Smad7* mRNA expression was faint throughout the embryo body (A-A'') as compared to the strong tail staining (B). Black arrow, pharyngeal mesenchyme; white arrow, endocardial lining; red arrow, myocardial lining; yellow arrowhead, pharyngeal ectoderm; white arrowhead, pharyngeal endoderm. CaV, cardinal vein;

DAo, dorsal aorta; EC, ectoderm; HG, hindgut; PA, pharyngeal arch; PE, pharyngeal endoderm; PM, pharyngeal mesenchyme; R/L, right/left.

3.5. The *Smad7* mutant phenotype

A recent study by Chen *et al.*, associated *Smad7* with cardiovascular development (Chen et al., 2009), however, the authors did not assess any 22q11DS-like phenotypic characteristics in the *Smad7* mutants. *Smad7*$^{GT/GT}$ embryos were examined as part of this project for the presence of thymic, palatal shelf, great vessel and intracardiac defects, in the context of the *Tbx1* mutant phenotype.

3.5.1. 22q11DS-like spectrum of defects

By E15.5 in the mouse embryo the great vessels have assumed the final asymmetric left-sided configuration (Hiruma et al., 2002), the ventricular septum (Webb et al., 1998) and secondary palate (Gritli-Linde, 2007; Meng et al., 2009) have formed completely and the thymic lobes have descended above the heart and lie as a pair (Grevellec and Tucker, 2010). Table 3.5 presents the defects observed in E15.5-E18.5 *Smad7* mutants, highlighting a potential contribution of the gene in great vessel and thymus development. Twenty-five out of the thirty (83%) *Smad7* gene-trap homozygous embryos had a thymic defect, including hypoplasia, aplasia, ectopic lobes or a single lobe (Figure 3.9.D', D''). Nine out of the thirty (30%) *Smad7*$^{GT/GT}$ embryos also presented with a great vessel defect, which was, with one exception, either a cervical RSCA (Figure 3.10.F), a cervical aortic arch (Figure 3.10.I) or an RAA (Figure 3.10.H). The single exception was a *Smad7*$^{GT/GT}$ embryo with a missing LCC. In both categories of phenotypes the gene-trap homozygotes were statistically different to the wild types ($p<0.01$, Fisher's exact test). There were also a few affected gene-trap heterozygotes, which exhibited a cervical RSCA (2%) or thymic hypoplasia (2%). Two *Smad7*$^{GT/GT}$ embryos displayed a cleft palate (Figure 3.9.C) and three presented with a membranous VSD (Figure 3.9.G), one of which had an overriding aorta too. These values, however, do not reach statistical significance. One *Smad7*$^{GT/GT}$ embryo exhibited subcutaneous oedema (Figure 3.9.E), while another presented with severe craniofacial malformation (Figure 3.9.A). No outflow tract defects were observed in any of the genotypes.

Genotype	n	Thymic hypo/aplasia	Great vessel defects
WT	37	0	0
Smad7$^{+/GT}$	82	2 (2%)	2 (2%)
Smad7$^{GT/GT}$	30	25* (83%)	9* (30%)
Total	**149**		

* p<0.01

Table 3. 5. Thymic and great vessel defects observed in the *Smad7* gene-trap embryos at E15.5-E18.5. P value from Fisher's exact test between the wild type and *Smad7*$^{GT/GT}$ groups. WT, wild type.

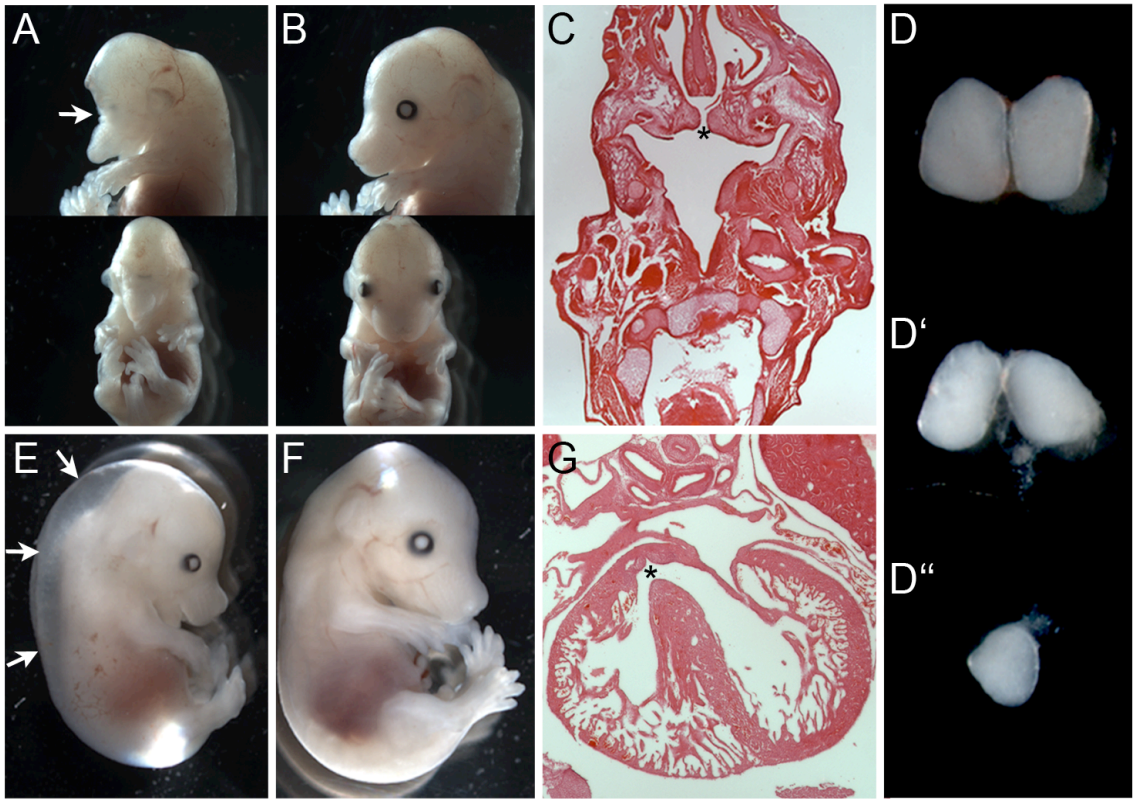

Figure 3. 9. 22q11DS-like spectrum of defects in *Smad7* gene-trap embryos. Craniofacial malformation (arrow) in *Smad7*$^{GT/GT}$ (A), compared to control embryo (B). Cleft palate in *Smad7*$^{GT/GT}$ embryo (C). *Smad7*$^{GT/GT}$ embryo thymic hypoplasia (D') and a single thymic lobe (D'') as compared to wild type (D). Subcutaneous oedema (arrows) in *Smad7*$^{GT/GT}$ (E) compared to control embryo (F). Membranous VSD in *Smad7*$^{GT/GT}$ embryo (G). Asterisks denote missing segments.

3.5.2. Great vessel and arch artery phenotype

Detailed analysis showed that the vast majority (7/9 affected) of the defects observed in E15.5-E18.5 *Smad7*$^{GT/GT}$ embryos reflected a left fourth or a right fourth arch defect, aside from the one exception of the left third arch-derived defect and one embryo that had a combined left and right fourth arch defect. The results of this analysis are summarised in Table 3.6.

E15.5-E18.5	**WT**	***Smad7*$^{+/GT}$**	***Smad7*$^{GT/GT}$**
Total embryos	37	82	30
Total normal	37	80	21
Total abnormal	**0**	**2 (2%)**	**9 (30%)**
L4th PAA	-	-	5
R4th PAA	-	2	2
L4th and R4h PAA	-	-	1
Other	-	-	1*

*L3rd PAA

Table 3. 6. Arch artery defects observed in the *Smad7* gene-trap embryos at E15.5-E18.5. L/R, left/right; PAA, pharyngeal arch artery; WT, wild type.

Smad7 mutant embryos were subsequently examined at an earlier developmental stage, to establish whether the great vessel phenotype is due to a formation defect or aberrant remodelling of the arch arteries. Pharyngeal artery patterning was initially examined at E10.5, a stage by which all caudal arch arteries should be formed (Hiruma et al., 2002; Yanagisawa et al., 1998). Very few abnormalities were detected (Figure 3.10.A-B'), which were scored in all the different genotypes (Table 3.7). The frequency of the defects between the wild types and the *Smad7*$^{GT/GT}$ embryos was not statistically significant ($p=0.50>0.05$, Fisher's exact test). A total of 105 embryos were collected at 10.5 days post coitum, but the majority of them had to be excluded because they were actually of earlier developmental stages, most likely due to animal housekeeping problems. The fact that the wild type embryos had a small but yet noticeable number of defects combined with the staging issues, led to the change of the stage at which arch artery patterning was examined to E11.5. This is the stage of initiation of arch artery remodelling (Hiruma et al., 2002; Yanagisawa et al., 1998). In all genotypes examined at E11.5 all the caudal arch arteries had formed normally, while the first and second pairs had regressed. One *Smad7*$^{GT/GT}$ embryo had an aplastic fourth arch artery, while in

a second embryo the right sixth arch artery was of equal size to the left counterpart, so it seemed that it was not regressing (Figure 3.10.C-D', Table 3.8). By E11.5, in wild type, gene-trap heterozygous or unaffected gene-trap homozygous embryos the right sixth arch artery is observed narrower that the left, as described in the literature (Hiruma et al., 2002; Yanagisawa et al., 1998). However, at E11.5 too the defects in the *Smad7*$^{GT/GT}$ embryos were not statistically different to the wild types (p=0.20>0.05, Fisher's exact test). Even by combining the populations of the two stages based on genotype, the differences between the wild type and the gene-trap homozygous mutant embryos still fail to reach statistical significance (p=0.20>0.05, Fisher's exact test) (Table 3.9). This indicates that the *Smad7* gene-trap mutation does not have a major effect on the formation of the pharyngeal arteries.

E10.5	**WT**	***Smad7*$^{+/GT}$**	***Smad7*$^{GT/GT}$**
Total embryos	16	43	10
Total normal	14	41	8
Total abnormal	**2 (12.5%)**	**2 (4.7%)**	**2 (20%)**
Persistent 1st &/or 2nd PAA	-	-	-
Hypo/aplastic 3rd PAA	-	-	-
Hypo/aplastic 4th PAA	1 (hypo), 1 (apl)	2 (hypo)	2 (hypo)
Hypo/aplastic 6th PAA	-	-	-
Aberrant branching	-	-	-

Table 3. 7. Arch artery defects observed in the *Smad7* gene-trap embryos at E10.5.
apl, aplastic; hypo, hypoplastic; PAA, pharyngeal arch artery; WT, wild type.

E11.5	**WT**	***Smad7*$^{+/GT}$**	***Smad7*$^{GT/GT}$**
Total embryos	17	24	14
Total normal	17	24	12
Total abnormal	**0**	**0**	**2 (14.3%)**
Persistent 1st &/or 2nd PAA	-	-	-
Hypo/aplastic 3rd PAA	-	-	-
Hypo/aplastic 4th PAA	-	-	1 (apl)
Hypo/aplastic 6th PAA	-	-	1 (not regr)
Aberrant branching	-	-	-

Table 3. 8. Arch artery defects observed in the *Smad7* gene-trap embryos at E11.5.
apl, aplastic; not regr, not regressing; PAA, pharyngeal arch artery; WT, wild type.

E10.5-E11.5	**WT**	***Smad7*$^{+/GT}$**	***Smad7*$^{GT/GT}$**
Total embryos	33	67	24
Total normal	31	65	20
Total abnormal	**2 (6%)**	**2 (3%)**	**4 (16.7%)**
Persistent 1st &/or 2nd PAA	-	-	-
Hypo/aplastic 3rd PAA	-	-	-
Hypo/aplastic 4th PAA	1 (hypo), 1 (apl)	2 (hypo)	2 (hypo), 1 (apl)
Hypo/aplastic 6th PAA	-	-	1 (not regr)
Aberrant branching	-	-	-

Table 3. 9. Arch artery defects observed in the *Smad7* gene-trap embryos at E10.5-E11.5. apl, aplastic; hypo, hypoplastic; not regr, not regressing; PAA, pharyngeal arch artery; WT, wild type.

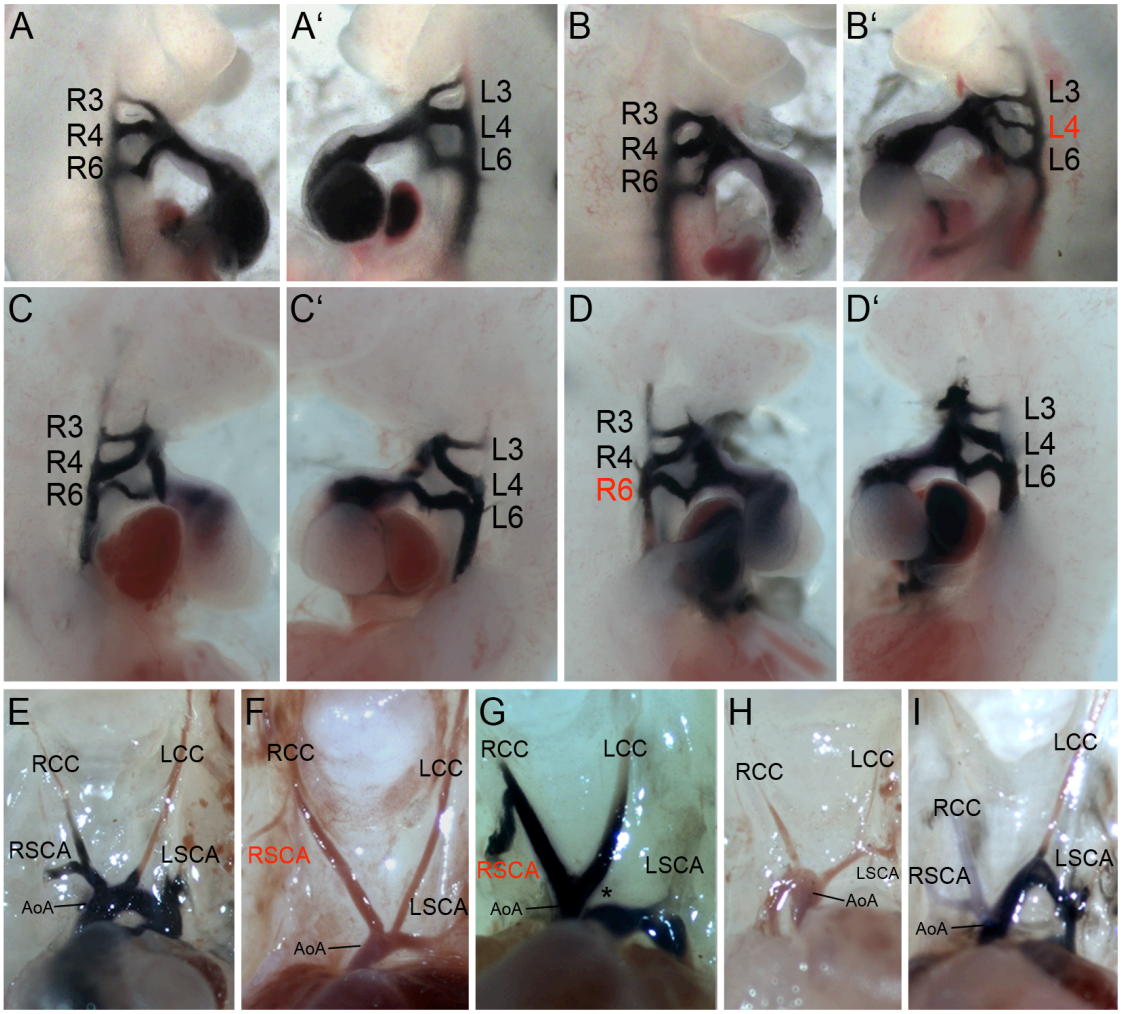

Figure 3. 10. Arch artery and great vessel defects in *Smad7* gene-trap embryos. Arch artery phenotype observed at E10.5 (A-B') or E11.5 (C-D') and great vessel defects observed at E15.5 (E-I). Right and left side of wild type embryos (A, A' and C, C'), and *Smad7*$^{GT/GT}$ embryos (B, B' and D, D'). Thin left fourth (B') and non regressing right sixth (D) arch arteries in *Smad7*$^{GT/GT}$ embryos. Wild type configuration (E) and *Smad7*$^{GT/GT}$ defects (F-I) at E15.5, cervical RSCA (F), cervical RSCA and IAA-B (G), RAA (H) and cervical aortic arch (I). Asterisks denote missing segments. AoA, aortic arch; RCC/LCC, right/left common carotid artery; RSCA/LSCA, right/left subclavian artery.

By comparing the defects observed in *Smad7*$^{GT/GT}$ mutants between the two developmental stages, prior to and after arch artery remodelling (E11.5 and E15.5-E18.5), statistical difference is not reached ($p=0.20>0.05$, Fisher's exact test). A trend,

however, exists, shown by the increase of frequency of vessel defects at E15.5-E18.5. This supports a role for *Smad7* in the remodelling of the great vessels. Furthermore, the gene-trap homozygous embryos at E11.5 are not different to the wild type controls considering the frequency of pharyngeal arch artery defects ($p=0.20>0.05$, Fisher's exact test). In contrast, at E15.5-E18.5 statistically significant difference is observed in the great vessel defects scored between the *Smad7*$^{GT/GT}$ and the wild type genotypes ($p<0.01$, Fisher's exact test) (Figure 3.11). The sample size at E11.5 may be small to prove a difference in the *Smad7*$^{GT/GT}$ populations between the two developmental stages.

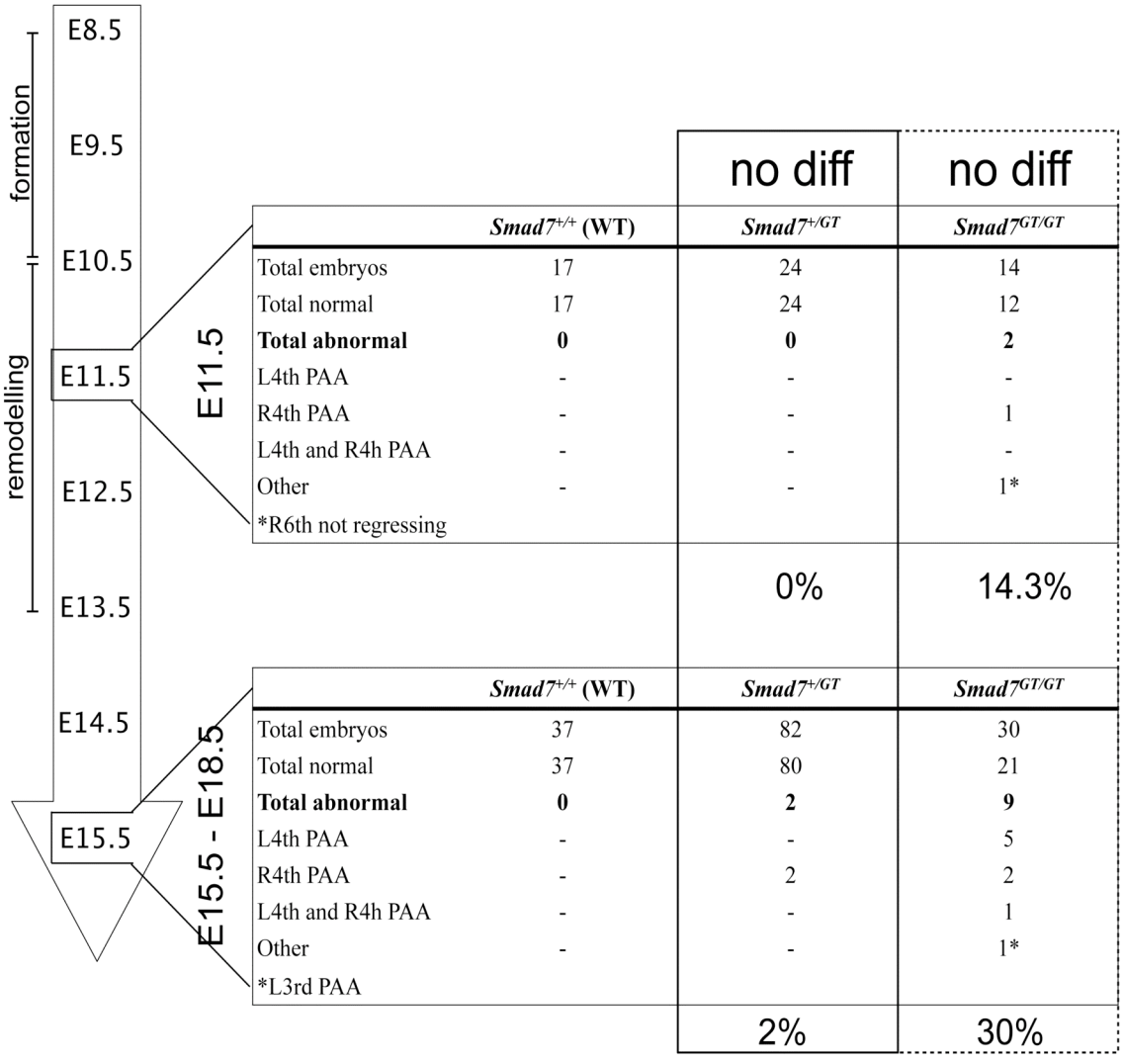

		no diff	no diff
	***Smad7*$^{+/+}$ (WT)**	***Smad7*$^{+/GT}$**	***Smad7*$^{GT/GT}$**
Total embryos	17	24	14
Total normal	17	24	12
Total abnormal	**0**	**0**	**2**
L4th PAA	-	-	-
R4th PAA	-	-	1
L4th and R4h PAA	-	-	-
Other	-	-	1*
*R6th not regressing			
		0%	14.3%

	***Smad7*$^{+/+}$ (WT)**	***Smad7*$^{+/GT}$**	***Smad7*$^{GT/GT}$**
Total embryos	37	82	30
Total normal	37	80	21
Total abnormal	**0**	**2**	**9**
L4th PAA	-	-	5
R4th PAA	-	2	2
L4th and R4h PAA	-	-	1
Other	-	-	1*
*L3rd PAA			
		2%	30%

Figure 3. 11. Arch artery defects observed in *Smad7* gene-trap embryos at E11.5 and E15.5-E18.5. Before the remodelling stage, at E11.5, a small proportion of the *Smad7*$^{GT/GT}$ embryos display arch artery defects. After complete remodelling of the

great vessels, at E15.5-E18.5, a greater population of the *Smad7*$^{GT/GT}$ embryos exhibit great vessel defects. Difference/ no difference, according to Fisher's exact test. L/R, left/right; PAA, pharyngeal arch artery; WT, wild type.

3.5.3. Neural crest migration

In several animal models arch artery development is affected by aberrant cardiac neural crest cell patterning that results in failed differentiation of post migratory crest (Liu et al., 2004) or reduced cellularisation of various structures (Kaartinen et al., 2004; Richarte et al., 2007). To investigate the underlying mechanisms of the *Smad7*$^{GT/GT}$ arch artery phenotype, neural crest migration was examined at E10.5 embryos, compared to stage-matched wild type littermates. This was assessed by whole mount *in situ* hybridisation for *Sox10*, a known neural crest marker (Kuhlbrodt et al., 1998). No defects were seen, although this experiment needs to be repeated for validation (Figure 3.12). Other neural crest markers can be used, like *HNK-1* (Vincent et al., 1983), *Crabp1* (Maden et al., 1991) or *Ap2α* (Mitchell et al., 1991).

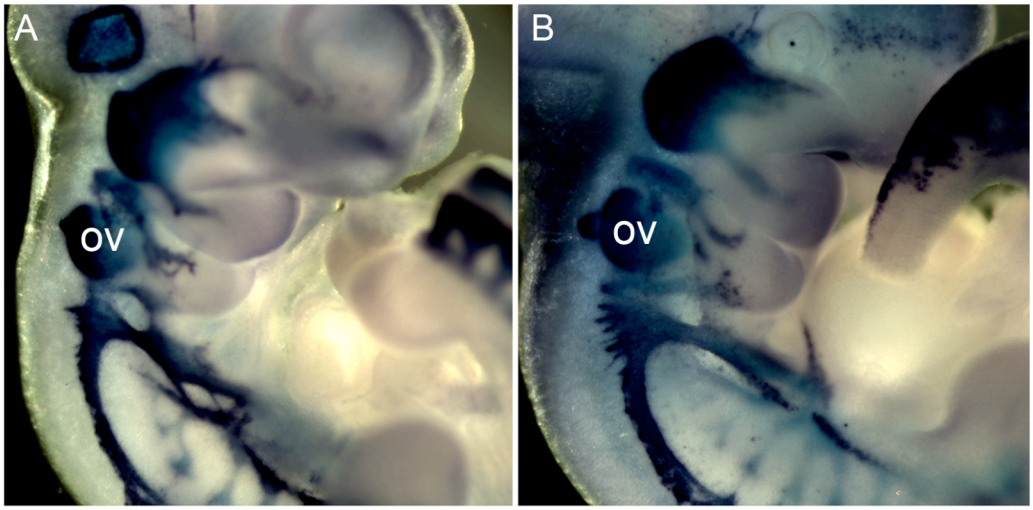

Figure 3. 12. Neural crest patterning in *Smad7* gene-trap embryos at E10.5. As detected by whole mount *in situ* hybridisation for *Sox10*, there was no difference between the neural crest migration pattern of the wild type (A) and the *Smad7*$^{GT/GT}$ embryo (B). ov, otic vesicle.

3.5.4. Shear stress related factors

Since no significant aberration was seen in the formation of the pharyngeal arch arteries in *Smad7*$^{GT/GT}$ embryos at E10.5/E11.5, it was hypothesised that lack of *Smad7*

affects the remodelling of the great vessels. Shear stress is important in angiogenesis (Ando and Yamamoto, 2009; Ando and Yamamoto, 2010). *Smad7* was first characterised as a shear stress responsive gene *in vitro* (Topper et al., 1997). In beginning to understand whether response to flow might be dysregulated in embryos that lack *Smad7*, a number of shear stress related genes were studied in *Smad7*$^{GT/GT}$ embryos. *Klf4* and *Klf10* were downregulated in our original microarray screen (van Bueren et al., 2010) so these, along with *Klf2* were evaluated in *Smad7*$^{GT/GT}$ embryos by real time quantitative PCR. At E9.5 neither *Klf4* nor *Klf10* seemed to be affected. In addition, *Klf10* only amplified at late cycles (Ct=30 out of 40 in total), resulting in differences among the triplicates. Conversely, *Klf2* was found upregulated progressively in gene-trap heterozygotes and homozygotes compared to the wild type controls (Figure 3.13). This implies a suppressive effect from *Smad7* on *Klf2*. A day later, at E10.5, the reverse phenomenon was seen, where *Klf2* was downregulated in the gene-trap heterozygous and homozygous embryos (Figure 3.13). Nonetheless, none of the values was statistically different to the respective wild type value in either stage.

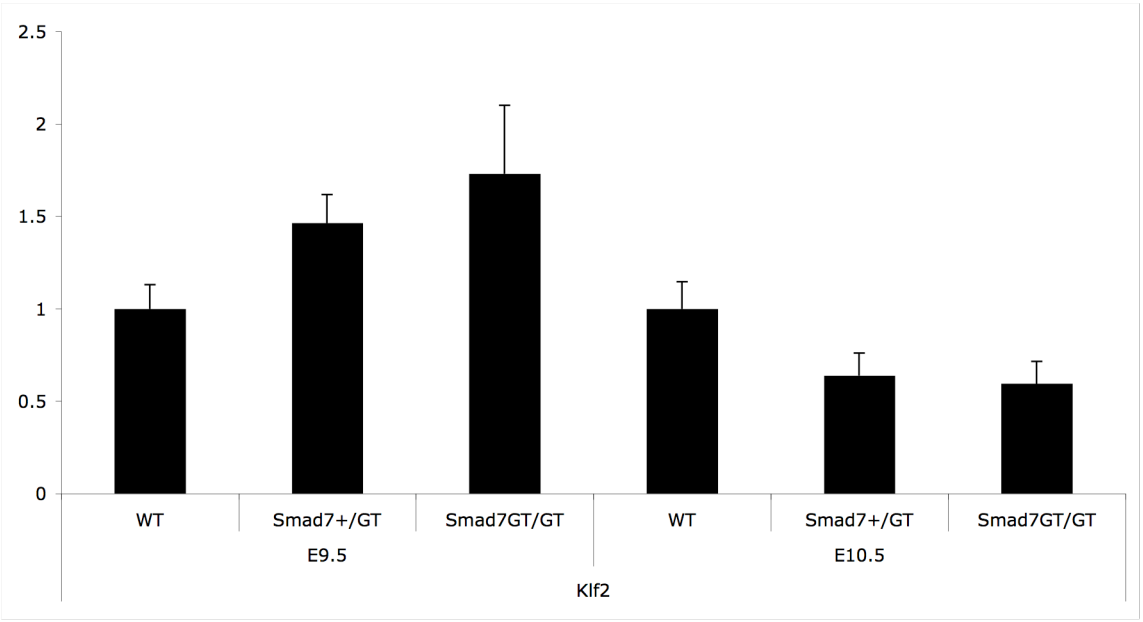

Figure 3. 13. *Klf2* expression levels in *Smad7* gene-trap embryos. Graphical representation of the relative expression levels of *Klf2* by quantitative real time PCR in E9.5 and E10.5 *Smad7* wild type, heterozygous and homozygous gene-trap embryos. WT, wild type.

3.5.5. TGFβ/BMP pathway

Smad7 is an inhibitor of both the TGFβ and BMP pathways (Moustakas and Heldin, 2009; Park, 2005; Ross and Hill, 2008; Yan et al., 2009), so it is important to establish whether either or both branches are affected in the *Smad7* gene-trap mutants. Whole embryo lysate from E9.5 wild type, gene-trap heterozygous and homozygous embryos was used for western blotting, to identify alterations in the levels of phosphorylated proteins representing activation of either branch of the pathway, namely the pSmad2/3 and pSmad1/5/8 complexes. Equal levels of pSmad2/3 were detected in all three genotypes (Figure 3.14), while a higher concentration of pSmad1/5/8 was observed in $Smad7^{GT/GT}$ versus $Smad7^{+/GT}$ embryos (Figure 3.14); no wild type controls were available for this experiment. This suggests that lack of *Smad7* at E9.5 impacts on the BMP branch of the pathway. Dilution effects from the whole embryo lysates are likely to mask tissue-specific alterations in the phosphorylation of these complexes. Finer dissection or immunohistochemical methods can be employed to examine this further.

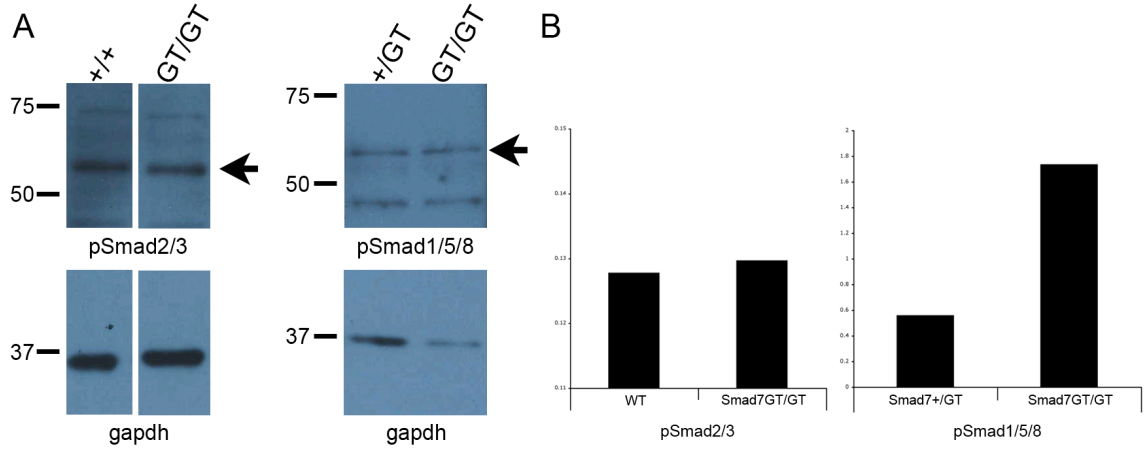

Figure 3. 14. pSmad2/3 and pSmad1/5/8 levels in *Smad7* gene-trap embryos. Western blots on $Smad7^{+/+}$, $Smad7^{+/GT}$ and $Smad7^{GT/GT}$ whole embryo lysates with antibodies against pSmad2/3 and pSmad1/5/8 complexes at the 60 kDa band (black arrows) and Gapdh at the 37 kDa band (A). Graphical representation of the quantification of the pSmad2/3 and pSmad1/5/8 in the respective genotypes normalised to Gapdh (B).

3.6. *Tbx1*;*Smad7* mutant phenotype

Tbx1 mutation in heterozygosity or homozygosity produces fourth arch-derived great vessel defects or a single truncus arteriosus respectively (Jerome and Papaioannou, 2001; Merscher et al., 2001). Since the vast majority of the *Smad7*$^{GT/GT}$ abnormalities considered fourth arch-derived defects, the genetic interaction between *Tbx1* and *Smad7* was studied, by producing double heterozygous embryos for these genes. A general study of the 22q11DS-affected structures was undertaken, including intracardiac septation, thymus and secondary palate development, as well as a more detailed analysis of the great vessel anatomy of these animals.

3.6.1. 22q11DS-like spectrum of defects

Embryos were collected at E15.5 and the great vessel, cardiac, thymic and palate phenotypes were assessed. Table 3.10 presents the defects observed in E15.5 *Tbx1*;*Smad7* mutants, highlighting a possible interaction between the two genes in thymus and great vessel development. Six out of the nineteen (31.5%) double heterozygous embryos had a hypoplastic thymus. Thirteen out of the nineteen (68%) double heterozygotes presented with a great vessel defect, which was fourth arch-derived in every case. The penetrance of the defects in the *Tbx1*;*Smad7* double heterozygotes was significantly different to all the other genotypes, including the additive effect of the *Tbx1* and *Smad7* mutations ($p<0.05$ or $p<0.01$, detailed in Table 3.10, Fisher's exact test). The phenotypes ranged among cervical or retro-oesophageal RSCA and cervical aortic arch, defects caused by an early unilateral fourth arch artery defect, and IAA-B or cervical arch combined with a cervical RSCA, denoting an earlier bilateral fourth arch defect (Figure 3.15.H-I). The *Tbx1* heterozygous embryos had the same spectrum of defects but always presented with unilateral fourth arch-derived defects (Figure 3.15.F-G). A detailed analysis of the arch artery defects observed in all genotypes at E15.5 is summarised in Table 3.11. An RAA, seen in almost half the *Smad7* gene-trap homozygous embryos with a defect, was not scored in any genotype here. None of the double heterozygotes presented with a VSD while one had a small cleft on the secondary palate. No outflow tract defects were observed in any of the genotypes.

Genotype	n	Thymic hypo/aplasia	Great vessel defects
WT	37	0	0
Tbx1$^{+/lacZ}$	17	0	5 (29%)
Smad7$^{+/GT}$	82	0	1 (1%)
Smad7$^{+/GT}$;*Tbx1*$^{+/lacZ}$	19	6 (31.5%)	13 (68%)
Total	**155**		

Table 3. 10. Thymic and great vessel defects observed in the *Tbx1*;*Smad7* double heterozygous embryos at E15.5-E18.5. P values from Fisher's exact test between the following comparisons: *Smad7*$^{+/GT}$;*Tbx1*$^{+/lacZ}$ and wild type (††,**), *Smad7*$^{+/GT}$;*Tbx1*$^{+/lacZ}$ and *Tbx1*$^{+/lacZ}$ (††,*), *Smad7*$^{+/GT}$;*Tbx1*$^{+/lacZ}$ and *Smad7*$^{+/GT}$ (††,**) and *Smad7*$^{+/GT}$;*Tbx1*$^{+/lacZ}$ and the additive effect of *Tbx1*$^{+/lacZ}$ and *Smad7*$^{+/GT}$ (††,**) groups. † p<0.05, †† p<0.01 for thymic defects; * p<0.05, ** p<0.01 for great vessel defects; WT, wild type.

E15.5	WT	*Smad7*$^{+/GT}$	*Tbx1*$^{+/lacZ}$	*Smad7*$^{+/GT}$;*Tbx1*$^{+/lacZ}$
Total embryos	37	82	17	19
Total normal	37	81	12	6
Total abnormal	**0**	**1 (1%)**	**5 (29%)**	**13 (68%)**
L4th PAA	-	-	2	2
R4th PAA	-	1	3	8
L4th and R4h PAA	-	-	-	3

Table 3. 11. Arch artery defects observed in the *Tbx1*;*Smad7* double heterozygous embryos at E15.5. L/R, left/right; PAA, pharyngeal arch artery; WT, wild type.

3.6.2. Great vessel and arch artery phenotype - genetic interaction

The great vessel phenotype of the double heterozygous embryos for *Tbx1* and *Smad7* was subsequently examined at an earlier developmental stage, to assess if the genetic interaction between the two genes affects the formation of the pharyngeal arteries, or their remodelling. Embryos were collected at E11.0, and the pharyngeal patterning was assessed. At this stage, the double heterozygous embryos had comparable penetrance of fourth arch artery defects as the *Tbx1* heterozygotes (Figure 3.15.A-D'), (p=0.58>0.05, Fisher's exact test), while they shared the same proportion of bilateral versus unilateral defects (Table 3.12). This indicates that there is no interaction between the two genes at E11.0. Consistent with the literature (Calmont et al., 2009;

Lindsay et al., 2001; Vitelli et al., 2002b Vitelli et al., 2006; Zhang and Baldini, 2008), *Tbx1* heterozygotes produced here partially recovered from the fourth arch defects by E15.5. The penetrance of the great vessel defects observed in the $Tbx1^{+/lacZ}$ embryos was reduced between E11.0 and E15.5 from 65% to 29%, which is statistically significant, with a p value of 0.042 ($p<0.05$, Fisher's exact test). Conversely, the double heterozygous animals did not recover from the original *Tbx1* haploinsufficiency-induced defect, and presented with the same penetrance of defects at both stages, 67% at E11.0 as compared to 68% at E15.5. Hence, at E15.5, the *Tbx1* heterozygotes are different to the double heterozygous population ($p<0.05$, Fisher's exact test) (Figure 3.16). This suggests that the *Tbx1* mutation produces fourth arch artery defects during arch artery formation stages, but the concurrent presence of one gene-trap allele for *Smad7* hinders the recovery of the *Tbx1* haploinsufficient phenotype during the remodelling stages (Figure 3.17).

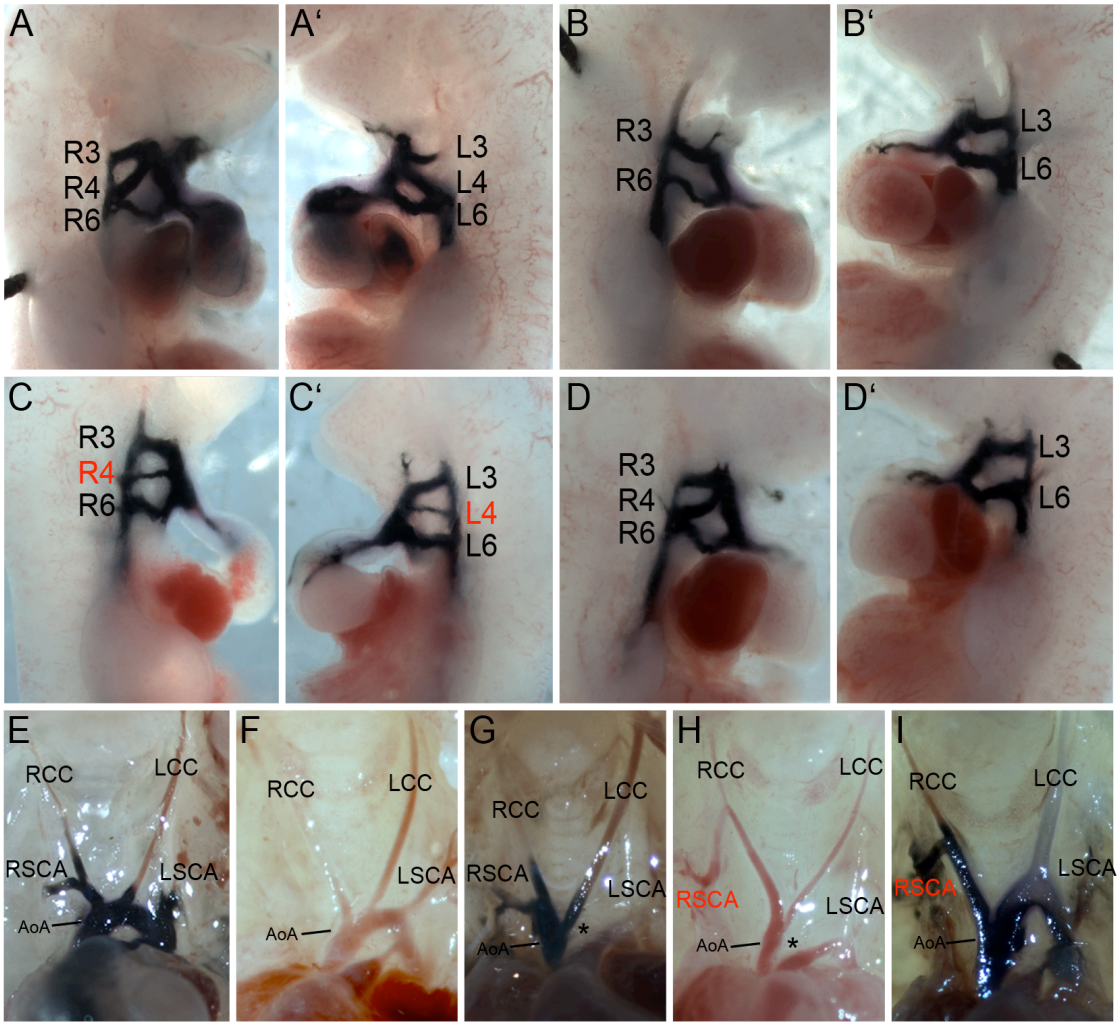

Figure 3. 15. Arch artery and great vessel defects in *Tbx1*;*Smad7* double heterozygous embryos. Arch artery phenotype observed at E11.0 (A-D') and great vessel defects observed at E15.5 (E-I). Right and left side of a wild type embryo (A, A'), *Smad7*$^{+/GT}$;*Tbx1*$^{+/lacZ}$ embryos (B, B' and C, C') and a *Tbx1*$^{+/lacZ}$ embryo (D, D'). Bilaterally absent fourth (B, B'), bilaterally hypoplastic fourth (C, C') and absent left fourth (D') arch arteries. Wild type configuration (E), *Tbx1*$^{+/lacZ}$ (F-G) and *Smad7*$^{+/GT}$;*Tbx1*$^{+/lacZ}$ phenotypes (H-I), absent RSCA (F), IAA-B (G), cervical RSCA and IAA-B (H) and cervical RSCA and cervical aortic arch (I). Asterisks denote missing segments. AoA, aortic arch; RCC/LCC, right/left common carotid artery; RSCA/LSCA, right/left subclavian artery.

E11.0	**WT**	***Smad7*$^{+/GT}$**	***Tbx1*$^{+/lacZ}$**	***Smad7*$^{+/GT}$;*Tbx1*$^{+/lacZ}$**
Total embryos	19	13	17	24
Total normal	19	12	6	8
Total abnormal	**0**	**1 (8%)**	**11 (65%)**	**16 (67%)**
Persistent 1st &/or 2nd PAA	-	-	-	-
Hypo/aplastic 3rd PAA	-	-	-	-
Hypo/aplastic 4th PAA	-	1 (apl)	7 (hypo), 4 (apl)	7 (hypo), 9 (apl)
Hypo/aplastic 6th PAA	-	-	-	-
Aberrant branching	-	-	-	-
Unilateral/Bilateral		unilateral	5/11 bilateral	7/16 bilateral

Table 3. 12. Arch artery defects observed in the *Tbx1*;*Smad7* double heterozygous embryos at E11.0. apl, aplastic; hypo, hypoplastic; PAA, pharyngeal arch artery; WT, wild type.

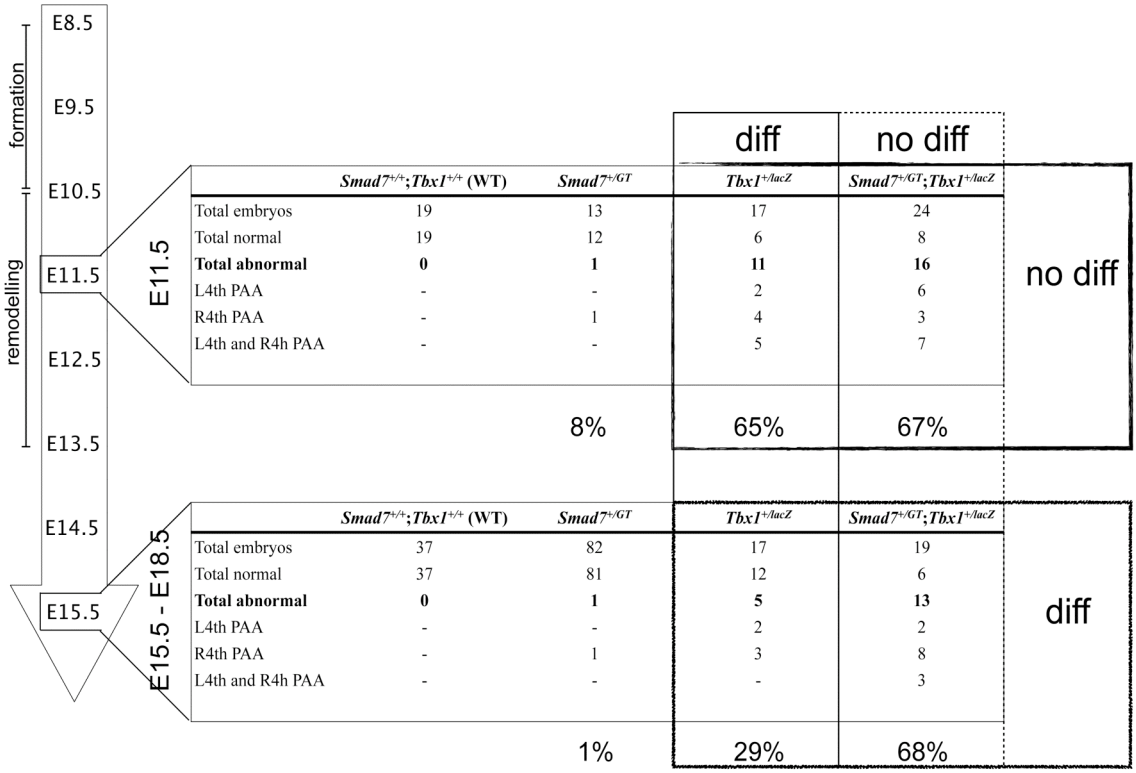

Figure 3. 16. Arch artery defects observed in *Tbx1*;*Smad7* double heterozygous embryos at E11.0 and E15.5. Before the remodelling stage, at E11.0, the *Smad7*$^{+/GT}$;*Tbx1*$^{+/lacZ}$ embryos have comparable frequency of fourth arch artery defects to the *Tbx1*$^{+/lacZ}$ embryos. After complete remodelling of the great vessels, at E15.5, although the *Tbx1*$^{+/lacZ}$ embryos partially recover from the fourth arch related defects,

the *Smad7*$^{+/GT}$;*Tbx1*$^{+/lacZ}$ embryos fail to do so and present with the same frequency of defects between the earl and the late stage. Difference/ no difference, according to Fisher's exact test. L/R, left/right; PAA, pharyngeal arch artery; WT, wild type.

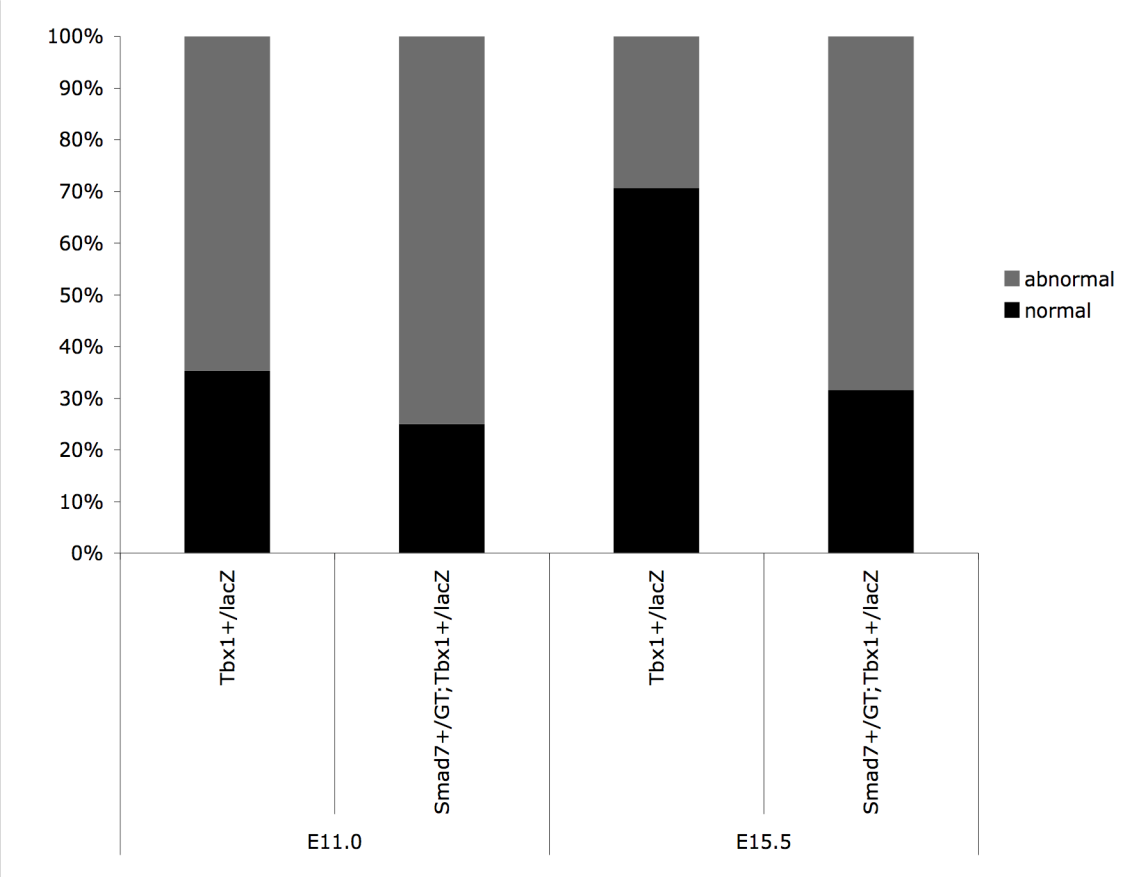

Figure 3. 17. Proportional representation of the fourth arch artery phenotype scored at E11.0 and E15.5 in *Tbx1* heterozygous and *Tbx1*;*Smad7* double heterozygous embryos.

3.6.3. Shear stress related factors

Klf2 was observed to be downregulated in *Smad7* gene-trap heterozygous and homozygous embryos at E10.5 (Figure 3.13). Although not consistently, it appeared to be downregulated in Tbx1 heterozygotes, and further decreased in *Tbx1*;*Smad7* double heterozygous embryos (Figure 3.18). This may suggest a common pathway whereby *Tbx1* is acting on *Smad7*, which subsequently reduces *Klf2* levels. However, neither of the values was statistically different to the wild type value.

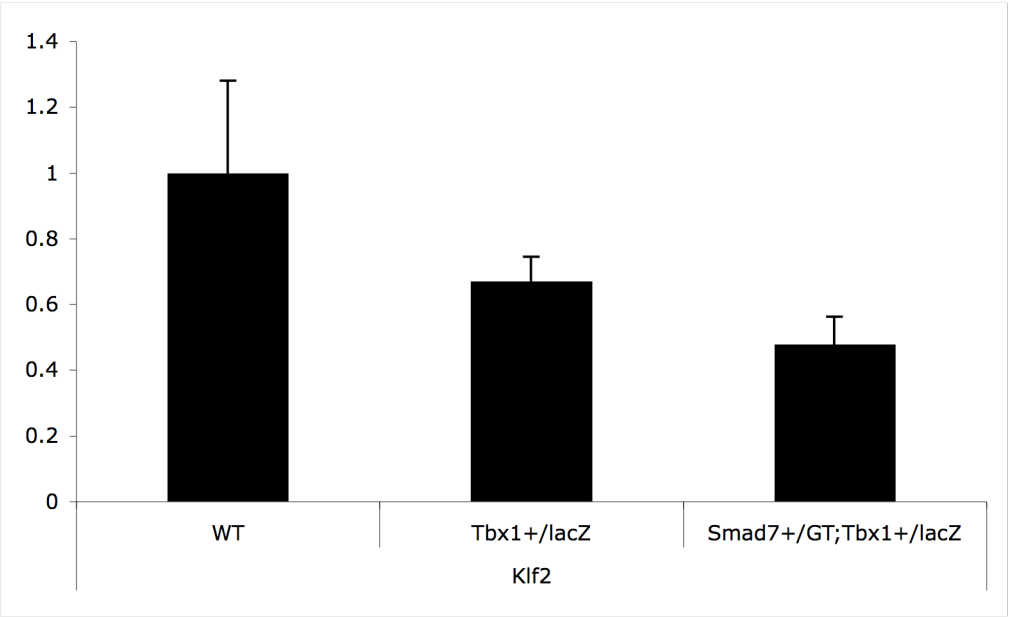

Figure 3. 18. *Klf2* expression levels in *Tbx1* heterozygous and *Tbx1*;*Smad7* double heterozygous embryos. Graphical representation of the relative expression levels of *Klf2* by quantitative real time PCR in E10.5 wild type, *Tbx1* heterozygous and *Tbx1*;*Smad7* double heterozygous embryos. WT, wild type.

3.7. *Smad7* gene-trap time-dependent excision

The *Smad7* gene-trap model used for this study is designed with two lox sites to implement excision of the splice acceptor sequence and thus *Cre*-dependent restoration of normal gene transcription (Figure 3.6.C). The potential to restore *Smad7* function to normal, combined with a time control element, is critical for the study of *Smad7* in the arch artery remodelling process. A tamoxifen inducible model that ubiquitously expresses *Cre* recombinase under the *Caggs* promoter was used for this purpose. The tamoxifen administration time-point, method and concentration were standarised on the

basis of gene-trap recombination efficiency. This was assessed by quantitative real time PCR for *Smad7* mRNA transcripts, compared to the wild type levels, in whole embryo lysates. The previously published optimal tamoxifen administration protocol for this line, for maximum recombination efficiency 24 hrs post administration, is IP injection of 3mg of tamoxifen per 40g body weight, equal to 75mg/ kg body weight (Hayashi and McMahon, 2002; Xu et al., 2005). Higher dosages are toxic and lead to embryonic lethality, while almost complete recombination is achieved 48 hrs post administration (Hayashi and McMahon, 2002).

The aim of this experiment was to restore *Smad7* mRNA transcripts in the $Smad7^{GT/GT}$ embryos at E10.5 or E10.75, a time point by which all the pharyngeal arch arteries have formed and the remodelling of the vessels commences (Hiruma et al., 2002; Yanagisawa et al., 1998). The embryos used were produced by intercrossing $Smad7^{+/GT}$ to $Smad7^{+/GT}$;*CaggsCre* animals and by treating the pregnant mothers with tamoxifen. Due to lack of animal availability, a second cross was used, $Tbx1^{+/lacZ}$ to $Smad7^{+/GT}$;*CaggsCre*. In this setting restoration of *Smad7* was examined at the gene-trap heterozygous level. A total of four different dosages or drug administration time points were tested using the free salt tamoxifen and one using the activated derivative (4OH), as summarised in Table 3.13. When administration was via the oral route, a final concentration of 4.8mg per 40g body weight, equal to 120mg/ kg body weight was given (Park et al., 2008).

CROSS	TAMOXIFEN ADMINISTRATION			TAMOXIFEN CONCENTRATION (DURATION)	RECOMBINATION AT E10.5 or E10.75*
	method	doses	stage		
Smad7$^{+/GT}$x*Smad7*$^{+/GT}$;*CaggsCre*	IP	1	E9.5	75mg/kg bw (24hrs)	26%
	IP IP 1/2	2	E9.0 E10.0	75mg/kg bw (24hrs) 37.5mg/kg bw (6hrs)	17%
	OG	1	E10.0	120mg/kg bw (10hrs)	0.5%*
Tbx1$^{+/lacZ}$x*Smad7*$^{+/GT}$;*CaggsCre*	IP	1**	E9.5	75mg/kg bw (24hrs)	12% and X-gal staining
	IP	1	E9.0	75mg/kg bw (30hrs)	15% and X-gal staining

** 4OH tamoxifen

Table 3. 13. Tamoxifen administration and *CaggsCre*-dependent recombination efficiency of the *Smad7* gene-trap vector. The different genetic crosses, tamoxifen administration protocols followed and the recombination efficiency of the *Smad7* gene-trap vector as assessed by quantitative real time PCR for the *Smad7* mRNA levels in *Smad7*$^{GT/GT}$;*CaggsCre* or *Smad7*$^{+/GT}$;*Tbx1*$^{+/lacZ}$;*CaggsCre* embryos are summarised here. IP, intraperitoneal; OG, oral gavage.

Smad7 mRNA expression at E10.5, as detected by quantitative real time PCR in whole embryos, was around 40% in *Smad7*$^{+/GT}$ embryos, between 40%-60% in *Smad7*$^{+/GT}$;*Tbx1*$^{+/lacZ}$ embryos and around 100% in *Tbx1*$^{+/lacZ}$ embryos, relative to the wild type levels (Figure 3.19). The *Smad7*$^{+/GT}$ embryos have not presented with significant phenotypic defects to date. Therefore, for safe interpretation of subsequent results, restored gene expression in *Smad7*$^{GT/GT}$ mutants would be considered effective if it reached at least 40% of the wild type *Smad7* mRNA levels.

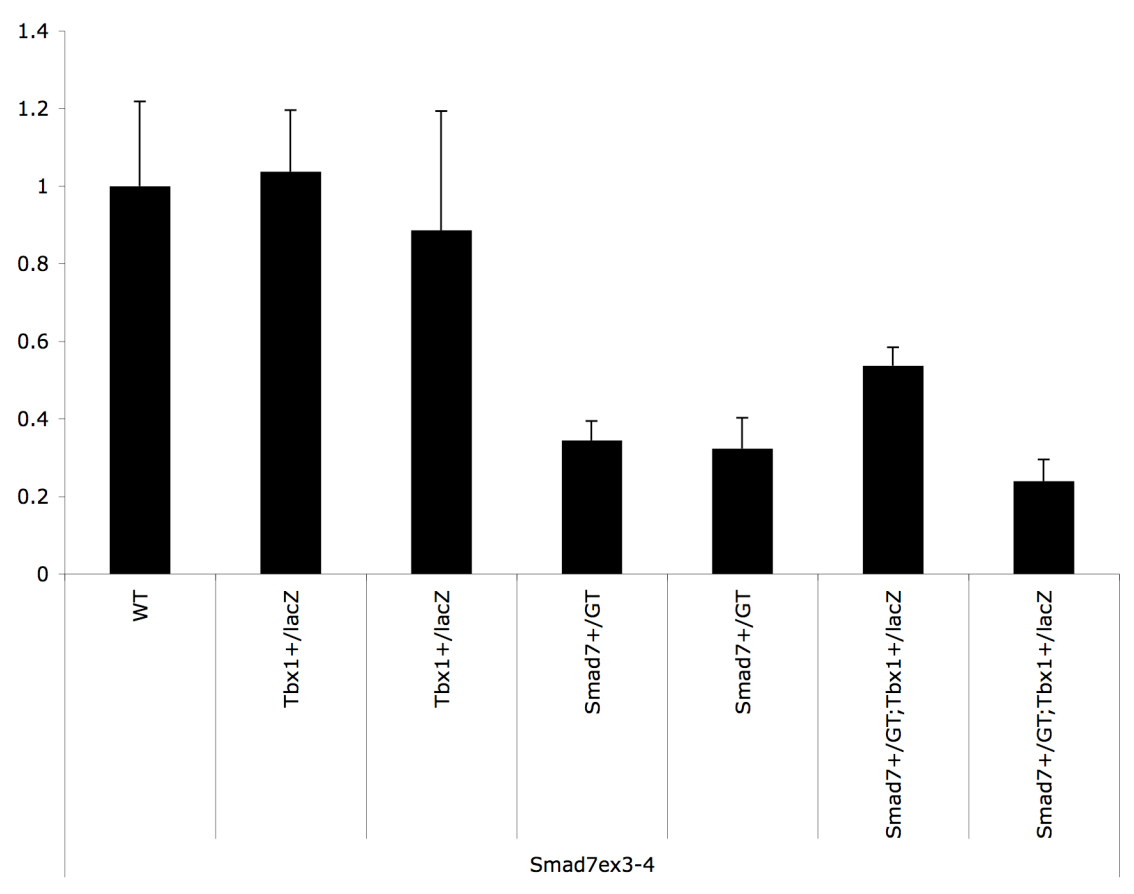

Figure 3. 19. *Smad7* expression levels in *Tbx1* or *Smad7* heterozygous and *Tbx1*;*Smad7* double heterozygous embryos. Graphical representation of the relative expression levels of *Smad7* by quantitative real time PCR in E10.5 wild type, *Tbx1* heterozygous, *Smad7* heterozygous and *Tbx1*;*Smad7* double heterozygous embryos. WT, wild type.

As depicted on the graphs below, the best recombination efficiency at E10.5 or E10.75, achieved within 24 hours, was an increase to 26% of the wild type dosage of *Smad7* mRNA in a $Smad7^{GT/GT}$ embryo carrying the *CaggsCre* allele. It was induced after a single IP injection of free salt tamoxifen at E9.5. The levels of *Smad7* expression in the $Smad7^{GT/GT}$;*CaggsCre* embryo were statistically different to the wild type value (p=0.05, t-test). Prolonging the duration of the drug activity may induce greater recombination of the gene-trap vector and eliminate this difference between the $Smad7^{GT/GT}$;*CaggsCre* and the wild type embryos. Free salt tamoxifen administered in a series of two IP injections, one full dosage at E9.0 and half the dosage at E10.0, induced at maximum expression of 17% of the wild type levels in E10.5 $Smad7^{GT/GT}$;*CaggsCre*

embryos. The levels of *Smad7* expression between the *Smad7*$^{GT/GT}$;*CaggsCre* embryos and the wild type embryo were statistically different ($p<0.01$, t-test). Administration of free salt tamoxifen by OG at E10.0 induced no recombination (0.5% of the wild type levels) by E10.75. *Smad7* mRNA expression in the *Smad7*$^{GT/GT}$;*CaggsCre* embryo was statistically different to the wild type ($p<0.01$, t-test) (Figure 3.20).

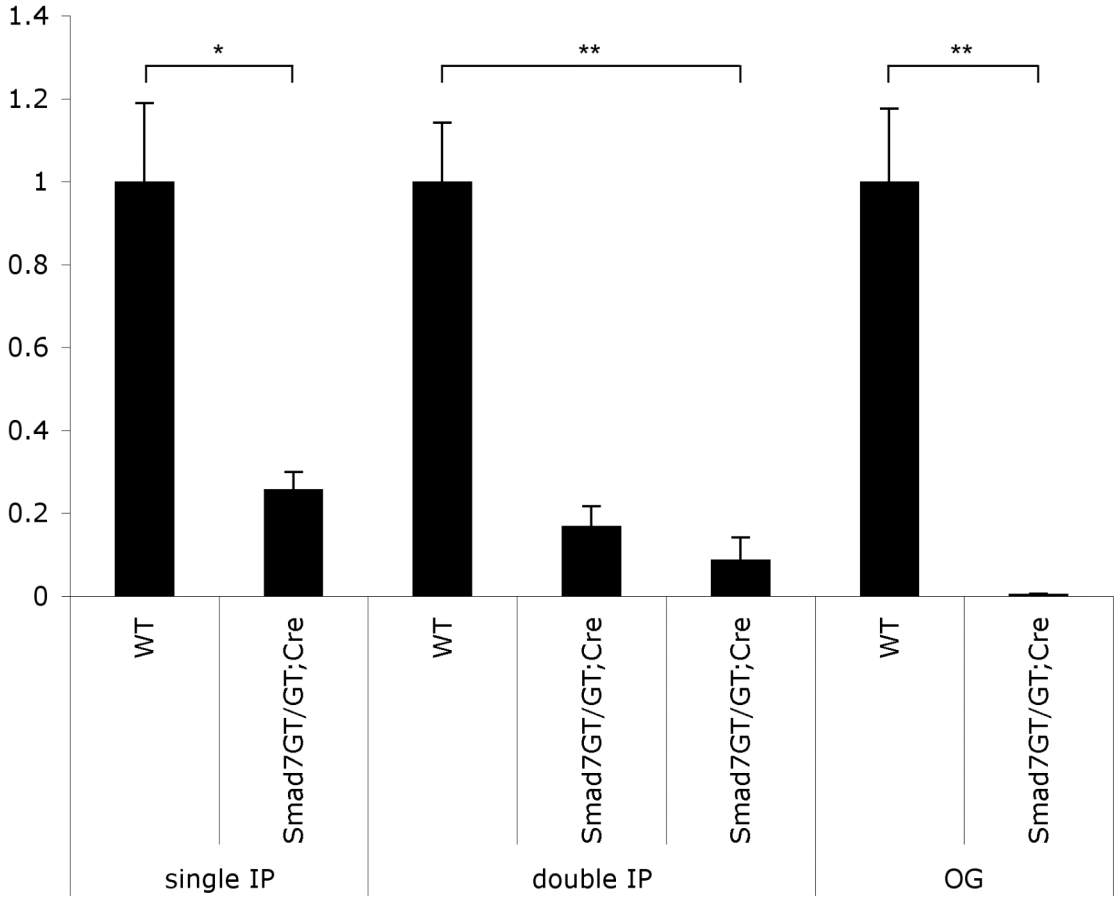

Figure 3. 20. *Smad7* gene-trap vector recombination efficiency in *Smad7*$^{GT/GT}$;*CaggsCre* embryos under different protocols of tamoxifen administration. Graphical representation of the relative expression levels of *Smad7* by quantitative real time PCR in E10.5 wild type and *Smad7*$^{GT/GT}$;*CaggsCre* embryos after tamoxifen induction with a single or double IP dosage, or OG (*p=0.05, **p<0.01). IP, intraperitoneal; OG, oral gavage; WT, wild type.

The comparison in the second genetic setting was between the double heterozygote levels and the double heterozygote carrying the *Cre* allele, within littermates. IP injection of the activated derivative (4OH) tamoxifen at E9.5 resulted in an absolute difference of 12% of the *Smad7* mRNA levels by E10.5 between a

Smad7$^{+/GT}$;*Tbx1*$^{+/lacZ}$;*CaggsCre* embryo and a *Smad7*$^{+/GT}$;*Tbx1*$^{+/lacZ}$ mutant. Relative to the wild type levels, the *Smad7*$^{+/GT}$;*Tbx1*$^{+/lacZ}$ embryo had 23% *Smad7* transcripts and the *Smad7*$^{+/GT}$;*Tbx1*$^{+/lacZ}$;*CaggsCre* embryo had 35%. IP injection of free salt tamoxifen at E9.0 induced an absolute difference of 15% of the *Smad7* mRNA levels by E10.5 in *Smad7*$^{+/GT}$;*Tbx1*$^{+/lacZ}$;*CaggsCre* embryos, compared to a *Smad7*$^{+/GT}$;*Tbx1*$^{+/lacZ}$ mutant. In this experiment the *Smad7*$^{+/GT}$;*Tbx1*$^{+/lacZ}$ embryo had 39% of the wild type *Smad7* mRNA and the *Smad7*$^{+/GT}$;*Tbx1*$^{+/lacZ}$;*CaggsCre* embryos had 54%. None of these values were statistically different to the wild type levels, so potentially both protocols can be used in future experiments (Figure 3.21).

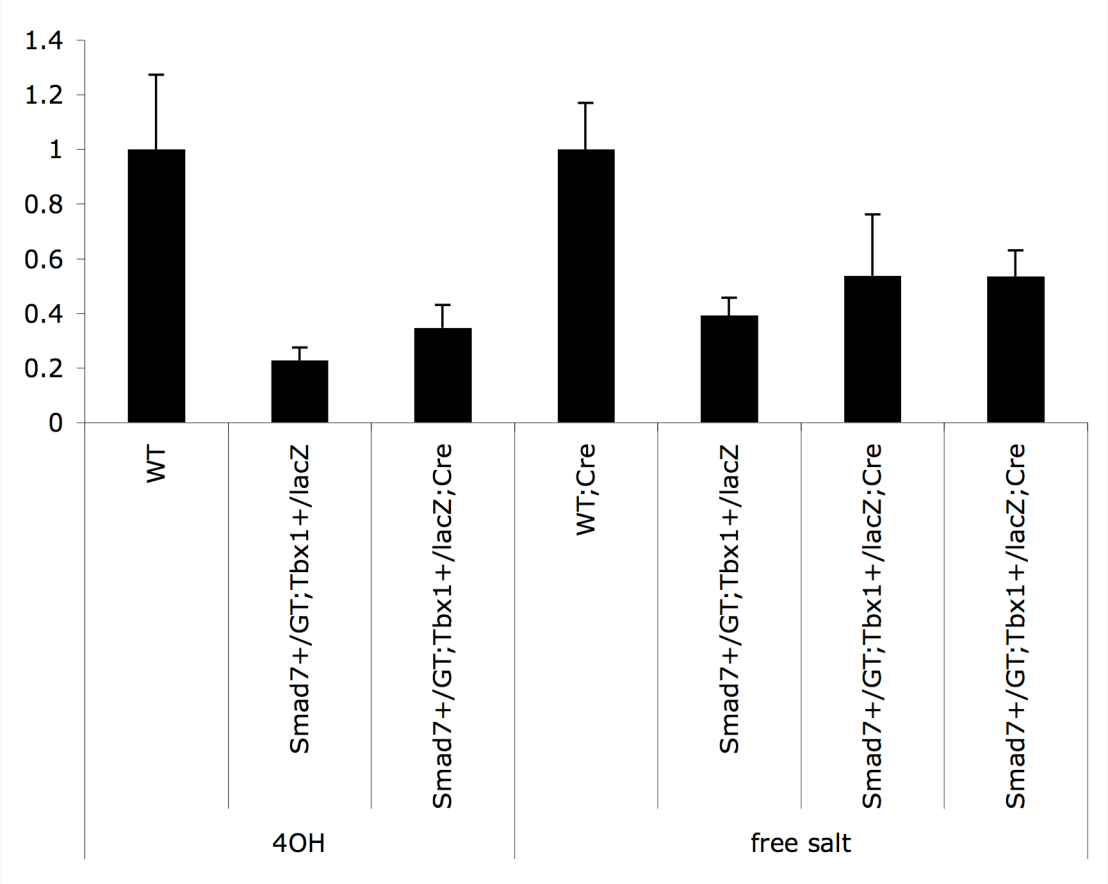

Figure 3. 21. *Smad7* gene-trap vector recombination efficiency in *Smad7*$^{+/GT}$;*Tbx1*$^{+/lacZ}$;*CaggsCre* embryos under different protocols of tamoxifen administration. Graphical representation of the relative expression levels of *Smad7* by quantitative real time PCR in E10.5 wild type, *Tbx1*$^{+/lacZ}$;*Smad7*$^{+/GT}$ and *Smad7*$^{+/GT}$;*Tbx1*$^{+/lacZ}$;*CaggsCre* embryos after induction with free salt tamoxifen or the activated derivative tamoxifen (4OH). WT, wild type.

To further validate the system's efficiency, recombination was assessed through X-gal staining using a *ROSA26* reporter line (Soriano, 1999), crossed to *Smad7*$^{+/GT}$;*CaggsCre* animals. Two different drug administration protocols were used, IP injection of 4OH tamoxifen at E9.5 and IP injection of free salt tamoxifen at E9.0. Both showed minimal recombination, while the *β-galactosidase* gene driven from the *Smad7* gene-trap was still highly expressed. Expression of the *Cre* gene was also tested by quantitative real time PCR and was found in abundance in all the expected genotypes. As shown in Figure 3.22, the levels of activated *Cre* are not sufficient for the level of recombination required. Changing the tamoxifen administration protocol to achieve prolonged activity of the drug, or a slightly higher dosage may produce better results.

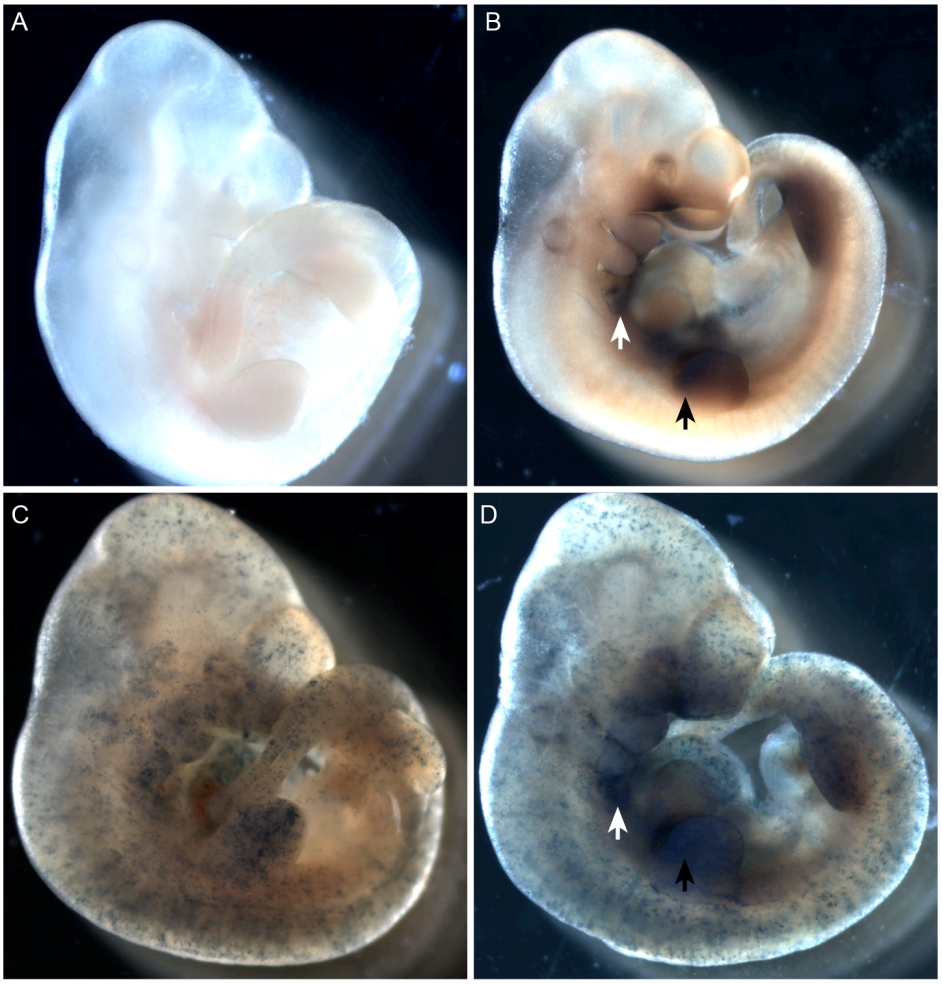

Figure 3. 22. Reporter expression indicating recombination efficiency in *Smad*$^{GT/GT}$*;CaggsCre* embryos. X-gal staining for the β-galactosidase reporter in E10.5 *ROSA26* embryos without the *CaggsCre* or the *Smad7* gene-trap allele (WT, A), with a

Smad7 gene-trap allele (*Smad7*$^{+/GT}$, B), with the *CaggsCre* allele (*CaggsCre*, C) and with both the *CaggsCre* and a *Smad7* gene-trap alleles (*Smad7*$^{+/GT}$;*CaggsCre*, D), after free salt tamoxifen induction for 30 hrs. White/ black arrows denote expression off the *Smad7* gene-trap vector, indicating inefficient recombination of the vector in (D). WT, wild type.

Genomic amplification and subsequent quantification of the wild type, gene-trap and recombined gene-trap locus showed similar levels of recombination to the quantitative real time PCR data (Figure 3.23). These results further support the notion that the current methods, including the type of tamoxifen, time of administration and administration method are not adequate. In conclusion, the lack of robust tamoxifen-induced recombination achieved to date precluded the conditional "rescue" experiments originally envisaged.

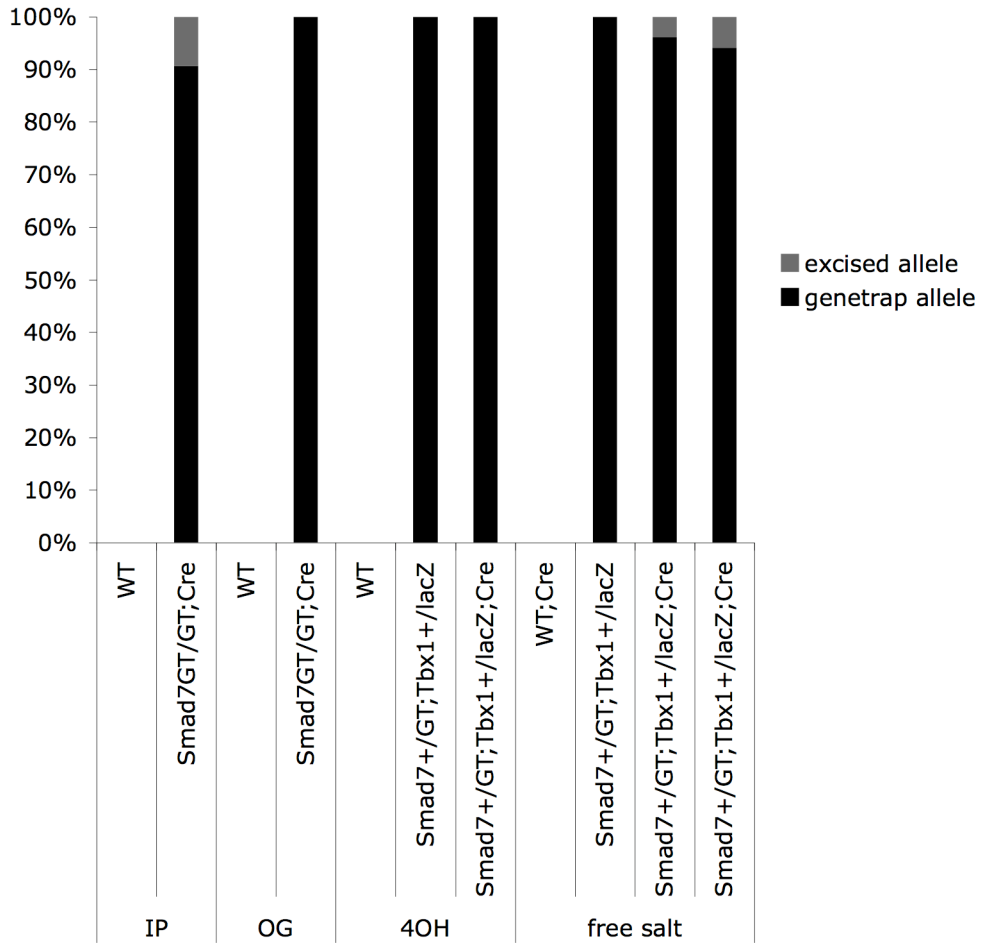

Figure 3. 23. Genomic amplification of the gene-trap and recombined gene-trap vector in different genotypes. Proportional representation of the genomic amplification of *Smad7* gene-trap (black) or recombined gene-trap alleles (grey) in E10.5 wild type, *Tbx1*;*Smad7* double heterozygous and *Smad7* gene-trap homozygous or *Tbx1*;*Smad7* double heterozygous embryos carrying the *Cre* allele, for the different tamoxifen administration protocols. There is no amplification of either of the alleles in wild type or wild type embryos carrying the *Cre* allele. Amplification of only the gene-trap allele is observed in $Smad7^{+/GT}$;$Tbx1^{+/lacZ}$ embryos, while amplification of both the gene-trap and the recombined alleles is observed in the $Smad7^{GT/GT}$;*CaggCre* and $Smad7^{+/GT}$;$Tbx1^{+/lacZ}$;*CaggsCre* embryos. Note that there is no recombination when tamoxifen is administered by OG, confirming the quantitative real time PCR data and none detected by this method in the embryos treated with the activated derivative tamoxifen (4OH). IP, intraperitoneal; OG, oral gavage; WT, wild type.

4. Discussion - Future directions

4.1. *Smad7* as a Tbx1 target

Smad7 was selected for this project as a putative Tbx1 downstream effector for a multitude of reasons. These included its expression profile during embryogenesis in heart and pharyngeal structures (Liu et al., 2007; Luukko et al., 2001; Zwijsen et al., 2000) and its differential regulation in *Tbx1*-expressing heterozygous and null cells (van Bueren et al., 2010). Interestingly, *Smad7* does not appear in two other array screens, one by us and one by an independent group that analysed the pharyngeal region of E9.5 (Ivins et al., 2005) or the secondary heart field of E8.75, E9.75 or E10.75 (Liao et al., 2008) mouse embryos respectively. This may reflect dilution effects, since both these arrays used entire embryonic segments that include non *Tbx1*-expressing cell populations. Also, as it was demonstrated in this thesis, a single null allele for *Tbx1* or even 34% of its wild type dosage are not sufficient to affect *Smad7* expression, when examined by whole mount *in situ* hybridisation. Stage, tissue and dosage-specific effects are probably characterising the *Tbx1*-*Smad7* relationship.

4.2. Direct or indirect target?

Smad7 mRNA was reduced in pharyngeal and cardiac tissues of E9.5 *Tbx1* null embryos, although not in heterozygotes or hypomorphs that express 34% of *Tbx1*. Limitations of the technique used here to identify changes in gene expression should not be disregarded. A more refined, quantitative approach can be followed, for example FACS sorting of $Tbx1^{Neo2/Neo2}$ cells, to examine *Smad7* levels on a cell autonomous setting and establish the *Tbx1* dosage requirements for *Smad7* expression. Nevertheless, these results indicate that *Tbx1* is necessary for the expression of *Smad7* in some embryonic domains, potentially in a dosage-dependent fashion.

It was recently demonstrated that a 4.3 kb *Smad7* promoter can recapitulate gene-specific expression during mouse development (Liu et al., 2007). No putative Tbx1 binding sites (Sinha, 2000) were found within this region and *in vitro* experiments within 2 kb upstream of the 5‘UTR of Smad7 did not conclusively show Tbx1 dependent activation of these subregions of the *Smad7* promoter. Putative Tbx1 binding elements have been identified in regulatory regions of the *VEGFR3* (Chen et al., 2010),

Pitx2c (Nowotschin et al., 2006), *Fgf8* (Hu et al., 2004) and *Fgf10* (Xu et al., 2004) genes. Tbx1 activates reporter constructs harboring these elements. However, only *VEGFR3* has been validated by ChIP (Chen et al., 2010) and *Pitxc2* has been verified by an electromobility sift assay (EMSA) (Nowotschin et al., 2006). Tbx1 additionally required Nkx2.5 to activate the *Pitx2c* enhancer reporter construct (Nowotschin et al., 2006). Ablating putative T-box binding elements from the *Mef2c* (Antonio Baldini, pers. comm.) or *Pax9* (Rumiko Matsuoka**,** pers. comm.) promoters did not affect Tbx1 activation at these promoters, indicating that elements other than canonical TBEs must be important for Tbx1 driven transcription.

A recent study used ChIP with massively parallel sequencing (ChIP-Seq) to identify active tissue-specific enhancers that are bound by the ubiquitously expressed coactivator protein p300 (Blow et al., 2010). This assay was performed in E11.5 mouse heart tissue and yielded 3,597 regions that did not overlap with known promoters or with p300 peaks identified in E11.5 forelimb, midbrain and limb tissues (Blow et al., 2010). An enhancer was detected 136 kb from *Smad7*, and in no closer proximity to any other known cardiac gene (Blow et al., 2010). This enhancer appeared to have activity in the outflow tract, as shown *in vivo* by transgene reporter expression (Blow et al., 2010). The reporter expression resembles E11.5 *Smad7* expression in the cardiac outflow tract but does not recapitulate all the *Smad7* expression domains. The distance the site was identified at and the restricted expression pattern of the reporter denote that enhancer elements are not necessarily located close to the transcription initiation site of a gene and that different enhancers may regulate tissue-specific expression of a gene.

Given the above, the presence or absence of putative Tbx1 binding sites in the immediate regulatory region of a gene does not conclusively indicate whether the gene of interest is directly regulated by Tbx1 or not. *Smad7* may therefore be Tbx1 controlled through elements not yet identified or it may be an indirect Tbx1 target. The single putative Tbx1 binding site located approximately 13 kb upstream the 5' UTR of *Smad7* could be examined in the future for *in vitro* Tbx1 binding.

4.3. *Smad7* is expressed in heart and pharyngeal structures during development

Smad7 expression was detected in multiple different cell types, structures and organs from E8.5 to E11.5. Whole mount *in situ* hybridisation and X-gal staining were used to confirm that the expression pattern of the β-galactosidase reporter matched that of the *Smad7* mRNA. Consistent with previous reports (Luukko et al., 2001; Zwijsen et al., 2000), *Smad7* expression was detected by whole mount *in situ* hybridisation in extraembryonic tissues at E7.5, in the heart endocardium and myocardium from as early as E8.5, and in the outflow tract and AV cushions as well as in veins and arteries from E10.5-E11.5. Conversely to Luukko *et al.*, however, expression in the cardinal veins identified here preceded DAo expression (Luukko et al., 2001). Zwijsen *et al.*, have demonstrated strong *Smad7* expression from as early as E8.0 in the lateral plate and cardiac mesoderm and weaker in the endoderm, neuroectoderm and paraxial and cephalic mesoderm (Zwijsen et al., 2000). These results were not reproduced here, although the same probe (Zwijsen et al., 2000) was used for whole mount *in situ* hybridisation. At E8.5, strong expression was only identified in the distal part of the tail and yolk sac tissues, while very faint expression was seen in the rest of the embryo proper, mainly in the myocardial and endocardial lining of the heart. This inconsistency with the previously published expression pattern may be attributed to the different methods used, chromophore versus radioactive labelling. Additionally, the myocardial and endocardial *Smad7* staining detected here in all the embryonic stages examined is contradictory to the endocardial-specific reporter expression identified with the use of a *Smad7Cre* line (Snider et al., 2009). The particular line was established with the 4.3 kb *Smad7* promoter (Liu et al., 2007). Nonetheless, the promoter itself has only been tested from E11.5 onwards (Liu et al., 2007); exclusion of earlier expression domains through different promoter elements cannot be ruled out.

Tbx1 is expressed in the pharyngeal epithelia and mesoderm from as early as E7.5 (Chapman et al., 1996; Huynh et al., 2007; Lindsay et al., 2001; Vitelli et al., 2002a) and hence partially overlaps with *Smad7* between E8.5-E10.5. This supports the potential for an interaction between the two genes, while the *Smad7* expression pattern in cardiac structures throughout embryogenesis suggests independent roles for *Smad7* during cardiovascular development.

4.4. *Smad7* mutation produces aspects of the 22q11DS-like phenotype

The gene-trap effectively introduces a null *Smad7* mutation, at least at the mRNA level. *Smad7*$^{GT/GT}$ embryos exhibit a cardiovascular phenotype that includes great vessel and intracardiac septation defects. This is in agreement with systemic *Smad7* deletion under the *Tie2Cre* promoter in female carriers, or the *EIIaCre* promoter (Chen et al., 2009). However, no valve defects were seen in any of the thirty gene-trap homozygotes examined in this thesis, while only three had a VSD, in contrast with the previous study (Chen et al., 2009). Genetic background modifiers or factors related to timing and/or efficiency of the recombination of the *Smad7* locus in the work by Chen *et al.*, may have resulted in these different phenotypes (Chen et al., 2009). The construct used to produce the conditional mouse model contains two loxP sites flanking exon 4 and the stop codon of the gene (Chen et al., 2009). Exon 4 harbors the entire MH2 domain located on the C-terminus of the protein (Chen et al., 2009), however, both the N-terminus and MH2 domains participate in the Smad7-specific inhibition of TGFβ/activin signalling (Yan et al., 2009). In that respect the truncated protein may still have limited functionality, causing inconsistencies between the phenotypes of the different mutants.

Despite *Smad7* expression in heart and outflow tract septation regions during embryogenesis, septation defects were not seen at all in the outflow tract, and with very reduced penetrance in the heart of the gene-trap homozygous mutants. This suggests that Smad7 is dispensable in these areas, and may be compensated for by Smad6, the other inhibitor of the TGFβ/BMP pathways. The majority of the animal models with a mutation in a BMP factor display valve abnormalities, outflow tract and heart septation defects (Chen et al., 2004; Gaussin et al., 2005; Gaussin et al., 2002; Jiao et al., 2003; Kaartinen et al., 2004; Kim et al., 2001; Liu et al., 2004; Ma et al., 2005; Solloway and Robertson, 1999; Stottmann et al., 2004). *TGFβ* gene mutations are additionally associated with great vessel malformations (Bartram et al., 2001; Choudhary et al., 2006; Todorovic et al., 2007; Wang et al., 2006; Wurdak et al., 2005). Both Smad7 and Smad6 act on the BMP branch of the pathway (Moustakas and Heldin, 2009; Park, 2005; Ross and Hill, 2008; Yan et al., 2009), and are strongly co-expressed in the cardiovasculature and mainly in the AV cushions, DAo and major arteries (Luukko et al., 2001). Therefore, if cardiac and outflow tract septation processes are primarily BMP

regulated, Smad6 may be compensating for the lack of Smad7. Additionally, no trabeculation abnormalities were observed in the *Smad7* gene-trap homozygous mutants in spite of the myocardial and endocardial expression of the gene and in contrary with the previous systemic deletion of *Smad7* (Chen et al., 2009). In this study the authors showed that Smad2/3 phosphorylation was increased in the ventricular endocardium of the *Smad7* mutant mice, suggesting that the TGFβ/activin pathway was affected in this process (Chen et al., 2009). Smad6 would not have a compensatory inhibiting role on this branch of the pathway, therefore genetic background modifiers or residual functionality of the proteins of either of the models may account for the differences in this phenotype.

In the context of 22q11DS, $Smad7^{GT/GT}$ embryos also display thymic and isolated palate malformations, partially phenocopying the *Tbx1* mutation. These phenotypes have not been previously reported for *Smad7*. The thymic defects were identified in the majority of the gene-trap homozygous embryos, indicating that *Smad7* is required for some or several of the steps of thymus formation and morphogenesis. At E9.5, when the thymic primordium evaginates into the underlying mesenchyme (Boehm, 2008; Gill et al., 2003; Hollander et al., 2006; Manley, 2000), the gene is expressed in the caudal pharyngeal endoderm, although no *Smad7* expression was detected in this tissue from E10.5 onwards. *Smad7* may participate in the early events of thymus development. Chicken-quail chimeras as well as *in vitro* studies have shown that the endoderm can induce non-pharyngeal mesenchyme to play a role in thymus organogenesis (Manley, 2000). *Smad7* may be modulating signalling originating from the gut endoderm at E9.5. Evidence shows that ectodermal signalling through *Tbx1* participates in thymic development (Randall et al., 2009); therefore, the ectodermal expression of *Smad7* between E9.5-E10.5 may similarly be involved in this developmental process. Previous studies have shown that overexpression of SMAD7 in the thymic epithelia results in severe hypoplasia of the organ (He et al., 2002). This, however, does not indicate that *Smad7* is important in thymic morphogenesis since this model effectively induces global inhibition of both TGFβ/BMP pathways. Expression analysis of thymic markers on $Smad7^{GT/GT}$ embryos could provide insight in the role of the gene in thymus development. The *Smad7* requirements in thymic development were not investigated further in this thesis, due to time restraints.

4.4.1. The *Smad7* mutant great vessel and arch artery phenotype in detail

The pharyngeal arch artery formation process completes by E10.5 in the mouse embryo (Hiruma et al., 2002; Yanagisawa et al., 1998), while by E15.5 the arch arteries have remodelled into the mature left-sided aortic arch configuration (Hiruma et al., 2002). *Smad7*$^{GT/GT}$ embryos have a very low penetrance of arch artery defects at E10.5-E11.5, but a higher frequency of such defects at E15.5-E18.5. This great vessel phenotype is therefore more likely due to abnormalities during the remodelling rather than the formation of the pharyngeal arch arteries. In the current sample size there is no statistically significant difference between the arch artery defects scored at E10.5-E11.5 versus E15.5-E18.5 in *Smad7*$^{GT/GT}$ embryos. However, a trend exists, supporting a later contribution of *Smad7* to the phenotype. The early stage (E10.5-E11.5) *Smad7*$^{GT/GT}$ embryos exhibit primarily hypoplastic fourth arches, or in a single case, non regressing right sixth artery. By the late stages (E15.5-E18.5) the defects observed in *Smad7*$^{GT/GT}$ mutants are mainly configurations that would have resulted from originally aplastic vascular segments and present with higher penetrance. Consequently, the type of the early stage defects does not sufficiently explain the late stage phenotype.

4.4.2. *Smad7* mutants display aberrant expression of *Klf2*, a shear stress related factor

Vessel walls respond to mechanical forces like shear stress or pressure with functional and phenotypic changes, including calcium signalling, NO production and gene expression regulation (Ando and Yamamoto, 2009; Ando and Yamamoto, 2010). Endothelial cells are specifically sensitive to shear stress and can discriminate between that and stretch forces (Andersson et al., 2005). *Smad7* was originally discovered as a shear stress responsive gene, induced by physiologic fluid mechanical stimulus in HUVECs (Topper et al., 1997). Additionally, *Smad7* has an endothelial-specific expression pattern in human (Topper et al., 1997) and mouse (Zwijsen et al., 2000) tissues. Among others, *Klf2* is a shear stress responsive gene (Poelmann et al., 2008). Interestingly, it was found to be upregulated in E9.5 *Smad7* gene-trap homozygous and heterozygous embryos compared to wild type controls. This may be related to compromised vascular integrity and further to that, with the pharyngeal arch artery remodelling program, since blood flow influences vascular remodelling (Rudic et al., 1998; Wang et al., 2009; Yashiro et al., 2007). A day later, at E10.5, *Klf2* appeared

moderately downregulated in the *Smad7* gene-trap homozygotes and heterozygotes. This transient differential *Klf2* expression corresponds with the transient *Smad7* expression pattern in the pharyngeal tissues. At E8.5 and E10.5 *Smad7* is detected weakly in the ectodermal covering alone, while in the intermediate stage, at E9.5, it is also found in the pharyngeal endoderm and mesenchyme. Maybe *Klf2* is regulated by *Smad7* at E9.5 and returns to normal expression levels in consequent stages. Nonetheless, it should be taken into account that these expression data were acquired from whole embryo lysates, and dilution effects are likely to mask tissue-specific changes, for example transcriptional alterations in the endothelial cell lineage. The examination of shear stress response genes on whole embryos was a prelude to investigating whether deficiency of *Tbx1* and/or *Smad7* impact upon this important aspect of remodelling, which will be assessed in more refined approaches in future work.

4.4.3. *Smad7* mutants appear to have unaffected neural crest patterning

Several mouse models have been described to date displaying arch artery formation or remodelling defects. These defects are in many cases caused by defective neural crest cell patterning that results in failed differentiation of post migratory crest (Liu et al., 2004) or reduced cellularisation of various structures (Kaartinen et al., 2004; Richarte et al., 2007). The neural crest migration pattern appeared unaffected in the $Smad7^{GT/GT}$ embryos by whole mount *in situ* hybridisation, although this experiment needs to be repeated, potentially with other crest markers too. The neural crest-derived VSM composition of the arch arteries has not yet been assessed in the mutant setting. All in all, solid conclusions regarding the role of the neural crest in the arch artery defects observed in $Smad7^{GT/GT}$ embryos cannot be drawn as yet.

Smad7 overexpression in the neural crest caused a spectrum of abnormalities, due to cell death in the pharyngeal arch arteries, craniofacial structures, and outflow tract cushions (Tang et al., 2010). Neural crest migration into the pharyngeal arches and subsequent differentiation in VSM cells was not affected (Tang et al., 2010). Nevertheless, this overexpression model does not provide insight into the roles of *Smad7* in the neural crest cell lineage as it induces general knock-down of the TGFβ/BMP pathways, so the resulting severe phenotype is hardly unexpected.

4.5. TGFβ/BMP pathway inhibition by Smad7

TGFβ signalling is important for endocardial and outflow tract cushion formation through mechanisms well characterised for many of the pathway components following knock-out or conditional models and expression studies (Person et al., 2005). As discussed previously, the majority of the models that ablate expression of *TGFβ* superfamily genes induce valve and/or septation defects and almost all of these genes are expressed in the embryonic heart (Person et al., 2005). *BMP* gene mutations predominantly produce septation anomalies (Chen et al., 2004; Gaussin et al., 2005; Gaussin et al., 2002; Jiao et al., 2003; Kaartinen et al., 2004; Kim et al., 2001; Liu et al., 2004; Ma et al., 2005; Solloway and Robertson, 1999; Stottmann et al., 2004), however, a number of *TGFβ* gene mutations induce great vessel malformations too (Bartram et al., 2001; Choudhary et al., 2006; Todorovic et al., 2007; Wang et al., 2006; Wurdak et al., 2005). Although Smad7 is an inhibitor of both pathways (Moustakas and Heldin, 2009; Park, 2005; Ross and Hill, 2008; Yan et al., 2009), the gene-trap mutation used in this thesis resulted primarily in arch artery abnormalities in the homozygotes, and only very few intracardiac defects. So, Smad7 may be acting via a TGFβ/activin route, towards the remodelling of the great vessels. Smad6 preferentially blocks the BMP branch (Moustakas and Heldin, 2009; Park, 2005; Ross and Hill, 2008; Yan et al., 2009), therefore, there is more reason to expect compensatory effects in the BMP rather than the TGFβ pathway, if there are any.

To date it has not been possible to conclusively establish which pathway is affected in the *Smad7* gene-trap mutants, by examining the levels of pSmad2/3 and pSmad1/5/8 in whole embryo lysates. An indication exists that in whole embryos, lack of Smad7 affects the BMP branch of the pathway, shown by a higher concentration of the pSmad1/5/8 complex in *Smad7* gene-trap homozygous as compared to heterozygous embryos. Potentially, assessment of these phosphorylated complexes on a fine dissection of the pharyngeal apparatus and heart of $Smad7^{GT/GT}$ embryos will address this more effectively. Moreover, *Smad7* is probably involved in both pathways towards the development of different embryonic structures, so tissue-specific examination of the pSmad2/3 and pSmad1/5/8 readouts will further define the discrete pathway requirements for *Smad7* in pharyngeal arch artery, cardiac, thymus and palatal shelf development. Immunohistochemical methods can be employed to that end.

TGFβ/BMP signalling is involved in the EMT process during palatal shelf fusion (Nawshad and Hay, 2003). Cleft palate was scored in only two *Smad7*$^{GT/GT}$ embryos, in combination with thymic, great vessel defects and in one of the two embryos with a VSD too. Consequently, *Smad7* probably has a minor role in palate morphogenesis, as demonstrated by this low penetrant phenotype. This may be attributed to gene dosage effects and/or compensatory roles from other genes of the TGFβ/BMP pathways.

4.6. Double heterozygosity for *Tbx1* and *Smad7* induces thymic and cardiovascular anomalies

At E15.5 *Tbx1*;*Smad7* double heterozygotes present with a higher penetrance of some 22q11DS-related phenotypes, namely thymic hypoplasia and fourth arch-derived great vessel defects, than the single gene heterozygotes or the wild type littermates. The defects scored in the double heterozygotes were statistically different to all other genotypes including the additive phenotypic outcome of each single mutation, therefore, a synergistic interaction is more likely than an additive effect of the two genes. For the purposes of this thesis the thymic phenotype was not studied any further and the focus was turned to the cardiac phenotype.

4.6.1. The great vessel and arch artery phenotype in detail

In order to investigate the relationship between *Tbx1* and *Smad7* more deeply, the great vessel phenotype of the *Smad7*$^{+/GT}$;*Tbx1*$^{+/lacZ}$ embryos was examined in detail. During early stages, at E11.0, these embryos present with a frequency of fourth arch artery abnormalities comparable to the *Tbx1* heterozygotes. There is no statistical difference between the *Tbx1* and *Tbx1*;*Smad7* heterozygotes at this stage and this reflects the sole contribution of *Tbx1* to this phenotype. This is further supported by the fact that *Smad7*$^{+/GT}$ embryos have normal arch artery formation. After arch artery remodelling has completed, at E15.5, the *Tbx1* heterozygotes present with a reduced penetrance of fourth arch defects compared to the earlier stage, as reported in several previous studies (Calmont et al., 2009; Lindsay et al., 2001; Vitelli et al., 2002b Vitelli et al., 2006; Zhang and Baldini, 2008). The double heterozygotes however do not show similarly reduced penetrance in great vessel defects. This is indicated by the statistically significant difference in the frequency of abnormalities between the *Tbx1*$^{+/lacZ}$ and *Smad7*$^{+/GT}$;*Tbx1*$^{+/lacZ}$ embryos of this stage. The great vessel defects observed in the

E15.5 double heterozygotes are exclusively fourth arch-derived, with similar frequency as scored at E11.0, prior to the remodelling process. No statistical difference exists in the double heterozygous populations between the two different time points. This suggests that recovery does not occur in the double heterozygotes and the defects initially caused by *Tbx1* haploinsufficiency result in an abnormal phenotype due to diminished Smad7, which compromises the rescue.

Similarly to what was observed in the $Smad7^{GT/GT}$ embryos at E10.5, *Klf2*, a shear stress responsive gene appeared reduced at E10.5 in the $Smad7^{+/GT}$;$Tbx1^{+/lacZ}$ mutants, compared to both the wild type and *Tbx1* heterozygous levels. Although this is insufficient evidence, it is supportive of a common pathway, further linking *Smad7* with *Tbx1*.

Another aspect that should be discussed here is the time-specific requirements for *Tbx1* in the development of the different heart and pharyngeal structures. Xu *et al.*, elucidated these requirements using a tamoxifen activatable model that induces ubiquitous deletion of *Tbx1* within 24 hrs post drug administration (Xu et al., 2005). The haploinsufficient aortic arch phenotype was produced only with the earliest heterozygous deletion of *Tbx1*, by E8.5, and it was scored with a penetrance of 44% in term embryos (Xu et al., 2005). The penetrance of the phenotype was incomplete but did recapitulate the $Tbx1^{+/-}$ phenotype expected (Calmont et al., 2009; Lindsay et al., 2001; Vitelli et al., 2002b Vitelli et al., 2006; Zhang and Baldini, 2008) for the stage examined. These results indicated that *Tbx1* is required before E8.5 for aortic arch patterning (Xu et al., 2005). Pharyngeal arch artery formation, prior to the remodelling process, was not assessed in these embryos (Xu et al., 2005). In summary, *Tbx1* is probably required before E8.5 for pharyngeal arch artery formation, but does not appear to regulate the recovery of the fourth arch defects.

4.6.2. *Tbx1* genetically interacts with other genes towards fourth arch artery development

4.6.2.1. Defining "genetic interaction"

Addressing the functional relationships between genes can be a useful tool in understanding the basic principles of the underlying genetic networks (Wong et al., 2004). A common approach includes intercrossing of single mutants with distinct

phenotypes and comparing these with the phenotype of the resulting double mutants (Perez-Perez et al., 2009). The phenotype of the double mutation is considered additive when it displays features present in the single mutants, or epistatic when it is reminiscent of the phenotype of one of the single mutants, but not the other. Alternatively, the double mutant phenotype can be regarded as suppressed when it is closer to the wild type condition than either of the single mutants (Perez-Perez et al., 2009), or synergistic, when it is significantly different to the phenotype of either single mutations alone or the additive effects of the individual mutations (Perez-Perez et al., 2009; Wong et al., 2004). Additivity is generally accepted as indication of absence of a functional relationship between the mutated genes under study (Perez-Perez et al., 2009). Conversely, epistasis and suppression are considered as the phenotypic outcomes of genetic interaction (Perez-Perez et al., 2009). Interpreting synergistic interactions, however, is somewhat more controversial, mainly because of the difficulties in distinguishing synergy from additivity (Perez-Perez et al., 2009). Synergy can often be the result of functional redundancy between paralogous genes or haploinsufficiency effects, but it can also be observed when converging pathways are disrupted, or when a mutation enhances the sensitivity to the effects of another mutation (Perez-Perez et al., 2009).

The use of statistical methods that estimate the average deviation of combinations of alleles against the rest of the genotypes within a population has proved to be a safe tool for establishing the genetic interactions on a specific genetic context (Phillips, 2008). Here, Fisher's exact test was used to compare the populations of different genotypes or of different time points produced by intercrossing *Tbx1*$^{+/lacZ}$ to *Smad7*$^{+/GT}$ animals.

4.6.2.2. Pooling data from the literature

Several studies to date have examined possible interactions between *Tbx1* and other genes in pharyngeal arch artery formation or remodelling (Aggarwal et al., 2006; Calmont et al., 2009; Guris et al., 2006; Morishima et al., 2003; Randall et al., 2009; Vitelli et al., 2002b). Most commonly, the single and double heterozygous embryos are assessed for arch artery formation defects. In some cases, they are also examined at a later stage, after the completion of arch artery remodelling, for great vessel defects. For the purposes of this thesis, the results of such studies were pooled and where

possible/available fourth arch artery hypoplasia and aplasia were recorded (Table 3.14). A hypoplastic vessel was considered thin patent (Th-P) while an aplastic one was classified as non patent (NP). If we consider that a hypoplastic vessel has the capacity to revert its state through molecular signalling, mechanical forces or the combination of these and recover into a functional part of the mature configuration, then a number of genes would be involved in regulating these mechanisms. Conversely, an absent (aplastic) vessel would not have this potential, and in order for a viable system to be produced by the end of embryonic development, arterial rearrangements might occur to compensate for the lost segment, providing alternative routes for blood circulation. These rearrangements, however, would produce a distinguishable anatomical outcome, unrelated to whether the final configuration is viable or not. During the pooling of these studies, there was no discrimination between unilateral and bilateral defects if both sides presented the same type of anomaly, while the cases of bilateral abnormalities with one Th-P and one NP vessel were classified as NP, in the sense that they are predicted to produce an abnormal phenotype at the later stage, should the embryo survive. Fisher's exact test was used on the data gathered from all the previously published studies, and the statistical result of this meta-analysis is denoted by a latin cross (†).

4.6.2.3. Description and interpretation of the fourth arch artery phenotype in *Tbx1* heterozygotes

All the studies addressing *Tbx1* haploinsufficiency have to consider the fact that *Tbx1* heterozygotes partially recover from the initial fourth arch artery defect in subsequent stages of development (Calmont et al., 2009; Lindsay et al., 2001; Vitelli et al., 2002b Vitelli et al., 2006; Zhang and Baldini, 2008). Whether or not this recovery is a *Tbx1* controlled process has not been studied yet. Essentially, combining all these studies is useful in clarifying if *Tbx1* plays an additional part in arch artery remodelling, aside from its known earlier role in arch artery formation (Jerome and Papaioannou, 2001; Lindsay et al., 2001; Merscher et al., 2001). Such a role may be masked by the severity and penetrance of the earlier formation defect. From the data collected from the literature it is apparent that during early stages of development *Tbx1* haploinsufficiency induces both hypoplastic and aplastic vascular segments. This difference may be due to genetic dosage, fine tuning in genetic networks, or purely the result of a set of stochastic events.

4.6.2.4. Reviewed gene interactions with *Tbx1* in pharyngeal arch artery morphogenesis

Morishima *et al.*, only checked the early stage of arch artery formation in *Tbx1* and *endothelin converting enzyme* (*Ece1*) double heterozygous embryos (Morishima et al., 2003). At E10.5 80% of the *Tbx1* heterozygotes had a hypoplastic fourth vessel with no statistically significant difference to the complete penetrance in hypoplastic fourth vessels of the double heterozygotes (Morishima et al., 2003). The *Ece1* heterozygotes were normal with the exception of one displaying a persistent second arch artery (Morishima et al., 2003). No later developmental stages were examined and although it was a small sample size, the data indicate that *Ece1* has no contribution in fourth arch artery formation.

Tbx1 is shown to interact with *Gbx2* in the formation of the fourth arch artery (Calmont et al., 2009). Although in this sample size the recovery of the fourth arch artery defect cannot be proven, the NP vessels alone at E10.5 (36% out of a total of 45%) were sufficient to cause the fourth-related defects scored at E15.5 in 26% of the population ($p=0.43>0.05$, no difference †) (Calmont et al., 2009). The same was true in the double heterozygous setting, where 79% of the $Gbx2^{+/-}$;$Tbx1^{+/lacZ}$ embryos displayed NP fourth arches, and this was not different to the 59% of fourth arch related defects scored at E15.5 in the same genotype ($p=0.20>0.05$, no difference †) (Calmont et al., 2009).

Likewise, *Tbx1* is shown to interact with *Chd7* in the formation of the fourth arch arteries (Randall et al., 2009). In single gene heterozygosity on this background, *Tbx1* produced 21% of NP fourth arches at E10.5, correlating well with the 24% of fourth-related defects scored at E15.5 ($p=0.60>0.05$, no difference †) (Randall et al., 2009). In the double heterozygous groups, 100% penetrance of non patency was comparable to 100% penetrance of fourth arch related defects observed at the two stages respectively (Randall et al., 2009).

Different studies have assessed the genetic interaction between *Tbx1* and the FGF pathway. Aggarwal *et al.*, examined *Tbx1* heterozygosity in combination with *Fgf8*, *Fgf10* or *Fgf8* and *Fgf10* heterozygosity (Aggarwal et al., 2006). Although in a very small sample size, a difference was observed between the $Tbx1^{+/-}$ and $Fgf8^{+/-}$;$Fgf10^{+/-}$;$Tbx1^{+/-}$ genotypes ($p<0.05$) (Aggarwal et al., 2006). In this study only the late

embryonic stage was studied, when the left-sided arch is fully formed (Aggarwal et al., 2006). The triple heterozygotes had either a left or a right fourth arch artery related defect (Aggarwal et al., 2006). These results indicate a contribution of the *FGF* genes to the resulting phenotype, but there is not enough data to examine the fourth arch artery recovery processes in these mutants. Vitelli *et al.*, showed that *Fgf8* and *Tbx1* genetically interact in the formation of the fourth arch arteries by studying the severity of the defects scored in the different genotypes at E10.5 (Vitelli et al., 2002b). At this stage a total of 93% of $Tbx1^{+/lacZ}$ embryos presented with a fourth arch defect but only 50% exhibited an NP vessel. (Vitelli et al., 2002b) Similarly, 93% of the E10.5 $Fgf8^{+/-}$;$Tbx1^{+/lacZ}$ transheterozygotes displayed a fourth arch defect, while 86% had an NP vessel (Vitelli et al., 2002b). The authors added the individual NP defects in each group (i.e. 2 vessels per embryo so the number of defects is double the number of embryos) and concluded that *Tbx1* and *Fgf8* interact towards the formation of the fourth arch ($p<0.01$) (Vitelli et al., 2002b). By comparing the NP defects per embryo, disregarding the unilateral or bilateral nature as approached here in all the studies analysed, the two groups are barely significant ($p=0.05$, †) Also, in terms of total defect penetrance there is no difference between the *Tbx1* heterozygous and the double heterozygous embryos (93% penetrance in both groups). Moreover, the great vessel defects scored in these two genotypes at E18.5, after complete remodelling of the arch arteries, indicate that both the $Tbx1^{+/lacZ}$ and $Fgf8^{+/-}$;$Tbx1^{+/lacZ}$ embryos partially rescued the fourth arch defects ($p=0.09>0.05$, no difference †), as expected in *Tbx1* heterozygosity. Therefore, it is probably not safe to say that *Fgf8* interacts with *Tbx1* towards fourth arch artery formation, at least not in the current sample size. Regardless of a formation role, however, *Fgf8* does not appear to have any contribution to the arch artery remodelling process.

The study relating most closely to the *Tbx1*-*Smad7* interaction theory discussed in this thesis is the genetic interaction between *Crkl* and *Tbx1* (Guris et al., 2006). *Crkl* heterozygotes did not display any early formation defect in the arch arteries while at the same stage the double heterozygotes exhibited only *Tbx1*-related defects and failed to recover from these in the course of development (Guris et al., 2006). A total of 87% *Tbx1* heterozygotes displayed a fourth arch artery defect at E10.5-E11.0 but only 20% had one or both vessels NP, which correlates well with the 28% of the $Tbx1^{+/-}$ embryos that displayed a fourth related defect after remodelling of the great vessels, at E16.5

(p=0.46>0.05, no difference †) (Guris et al., 2006). Similarly, out of the total of 100% of $Crkl^{+/-}$;$Tbx1^{+/-}$ transheterozygotes with an early fourth arch artery defect, 88% of those exhibited unilateral or bilateral non patency as compared to 100% of the same genotype at the later stage that displayed a fourth arch related defect (p=0.22>0.05, no difference †) (Guris, 2006).

A similar pattern is observed in the progeny of $Tbx1^{+/lacZ}$ (x) $Smad7^{+/GT}$ crosses. At E11.0 $Tbx1^{+/lacZ}$ embryos exhibited a fourth arch defect with a penetrance of 65% but only 24% displayed non patency of the vessels. At E15.5 the frequency of the fourth arch related defects was 29%, and although the two populations are statistically different in terms of total defects, they are the same if only the NP defects are compared to the later stage (p=0.5>0.05, no difference). However, in contrast to all previous studies, in the $Smad7^{+/GT}$;$Tbx1^{+/lacZ}$ embryos the 38% of NP vessels seen does not suffice to cause the 68% of fourth-related defects scored at E15.5 (p<0.05, difference). This implies that during normal development, *Smad7* is part of a mechanism remodelling vessel architecture that can potentially sustain hypoplastic vessels and rescue a Th-P vessel phenotype. Therefore, *Smad7* does not necessarily share a common pathway with *Tbx1* in the remodelling process of the pharyngeal arteries, rather, lack of Smad7 in the *Tbx1*;*Smad7* heterozygotes prevents them from rescuing the hypoplastic vessels formed aberrantly earlier, due to lack of Tbx1 (Figure 3.24).

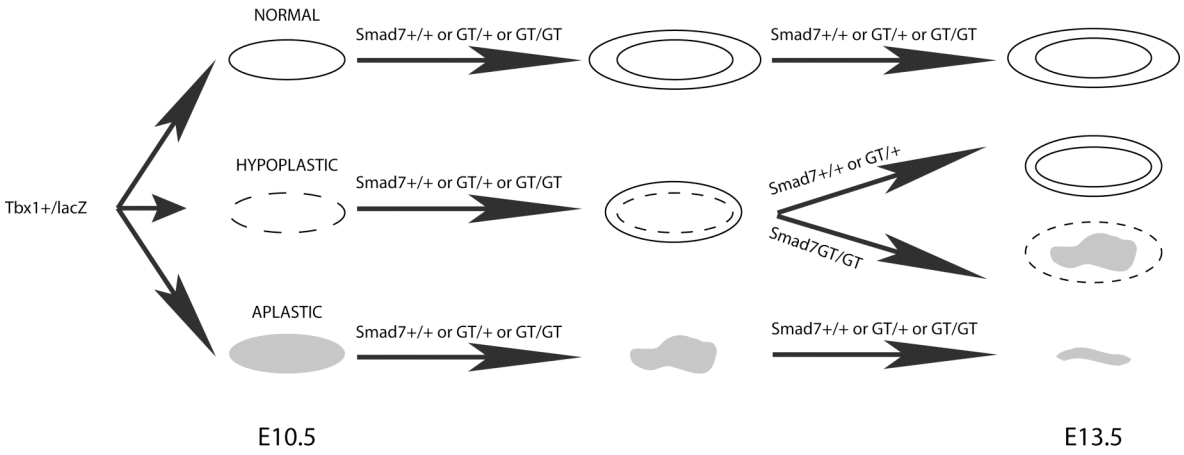

Figure 3. 24. Schematic representation of the presumptive requirement for *Tbx1* and *Smad7* during vessel development. *Tbx1* haploinsufficiency can result in normal, hypoplastic or aplastic vascular segments due to abnormalities in the formation process. During the remodelling process, a normal vessel or an aplastic one will produce a normal or a missing segment of the mature configuration respectively, regardless of the

Smad7 dosage. A hypoplastic vessel has the potential to recover, above a threshold of *Smad7* expression, which does not occur in the *Smad7* null setting.

	E10.5				E15.5-E18.5			
	WT	***Ece1*$^{+/-}$**	***Tbx1*$^{+/lacZ}$**	***Ece1*$^{+/-}$;*Tbx1*$^{+/lacZ}$**	**WT**	***Ece1*$^{+/-}$**	***Tbx1*$^{+/lacZ}$**	***Ece1*$^{+/-}$;*Tbx1*$^{+/lacZ}$**
Total embryos	7	8	5	9				
Total normal	7	7	1	0				
Total abnormal	**0**	**1* (12.5%)**	**4 (80%)**	**9* (100%)**		**NOT EXAMINED**		
L4th PAA	-	-						
R4th PAA	-	-						
L4th and R4h PAA	-	-						
Th-P/NP vessels			4 Th-P	9 Th-P	* persistent 1st &/or 2nd PAA			Morishima et al., 2003

	E10.5				E15.5			
	WT	***Gbx2*$^{+/-}$**	***Tbx1*$^{+/lacZ}$**	***Gbx2*$^{+/-}$;*Tbx1*$^{+/lacZ}$**	**WT**	***Gbx2*$^{+/-}$**	***Tbx1*$^{+/lacZ}$**	***Gbx2*$^{+/-}$;*Tbx1*$^{+/lacZ}$**
Total embryos	6	11	11	14	29	16	19	22
Total normal	6	11	6	2	29	16	14	9
Total abnormal	**0**	**0**	**5 (45%)**	**12 (86%)**	**0**	**0**	**5 (26%)**	**13 (59%)**
L4th PAA	-	-	1	1	-	-	-	1
R4th PAA	-	-	2	1	-	-	2	5
L4th and R4h PAA	-	-	2	10	-	-	2	7
Th-P/NP vessels			1 Th-P, **4 NP (36%)**	1 Th-P, **11 NP (79%)**				Calmont et al., 2009

	E10.5				E14.5			
	WT	***Chd7*$^{+/-}$**	***Tbx1*$^{+/lacZ}$**	***Chd7*$^{+/-}$;*Tbx1*$^{+/lacZ}$**	**WT**	***Chd7*$^{+/-}$**	***Tbx1*$^{+/lacZ}$**	***Chd7*$^{+/-}$;*Tbx1*$^{+/lacZ}$**
Total embryos		6	14	6		26	25	17
Total normal		2	5	0		21	19	0
Total abnormal		**4 (67%)**	**9 (64%)**	**6 (100%)**		**5 (19%)**	**6 (24%)**	**17 (100%)**
L4th PAA		1	2	-		2	2	10
R4th PAA		3	4	-		3	4	6
L4th and R4h PAA		-	3	6		-	-	1
Th-P/NP vessels			**3 NP (21%)**	**6 NP (100%)**				Randall et al., 2009

	E17.5					
	WT	***Tbx1*$^{+/tm1Rak}$**	***Fgf8*$^{+/-}$;*Fgf10*$^{+/-}$**	***Fgf10*$^{+/-}$;*Tbx1*$^{+/tm1Rak}$**	***Fgf8*$^{+/-}$;*Tbx1*$^{+/tm1Rak}$**	***Fgf8*$^{+/-}$;*Fgf10*$^{+/-}$;*Tbx1*$^{+/tm1Rak}$**
Total embryos	6	5	5	7	6	6
Total normal	6	5	5	7	5	2
Total abnormal	**0**	**0**	**0**	**0**	**1 (17%)**	**4 (67%)**
L4th PAA	-	-	-	-	-	2
R4th PAA	-	-	-	-	1	2
L4th and R4h PAA	-	-	-	-	-	-
Th-P/NP vessels						Aggarwal et al., 2006

	E10.5				E18.5			
	WT	***Fgf8*$^{+/-}$**	***Tbx1*$^{+/lacZ}$**	***Fgf8*$^{+/-}$;*Tbx1*$^{+/lacZ}$**	**WT**	***Fgf8*$^{+/-}$**	***Tbx1*$^{+/lacZ}$**	***Fgf8*$^{+/-}$;*Tbx1*$^{+/lacZ}$**
Total embryos	18	10	14	14	30	30	35	36
Total normal	18	10	1	1	30	30	24	18
Total abnormal	**0**	**0**	**13 (93%)**	**13 (93%)**	**0**	**0**	**11 (31%)**	**18 (50%)**
L4th PAA			-	-			-	-
R4th PAA			5	1			6	6
L4th and R4h PAA			8	12			5	12
Th-P/NP vessels			6 Th-P, **7 NP (50%)**	1 Th-P, **12 NP (86%)**				Vitelli et al., 2002b
	E10.75-E11.0				E16.5-P2			
	WT	***Crkl*$^{+/-}$**	***Tbx1*$^{+/tm1Pa}$**	***Crkl*$^{+/-}$;*Tbx1*$^{+/tm1Pa}$**	**WT**	***Crkl*$^{+/-}$**	***Tbx1*$^{+/tm1Pa}$**	***Crkl*$^{+/-}$;*Tbx1*$^{+/tm1Pa}$**
Total embryos	24	10	15	25	21	15	18	16
Total normal	23	10	2	0	21	15	13	0
Total abnormal	**1 (4%)**	**0**	**13 (87%)**	**25 (100%)**	**0**	**0**	**5 (28%)**	**16 (100%)**
L4th PAA	-	-	6	24	-	-	1	-
R4th PAA	1	-	11	23	-	-	4	8
L4th and R4h PAA	-	-	4	22	-	-	-	8
Th-P/NP vessels	Th-P		10 Th-P, **3 NP (20%)**	3 Th-P, **22 NP (88%)**				Guris et al., 2006

	E11.0				E15.5			
	WT	***Smad7*$^{+/GT}$**	***Tbx1*$^{+/lacZ}$**	***Smad7*$^{+/GT}$;*Tbx1*$^{+/lacZ}$**	**WT**	***Smad7*$^{+/GT}$**	***Tbx1*$^{+/lacZ}$**	***Smad7*$^{+/GT}$;*Tbx1*$^{+/lacZ}$**
Total embryos	19	13	17	24	37	82	17	19
Total normal	19	12	6	8	37	81	12	6
Total abnormal	**0**	**1 (8%)**	**11 (65%)**	**16 (67%)**	**0**	**1 (1%)**	**5 (29%)**	**13 (68%)**
L4th PAA	-	-	2	6	-	-	2	2
R4th PAA	-	1	4	3	-	1	3	8
L4th and R4h PAA	-	-	5	7	-	-	-	3
Th-P/NP vessels		**NP (8%)**	7 Th-P, **4 NP (24%)**	7 Th-P, **9 NP (38%)**				this thesis

Table 3. 14. Arch artery defects observed in embryos with compound mutations for *Tbx1* and other genes, at early or late developmental stages in the different studies. The *Tbx1*;*Smad7* arch artery defects studied here were included for convenience purposes. L/R, left/right; NP, non patent; PAA, pharyngeal arch artery; Th-P, thin patent; WT, wild type.

The notion of prevention of recovery of the early fourth arch defect has been suggested for a different set of genetic mutations, *Fgf8* and *Crkl* combined (Moon et al., 2006). *Fgf8* heterozygosity combined with a heterozygous or null *Crkl* mutation profoundly disrupts fourth arch artery formation (Moon et al., 2006). *Fgf8* hypomorphs and conditional mutants were mildly affected while *Crkl* null mutants and *Fgf8* heterozygotes had normal arch arteries (Moon et al., 2006). During development $Fgf8^{+/-}$;$Crkl^{-/-}$ mutants did not recover and presented with complete penetrance of fourth arch related defects (Moon et al., 2006). Conversely, the $Fgf8^{+/-}$;$Crkl^{+/-}$ mutants had an incidence of 13% of defects at E15.5, as compared to 50% at E10.5 (Moon et al., 2006). The authors showed that there was compromised neural crest cell survival and population of the pharyngeal arches in the $Crkl^{-/-}$ embryos, while Crkl bound activated Fgf receptors and was required for subsequent downstream signalling *in vitro* (Moon et al., 2006).

4.6.3. *Tbx1* is involved in pathways affecting pharyngeal arch artery remodelling

To date, two independent pathways have been described specifically in pharyngeal arch artery remodelling. Huh *et al.*, studied the canonical Wnt pathway (Huh and Ornitz, 2010), while Ryckebusch *et al.*, examined the RA signalling (Ryckebusch et al., 2010) in the remodelling process. Both studies additionally assessed *Tbx1* in their respective context, due to the well established *Tbx1* role in arch artery development.

4.6.3.1 *Tbx1*, Wnt signalling and arch artery remodelling

By performing conditional deletion of *β-catenin* in the pharyngeal mesenchyme, effective in the entirety of the mesenchyme from E10.5 onwards, Huh *et al.*, showed that lack of canonical Wnt signalling leads to cardiovascular defects, among other abnormalities (Huh and Ornitz, 2010). The mutant phenotype included A-RSCA, increased spacing between the right brachiocephalic and LCC arteries, lower positioning of the LSCA on the DAo as well as outflow tract and intracardiac septation defects, compared to wild type controls (Huh and Ornitz, 2010). The pharyngeal arch artery defects described in this study were right fourth arch (A-RSCA), aortic sac (brachiocephalic-LCC artery distance) or left seventh ISA (LSCA positioning) derived. The formation versus the remodelling of the arch arteries was examined, and it was concluded that the conditional mutant embryos had defects in the remodelling process,

dictated by failure of both carotid ducts to regress normally by E13.5 (Huh and Ornitz, 2010). The conditional mutants did not display the normal pattern of cellular apoptosis in the mesenchyme surrounding the carotid ducts, explaining the persistence of these vascular segments (Huh and Ornitz, 2010). Further to describing the cardiovascular phenotype, the authors addressed the genetic mechanism underlying it, and demonstrated that lack of β-catenin is sufficient to increase *Tbx1* expression and the *Tbx1*-related downstream FGF signalling in the embryonic pharynx at E9.5 (Huh and Ornitz, 2010). It should be noted that *Cre* recombinase was active only in the non neural crest mesenchyme at this stage in the conditional embryos, as shown by reporter expression (Huh and Ornitz, 2010). Reducing *Fgf8* dosage in the conditional *β-catenin* ablated mutants partially rescued the carotid duct persistence phenotype (Huh and Ornitz, 2010). Constitutive or temporal activation of the Wnt-β-catenin signalling resulted in reduced expression of *Tbx1* in the pharyngeal apparatus at E9.5 and E10.5 and *Fgf8* at E9.5 (Huh and Ornitz, 2010). The authors additionally showed that temporal activation of the Wnt-β-catenin signalling increased the penetrance of the *Tbx1* haploinsufficient fourth arch phenotype at E10.5 (Huh and Ornitz, 2010). Through this study, the Wnt pathway, via *β-catenin*, has been associated with the arch artery remodelling process as well as with the *Tbx1* pathway. This however does not necessarily link *Tbx1* with the remodelling of the pharyngeal arch arteries, since the impact activated β-catenin had on the *Tbx1* haploinsufficient phenotype considered formation rather than remodelling defects.

These data indicate potential future directions on the *Tbx1-Smad7* study. Functional interaction between Smad7 and β-catenin has been previously described (Edlund et al., 2005; Han et al., 2006; Tang et al., 2008). Tang *et al.*, demonstrated that Smad7 stabilises cytoplasmic β-catenin *in vitro*, by inhibiting its phosphorylation by Gsk3-β (Tang et al., 2008). Huh *et al.*, used LiCl injections to temporally inhibit Gsk3-β and activate β-catenin *in vivo* (Huh and Ornitz, 2010). In that respect it might be interesting to employ the same system and temporally activate β-catenin in $Smad7^{GT/GT}$ embryos and examine the potential rescue of the arch artery remodelling phenotype. Depending on the cell line used, Smad7 affected β-catenin related transcriptional activity (Edlund et al., 2005) or not (Tang et al., 2008). A potential role for *Smad7* upstream of *Tbx1* through *β-catenin* can therefore be addressed too. Nevertheless, a linear pathway, whereby *Tbx1* transcriptionally regulates Smad7, which in turn

modulates cytoplasmic β-catenin towards arch artery remodelling appears more plausible. In support of that, the *Tbx1-Smad7* model discussed in this thesis involves aberrant remodelling of the fourth arch artery, solely inducing fourth arch related defects during development, rather than carotid duct persistence that leads to a range of defects observed in the *β-catenin* conditional mutants (Huh and Ornitz, 2010).

4.6.3.2. *Tbx1*, retinoic acid signalling and arch artery remodelling

RA signalling has also been recently discussed as an influencing factor in the arch artery remodelling process, although maybe without sufficient evidence. *Raldh2* homozygous mutants die at E10.5 and by then display a range of disfiguring phenotypes (Niederreither et al., 1999), so studying arch artery development in the null setting is not possible. Ryckebusch *et al.*, generated double heterozygotes for the *Raldh2* and *Tbx1* genes and scored the fourth arch artery defects at different developmental stages (Ryckebusch et al., 2010). The penetrance of the early fourth arch artery defects (E10.5) in *Tbx1* heterozygotes is 45% (Jerome and Papaioannou, 2001), but varies depending on the genetic background, and for this study it was found to be 82% (Ryckebusch et al., 2010). The frequency of the fourth arch defects was 8% in the *Raldh2* heterozygotes and 85% in the $Raldh2^{+/-}$;$Tbx1^{+/-}$ mutants, suggesting that the single *Raldh2* null allele has no contribution to the phenotype (Ryckebusch et al., 2010). The authors scored the arch artery defects at a later stage (E11.5) and established 57% penetrance for the *Tbx1* heterozygotes and 29% penetrance for the double heterozygotes (Ryckebusch et al., 2010). The *Tbx1* haploinsufficient fourth arch phenotype partially recovers during development (Calmont et al., 2009; Lindsay et al., 2001; Vitelli et al., 2002b Vitelli et al., 2006; Zhang and Baldini, 2008). Given the reduced penetrance of the defects in the $Raldh2^{+/-}$;$Tbx1^{+/-}$ embryos between E10.5 and E11.5 (85% compared with 29%) it was rationalised that the presence of one *Raldh2* null allele accelerated the recovery of the double heterozygous phenotype (Ryckebusch et al., 2010). The aortic arch pattering defects scored at E14.5-E18.5 were 25% penetrant in the $Tbx1^{+/-}$ embryos and 19% penetrant in the $Raldh2^{+/-}$;$Tbx1^{+/-}$ embryos (Ryckebusch et al., 2010). Statistical analysis shows no difference in the occurrence of great vessel defects between these two populations ($p=0.39>0.05$, Fisher's exact test †). Essentially, the intermediate stage the authors chose to test for an RA signalling role in the recovery of the fourth arch defects was unnecessary, since judging by the other two stages (E10.5 and E14.5 onwards)

there is an expected pattern of occurrence of fourth arch artery defects. The difference that was nonetheless identified among the *Raldh2*$^{+/-}$;*Tbx1*$^{+/-}$ mutants between E10.5 and E11.5 probably reflects experimental errors in scoring of the phenotypes, changes in genetic background or other inconsistencies not related to a true mechanism. In general, recovery of an arch artery defect relates to either compensation of an absent vascular segment by another, resulting in an alternative configuration (see introduction: 4.3) or reversal of the regression fate of a vascular segment by signalling from the surrounding tissues, haemodynamic forces or the combination of both. The *Tbx1* haploinsufficient fourth arch artery defect can be unilateral or bilateral hypoplasia or aplasia of the vessels (Lindsay et al., 2001). The *Raldh2*$^{+/-}$;*Tbx1*$^{+/-}$ embryos displayed all the expected types of fourth arch defects at both E10.5 and E11.5, but the notable difference was in the vessel aplasia frequencies between the two stages. The double heterozygotes examined at E10.5 exhibited NP vessels with a penetrance of 50% while the same genotype at E11.5 displayed 16% penetrance of NP fourth arch arteries. However, the formation of the caudal pharyngeal arches is completed by E10.5-E11.0 (Hiruma et al., 2002; Yanagisawa et al., 1998) and there is not enough time for a vessel to collapse and recover between E10.5-E11.5, as the authors claim (Ryckebusch et al., 2010). The difference in the hypoplastic vessel frequencies between the two stages in *Raldh2*$^{+/-}$;*Tbx1*$^{+/-}$ embryos was more subtle, with a frequency of 35% at E10.5 as compared to 25% at E11.5. In conclusion, even if RA signalling improves the VSM cellularisation of the fourth arch arteries and aids the recovery of hypoplastic fourth arches, as the authors support (Ryckebusch et al., 2010), there is still no sufficient explanation for the difference in the vessel aplasia frequencies in the double heterozygotes between E10.5 and E11.5, rendering the current conclusions of this study open to doubt.

Raldh2 homozygous mutants arrest developmentally at around E8.5 (Niederreither et al., 1999) so it is impossible to assess the *Smad7* levels in these embryos. The *Raldh2* null phenotype suggests that the gene is required in the embryo before E8.5. However, the onset of *Smad7* expression is at E8.5, which makes it unlikely for *Raldh2* and *Smad7* to be part of the same pathway at an early stage. A later interaction cannot be excluded, and can be assessed by examining *Raldh2* expression in *Smad7* gene-trap embryos and conversely, by examining *Smad7* expression in *Raldh2* hypomorph embryos that survive to mid-gestation (Vermot et al., 2003).

4.6.4. Concluding remarks on *Tbx1-Smad7* interaction in pharyngeal arch artery morphogenesis

The genetic network regulating pharyngeal arch artery formation is likely to be distinct from that controlling arch artery remodelling. So far no links have been described between these two networks. *Tbx1*, a well known regulator of arch artery formation (Lindsay et al., 2001; Xu et al., 2005; Zhang and Baldini, 2008), appears to regulate the early expression of *Smad7* or the survival/proliferation of a cell population that will express *Smad7*, a gene involved in the remodelling process of the arch arteries (Figure 3.25). Expression studies demonstrated that *Smad7* transcripts are reduced in the absence of *Tbx1* at E9.5, by microarray analysis, quantitative real time PCR (van Bueren et al., 2010) and whole mount *in situ* hybridisation (this thesis). It was also shown by quantitative real time PCR that at E10.5 *Smad7* mRNA levels were comparable between *Smad7* heterozygotes and *Tbx1*;*Smad7* double heterozygotes, while remaining unaffected in *Tbx1* heterozygotes. In that respect, *Tbx1* haploinsufficiency, acting at an earlier stage than E10.5, maybe an indirect regulator of arch artery remodelling through *Smad7*. This hypothesis has implications for the human disease of 22q11DS, caused by the hemizygous deletion of chromosome 22q11.2. Approximately 15% of the 22q11DS patients that have cardiovascular manifestations present with IAA-B, a fourth arch artery related defect (Yamagishi, 2002). There is a small proportion of patients that do not carry the typical or atypical deletions but only a subset of these carry point mutations in *TBX1* (Paylor et al., 2006; Stoller and Epstein, 2005a; Torres-Juan et al., 2007; Yagi et al., 2003; Zweier et al., 2007). The phenotype of *TBX1* haploinsufficiency caused by the deletion may be modified by *SMAD7* mutations or sequence variants, resulting in the definite great vessel phenotype. To date, no *SMAD7* mutations have been reported in human heart disease.

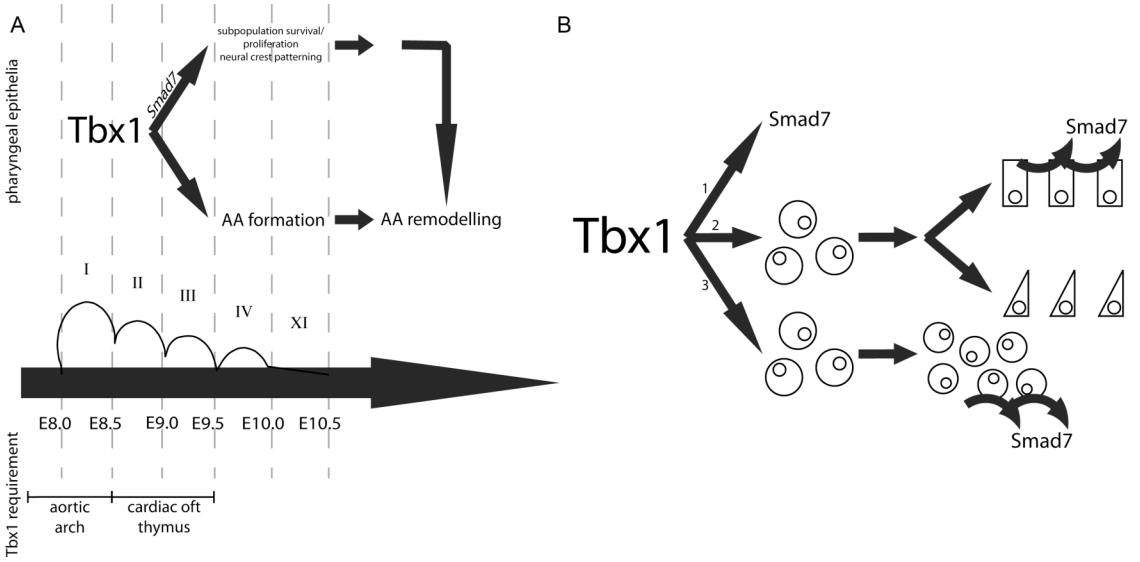

Figure 3. 25. Schematic representation of the presumptive modes of interaction between *Tbx1* and *Smad7* during development. The potential model and timing of interaction between *Tbx1* and *Smad7* (A). *Tbx1* is required during early embryogenesis for multiple developmental processes. *Tbx1* may regulate *Smad7* or the survival/proliferation of a population that will express *Smad7*, at an early stage, prior to arch artery formation. *Smad7* is subsequently required for arch artery remodelling. Possible types of interaction between *Tbx1*-*Smad7* (1) direct (unlikely), (2) indirect, whereby *Tbx1* regulates the differentiation of a progenitor population that will eventually express *Smad7*, or (3) indirect, whereby *Tbx1* regulates the survival or proliferation of a progenitor population that will eventually express *Smad7* (B). I-XI, pharyngeal arches; E, day of embryonic development.

4.7. *Smad7* gene-trap time-dependent rescue

An elegant way of assessing if *Smad7* is indeed required at E10.5-E11.5 onwards for the actual remodelling of the pharyngeal arteries is through a time-controlled inducible *Cre*/*lox* system. *CaggsCre* was used to provide ubiquitous recombination and excise the splice acceptor of the *Smad7* gene-trap vector in a timely controlled fashion. This model, however, is still being standarised and currently cannot be used, since the published methods (Hayashi and McMahon, 2002; Xu et al., 2005) do not provide sufficient recombination efficiency, as examined here by DNA, RNA and protein assays. Hayashi and McMahon took advantage of the *ROSA26* reporter line and assessed the recombination efficiency at the protein level (Hayashi and McMahon, 2002). The authors concluded that 3mg per 40g body weight injected intraperitonealy

are sufficient to induce up to 75% ubiquitous recombination within 24 hrs, from as early as E8.5 (Hayashi and McMahon, 2002). A higher dosage of 9mg per 40g body weight induced quicker recombination but the embryos died around E13.5 and none survived to term (Hayashi and McMahon, 2002). Recombination varied among the different embryonic tissues and even with a high tamoxifen dosage a small percentage of cells in all tissues failed to undergo recombination within 24 hrs (Hayashi and McMahon, 2002). Prolonged drug activity induced up to 95% recombination in the embryos injected with 3mg per 40g body weight (Hayashi and McMahon, 2002). Xu *et al.*, addressed the recombination efficiency issue at the genomic, RNA and protein level (Xu et al., 2005). They showed that IP injection of 3mg per 40g body weight induced complete recombination within 24 hrs by estimating the levels of the recombined and non recombined genomic locus. Also, no mRNA transcripts of the gene were detectable, or at very low levels, at the same stage, examined by reverse transcriptase PCR (Xu et al., 2005). Ubiquitous recombination was demonstrated through reporter expression with the use of the *ROSA26* line (Xu et al., 2005).

A more refined method was used in this study to examine the recombination efficiency of the system, given that reconstitution of the gene is required here, rather than deletion. By quantitative real time PCR it was shown that the maximum efficiency achieved in our system was production of 26% of the wild type *Smad7* mRNA levels in *Smad7*$^{GT/GT}$;*CaggsCre* embryos, which is not considered sufficient. An arbitrary threshold of 40% of the wild type levels was set to achieve gene dosage greater than the *Smad7* heterozygote, to safely interpret the results of this experiment. The *Smad7* heterozygotes have no phenotypic defects, so restoring gene dosage in the gene-trap homozygous embryos to a level greater than the heterozygote may be sufficient to rescue the gene-trap homozygous phenotype. The time control element of the system will help clarify the developmental stage at which *Smad7* acts on arch artery remodelling. In combination with *Tbx1* heterozygosity, this system can also ascertain whether *Smad7* and *Tbx1* are required in a linear pathway during the remodelling process.

The discrepancy in the induction of the system among the different studies may be due to the different genetic backgrounds, inaccessibility of the *Smad7* genomic locus or the methods used to test the recombination efficiency. Whichever the reasons, the system should be standarised in every new setting. A different approach in examining

the *Smad7* role in arch artery remodelling is a *Cre*/*lox* system that conditionally deletes *Smad7* in a timely controlled fashion, instead of the $Smad7^{GT}$;*CaggsCre* model.

4.8. Conclusion and future directions

In this chapter I have shown that *Smad7*, a gene identified by a microarray screen as a potential Tbx1 target, is indeed related to *Tbx1*. The interaction between the two genes is more likely indirect. *Smad7* expression depends upon tissue-specific Tbx1 activation at an early developmental stage. *Tbx1* is a major regulator of pharyngeal development (Zhang and Baldini, 2008). In that respect, it controls a great number of genes that will eventually play roles in different processes and at different time points. The developmental roles of *Smad7* are apparent at a much later stage than its initial activation from Tbx1, during the remodelling of the great vessels. Therefore, a synergistic interaction between the two genes is proposed.

To elucidate the role of *Smad7* in the remodelling of the pharyngeal arteries, initially a neural crest patterning defect has to be conclusively ruled out, for example by *Sox10*, *HNK-1*, *Ap2a* or *Crabp1* whole mount *in situ* hybridisation on *Smad7* gene-trap homozygous versus wild type embryos. Next, the VSM population of the pharyngeal arch arteries has to be assessed, in case the neural crest cells migrate efficiently into the pharyngeal arches but fail to differentiate *in situ* and create this supportive lining. The mesodermally-derived arch artery endothelium should also be examined. Immunohistochemical methods can address both these issues. *In vitro* experiments can also be employed to assess for shear stress responsiveness of *Smad7* deprived endothelium. HUVEC cultures can be used, where in a customised chamber differential stress forces and be applied, allowing for the measurement of the transcriptional response. Alternatively, FACS sorted endothelial cells from *Smad7* gene-trap homozygous embryos can be examined for shear stress responsive or other haemodynamic related factors. Increasing the sample size of the E11.5 $Smad7^{GT/GT}$ embryos and scoring the arch artery defects will make a stronger argument towards a remodelling rather than a formation role of the gene. Interestingly, *Tgfβ2* mutants exhibit fourth arch artery remodelling defects too (Bartram et al., 2001; Molin et al., 2002), associated with reduction in Smad2 expression in the fourth arch (Molin et al., 2002). Future analysis of the *Smad7* mutants at subsequent developmental stages during arch artery remodelling can address whether it acts via or dependent on *Tgfβ2*, or if it is

part of a completely independent pathway. *Tgfß2* null embryos have a 33% penetrance of aortic arch anomalies, which are hypoplasia of the ascending aorta and fourth arch-related defects (Bartram et al., 2001), correlating well with the 30% penetrance of great vessel defects scored in *Smad7* homozygotes, concerning almost exclusively fourth arch-related defects. A possible interaction between *Smad7* and the Wnt-β-catenin pathway can be addressed by temporally inhibiting Gsk3-β and activating β-catenin in $Smad7^{GT/GT}$ embryos, to examine the potential rescue of the arch artery remodelling phenotype. The proliferation and apoptosis rates need to be scored in the developing vasculature of $Smad7^{GT/GT}$ and $Smad7^{+/GT}$;$Tbx1^{+/lacZ}$ embryos, in order to investigate the precise mechanism by which *Smad7* is part of the pharyngeal arch artery remodelling scheme. Finally, in terms of future work, a *Cre*/*lox* system can be employed to conditionally delete *Smad7* in a timely controlled fashion, as a way of addressing its role in great vessel remodelling, instead of the $Smad7^{GT}$;*CaggsCre* model.

IV. HES1

1. Introduction – Literature review

1.1. Notch pathway

1.1.1. Biological functions

Notch signalling is an evolutionary conserved pathway that influences cell fate specification, progenitor cell maintenance, boundary formation, cell proliferation and apoptosis and is involved in several developmental processes (Artavanis-Tsakonas et al., 1999; High and Epstein, 2008; High et al., 2007; Nemir and Pedrazzini, 2008). Dysregulation of the Notch pathway contributes to a number of human pathologies including congenital heart disease, cancer (Nemir and Pedrazzini, 2008), Alagille syndrome, Cerebral Autosomal Dominant Arteriopathy with Subcortical Infarcts and Leukoencephalopathy (CADASIL), and T-cell leukemia (Fischer and Gessler, 2007).

1.1.2. Notch pathway genes

Four type I transmembrane Notch receptors (*Notch1-4*) and five type I transmembrane Notch ligands (*Jagged1-2* and *Delta-like1,-3*, and *-4*) have been identified in mammals (High et al., 2007; Jain et al., 2010; Niessen and Karsan, 2008). Both the receptors and ligands are expressed on the cell surface, promoting communication between two adjacent cells (High et al., 2007; Nemir and Pedrazzini, 2008; Niessen and Karsan, 2008). Ligand binding induces two sequential cleavage events of the Notch receptor (Fischer and Gessler, 2007; Niessen and Karsan, 2008). The first cleavage occurs on the membrane and is mediated by the metalloprotease tumor necrosis factor-α-converting enzyme (TACE/ADAM17) (Nemir and Pedrazzini, 2008; Niessen and Karsan, 2008). This is followed by proteolytic cleavage by a γ-secretase complex (High et al., 2007; Nemir and Pedrazzini, 2008; Niessen and Karsan, 2008). The receptor eventually releases the intracellular domain of Notch (NICD), which translocates to the nucleus (Fischer and Gessler, 2007; High et al., 2007; Kageyama et al., 2005; Nemir and Pedrazzini, 2008; Niessen and Karsan, 2008). In the nucleus the NICD interacts with the DNA binding recombination signal binding protein for immunoglobulin kappa J region (RBP-Jkappa or RBP-J) and transcriptional co-activators like the mastermind-like (MAML), promoting transcription of Notch target genes (Fischer and Gessler, 2007; High et al., 2007; Jain et al., 2010; Kageyama et al.,

2005; Nemir and Pedrazzini, 2008; Niessen and Karsan, 2008). The most extensively studied target genes are those of the hairy and enhancer of split (HES) and HES-related (HRT or Hey) transcription factor families (Figure 4.1) (Fischer and Gessler, 2007; High et al., 2007; Jain et al., 2010; Kageyama et al., 2005; Nemir and Pedrazzini, 2008; Niessen and Karsan, 2008).

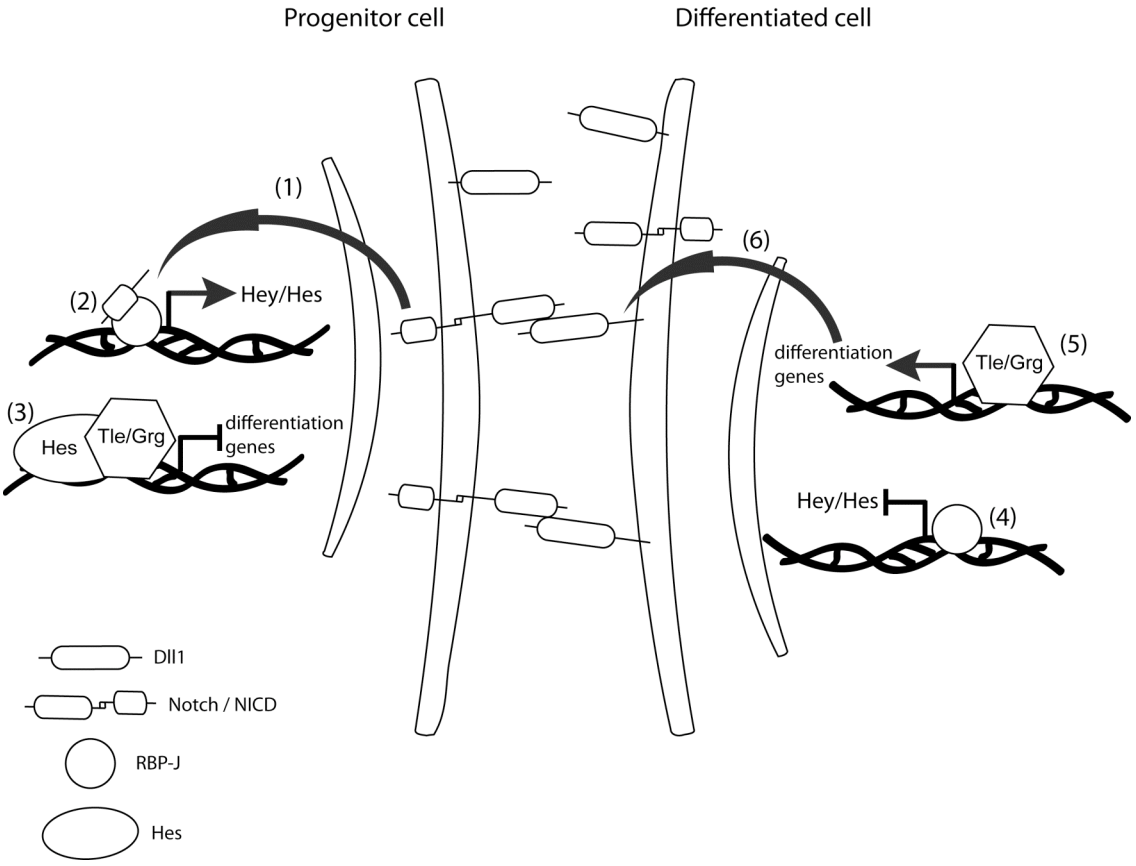

Figure 4. 1. Simplified schematic representation of Notch signalling in two adjacent cells. (1) Notch is activated by Delta in a progenitor cell, (2) which leads to translocation of the intracellular domain of Notch (NICD) into the nucleus where it forms a complex with RBP-J, which in turn induces target gene transcription. (3) Hes proteins recruit Tle/Grg corepressors and inhibit transcription of activator-type bHLH genes by binding to their promoters. Differentiation genes are essentially not expressed. (4) In the absence of activated Notch in a differentiating cell, RBP-J promotes transcriptional repression of *Hes* genes, (5) while the activator-type bHLH genes are being expressed, subsequently inducing differentiation genes, (6) and Delta activation, promoting Notch signalling in neighboring cells. NICD, intracellular domain of Notch.

1.1.3. Notch target genes

Generally, the Notch downstream effectors remain largely unknown (Nemir and Pedrazzini, 2008). The first Notch targets that were identified were genes encoding basic helix-loop-helix (bHLH) proteins of the Hes and Hey families, related to the *Drosophila Hairy* and *Enhancer-of-Split* (Nemir and Pedrazzini, 2008). Seven *Hes* genes (*Hes1-7*) have been described in mammals, of which only *Hes1, 5* and *7* are activated by Notch (Fischer and Gessler, 2007; Kageyama et al., 2005; Nemir and Pedrazzini, 2008). All three members of the Hey family, *Hey1*, *Hey2* and *HeyL*, are induced by Notch (Fischer and Gessler, 2007; Nemir and Pedrazzini, 2008). As effectors of Notch signalling, these genes are considered as central regulators of fate-specific gene transcription (Nemir and Pedrazzini, 2008). Hes and Hey proteins form homo- or heterodimers, and generally act as transcriptional repressors, either actively, by direct association with E- and N-box DNA sequences on target gene promoters (Fischer and Gessler, 2007; Kageyama et al., 2005; Nemir and Pedrazzini, 2008; Pedrazzini, 2007) or passively, through interaction with other DNA-binding transcription factors, and transcription factor sequestration (Nemir and Pedrazzini, 2008; Pedrazzini, 2007). Hes and Hey genes have a wide range of expression domains, indicative of their involvement in transcriptional regulation during development (Nemir and Pedrazzini, 2008). Until recently it was thought that, among the Notch effectors, only *Hey* genes were involved in cardiovascular development (Nemir and Pedrazzini, 2008). However, we and others have shown that *Hes1* deficiency induces aortic arch, outflow tract and intracardiac defects (Rochais et al., 2009b; van Bueren et al., 2010).

1.1.3.1. Hes1 protein, interactors and biological functions

Hes1 is a repressor bHLH protein involved in many developmental processes, such as regulation of binary cell decisions, T-cell development, (Kageyama et al., 2000), maintenance and proliferation of neural stem cells, gliogenesis (Kageyama et al., 2005) and boundary formation in the central nervous system (CNS) (Baek et al., 2006). It is expressed by almost all undifferentiated cells and it is required to maintain these cells in an undifferentiated state, while missexpression of *Hes1* inhibits cell differentiation (Kageyama et al., 2000). *Hes1* expression is activated by Notch through RBP-J (Jarriault et al., 1995; Nishimura et al., 1998). RBP-J can also act independently and repress *Hes1* transcription by binding onto the *Hes1* promoter (Kageyama et al.,

2005). Of particular note is the fact that in the CNS *Hes1* is expressed at the neuroepithelial stage, which precedes *Notch* and *Delta* expression, suggesting that Notch is not the sole regulator of *Hes1* expression, at least in the neuronal cell lineage (Kageyama et al., 2005).

Like the rest of the Hes proteins, Hes1 has an N-terminal domain used for dimerisation and DNA binding, a proline residue in the middle of the basic region producing high affinity to N-boxes (instead of E-boxes) and a less conserved Orange domain, involved in protein-protein interactions (Kageyama et al., 2005). Hes1 acts through promoter binding and transcriptional repression or by inactivating dimerisation with activator bHLH proteins, such as Mash1, a neuronal determination protein (Kageyama et al., 2005; Kageyama et al., 2000). Hes proteins additionally recruit Tle/Grg corepressors through their WRPW tetrapeptide, unlike the Hey proteins that lack this domain (Fischer and Gessler, 2007; Kageyama et al., 2005; Kageyama et al., 2000).

Hes1 has the ability of negatively regulating its own promoter (Takebayashi et al., 1994) and thus functioning as a cellular oscillator both *in vitro*, in cultured cells, and *in vivo*, in the presomitic mesoderm during somitogenesis (Hirata et al., 2002). *Hes1* mRNA and protein have short half lives (~20 min) and oscillate in a 2-hour cycle *in vitro* (Hirata et al., 2002). Kobayashi *et al.*, recently demonstrated that *Hes1* exerts oscillatory roles in embryonic stem (ES) cells too, through a Notch independent pathway (Kobayashi et al., 2009).

Hes genes are also suggested to modulate the timing of cell differentiation by repressing the premature onset of the activator bHLH genes (Kageyama et al., 2005). *Hes1* together with *Hes3* and *Hes5* are expressed in neural stem cells and inhibit differentiation into neuronal fates, thereby maintaining the stem cell potential (Kageyama et al., 2005). Double mutation for *Hes1* and *Hes5* induces premature glial cell differentiation into neurons while triple knock-out for *Hes1*, *Hes3* and *Hes5* results in premature neuroepithelial cell differentiation into neurons, from as early as E8.5 (Kageyama et al., 2005). Kobayashi *et al.*, additionally studied *Hes1* in ES cell differentiation (Kobayashi et al., 2009). ES cells expressing low levels of *Hes1* differentiated more efficiently into neural lineages, while ES cells expressing high levels of *Hes1* tended to acquire mesodermal fates (Kobayashi et al., 2009). These

reflected different phases in ES cell differentiation and not different subpopulations, as both high and low *Hes1*-expressing populations returned to the original distribution of variable *Hes1* expression levels within a day (Kobayashi et al., 2009). Inactivation of the gene in ES cells under neural differentiation conditions induced neural fates for almost all *Hes1* null cells and at an earlier time point, compared to wild type ES cells (Kobayashi et al., 2009).

1.1.4. Notch pathway in cardiovascular development

Notch signalling functions via three distinct modes of action (Bray, 2006). First, through inductive signals between different cell populations Notch pathway promotes the formation of boundaries (Bray, 2006; Nemir and Pedrazzini, 2008; Pedrazzini, 2007). Notch pathway is also involved in cell lineage determination by controlling asymmetric cell division, in which one cell divides to produce two daughter cells that adopt two different fates (Bray, 2006; Pedrazzini, 2007). Last, Notch acts through lateral inhibition between adjacent cells, whereby a cell assuming a particular fate inhibits its neighboring cells from adopting the same fate (Bray, 2006; Nemir and Pedrazzini, 2008; Pedrazzini, 2007).

Several Notch receptors, ligands and targets are expressed in the developing cardiovasculature (Nemir and Pedrazzini, 2008). *Notch1* and *Notch2* are the predominant receptors expressed in the developing heart, whereas *Notch3* is restricted to the smooth muscle and *Notch4* to the endothelium of the vascular system (Nemir and Pedrazzini, 2008). The Notch ligand *Jag1* is detected in the outflow tract, AVC and ventricular trabeculae, while *Dll1* and *Dll4* are expressed in the endocardium during different stages of development (Nemir and Pedrazzini, 2008). *Dll4* is also observed in the cardiac crescent in early stages of cardiogenesis (Nemir and Pedrazzini, 2008). Notch target genes are also expressed in the developing cardiovasculature. *Hey1* is initially expressed in the cardiac crescent, later in development it is detected in the endocardium and ultimately becomes restricted to the atrial myocardium and epicardium (Nemir and Pedrazzini, 2008). *Hey2* is found in the presumptive ventricles at the heart tube stage and later it is limited to the compact myocardium (Nemir and Pedrazzini, 2008). *Hey2* is also found highly expressed in the AV canal endocardium but not the mesenchyme at the onset of EMT (Nemir and Pedrazzini, 2008). *HeyL* is

expressed in the AV cushions between E9.5 and E12.5 and in an overlapping fashion with *Notch1*, *Notch2*, *Jag1*, *Hey1* and *Hey2* (Fischer et al., 2007).

The spatiotemporal expression pattern of Notch receptors, ligands and targets in the embryonic heart, combined with the phenotype of animal mutants of components of the Notch pathway demonstrate the importance of Notch signalling during heart development (Nemir and Pedrazzini, 2008). Developmental processes the Notch pathway has been described in include cardiomyocyte differentiation, ventricular trabeculation, boundary formation of the AV canal, outflow tract remodelling and valve development (High and Epstein, 2008; Jain et al., 2010). Moreover, in the early stages of cardiogenesis, signalling through Notch1, Notch2 and Dll1 is essential for determination of the left-right embryonic axis and subsequently for normal looping of the heart tube (Niessen and Karsan, 2008).

1.2. Notch gene mutations

Inactivating mutations on factors of the Notch pathway or its targets have been associated with the etiology of cardiovascular anomalies (Cau et al., 2000; Fischer et al., 2007; High et al., 2007; Hirata et al., 2004; Hirata et al., 2001; Nemir and Pedrazzini, 2008; Rochais et al., 2009b; Stauber et al., 2009; van Bueren et al., 2010).

1.2.1. Notch pathway gene mutations

In humans, mutations in the *NOTCH1* gene have been associated with T-cell acute lymphoblastic leukemia (Weng et al., 2004) and aortic valve disease (Garg et al., 2005) while mutations in the *NOTCH3* gene have been identified in CADASIL patients (Shawber and Kitajewski, 2004). Moreover, Allagile syndrome has been linked to haploinsufficiency of the Notch ligand *JAGGED1* (Shawber and Kitajewski, 2004; Warthen et al., 2006). Mutations in the *DLL3* gene causes one form of autosomal recessive Spondylocostal Dysostosis (Gridley, 2003).

In mice, interference with Notch signalling in the neural crest lineage through a dominant negative inhibitor induced cardiac outflow tract and aortic arch patterning defects (High et al., 2007). The neural crest cell migration was not affected in these mutants, however, localised downregulation of Notch target genes and diminished expression of SMC markers was observed (High et al., 2007). The authors concluded that Notch signalling has a cell-autonomous role in neural crest cell differentiation into

VSM (High et al., 2007). Other Notch gene mutants, including *Notch1*, *RBP-J*, *Jag1*, and *Dll4*, also display cardiovascular phenotypes, which are predominantly outflow tract, ventricular septation or trabeculation defects (Nemir and Pedrazzini, 2008).

1.2.2. Notch target gene mutations

Deficiency in *Hey1* or *HeyL* does not result in heart anomalies, *Hey2* deficient mice however display perinatal lethality and cardiovascular malformations, including ASDs and VSDs, enlargement of the atrial and ventricular cavities, thin ventricular walls, pulmonary stenosis and tricuspid atresia (Fischer et al., 2007). Double mutants for *Hey1* and *Hey2* die in utero due to severe cardiovascular insufficiency, reminiscent of the phenotype observed in *Notch1* mutant mice (Fischer et al., 2007). Consistently, combined mutation for *Hey1* and *HeyL* causes defects in the EMT processes of the AVC and results in congenital heart defects including chamber enlargement, membranous VSDs and dysplastic valves (Fischer et al., 2007).

Null mutation of either the *Hes3* (Hirata et al., 2001) or the *Hes5* (Cau et al., 2000) genes produces viable and fertile mice. Homozygosity for a targeted null mutation in *Hes7* disrupts somite formation that leads to skeletal defects and neonatal death (Hirata et al., 2004; Stauber et al., 2009). Animal models for *Hes2* or *Hes6* mutations have not been established yet, while for the purposes of this thesis, the phenotype of the *Hes1* mutation will be discussed in greater detail here.

During mouse embryogenesis *Hes1* participates in neural tube (Ishibashi et al., 1995), eye (Lee et al., 2005; Takatsuka et al., 2004; Tomita et al., 1996), thymus (Tomita et al., 1999), lung (Ito et al., 2000) and pancreas development (Jensen et al., 2000), while homozygous knock-down of the gene results in a range of defects affecting these organs and is embryonic lethal (Ishibashi et al., 1995). We and others have shown that *Hes1* null embryos additionally exhibit cardiovascular (Rochais et al., 2009b; van Bueren et al., 2010) and craniofacial anomalies (van Bueren et al., 2010). During early stages of development (E10.5), a proportion of the *Hes1* homozygous embryos exhibit pharyngeal arch artery defects (van Bueren et al., 2010) (Table 4.1).

	WT	***Hes1*$^{+/-}$**	***Hes1*$^{-/-}$**
Total embryos	77	80	40
Total normal	76	67	27
Total abnormal	**1 (1%)**	**13* (16%)**	**13* (32.5%)**
Persistent 1st &/or 2nd PAA	-	2	6
Hypo/aplastic 3rd PAA	-	-	1 (apl)
Hypo/aplastic 4th PAA	1 (hypo)	8 (hypo)	3 (hypo), 3 (apl)
Hypo/aplastic 6th PAA	-	-	1 (hypo)
Aberrant branching	-	4	4

*$p<0.01$

Table 4. 1. Arch artery defects observed in *Hes1* embryos at E10.5. P value from Fisher's exact test against the wild type group. apl, aplastic; hypo, hypoplastic; PAA, pharyngeal arch artery; WT, wild type. Nb. Total WT embryos include additional WT non-littermates examined for the presence of arch artery defects (van Bueren et al., 2010).

At later stages of development (E14.5-E15.5), *Hes1* null embryos present with high penetrance of thymic defects and moderate penetrance of secondary palate defects, depending on the genetic background (van Bueren et al., 2010). At the same stage and with variable penetrance the *Hes1* mutants exhibit cardiovascular defects. These include great vessel defects, like RAA on an MF1;C57BL/6J background (van Bueren et al., 2010) or isolated RSCA on an MF1 background (van Bueren et al., 2010) and outflow tract defects, like dextroposed aorta on a CD1 background (Rochais et al., 2009b) and DORV on an MF1 or MF1;C57BL/6J background (van Bueren et al., 2010). Intracardiac septation defects have also been reported in all genetic backgrounds examined (Table 4.2) (Rochais et al., 2009b; van Bueren et al., 2010).

Strain	Genotype	n	Total CV defects			Cleft Palate	Thymic hypo/ aplasia
				Great vessel defect	OFT defect		
MF1*	WT	2	0	0	0	0	0
	Hes1$^{+/-}$	15	1[a] (7%)	0	0	0	0
	Hes1$^{-/-}$	15	2 (13%)	1	1	9 (60%)	13 (87%)
MF1;C57BL/6J*	WT	7	0	0	0	0	0
	Hes1$^{+/-}$	21	0	0	0	1 (5%)	0
	Hes1$^{-/-}$	23	5 (22%)	4	1	9 (39%)	23 (100%)
CDI**	WT	N/A	N/A	N/A	N/A	N/S	N/S
	Hes1$^{+/-}$	N/A	N/A	N/A	N/A	N/S	N/S
	Hes1$^{-/-}$	21	8 (38%)	0	8	N/S	N/S

Table 4. 2. Thymic cardiovascular and palate defects observed in *Hes1* embryos at E14.5-E15.5. OFT, outflow tract; CV, cardiovascular; N/A, not available; N/S, not studied; WT, wild type. [a] Dextroposition of the heart, * van Bueren et al., 2010, ** Rochais et al., 2009b.

Although heterogeneity is observed in the cardiovascular phenotype among the different genetic backgrounds, *Hes1* appears to participate in the development of both the great vessel and the outflow tract. Interestingly, the *Hes1* null mutant is the first Notch effector mutant described with pharyngeal arch artery anomalies (van Bueren et al., 2010). Functional redundancy among related Notch pathway members may explain this inconsistency (van Bueren et al., 2010).

2. Project overview

Hes1 was identified as a potential Tbx1 target through our microarray screen on *Tbx1*-expressing heterozygous and null cells, and validated by quantitative real time PCR (van Bueren et al., 2010). Preliminary experiments by a member of our lab demonstrated that *Hes1* is expressed in an overlapping fashion with *Tbx1* in E9.5 pharyngeal tissues, while it was detected downregulated in all these tissues in E9.5 $Tbx1^{lacZ/lacZ}$ embryos, compared to stage matched wild type controls, by whole mount *in situ* hybridisation (van Bueren, 2008). Expression analysis was undertaken to further refine the *Hes1* expression domains during early mouse embryogenesis, in relation to *Tbx1* expression. Conditional knock-out embryos of *Hes1* were generated for different tissues, using the *Cre*/*loxP* system, to establish the tissue-specific contributions of *Hes1* to the null phenotype. Neural crest cell patterning was assessed in *Hes1* null and conditional embryos. Last, elements of the Notch and FGF pathways were also examined in the context of the phenotypes observed.

3. Results

3.1. *Hes1* in the mouse embryo

Tbx1 is expressed in the pharyngeal epithelia and mesoderm from as early as E7.5 (Chapman et al., 1996; Huynh et al., 2007; Lindsay et al., 2001; Vitelli et al., 2002a) while *Tbx1* expression is required for fourth arch artery formation prior to its morphological appearance, before E9.5 (Xu et al., 2005). Immunohistochemistry was employed to study the localisation of Hes1 and Tbx1 proteins in the mouse embryo at E8.5. Both were found co-expressed in the pharyngeal ectoderm, endoderm and mesenchyme (Figure 4.2.E). Whole mount *in situ* hybridisation was used to demonstrate that at E9.5 *Hes1* mRNA is also expressed in an overlapping fashion with *Tbx1* in the pharyngeal endoderm, mesenchyme and ectoderm (Figure 4.2.A-B'). Furthermore, *Hes1* expression was identified as downregulated by whole mount *in situ* hybridisation in E9.5 $Tbx1^{lacZ/lacZ}$ embryos in the pharyngeal endoderm and mesenchyme but not ectoderm, compared to littermate stage matched wild type controls (Figure 4.2.C-D').

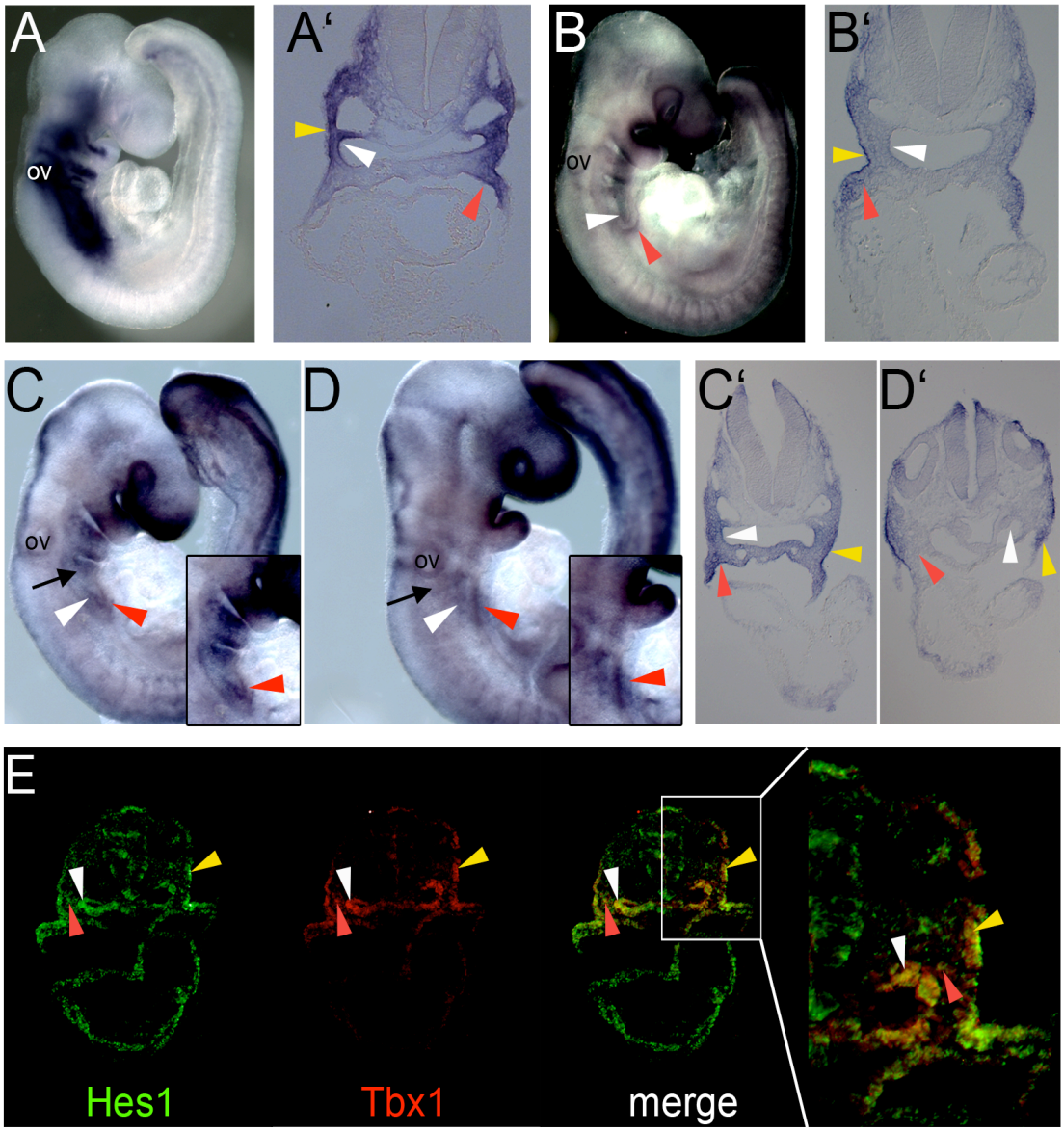

Figure 4. 2. Tbx1 and Hes1 expression detected by immunofluorescence at E8.5 and *in situ* hybridisation at E9.5. (A, A') Wild type *Tbx1* mRNA expression in whole mount (A) and transverse section at the caudal pharyngeal level at E9.5 (A'). (B, B') Wild type *Hes1* mRNA expression in whole mount (B) and transverse section at the caudal pharyngeal level at E9.5 (B'). (C, C', D, D') E9.5 *Hes1* mRNA expression in wild type control embryo in whole mount (C) and transverse section at the caudal pharyngeal level (C') and in *Tbx1*$^{lacZ/lacZ}$ embryo in whole mount (D) and transverse section at the caudal pharyngeal level (D'). Hes1 (green) and Tbx1 (red) protein expression in wild type embryo at E8.5 in transverse section at the caudal pharyngeal level (E). Black arrow, pharyngeal mesenchyme; yellow arrowhead, pharyngeal

ectoderm; red arrowhead, SHF mesoderm; white arrowhead, pharyngeal endoderm; SHF, second heart field; ov, otic vesicle.

3.2. Tissue-specific contributions of *Hes1*

The pharyngeal expression profile of the gene during early mouse embryogenesis led us to conditionally ablate *Hes1* in the neural crest, ectoderm and neural crest, anterior heart field and finally endoderm and study the resulting phenotype. The gene was deleted in each tissue through a *Cre*/*loxP* model, on a *Hes1* heterozygous background, by combining the *Hes1* null and flox alleles with the respective *Cre* transgene. This induced complete inactivation of *Hes1* in the tissue of interest and heterozygous inactivation of the gene in the rest of the embryo in the $Hes1^{Fl/-}$;*Cre* genotypes. The fact that *Hes1* heterozygous mutants have some pharyngeal arch artery defects at E10.5 but appear normal in subsequent stages of development (van Bueren et al., 2010) was considered when interpreting the results of the conditional deletions. Reporter expression through the *ROSA26* line (Soriano, 1999) on a $Hes1^{Fl/+}$ or $Hes1^{Fl/-}$ background was used as a proxy to assess the recombination efficiency of each *Cre* system.

3.2.1. *Hes1* in the neural crest

The *Wnt1Cre* model (Danielian et al., 1998) was used to achieve conditional deletion of the gene in the neural crest. Timed matings of $Hes1^{Fl/Fl}$ (C57BL/6J) to $Hes1^{+/-}$;*Wnt1Cre* (MF1;C57BL/6J) mice were used to produce embryos to study the neural crest *Hes1* contribution to the *Hes1* null phenotype. This cross should ablate *Hes1* in the *Wnt1* expressing cells, which are predominantly neural crest cells, from E8.5 onwards (Figure 4.3.A-A'') (Danielian et al., 1998; Echelard et al., 1994).

3.2.1.1. *Hes1* may have a minor role in the neural crest towards arch artery morphogenesis

The pharyngeal arch artery phenotype of these mutants was assessed at two stages, the arch artery formation and the mature left-sided aortic arch stage. At E10.5, when all pairs of the caudal arch arteries have formed (Hiruma et al., 2002; Yanagisawa et al., 1998), two (10.5%) $Hes1^{Fl/+}$;*Wnt1Cre* and two (12.7%) $Hes1^{Fl/-}$;*Wnt1Cre* embryos (hereafter *Wnt1Cre* conditional mutants) presented with a defect, but this was

not statistically different to the wild type phenotype (p>0.05, Fisher's exact test) (Table 4.3).

	***Hes1*$^{Fl/+}$ (WT)**	***Hes1*$^{Fl/-}$**	***Hes1*$^{Fl/+}$;*Wnt1Cre***	***Hes1*$^{Fl/-}$;*Wnt1Cre***
Total embryos	23	21	19	16
Total normal	23	21	17	14
Total abnormal (%)	0	0	2 (10.5%)	2 (12.7%)
Persistent 1st &/or 2nd PAA	-	-	1	-
Hypo/aplastic 3rd PAA	-	-	1 (apl)	-
Hypo/aplastic 4th PAA	-	-	-	2 (hypo)
Hypo/aplastic 6th PAA	-	-	-	-

Table 4. 3. Arch artery defects observed in the *Wnt1Cre* conditional embryos at E10.5. apl, aplastic; hypo, hypoplastic; PAA, pharyngeal arch artery; WT, wild type.

By E15.5 the pharyngeal arch arteries have completely remodelled into the mature left-sided configuration (Hiruma et al., 2002). At this stage three (11.5%) *Wnt1Cre* conditional mutants displayed cervical origin of the RSCA (Figure 4.3.C), which occurs after aberrant formation or remodelling of the right fourth arch artery. This however was not statistically different to the rest of the genotypes (p>0.05, Fisher's exact test) (Table 4.4), suggesting that *Hes1* in the neural crest is probably not required for great vessel development. No outflow tract defects were observed in any of the genotypes.

Genotype	**n**	**Thymic hypoplasia**	**Great vessel defects**	**Eye defects**
Hes1$^{Fl/+}$ (WT)	17	0	0	0
Hes1$^{Fl/-}$	21	3 (14%)	0	0
Hes1$^{Fl/+}$;*Wnt1Cre*	31	2 (6%)	0	0
Hes1$^{Fl/-}$;*Wnt1Cre*	26	10* (38%)	3 (11.5%)	0
Total	**95**			

* p<0.05

Table 4. 4. Thymic, great vessel and eye defects observed in the *Wnt1Cre* conditional embryos at E15.5. P value from Fisher's exact test between the wild type and *Hes1*$^{Fl/-}$;*Wnt1Cre* groups. WT, wild type.

In summary, *Wnt1Cre* conditional deletion of *Hes1* resulted in isolated fourth arch artery defects at both E10.5, after complete formation of the arch arteries, and E15.5,

after complete remodelling of the arch arteries. In that respect, *Hes1* may have a minor contribution in fourth arch artery morphogenesis.

3.2.1.2. *Hes1* is required in the neural crest for thymus development

Lack of *Hes1* either at the heterozygous (*Hes1*$^{Fl/-}$ or *Hes1*$^{Fl/+}$;*Wnt1Cre*) or homozygous level (*Hes1*$^{Fl/-}$;*Wnt1Cre*) in the neural crest induced thymic defects at E15.5, which ranged from a single thymic lobe to hypoplastic and/or ectopic lobes (Figure 4.3.D-F). By this stage the thymic lobes have normally descended above the heart and lie as a pair (Grevellec and Tucker, 2010). Ten out of twenty six (38%) *Wnt1Cre* conditional mutants exhibited thymic defects, in comparison to none out of seventeen wild type controls, which was significantly different ($p<0.05$, Fisher's exact test). Defects were also seen in three out of twenty one (14%) of the *Hes1*$^{Fl/-}$ and two out of thirty one (6%) of the *Hes1*$^{Fl/+}$;*Wnt1Cre* embryos, but these values did not reach statistical significance (Table 4.4). The thymic defects scored in these genotypes also included hypoplasia, single or ectopic lobes.

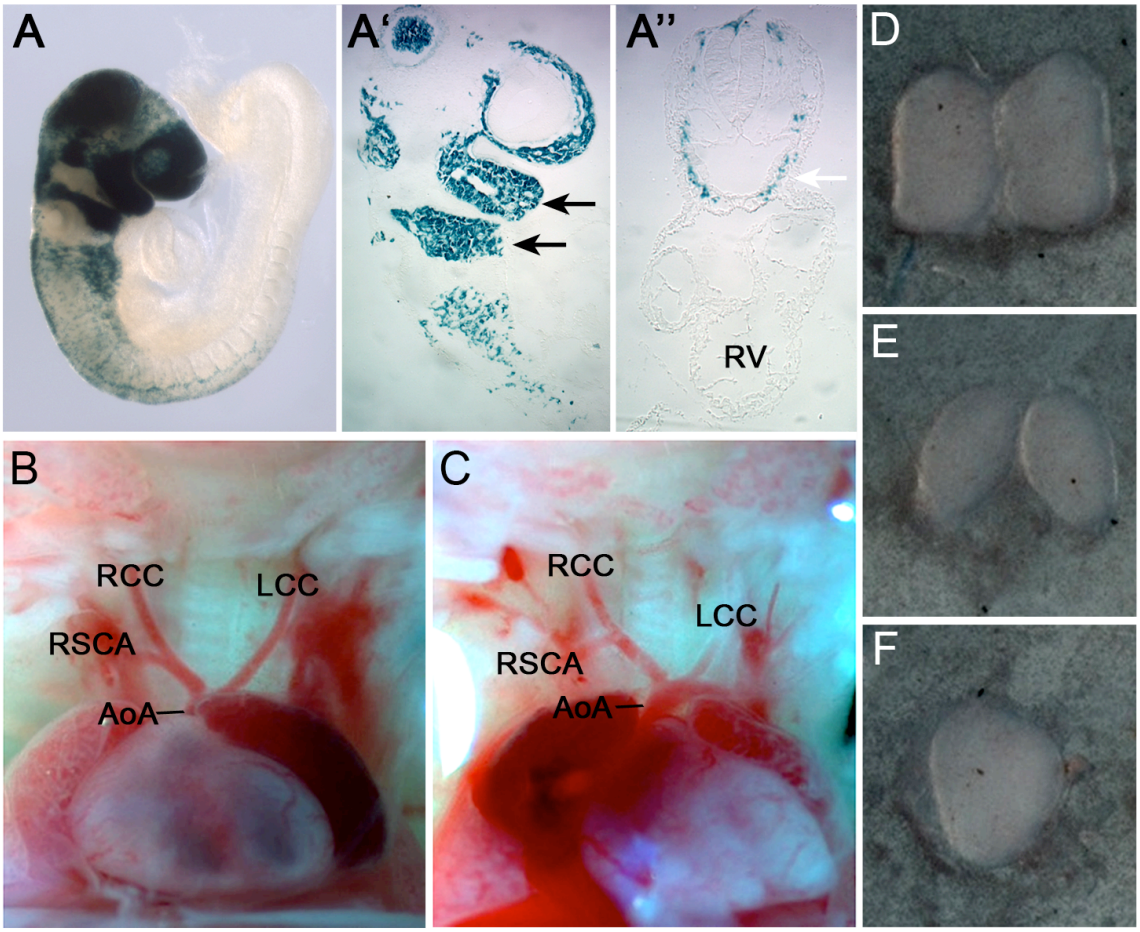

Figure 4. 3. *Wnt1Cre* conditional deletion. Reporter expression as detected by X-gal staining in *Wnt1Cre*;*ROSA26* embryos indicating *Cre* activity in whole mount (A), parasagittal (A') and transverse section at the caudal pharyngeal level (A''). (B-C) Great vessel defects at E15.5. Wild type configuration (B) and *Wnt1Cre* conditional embryo displaying cervical RSCA (C). (D-F) Thymic defects at E15.5. Wild type thymus (D) and *Wnt1Cre* conditional embryos with hypoplastic thymus (E) or a single thymic lobe (F). Black arrow, recombination in the neural crest of the pharyngeal arches; white arrow, recombination in the neural crest at the SHF level; AoA, aortic arch; RCC/LCC, right/left common carotid artery; RSCA/LSCA, right/left subclavian artery; RV, right ventricle; SHF, second heart field.

3.2.1.3. *Hes1* may have a minor role in the neural crest towards secondary palate and ventricular septum development

By E15.5 the ventricular septum (Webb et al., 1998) and secondary palate (Gritli-Linde, 2007; Meng et al., 2009) have formed completely. A minor population of *Hes1*$^{Fl/+}$;*Wnt1Cre* (one out of thirty one, 3%) and *Hes1*$^{Fl/-}$;*Wnt1Cre* (three out of twenty

six, 11.5%) embryos displayed intracardiac septation defects while none of the wild type embryos had the phenotype, but the values were not statistically significant. Also, one (3%) of the *Hes1*$^{Fl/+}$;*Wnt1Cre* embryos had a cleft palate.

3.2.1.3. *Hes1* is not required in the neural crest for eye development

No eye defects were scored in any of the genotypes, suggesting that *Hes1* is not involved in eye development through the neural crest (Table 4.4).

3.2.2. *Hes1* in the ectoderm

To assess the ectodermal role of *Hes1*, the *Ap2αCre* model was used (Macatee et al., 2003). Conditional mutant embryos were obtained and analysed from *Hes1*$^{Fl/Fl}$ (C57BL/6J) to *Hes1*$^{+/-}$;*Ap2αCre* (MF1;C57BL/6J) timed matings. This cross should delete *Hes1* in neural crest and ectodermal populations of the *Hes1*$^{Fl/+}$;*Ap2αCre* and *Hes1*$^{Fl/-}$;*Ap2αCre* embryos (hereafter *Ap2αCre* conditional mutants) (Figure 4.4.A-A''). *Ap2α* driven expression of *Cre* recombinase should begin at E8.5 in the surface ectoderm and head mesenchyme and later in the neural crest lineages and the ectoderm of the pharyngeal region (Macatee et al., 2003; Mitchell et al., 1991). The already characterised phenotype of the *Wnt1Cre* conditional mutants was considered when discussing the *Ap2αCre* conditional mutant phenotype.

3.2.2.1. *Hes1* is required in the neural crest and ectoderm towards arch artery morphogenesis

The pharyngeal arch artery phenotype of the *Ap2αCre* conditional mutants was also assessed at both stages, after arch artery formation and after arch artery remodelling. Conditional deletion of the gene in the neural crest and ectoderm induced persistent second arch arteries as well as hypoplasia or aplasia of the third arches in all the genotypes examined at E10.5. These, however, were isolated defects that did not reach statistical significance in any of the genotypes ($p>0.05$, between *Ap2αCre* conditional mutants and wild types, Fisher's exact test) (Table 4.5).

	***Hes1*$^{Fl/+}$ (WT)**	***Hes1*$^{Fl/-}$**	***Hes1*$^{Fl/+}$;*Ap2αCre***	***Hes1*$^{Fl/-}$;*Ap2αCre***
Total embryos	14	9	12	16
Total normal	13	8	11	14
Total abnormal (%)	1 (7.1%)	1 (11%)	1 (8.3%)	2 (12.5%)
Persistent 1st &/or 2nd PAA	-	1	1	1
Hypo/aplastic 3rd PAA	1 (hypo)	-	-	1 (apl)
Hypo/aplastic 4th PAA	-	-	-	-
Hypo/aplastic 6th PAA	-	-	-	-

Table 4. 5. Arch artery defects observed in the *Ap2αCre* conditional embryos at E10.5. apl, aplastic; hypo, hypoplastic; PAA, pharyngeal arch artery; WT, wild type.

Deleting *Hes1* in the neural crest and ectoderm produced great vessel defects in seven out of thirty two (22%) *Ap2αCre* conditional mutants at E15.5 against none out of twenty seven wild type embryos, which is statistically significant ($p<0.01$, Fisher's exact test) (Table 4.6). Five *Ap2αCre* conditional embryos exhibited cervical RSCAs (Figure 4.4.E) and one had retro-oesophageal origin of the RSCA, which branched off the pulmonary artery instead of connecting to the RCC artery (Figure 4.4.D). These defects occur when there is aberrant formation or remodelling of the right fourth arch artery and are in agreement with the *Hes1*$^{-/-}$ phenotype (van Bueren et al., 2010). One *Ap2αCre* conditional mutant presented with duplication of the RCC (Figure 4.4.C), potentially a right third arch artery defect, which has not been observed in the Hes1 null setting (van Bueren et al., 2010). No outflow tract defects were observed in any of the genotypes.

Genotype	n	Thymic hypo/aplasia	Great vessel defects	Eye defects
Hes1$^{Fl/+}$ (WT)	27	2 (7%)	0	0
Hes1$^{Fl/-}$	23	2 (8%)	0	0
Hes1$^{Fl/+}$;*Ap2αCre*	20	0	0	0
Hes1$^{Fl/-}$;*Ap2αCre*	32	25** (78%)	7** (22%)	5* (16%)
Total	**102**			

*p<0.05
**p<0.01

Table 4. 6. Thymic, great vessel and eye defects observed in the *Ap2αCre* conditional embryos at E15.5. P value from Fisher's exact test between the wild type and *Hes1*$^{Fl/-}$;*Ap2αCre* groups. WT, wild type.

In summary, ablating *Hes1* from both the ectodermal and neural crest lineages induced isolated second or third arch artery defects in the *Ap2αCre* conditional mutants, but no fourth arch defects at E10.5. These abnormalities did not reach statistical significance compared to the wild type controls (p>0.05, Fisher's exact test). At E15.5 the *Ap2αCre* conditional mutants exhibited fourth arch artery-derived and in one case third arch artery-derived great vessel defects, which were statistically different to the wild type controls (p<0.01, Fisher's exact test). When comparing the *Ap2αCre* conditional mutant defects between the two developmental stages there is no statistical difference (p>0.05, Fisher's exact test), suggesting that the early formation defects are potentially sufficient to induce the late stage phenotype. Increasing the sample size of the E10.5 populations may provide safer conclusions.

3.2.2.2. *Hes1* is required in the neural crest and ectoderm for thymic development

Thymic defects were observed in twenty five out of thirty two (78%) *Ap2αCre* conditional mutants against two out of twenty seven (7%) wild type embryos at E15.5. The difference was statistically significant (p<0.01, Fisher's exact test) (Table 4.6). The conditional mutant defects ranged from hypoplasia, single or ectopic lobes to complete aplasia (Figure 4.4.F-J). The two wild type embryos presented with a hypoplastic thymus. It should be noted that the great vessel defects were always accompanied by a thymic defect. Two out of twenty three (8%) *Hes1*$^{Fl/-}$ embryos also displayed thymic hypoplasia, which was not however statistically significant.

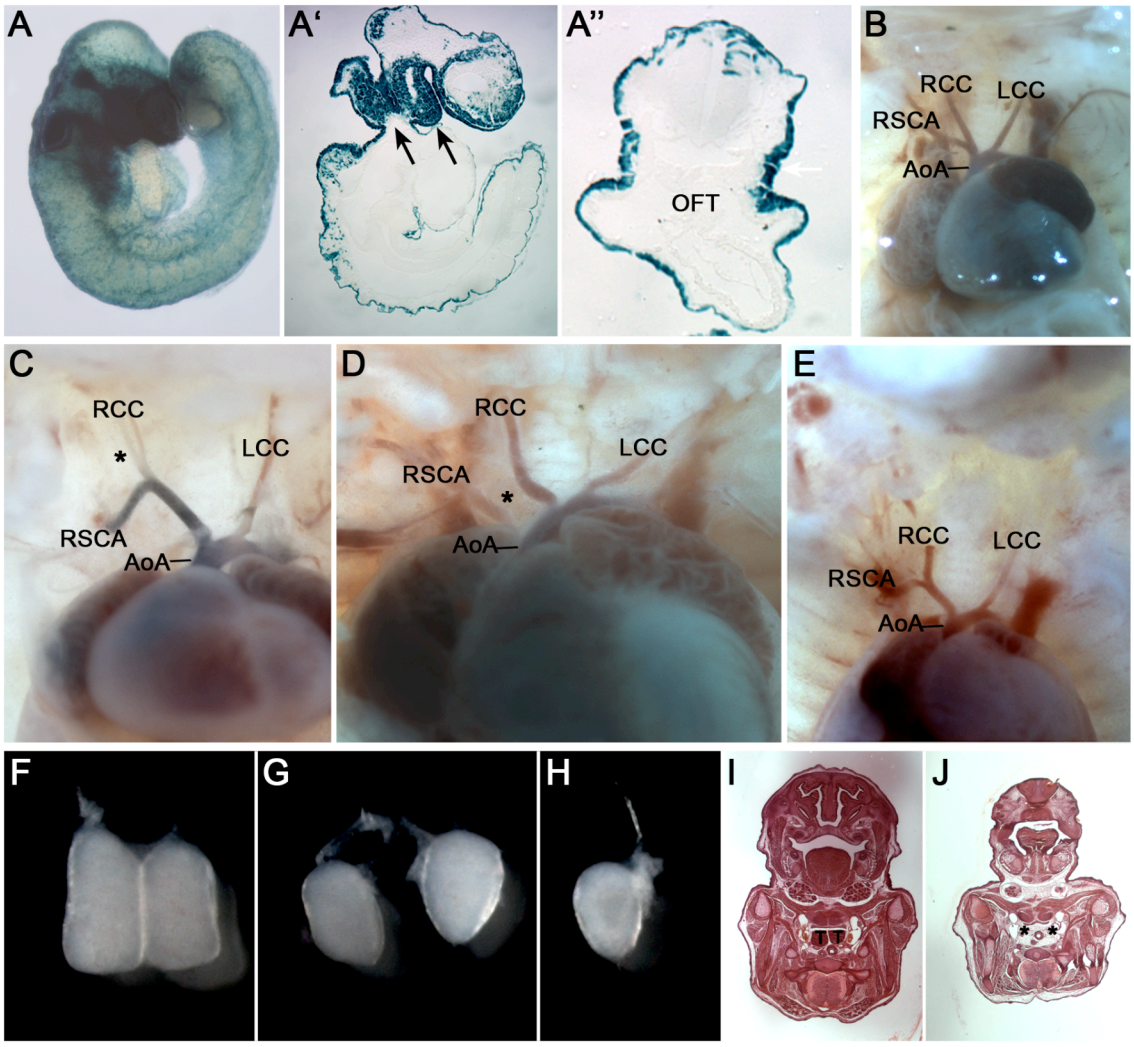

Figure 4. 4. *Ap2αCre* conditional deletion. Reporter expression as detected by X-gal staining in *Ap2αCre*;*ROSA26* embryos indicating *Cre* activity in whole mount (A), parasagittal (A’) and transverse section at the caudal pharyngeal level (A’’). Great vessel defects at E15.5. Wild type configuration (B) and *Ap2αCre* conditional embryos displaying duplication of the RCC (C), retro-oesophageal RSCA (D) and cervical RSCA (E). (F-J) Thymic defects at E15.5. Wild type thymus (D, I) and *Ap2αCre* conditional embryos with hypoplastic thymus (G), a single thymic lobe (H), or aplastic thymus (J). Asterisks denote abnormal vascular segments or missing thymic lobes in (J). Black arrow, recombination in the neural crest of the pharyngeal arches; white arrow, recombination in the ectoderm at the caudal pharyngeal level; AoA, aortic arch; OFT, outflow tract; RCC/LCC, right/left common carotid artery; RSCA/LSCA, right/left subclavian artery.

3.2.2.3. *Hes1* may have a minor role in the neural crest and ectoderm during secondary palate and ventricular septum development

One (3%) *Ap2αCre* conditional mutant exhibited exencephaly, was overall delayed versus the gestational age and had a cleft lip/palate and VSD (Figure 4.5). It was also amongst the embryos with a cervical RSCA. There was also a second *Ap2αCre* conditional mutant with unfused palatal shelves.

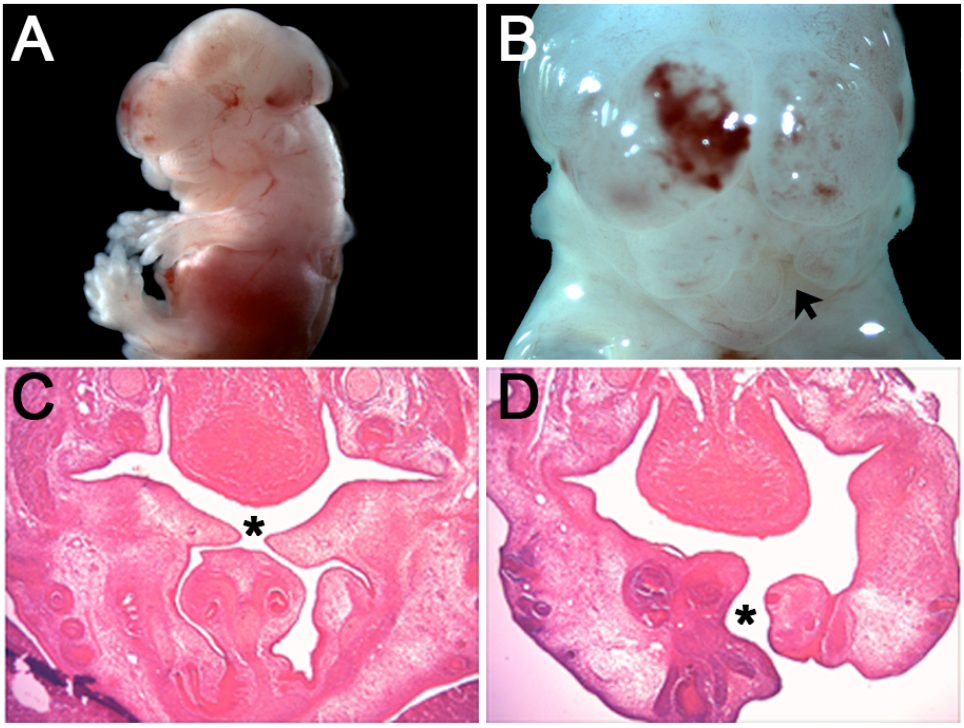

Figure 4. 5. Craniofacial defects in the *Ap2αCre* conditional embryos at E15.5. (A-B) Whole mount views and (C-D) transverse histological sections. An *Ap2αCre* conditional mutant displaying exencephaly (A), cleft lip (B, D), and cleft palate (C). Asterisks denote missing segments. Black arrow, cleft lip.

3.2.2.4. *Hes1* is required in the neural crest and ectoderm for eye development

Five out of the thirty two (16%) *Ap2αCre* conditional mutants presented with bilaterally missing eyes, which is statistically different to the wild type phenotype in the current sample size (Table 4.6). The eye defects previously reported for *Hes1*$^{-/-}$ embryos range between reduced lenses with small optic cups and abnormal rosette-like structures in the retina to complete absence of the lens and an arrested optic cup (Lee et al., 2005; Takatsuka et al., 2004; Tomita et al., 1996). In all cases the *Ap2αCre* conditional

mutants exhibited complete absence of the lens and disorganisation of the whole organ, the optic nerves and CNS structures like the optic chiasmata (Figure 4.6).

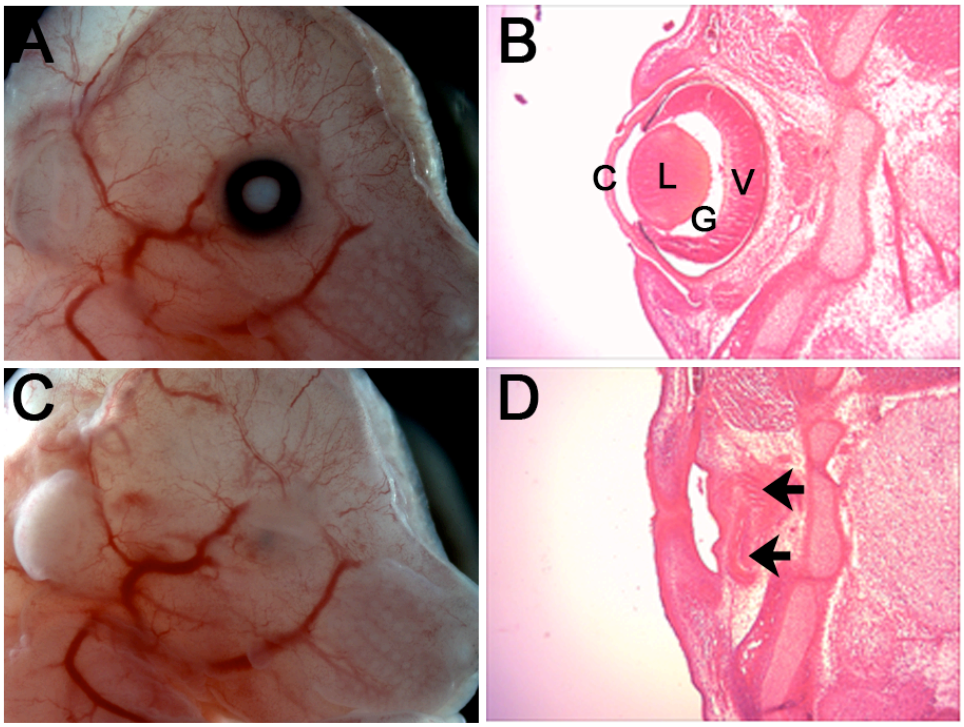

Figure 4. 6. Eye defects in the *Ap2αCre* conditional embryos at E15.5. (A, C) Whole mount views and (B, D) transverse histological sections. Normal eye development in wild type embryos (A, B) and undeveloped eye in *Ap2αCre* conditional embryos displaying disorganisation of the organ without distinct cell layers (C, D). Black arrow, abnormal structures; C, cornea; G, ganglion cell layer; L, lens; V, ventricular zone.

3.2.3. *Hes1* in the anterior heart field

The anterior heart field role of *Hes1* was investigated through the *Mef2c-AHF-Cre* model (Verzi et al., 2005). Conditional mutant embryos from $Hes1^{Fl/Fl}$ (C57BL/6J) to $Hes1^{+/-}$; *Mef2c-AHF-Cre* (mixed background) timed matings were produced, to delete *Hes1* in the anterior heart field of the $Hes1^{Fl/+}$; *Mef2c-AHF-Cre* embryos (hereafter *Mef2cCre* conditional mutants) (Figure 4.7.A-A''). The promoter and enhancer of the *Mef2c* gene that drive *Cre* recombinase expression in this model are active from the cardiac crescent stage, at E7.5 (Dodou et al., 2003; Verzi et al., 2005). During the linear heart tube stage *Cre* recombinase expression is detected in the pharyngeal mesoderm and arterial pole of the heart, and later it is identified in the outflow tract and RV of the heart (Dodou et al., 2003; Verzi et al., 2005).

3.2.3.1. *Hes1* is not required in the anterior heart field for arch artery morphogenesis

Similarly to the previous analyses, *Mef2cCre* conditional mutants were assessed after arch artery formation and after arch artery remodelling. Conditional deletion of the gene in the anterior heart field did not induce any pharyngeal arch artery defects at E10.5, apart from one case of a $Hes1^{Fl/+}$; *Mef2c-AHF-Cre* embryo that displayed persistent second arch artery (Table 4.7).

	$Hes1^{Fl/+}$ (WT)	$Hes1^{Fl/-}$	$Hes1^{Fl/+}$;*Mef2c-AHF-Cre*	$Hes1^{Fl/-}$;*Mef2c-AHF-Cre*
Total embryos	1	1	16	20
Total normal	1	1	15	20
Total abnormal (%)	0	0	1 (6%)	0
Persistent 1st &/or 2nd PAA	-	-	1	-
Hypo/aplastic 3rd PAA	-	-	-	-
Hypo/aplastic 4th PAA	-	-	-	-
Hypo/aplastic 6th PAA	-	-	-	-

Table 4. 7. Arch artery defects observed in the *Mef2cCre* conditional embryos at E10.5. PAA, pharyngeal arch artery; WT, wild type.

Conditional deletion of *Hes1* in the anterior heart field did not result in any great vessel or outflow tract defects at E15.5-E19.5 either, although the *Mef2cCre* conditional mutant and wild type populations appeared underrepresented during these stages (Table 4.8). One $Hes1^{Fl/+}$;*Mef2c-AHF-Cre* embryo exhibited thinning of the arch on the left fourth-derived fragment, potentially by an aortic coarctation (Figure 4.7.C). Increasing the sample size may clarify whether the *Mef2cCre* conditional embryos die embryonically and if they display a cardiovascular phenotype.

Genotype	n	Thymic hypo/aplasia	Great vessel defects	Eye defects
Hes1$^{Fl/+}$ (WT)	7	0	0	0
Hes1$^{Fl/-}$	10	1 (10%)	0	0
Hes1$^{Fl/+}$;*Mef2c-AHF-Cre*	20	1 (5%)	1 (5%)	0
Hes1$^{Fl/-}$;*Mef2c-AHF-Cre*	5	0	0	0
Total	**42**			

Table 4. 8. Thymic, great vessel and eye defects observed in the *Mef2cCre* conditional embryos at E15.5-E19.5. WT, wild type.

3.2.3.2. *Hes1* is not required in the anterior heart field for thymus, palate or eye development

Only isolated cases of thymic or secondary palate defects were scored in some of the genotypes of the *Hes1*$^{Fl/Fl}$ (x) *Hes1*$^{+/-}$;*Mef2c-AHF-Cre* cross. One *Hes1*$^{Fl/-}$ and one *Hes1*$^{Fl/+}$;*Mef2c-AHF-Cre* embryos displayed thymic hypoplasia. One *Hes1*$^{Fl/+}$;*Mef2c-AHF-Cre* embryo had cleft palate (Figure 4.7.D) and one *Hes1*$^{Fl/-}$ embryo had exomphalos (Figure 4.7.E). No eye defects were scored in any of the genotypes (Table 4.8). None of these values reached statistical significance.

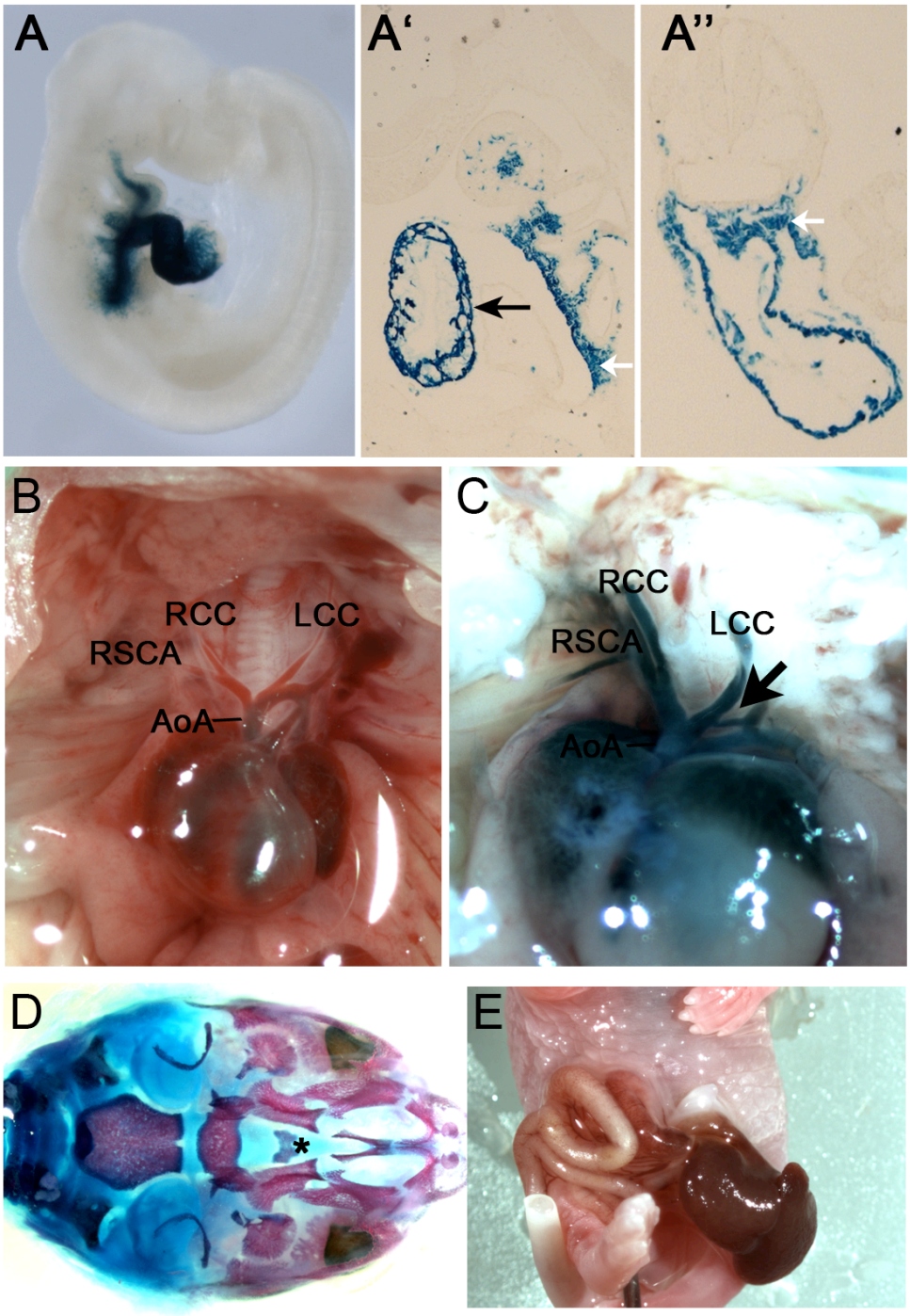

Figure 4. 7. *Mef2cCre* conditional deletion. Reporter expression as detected by X-gal staining in *Mef2c-AHF-Cre*;*ROSA26* embryos indicating *Cre* activity in whole mount (A), parasagittal (A') and transverse section at the caudal pharyngeal level (A''). (B-C) Great vessel defects. Control embryo normal configuration (B) and a $Hes1^{Fl/+}$;*Mef2c-AHF-Cre* embryo displaying thinning of the AoA (C). A $Hes1^{Fl/+}$;*Mef2c-AHF-Cre* embryo had cleft palate (D) and a $Hes1^{Fl/-}$ embryo had exomphalos (E). Asterisks denote missing segments. Black arrow, recombination in the ventricular myocardium;

white arrow, recombination in the mesoderm at the SHF level; AoA, aortic arch; RCC/LCC, right/left common carotid artery; RSCA/LSCA, right/left subclavian artery; SHF, second heart field.

3.2.4. *Hes1* in the endoderm

Two different models were employed to conditionally delete *Hes1* in the endoderm during embryogenesis. The *Foxa2mcm* (Park et al., 2008) and the *Sox17-2A-iCre* (Engert et al., 2009) transgenic animals were used. Timed matings of $Hes1^{Fl/Fl}$ (C57BL/6J) to $Hes1^{+/-}$;*Foxa2mcm* or $Hes1^{+/-}$;*Sox17-2A-iCre* (both MF1;C57BL/6J) mice were used to produce embryos to study the endodermal role of *Hes1*. Tamoxifen induction at E5.75 should induce *Cre* recombinase expression under the *Foxa2* driver in the definitive endoderm and in a few anterior mesoderm cells at the 0 somite stage (Park et al., 2008). By E8.5 *Cre* recombinase expression should be detected in the foregut endoderm, notochord, floorplate and a few head mesenchyme and myocardial and endocardial cells (Park et al., 2008). At E9.5 pharyngeal and gut endoderm as well as liver bud, notochord and floorplate specific *Cre* expression should be induced (Park et al., 2008). The optimal tamoxifen administration protocol for this line is 120mg/ kg body weight by OG at E5.75 and E6.75 (Anne Moon, pers. comm.). *Cre* expression under the *Sox17* promoter should be active in the extraembryonic visceral endoderm from E6.0, in the visceral and definitive endoderm from E7.5 and by E8.5 throughout the gut tube, the endocardial lining of the heart, the DAo, blood vessels in the head region and the allantois (Engert et al., 2009). From E9.5 onwards *Cre* recombinase should be expressed in the otic vesicle, the gut, the heart and all the blood vessels (Engert et al., 2009).

The initial approach was deletion of *Hes1* in the endoderm through the *Foxa2mcm* model. Although the optimal tamoxifen administration protocol for *Cre* recombinase induction was followed, the reporter expression showed that induction of the promoter was not reproducible (Figure 4.8). Unless the recombination efficiency can be assessed in each embryo, this model cannot be used to examine the endodermal requirements for *Hes1* during embryogenesis.

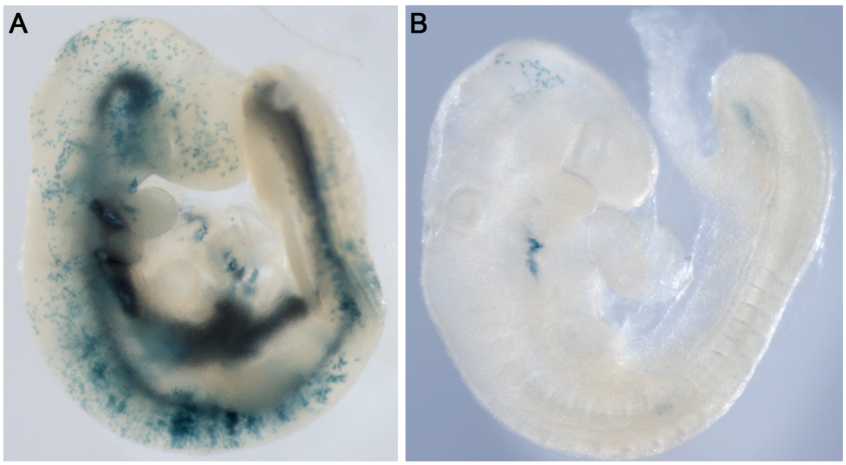

Figure 4. 8. *Foxa2mcm* system induction at E9.5. Reporter expression as detected by X-gal staining in *Foxa2mcm*;*ROSA26* embryos indicating maximal (A) and minimal (B) induction of the *Foxa2mcm* driver in two separate experiments following the same tamoxifen administration protocol.

The *Sox17-2A-iCre* model was therefore used instead of the *Foxa2mcm* model. This approach, however, was abandoned too, because the reporter expression indicated that a single *Hes1* null allele, potentially in combination with background modifiers, interferes with the *Sox17* promoter and induces ubiquitous recombination (Figure 4.9).

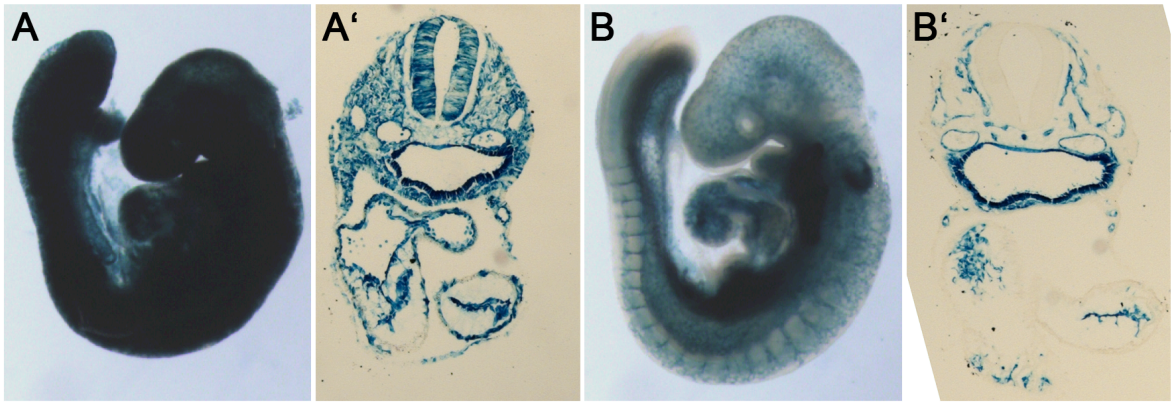

Figure 4. 9. *Sox17-2A-iCre* system induction at E9.5. Reporter expression as detected by X-gal staining in *Hes1*$^{+/-}$;*Sox17-2A-iCre*;*ROSA26* (A, A’) or *Hes1*$^{+/+}$;*Sox17-2A-iCre*;*ROSA26* (B, B’) embryos in whole mount (A, B) or transverse section at the caudal pharyngeal level (A’, B’) indicating ubiquitous activity of the *Sox17-2A-iCre* driver in the presence of one null *Hes1* allele.

3.3. *Hes1* in the neural crest lineage

As demonstrated in this thesis, *Hes1* is expressed in the pharyngeal mesenchyme at E9.5 and neural crest-specific deletion of the gene leads to thymic and isolated great vessel defects. Concurrent ectodermal and neural crest cell-specific ablation of the gene led to a more severe thymic phenotype and greater penetrance of cardiovascular anomalies. Abnormal neural crest patterning has been associated with pharyngeal arch artery defects (Kaartinen et al., 2004; Liu et al., 2004; Richarte et al., 2007) while conditional inhibition of the Notch pathway in the neural crest lineage induces outflow tract and arch artery defects and inhibits neural crest cell differentiation into VSM cells (High et al., 2007). Therefore, we sought to investigate potential cell-autonomous roles for *Hes1* in the neural crest cell population.

3.3.1. *Hes1* in neural crest cell patterning

Hes1, in co-operation with *Hes3* and *Hes5*, maintains the undifferentiated state of neuronal lineages (Kageyama et al., 2005) while Hes1 alone is shown to participate in ES cell differentiation (Kobayashi et al., 2009). Combined *Hes1* and *Hes5* deficiency induces premature glial cell differentiation into neurons (Kageyama et al., 2005). Moreover, Kobayashi *et al.*, showed that *Hes1* binds to and regulates several neural crest genes in ES cells, through microarray and ChiP-on-chip assays (Kobayashi et al., 2009).

To test the hypothesis that *Hes1* may be involved in maintaining cardiac neural crest cells in an undifferentiated state, thus allowing for migration into their target sites and subsequent *in situ* differentiation, neural crest cell patterning was examined at E10.5 in *Hes1*$^{-/-}$, *Hes1*$^{Fl/-}$;*Wnt1Cre* and *Hes1*$^{Fl/-}$;*Ap2αCre* embryos, compared to stage matched littermate controls. This was assessed by whole mount *in situ* hybridisation for *Sox10*, a known neural crest marker (Kuhlbrodt et al., 1998). A diminished population of neural crest cells was observed migrating through the post-otic streams in *Hes1* null and *Wnt1Cre* conditional embryos, while diminished population and disrupted migratory pathways of the neural crest cells were detected in the *Ap2αCre* conditional mutants (Figure 4.10).

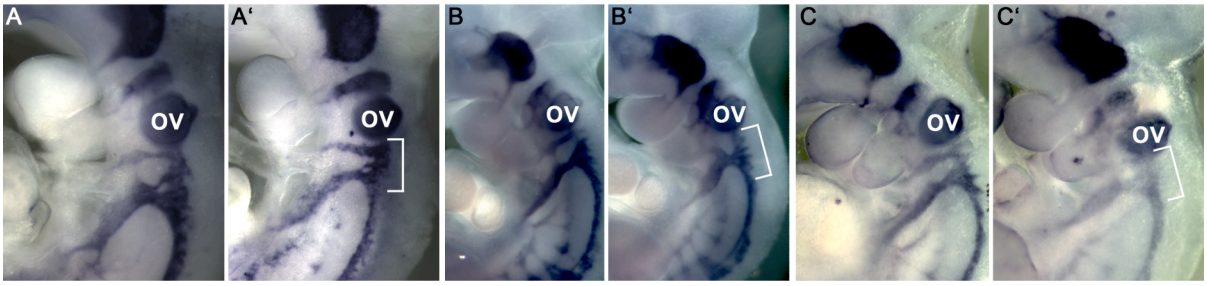

Figure 4. 10. Neural crest patterning in *Hes1* mutant embryos at E10.5. Whole mount *in situ* hybridisation for *Sox10* on *Hes1*$^{Fl/+}$ (WT) (A), *Hes1*$^{Fl/-}$;*Wnt1Cre* (A'), *Hes1*$^{Fl/+}$ (WT) (B), *Hes1*$^{Fl/-}$;*Ap2αCre* (B'), wild type (C) and *Hes1*$^{-/-}$ (C') embryos. White box, post otic neural crest streams; ov, otic vesicle; WT, wild type.

A day earlier, at E9.5, the post-otic neural crest migration streams also appear disorganised in *Hes1*$^{-/-}$ as compared to *Hes1*$^{+/-}$ stage matched littermate control embryos. In *Hes1*$^{+/-}$ embryos there are two distinct cardiac neural crest streams that will populate the third and fourth/sixth arches respectively. Conversely, the cardiac crest streams do not form discrete streams in the null embryos (Figure 4.11).

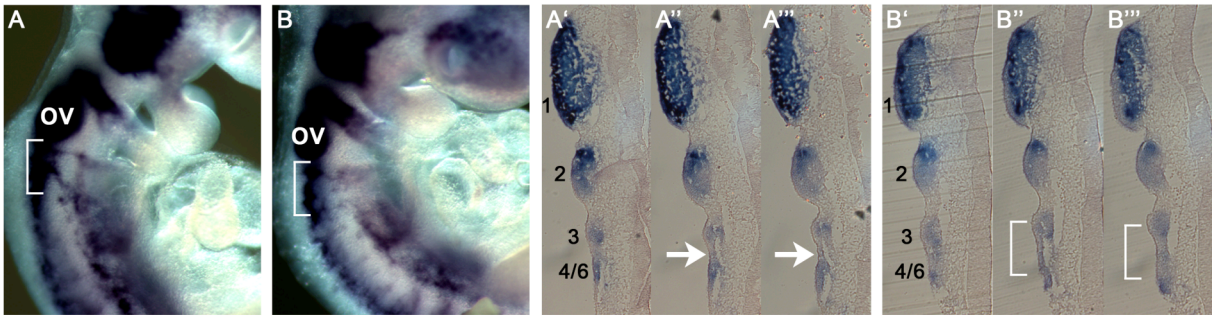

Figure 4. 11. Neural crest patterning in *Hes1* mutant embryos at E9.5. *In situ* hybridisation for *Sox10* on wild type (A-A''') and *Hes1*$^{-/-}$ (B-B''') embryos in whole mount (A, B) and coronal sections through the pharyngeal arches (A'-A''', B'-B'''). White box, post otic neural crest streams in whole mount and non segregated streams in section; white arrow, segregation of neural crest streams; ov, otic vesicle; 1-6, neural crest migratory streams depending on target pharyngeal arch.

3.3.2. *Hes1* in post migratory neural crest

To address whether neural crest cells become sequestered and fail to migrate into their target sites in *Hes1* null mutants, members of the *Hox* family of genes, *Hoxb4* and *Hoxd4* that are expressed in the neural crest cells populating the fourth pharyngeal arch (Minoux et al., 2009) were examined in E10.5 *Hes1*$^{-/-}$ versus stage matched littermate

control embryos by whole mount *in situ* hybridisation. *Hoxb4* mRNA could not be detected with the probe used, and this was not further pursued. Consistently, no differences were seen between the *Hes1* heterozygous and homozygous embryos in *Hoxd4* expression at E10.5 (Figure 4.12), a stage by which all caudal pharyngeal arches have formed (Hiruma et al., 2002; Yanagisawa et al., 1998). This indicates that even if cardiac neural crest cells appear misspatterned at E9.5 and E10.5 by *Sox10* labelling, neural crest cells eventually populate the fourth arch in the *Hes1*$^{-/-}$ embryos.

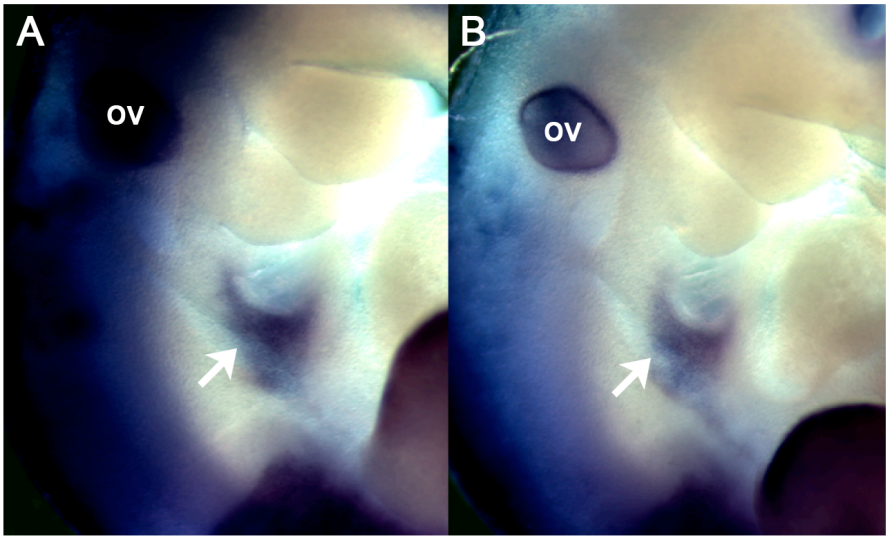

Figure 4. 12. Neural crest patterning in *Hes1* mutant embryos at E10.5. Whole mount *in situ* hybridisation for *Hoxd4* on control *Hes1*$^{+/-}$ (A) and *Hes1*$^{-/-}$ (B) embryos. White arrow, post migratory neural crest within the fourth; ov, otic vesicle.

3.4. *Hes1* and the Notch pathway during pharyngeal development

Notch pathway genes that directly interact with *Hes1*, like *Jag1* (Kobayashi et al., 2009), which is also expressed in the pharyngeal apparatus during embryogenesis (Barsi et al., 2005) and the *Hes1* upstream regulator *RBP-J* (Iso et al., 2003) and glial-specific genes, like *Neuregulin* (Meyer et al., 1997) were examined in E9.5 *Hes1*$^{-/-}$ versus stage matched littermate control embryos by whole mount *in situ* hybridisation. The *Hes1* mutation induces higher frequency of cardiovascular defects on a C57BL/6J background (van Bueren et al., 2010). Therefore, the embryos used for these experiments derived from crosses between *Hes1* heterozygous animals maintained on a C57BL/6J background for at least four generations.

Both Jag1 and *RBP-J* were differentially expressed in *Hes1*$^{-/-}$ embryos at E9.5, compared to heterozygous controls. *Jag1* was upregulated in the pharyngeal pouches in *Hes1* null compared to control embryos, while the rest of the expression domains remained unaltered (Figure 4.13.A-B'). Conversely, *RBP-J* was detected downregulated in the pharyngeal ectoderm and mesenchyme in the *Hes1* null embryos compared to the heterozygous controls (Figure 4.13.C-D').

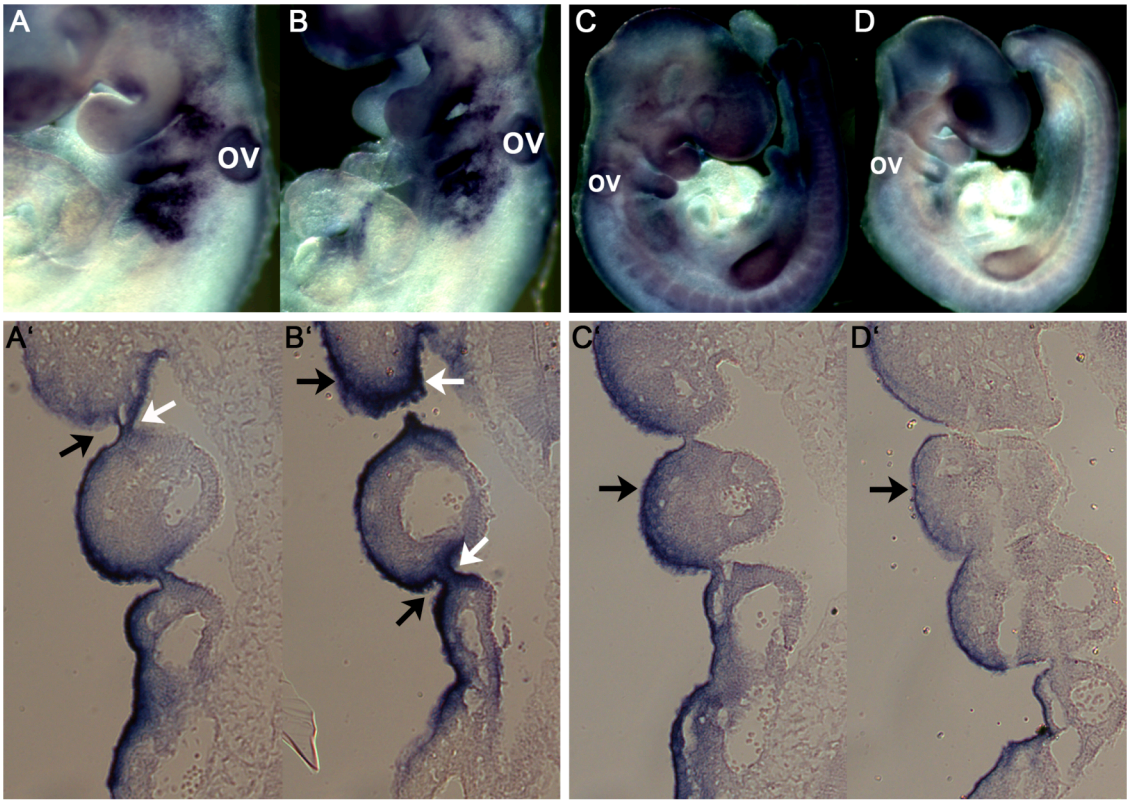

Figure 4. 13. Pharyngeal expression of Notch genes in *Hes1* mutant embryos at E9.5. *In situ* hybridisation for *Jag1* on control *Hes1*$^{+/-}$ (A, A') and *Hes1*$^{-/-}$ (B, B') embryos and *RBP-J* on control *Hes1*$^{+/-}$ (C, C') and *Hes1*$^{-/-}$ (D, D') embryos in whole mount (A-D) and coronal sections through the pharyngeal arches (A'-D'). Black arrow, pharyngeal ectoderm; white arrow, pharyngeal endoderm; ov, otic vesicle.

At E10.5, an attempt was made to assess cranial ganglia patterning through *Neuregulin 1* (*Nrg1*), but the probe used did not detect *Nrg1* transcripts, and this was not further pursued.

3.5. *Hes1* and the FGF pathway during pharyngeal development

Fgf8 has been associated with pharyngeal arch artery morphogenesis (Frank et al., 2002) and has been shown to genetically interact with *Tbx1* in great vessel development (Aggarwal et al., 2006; Vitelli et al., 2002b). Dominant negative inhibition of the Notch pathway in the SHF results in defective EMT in the outflow tract cushions, which can be rescued by *Fgf8* in *ex vivo* culture (High et al., 2009). In that respect, differential regulation of *Fgf8* may contribute to both the arch artery and outflow tract abnormalities observed in *Hes1* nulls. Nonetheless, no alteration of *Fgf8*, or *Etv4*, a readout for FGF activity (Mao et al., 2009) was detected at E8.5 by whole mount *in situ* hybridisation, while *Fgf8*, *Fgf10* and *Etv4* appeared unaffected at E9.5 as well (Figure 4.14). No quantitative change was detected in *Etv4* or *Etv5* expression at both stages by quantitative real time PCR (Figure 4.14.K, K'). The embryos used for these experiments derived from crosses between *Hes1* heterozygous animals maintained on an MF1 background.

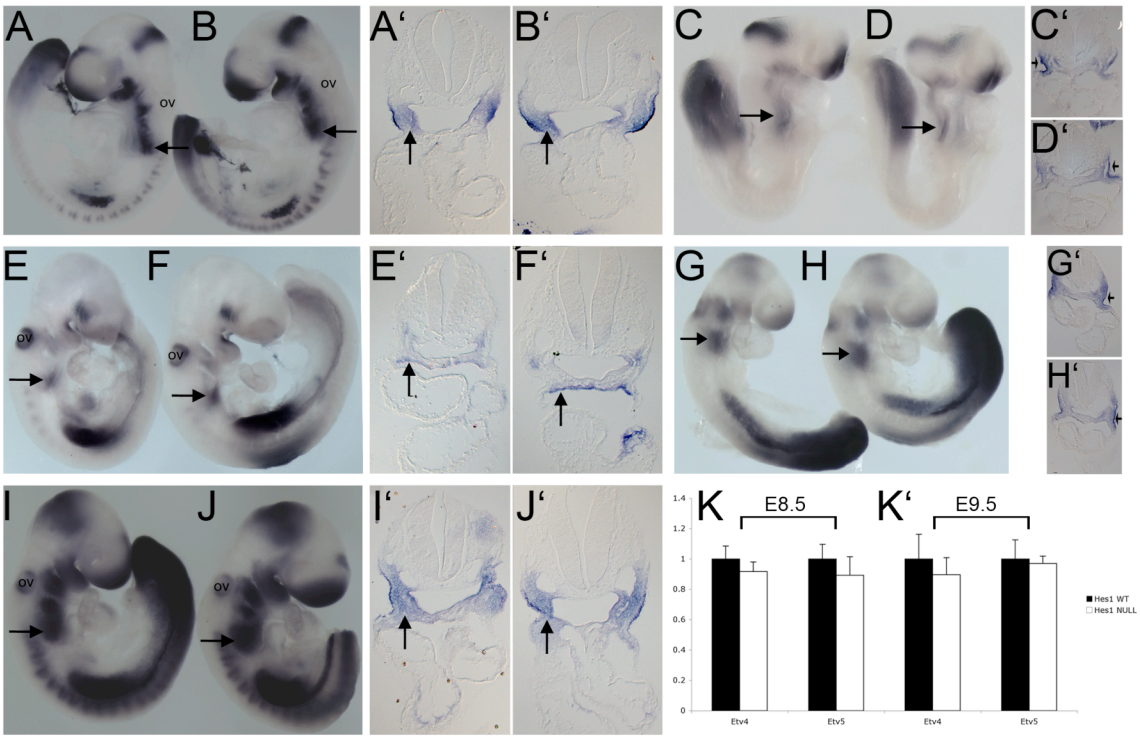

Figure 4. 14. Expression of FGF genes in *Hes1* mutant embryos at E8.5 and E9.5. *In situ* hybridisation for *Fgf8* at E9.5 (A-B') and E8.5 (C-D') on wild type (A, A', C, C') and *Hes1*$^{-/-}$ (B, B', D, D') embryos in whole mount (A, B, C, D) or transverse section at the caudal pharyngeal level (A', B', C', D'). *In situ* hybridisation for *Fgf10* at E9.5 (E-F') on wild type (E, E') and *Hes1*$^{-/-}$ (F, F') embryos in whole mount (E, F) or

transverse section at the caudal pharyngeal level (E', F'). *In situ* hybridisation for *Etv4* at E9.0 (G-H') and E9.5 (I-J') on wild type (G, G', I, I') and *Hes1*$^{-/-}$ (H, H', J, J') embryos in whole mount (G, H, I, J) or transverse section at the caudal pharyngeal level (G', H', I', G'). Graphical representation of the relative expression levels of Etv4 (K) and Etv5 (K') by quantitative real time PCR on E8.5 and E9.5 wild type and *Hes1*$^{-/-}$ embryos, in single embryos. Black arrow, pharyngeal mesenchyme; ov, otic vesicle; WT, wild type.

4. Discussion - Future directions

4.1. *Hes1* is expressed in overlapping domains with *Tbx1* during early embryogenesis

Hes1 was originally identified through a microarray screen as a putative Tbx1 target (van Bueren et al., 2010). Preliminary data by a member of our lab suggested that *Hes1* is expressed in an overlapping fashion with *Tbx1* at E9.5 in pharyngeal tissues, while *Hes1* transcripts appeared downregulated in these tissues in $Tbx1^{lacZ/lacZ}$ embryos of the same stage, compared to stage matched wild type controls (van Bueren, 2008). Hes1 expression was therefore examined during embryogenesis in this thesis, to confirm and extend these results. At E8.5 Tbx1 and Hes1 proteins were found co-expressed in the pharyngeal ectoderm, endoderm and mesenchyme. A day later, at E9.5 *Hes1* mRNA transcripts were also expressed in an overlapping fashion with *Tbx1*, in the pharyngeal endoderm, mesenchyme and ectoderm. *Hes1* expression was additionally detected downregulated in E9.5 $Tbx1^{lacZ/lacZ}$ embryos in the pharyngeal endoderm and mesenchyme but not ectoderm, compared to littermate stage matched wild type controls. These results support the potential for a *Tbx1-Hes1* interaction in subsequent stages of development.

Although it would be important to address the issue of a potential genetic interaction between *Tbx1* and *Hes1*, to date there is no evidence supporting such a relationship in a mammalian system. Previous work by a member of our lab has examined the interaction between the two genes by intercrossing heterozygous mice for *Tbx1* and *Hes1*. Double heterozygosity for the two genes did not have an effect on the *Tbx*1 haploinsufficient arch artery phenotype (van Bueren, 2008). Functional redundancy between Hes1 and other bHLH factors may partly explain these results. *Hes5* compensates for loss of *Hes1* expression in the CNS of *Hes1* null embryos (Hatakeyama et al., 2004). *Hey* genes have overlapping expression domains with *Hes1* within pharyngeal tissues including the neural crest and pharyngeal endoderm (High et al., 2007). Moreover, redundancy between the *Hey* genes has been previously demonstrated, considering that the *Hey2* mutation alone is sufficient to cause cardiovascular defects, but *Hey1* and *HeyL* induce similar phenotypes only in double mutations (Fischer and Gessler, 2007).

4.2. Tissue-specific contributions of *Hes1* to the null phenotype

The tissue-specific contribution of *Hes1* to the null phenotype previously reported was investigated through this work. The data collected (summarised in Table 4.9) indicate that *Hes1* is involved in great vessel development through ectodermal lineages and in thymus development through the neural crest and ectoderm. Additionally, *Hes1* may be acting through the ectoderm towards eye development.

Hes1 deletion	**Cardiovasculature**			**Thymus**	**Eye**
	great vessels	outflow tract	ventricular septum		
Neural crest	✔	-	✔	✔	-
Ectoderm/ Neural crest	✔	-	✔	✔	✔
Mesoderm	-	-	-	-	-
Endoderm	could not assess				

Table 4. 9. Summary of the *Hes1* conditional deletion phenotypes. ✔: statistically significant; ✔: potential minor contribution.

The role of *Hes1* via the endoderm has not been possible to be assessed with the models used in this thesis. The *Foxa2mcm* system is tamoxifen inducible and had variable activation, which was not consistent, while the *Sox17-2A-iCre* driver was ubiquitously activated in the presence of one null *Hes1* allele. *Hes1* is shown to repress *Sox17* in the pharyngeal endoderm at E9.5, an interaction required for the patterning and morphogenetic segregation of the ventral foregut lineages (Spence et al., 2009). In that respect, earlier interactions between the two genes are possible, making the *Sox17-2A-iCre* an inadequate model for *Hes1* targeted deletion in the endoderm.

4.2.1. Cardiovascular development

All the embryonic germ layers participate in cardiovascular development during embryogenesis. The ectoderm is shown to be a distant regulator of fourth arch artery development, through *Tbx1* (Calmont et al., 2009). The mesoderm provides the endothelial lining of the arch arteries (Graham, 2001; Graham, 2003; Graham, 2008;

Grevellec and Tucker, 2010) and through the SHF population contributes to the outflow tract, RV and parts of the LV and inflow region (Dunwoodie, 2007). The neural crest provides the VSM layer that supports the arch arteries (Hutson and Kirby, 2007; Scholl and Kirby, 2009) and a significant cellular contribution into the AP septum (Epstein et al., 2000; Nakamura et al., 2006), while the endoderm provides essential positional cues for the mesoderm and the invading neural crest of the arches (Graham, 2008). Deleting *Hes1* from the neural crest lineage or the ectoderm and neural crest combined, but not the anterior heart field, induced cardiovascular phenotypes.

Tissue-specific inactivation of *Hes1* in neural crest and ectodermal tissues resulted in great vessel defects in the *Ap2αCre* and in *Wnt1Cre* conditional mutants at E15.5, although with very reduced penetrance in the latter. The phenotype observed in both genetic settings included primarily right fourth arch artery related defects, with the exception of one $Hes1^{Fl/-}$;*Ap2αCre* embryo that displayed duplication of the RCC, a right third arch artery-derived defect. These defects are consistent with the *Hes1* null (MF1;C57BL/6J) great vessel phenotype at E14.5-E15.5 ($p>0.05$, no difference, Fisher's exact test) (van Bueren et al., 2010). Since *Hes1* ablation in the *Wnt1* expressing cells produced a weakly penetrant phenotype, *Hes1* may have a minor role in great vessel development through the neural crest and a major contribution to the process through ectodermal expression. *Hes1* may modulate signalling from the ectoderm to the neural crest or other mesenchymal lineages, acting non cell autonomously on great vessel development. Additive effects from both tissues cannot be excluded either.

Homozygous knock-out of the *Hes1* gene additionally induces outflow tract defects (Rochais et al., 2009b; van Bueren et al., 2010). However, no such defects were observed here, in any of the *Hes1* conditional mutations. Two different phenotypes have been identified on the genetic backgrounds examined, DORV on MF1 or MF1;C57BL/6J backgrounds with very low penetrance (6% or 4% respectively, van Bueren et al., 2010) and dextroposed aorta on CD1 background with higher penetrance (38%, Rochais et al., 2009b). Additionally, the $Hes1^{-/-}$ (CD1) embryos displayed shortening of the outflow tract and widening of the angle between the proximal and distal regions at E10.5, compared to littermate controls (Rochais et al., 2009b). Both the *Ap2αCre* and *Wnt1Cre Hes1* conditional mutants produced here were maintained on an MF1;C57BL/6J background, while the *Mef2cCre* conditional mutation was maintained

on a mixed background. The outflow tract anomalies may be difficult to demonstrate in the conditional deletions due to the fact that low penetrance (even in the constitutive nulls) is doubleed by genomic recombination at the $Hes1^{Fl}$ allele, which may not be fully efficient. Genetic background modifiers may be responsible for rescuing the dextroposed aorta phenotype seen in $Hes1^{-/-}$ CD1 embryos, in the *Hes1* tissue-specific deletions studied here. It should be noted that during ink filling of the pharyngeal arch arteries via the outflow tract in E10.5 embryos, the impression was gained that the *Wnt1Cre* conditional mutants exhibited shorter outflow tracts. This was not observed in any of the other conditional or control embryos. It may be worth examining the outflow tract length and angulation in all conditional mutants, according to Rochais *et al.*, to decisively answer whether *Hes1* participates in outflow tract development through any of its expression domains (Rochais et al., 2009b).

A small proportion of *Hes1* null embryos display ventricular septation anomalies (Rochais et al., 2009b; van Bueren et al., 2010), which was recapitulated by *Hes1* deletion in the neural crest and in smaller frequency by *Hes1* deletion in the ectoderm and neural crest lineages. *Hes1* may hence participate in intracardiac septation through the ectoderm and neural crest, although none of these values reached statistical significance.

Hes1 is expressed in the SHF as shown here by Tbx1-Hes1 protein overlap in the pharyngeal mesenchyme at E8.5 and the work by Rochais *et al.* (Rochais et al., 2009b). The anterior/secondary heart field is considered a subpopulation of the SHF (Perez-Pomares et al., 2009). Deletion of *Hes1* in the anterior heart field induced isolated arch artery defects in two $Hes1^{Fl/+}$;*Mef2c-AHF-Cre* embryos, but no outflow tract defects or other gross anomalies in any of the other genotypes. Both the wild type and the $Hes1^{Fl/-}$;*Mef2c-AHF-Cre* populations at E15.5-E19.5 appeared underrepresented compared to the other groups. Increasing the sample size may elucidate the role of *Hes1* in the anterior heart field during development. Moreover, refined analysis of the Hes1 expression domains in the splanchnic mesoderm will clarify if *Hes1* is expressed in the anterior heart field or complementary domains of the SHF. A *Cre* allele active in early cardiogenic mesoderm, like the *Mesp1Cre* (Saga et al., 1999) may be more informative towards dissecting the *Hes1* roles in the mesoderm.

4.2.2. Thymus development

The thymus arises from endodermal cells of the anterior pharyngeal region that evaginate the underlying mesenchyme, controlled by signalling from both the neural crest-derived mesenchyme and the adjacent mesoderm (Boehm, 2008). The neural crest gives rise to the perivascular mesenchyme of the adult organ (Muller et al., 2008). Deleting *Hes1* either in the neural crest lineage or in both the ectoderm and the neural crest populations induced thymic defects in the conditional mutants, highlighting the requirement of the gene's expression for normal thymus development. The *Wnt1Cre* conditional mutants displayed thymic hypoplasia, single or ectopic lobes, partially recapitulating the *Hes1*$^{-/-}$ phenotype characterised on MF1;C57BL/6J background ($p<0.01$, difference, Fisher's exact test) (van Bueren et al., 2010). The *Ap2αCre* conditional mutation induced more severe defects, ranging from thymic hypoplasia, single or ectopic lobes to thymic aplasia, which were also more penetrant. Hence, deletion of *Hes1* in the neural crest and ectoderm fully recapitulated the *Hes1* null thymic phenotype characterised on MF1 background ($p>0.05$, no difference, Fisher's exact test) although not on the MF1;C57BL/6J background ($p<0.05$, difference, Fisher's exact test) (van Bueren et al., 2010). No thymic abnormalities were detected in any of the *Mef2c-AHF-Cre* conditional mutants. These results suggest that *Hes1* is required in the neural crest and ectoderm for thymus development.

The mesenchyme surrounding the thymic primordium mediates cell proliferation and regulates morphogenesis of the thymic epithelium (Gill et al., 2003). Moreover, Kaneta *et al.* showed that in *Hes1*$^{-/-}$ thymi the cells were reduced to half the number of the wild type control, *ex vivo*, while the ratio of different cell phenotypes was normal (Kaneta, 2000). Taken together, these findings propose non cell autonomous roles for *Hes1* in thymus development, potentially as a mediator of the proliferative and morphogenetic actions of the mesenchyme surrounding the thymus. Since the perivascular mesenchyme of the adult thymus is of neural crest origin (Muller, 2008), *Hes1* may be important through the neural crest for the maturity and maintenance of the organ, while lack of it may lead to thymic hypoplasia.

4.2.3. Eye development

The embryonic eye begins to develop at E8.5, when the anterior neural plate evaginates at both sides to form depressions, called optic grooves (Lamb et al., 2007;

Lee et al., 2005). These regions balloon outwards creating the optic vesicles that come in contact with the surface ectoderm (Lamb et al., 2007; Lee et al., 2005). Reciprocal signalling causes the optic vesicles to invaginate and form the optic cups, while the ectoderm forms the lens pit and the lens (Lamb et al., 2007; Lee et al., 2005). Retinal neurogenesis begins at E11.0 in the dorso-central optic cup (Lamb et al., 2007; Lee et al., 2005). *Hes1* is required at several stages during eye morphogenesis (Lee et al., 2005; Takatsuka et al., 2004; Tomita et al., 1996). Lee *et al.*, have shown that *Hes1* is expressed in the anterior neural plate at E8.5, while Hes1 protein is also detected in the surface ectoderm and later in the developing optic vesicle, cup, lens and pigmented epithelium (Lee et al., 2005). The same study showed that in *Hes1*$^{-/-}$ embryos the optic vesicles fail to form a cup and the lens is smaller than normal or absent, suggesting that *Hes1* is required for normal development of these structures (Lee et al., 2005). Furthermore, *Hes1* is shown to regulate retinal morphogenesis by maintaining the precursor state of cells (Lee et al., 2005; Takatsuka et al., 2004). In the absence of *Hes1*, the precursors differentiate prematurely and scatter into the subretinal space, between neural retina and pigmented epithelium (Lee et al., 2005; Takatsuka et al., 2004). This may be the cause of the abnormal rosette-like structures seen in the *Hes1*$^{-/-}$ retinas (Takatsuka et al., 2004; Tomita et al., 1996). The prematurely differentiated neurons cannot divide further, which accounts for the smaller than normal overall size of the organ (Takatsuka et al., 2004).

Depending on the genetic background, the *Hes1* null eye phenotype has variable expressivity (Lee et al., 2005; Takatsuka et al., 2004; Tomita et al., 1996). On both MF1 and MF1;C57BL/6J backgrounds there is complete penetrance of absent eyes in *Hes1* null embryos (Kelly Lammerts van Bueren, pers. comm.). Eye defects were scored in *Ap2αCre* conditional mutants, which also presented with complete loss of the organ. No organised structure was apparent, while there were abnormal tissue condensations. No eye defects were scored in any of the *Wnt1Cre* conditional mutants. These results highlight an ectodermal requirement for *Hes1* in the development of the embryonic eye.

The gene may mediate the signalling between the surface ectoderm and the optic vesicle, since *Hes1* nulls present with absent lenses and an arrested optic vesicle (Lee et al., 2005; Tomita et al., 1996). From the previous studies it is apparent that *Hes1* has multiple roles in eye formation and is important at different time points during development (Lee et al., 2005; Takatsuka et al., 2004; Tomita et al., 1996). Expression

in the ectoderm may regulate the development of the optic cup from the optic vesicle as well as the formation of the lens. It is plausible that the phenotypically normal eyes of the *Wnt1Cre* conditional mutants may have had a subtle defect in the retina, caused by loss of *Hes1* in neural crest populations. This was not however examined. Generally, increased production of retinal ganglion cells, which is the *Hes1* null (Lee et al., 2005; Takatsuka et al., 2004) and *Shh* conditional phenotype (Wang et al., 2002), results in micropthalmia, which was not observed in the *Wnt1Cre* conditionals.

4.2.4. Neural tube closure

The neural tube formation in mice commences at E7.5, when the neural folds elevate and approach each other medially (Copp, 2005). These start to fuse at E8.5 and the process is completed by E10 (Copp, 2005). *Hes1* null embryos exhibit failure of closure of the cranial neural tube at E9.5 (Ishibashi et al., 1995). On ICR background, *Hes1* null mice exhibit neurulation defects with 70% penetrance (Ishibashi et al., 1995). Work done in our lab has shown that *Hes1*$^{-/-}$ embryos on MF1 background present with low frequency of neural tube defects (NTDs) while on mixed MF1;C57BL/6J background there are no neurulation defects **(**van Bueren et al., 2010). This suggests that modifiers within the C57BL/6J background may play a protective role against *Hes1*$^{-/-}$ NTDs. The mixed background of the *Ap2αCre* conditional mutants, which includes C57BL/6J, may account for the low frequency of NTDs observed. In the mouse models used, *Cre* recombinase begins to be expressed at E8.5, in the midbrain (*Wnt1Cre*) or the surface ectoderm and the head mesenchyme (*Ap2αCre*), suggesting overlapping patterns of *Hes1* deletion in the neural crest in both systems at this time point. However, no neurulation defects were observed in any of the *Wnt1Cre* conditional mutants, so *Hes1* may have a minor role in neural tube formation through the ectoderm. Studying neural tube development in *Hes1* conditional mutants maintained on an ICR background will probably provide greater insight in the tissue-specific roles of *Hes1* in this process.

4.3. Genetic background considerations

Within the genetic makeup of each strain there are different genetic modifiers that can affect the phenotype expressivity, penetrance and dominance of a gene of interest (Nadeau, 2001). In that respect, a mutation should be considered to induce a phenotype

in a specific genomic context (Montagutelli, 2000). Consequently, great caution should be taken when comparing data between different experiments, as the background modifiers may profoundly influence the resulting phenotype of a mutation.

The *Hes1* mutation is highly background-dependent. A low penetrance great vessel phenotype is seen on an MF1 or MF1;C57BL/6J background (van Bueren et al., 2010), while no great vessel defects are observed on a CD1 background (Rochais et al., 2009b). Conversely, the outflow tract phenotype is weakly penetrant on an MF1 or MF1;C57BL/6J background (van Bueren et al., 2010), while it has greater penetrance on a CD1 background (Rochais et al., 2009b). Thymic abnormalities are observed with incomplete (MF1) or complete (MF1;C57BL/6J) penetrance, depending on the genetic background (van Bueren et al., 2010). The eye phenotype observed in *Hes1* null embryos (Tomita et al., 1996) has variable expressivity on the different genetic backgrounds. On the original 129/Sv (x) ICR background *Hes1*$^{-/-}$ embryos display disorganised lens, rosette-like structures dispersed in the ventricular zone and poor cornea development (Tomita et al., 1996). However, complete absence of the organs is observed in *Hes1* nulls on both MF1 and MF1;C57BL/6J backgrounds (Kelly Lammerts van Bueren, pers. comm.). Moreover, approximately 70% of the *Hes1*$^{-/-}$ embryos kept on the original 129/Sv (x) ICR background exhibit severe NTDs (Ishibashi et al., 1995), while some embryos of the same genotype present with NTDs when kept on an MF1 background and none when kept on an MF1;C57BL/6J background (van Bueren, 2008).

As it has become apparent from the literature and the results of this thesis, the different features of the *Hes1* null phenotype have variable penetrance and expressivity on the different genetic backgrounds. Consideration is therefore required when discussing the results of different studies, while all comparisons should be made with reference to the respective genetic background. For this study, a mixed MF1;C57BL/6J background was used, so all comparisons between the *Hes1* conditional mutants and the *Hes1* knock-out phenotype are discussed based on this background, unless otherwise specified.

4.4. *Hes1* in the neural crest lineage

The neuropilin receptors Npr1 and Npr2, together with their class 3 semaphorin ligands, direct cranial neural crest migration (Schwarz et al., 2008). Embryos carrying homozygous null mutations of *Nrp1* or *Nrp2* (*Nrp1*$^{-/-}$ or *Nrp2*$^{-/-}$) or *Nrp2* null embryos

with reduced semaphorin signalling through neuropilins (*Nrp1*$^{sema3+/-}$;*Nrp2*$^{-/-}$) present with ectopically patterned neural crest cells that subsequently give rise to ectopic neurons (Schwarz et al., 2008). Although cardiac neural crest cell patterning defects were identified in *Hes1* null, *Wnt1Cre* and *Ap2αCre* conditional mutants, no ectopic neural crest-derived structures were detected in consequent developmental stages. However, the main defect identified here was compromised cellular contribution from the neural crest to the pharyngeal arches, rather than additional ectopic migratory streams. Moreover, fourth arch neural crest cells appeared normally localised by *Hoxd4* expression in *Hes1*$^{-/-}$ embryos compared to controls, suggesting normal population of cardiac crest cells within these arches. Potentially, the cardiac crest that reaches the pharyngeal arches is sufficient for subsequent arch artery and outflow tract development. The low penetrance of great vessel and outflow tract defects observed in *Hes1* null (Rochais et al., 2009b; van Bueren et al., 2010) and *Wnt1Cre* and *Ap2αCre* conditional mutants (this thesis, in van Bueren et al., 2010) may reflect stochastic events that additionally compromise neural crest contribution into the cardiovasculature, resulting in these defects.

4.5. *Hes1* and Notch pathway genes during pharyngeal development

In beginning to identify a mechanism by which *Hes1* is involved in cardiovascular and thymus morphogenesis, genes known to directly interact with *Hes1*, like *Jag1* (Kobayashi et al., 2009), also known to be expressed in pharyngeal structures during embryogenesis (Barsi et al., 2005) and the *Hes1* upstream regulator *RBP-J* (Iso et al., 2003) were examined in *Hes1* null embryos. Differential regulation of both *Jag1* and *RBP-J* was identified in the *Hes1* null pharyngeal apparatus compared to controls at E9.5. Hes1 probably normally represses *Jag1* and promotes *RPB-J* in the pharyngeal region of E9.5 mouse embryos. These results suggest that *Hes1* may be acting through an auto-regulatory loop through the Notch pathway in exerting its roles in pharyngeal development. Nonetheless, conditional deletion of *Jag1* in the anterior heart field, using the same *Mef2c-AHF-Cre* model implemented here, induced outflow tract and great vessel defects with high penetrance (High et al., 2009), conversely to the *Mef2c-AHF-Cre Hes1* conditional mutation.

4.6. *Hes1* and the FGF pathway

Fgf8 has been associated with pharyngeal arch artery morphogenesis (Frank et al., 2002) and has been shown to genetically interact with *Tbx1* in great vessel development (Aggarwal et al., 2006; Vitelli et al., 2002b). Recent evidence suggests that Notch functions via *Jag1* in the SHF to regulate *Fgf8*, which in turn modulates downstream pathways affecting neural crest invasion and endocardial cushion development (High et al., 2009). However, no alteration in *Fgf8* or elements of the FGF pathway were identified in *Hes1* null compared to wild type control embryos, by both whole mount *in situ* hybridisation and quantitative real time PCR between E8.5-E9.5. Therefore, *Hes1* probably does not interact with the FGF pathway towards arch artery and outflow tract morphogenesis.

4.7. Conclusion and future directions

In this chapter I have addressed the tissue-specific requirements for *Hes1* during embryogenesis and tried to study potential mechanisms of action. Non cell autonomous actions for *Hes1* were revealed in the ectoderm, towards great vessel and eye development, while *Hes1* is essential in both the ectodermal and neural crest lineages for thymus morphogenesis.

To further understand the *Hes1* requirements in mouse embryogenesis, the endodermal contribution of the gene has to be examined. This has not been possible through this thesis, so future work may implement a different endoderm-specific *Cre* line, like the Claudin-6*Cre* (Anderson et al., 2008) towards that end. Alternatively, both the standard knock-out and the conditional lines can be studied on the same background, to eliminate background specific modifiers.

Potential *Hes1* roles in the neural crest can be addressed further. During this project I have shown that *Hes1* deficiency can cause aberrant neural crest patterning, although the final neural crest contribution to the fourth arches appears unaffected. Kobayashi *et al.*, have demonstrated that lack of *Hes1* affects multiple neural crest related genes in ES cells (Kobayashi et al., 2009). Neural crest explant assays can be implemented to examine the *Hes1* role in differentiation and/or migration potential of this lineage. Last, *Hes1* was originally identified as a putative Tbx1 target through a microarray screen and validated by quantitative real time PCR (van Bueren et al., 2010).

I demonstrated that Hes1 and Tbx1 proteins overlap in pharyngeal structures at E8.5, while a day later, at E9.5 both genes also shared common expression domains. Additionally, *Hes1* was found downregulated in pharyngeal tissues in *Tbx1* null embryos at E9.5. Although, to date, no evidence exists supporting a genetic interaction between *Tbx1* and *Hes1* (van Bueren, 2008), examination of a potential interaction during endocardial cushion and outflow tract development stages may be more informative.

V. SLIT2

1. Introduction – Literature review

1.1. The Slit/Robo pathway

1.1.1. Biological functions

Slit was originally described in *Drosophila* as a secreted protein expressed in the midline of the developing CNS (Andrews et al., 2007; Hohenester, 2008). By binding to its receptor, *Roundabout* (*Robo*), it acts as a repellent and regulates guidance, migration as well as outgrowth and branching of axons (Andrews et al., 2008). Slit/Robo interactions have been described in cortical, olfactory tract, optic chiasm and optic tract development as well as midline axonal crossing and motor axon path finding in the hindbrain (Andrews et al., 2007). In chicken embryos Slit/Robo signalling is important for the confinement of trunk neural crest cells to the ventral migratory pathway (Jia et al., 2005) and for the prevention of trunk crest cells from invading the gut (De Bellard et al., 2003). The Slit/Robo pathway is also involved in the development of other systems, including lung, kidney and mammary gland (Hohenester, 2008). Interestingly, Slit/Robo mediated signalling is required for the assembly of the heart tube in *Drosophila*, by regulation of the migration and adhesive interactions of cardiac precursor cells (MacMullin and Jacobs, 2006; Santiago-Martinez et al., 2006). Moreover, through repulsive interactions, Slit/Robo is also required for lumen formation of the *Drosophila* heart (Medioni et al., 2008; Santiago-Martinez et al., 2008).

1.1.2. Protein interactions

There are at least three *Slit* homologs (*Slit1-3*) and four *Robo* homologs (*Robo1-4*) in mammals (Dickinson and Duncan, 2010). Slit proteins appear to lack hydrophobic sequences, which indicates transmembrane domains, and are predicted to be secreted proteins associated with the ECM (Dickinson and Duncan, 2010). The evolutionary conserved domains of the Slit proteins include four tandem leucine-rich repeats (D1-D4) at the N-terminus, six EGF-like domains, a laminin G-like domain, three more EGF-like domains and a C-terminal cystine knot domain (Dickinson and Duncan, 2010; Hohenester, 2008). Among the Robo proteins, Robo1-3 share a common extracellular domain that is reminiscent of cell adhesion molecules (CAMs) (Dickinson and Duncan,

2010) and consists of five immunoglobulin (IG)-like domains and three fibronectin type 3 (FN3) repeats (Andrews et al., 2007; Hohenester, 2008). Robo4, which unlike Robo1-3 is expressed exclusively in endothelial cells and not the CNS, has two IG-like and two FN3 domains (Andrews et al., 2007; Hohenester, 2008). Robo proteins also have a transmembrane region and a cytoplasmic domain suggested to interact with downstream signalling molecules (Andrews et al., 2007). Slit binding has been confirmed biochemically for all Robos, except for Robo4 (Hohenester, 2008), and it has been suggested that Robo4 may not be a true Robo receptor (Dickinson and Duncan, 2010).

Slit binding onto the Robo receptors leads to modifications in the cytoplasmic domain of the receptors and reorganisation of the actin cytoskeleton (Dickinson and Duncan, 2010). The Robo cytosolic domains do not have catalytic activity (Hohenester, 2008). It is believed that several catalytically inactive adaptors are bound to the Robo cytosolic domain and respond to Slit binding, subsequently promoting downstream signalling (Hohenester, 2008).

1.1.2.1. *Slit2*

Slit2 is expressed in the pharyngeal clefts from E8.5 while it is detected prominently in CNS structures throughout development (Yuan et al., 1999). It is involved in retinal axon growth and guidance (Plump et al., 2002) as well as ureteric bud formation (Grieshammer et al., 2004). In the developing kidney Slit2 associates with the receptor Robo2 to promote intracellular signalling (Grieshammer et al., 2004).

1.2. Slit/Robo gene mutations

Slit1 or *Slit2* targeted mutations lead to nervous system defects ((Plump et al., 2002). *Slit2* null embryos additionally exhibit defects in the renal/urinary system and display prenatal or perinatal lethality (Grieshammer et al., 2004). *Slit3* mutants exhibit right ventricular hypertrophy, diaphragm and kidney defects (Liu et al., 2003; Yuan et al., 2003). Targeting genes of the *Robo* family affects the nervous system and causes prenatal or perinatal lethality in all cases (Andrews et al., 2008; Andrews et al., 2006; Long et al., 2004; Sabatier et al., 2004), while systems like the respiratory, renal/urinary and vasculature are also affected in *Robo1* (Xian et al., 2001), *Robo2* (Grieshammer et al., 2004; Lu et al., 2007) and *Robo4* (Jones et al., 2008) mutants respectively.

2. Project overview

The initial indication that *Slit2* may be a Tbx1 regulated gene resulted from our microarray screen and subsequent quantitative real time PCR validation (van Bueren et al., 2010). Further study in our lab demonstrated that during early embryogenesis *Slit2* is expressed in an overlapping fashion with *Tbx1* in the surface ectoderm, while the receptor *Robo1* is expressed in the migrating neural crest (Calmont et al., 2009). *Slit2* was also found downregulated in pharyngeal tissues of *Tbx1* null embryos (Calmont et al., 2009). Previous studies have shown that the Slit/Robo pathway is involved in trunk neural crest migration in the chicken (De Bellard et al., 2003; Jia et al., 2005). Collectively, these data highlight a potential involvement of the Slit/Robo pathway in cardiac neural crest migration, potentially regulated by *Tbx1*, which motivated us to further study *Slit2*. As part of this thesis, the expression profiles of both *Slit1* and *Slit2* were examined at E9.5. Moreover, the *Slit2* null and double *Slit1*;*Slit2* null phenotypes were assessed in terms of cardiovascular and other 22q11DS-like defects. Finally, the potential *Tbx1*-*Slit2* genetic interaction was studied to establish whether the two genes act through a common pathway.

3. Results

3.1. *Slit1* and *Slit2* in the mouse embryo

3.1.1. Expression domains

At E9.5 both *Slit1* and *Slit2* are expressed in the pharyngeal apparatus, as identified by whole mount *in situ* hybridisation. *Slit1* is detected in the pharyngeal mesenchyme, potentially the core mesoderm (Figure 5.1.B, B'), while *Slit2* is found in the pharyngeal ectoderm and endoderm (Figure 5.1.C, C'). Hence, both genes share expression domains with *Tbx1*.

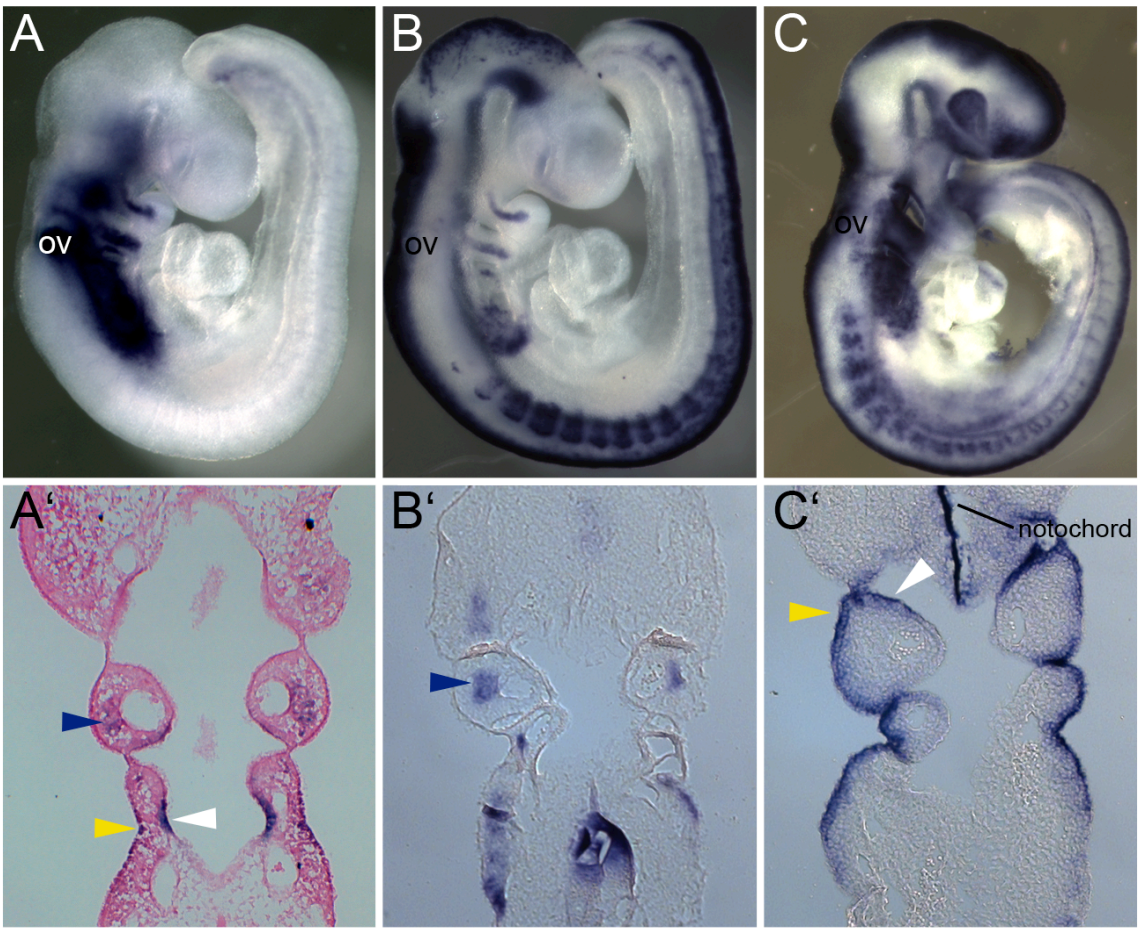

Figure 5. 1. *Tbx1*, *Slit1* and *Slit2* mRNA expression detected by *in situ* hybridisation at E9.5. (A, A') *Tbx1* mRNA expression in whole mount (A) and coronal section through the pharyngeal arches (Ivins et al., 2005) (A'). (B, B') *Slit1* mRNA expression in whole mount (B) and coronal section through the pharyngeal arches (B'). (C, C') *Slit2* mRNA expression in whole mount (C) and coronal section

through the pharyngeal arches (C'). Yellow arrowhead, pharyngeal ectoderm; blue arrowhead, core mesoderm; white arrowhead, pharyngeal endoderm; ov, otic vesicle.

3.1.2. *Slit2* mutant phenotype[1]

By E15.5 in the mouse embryo the great vessels (Hiruma et al., 2002) and the ventricular septum (Webb et al., 1998) have formed completely, while the thymic lobes have descended above the heart and lie as a pair (Grevellec and Tucker, 2010). *Slit2* mutant embryos were examined between E15.5-E18.5 but none exhibited any great vessel or thymic defects, whereas one out of the seventeen (6%) *Slit2*$^{-/-}$ embryos assessed had a VSD (Table 5.1). This however is not statistically significant. No outflow tract defects were observed in any of the genotypes.

Genotype	n	Thymic hypo/aplasia	Great vessel defects	Intracardiac septation
WT	17	0	0	N/S
Slit2$^{+/-}$	21	0	0	N/S
Slit2$^{-/-}$	17	0	0	1 (6%)
Total	**55**			

Table 5. 1. Thymic, great vessel and intracardiac defects observed in the *Slit2* embryos at E15.5-E18.5. N/S, not studied; WT, wild type.

3.1.3. *Slit1*;*Slit2* mutant phenotype[1]

Slit1 and *Slit2* act synergistically in the developing CNS regulating retinal axon guidance (Plump et al., 2002). In an effort to overcome any functional redundancy that might occur between the two genes in cardiovascular and thymic development, transheterozygous *Slit1*$^{+/-}$;*Slit2*$^{+/-}$ animals were intercrossed and embryos were analysed between E14.5-E18.5 for thymic and great vessel defects. The E14.5 embryos were examined for great vessel and outflow tract defects only, since the mature left-sided configuration is fully remodelled by E13.5 (Hiruma et al., 2002). No defects were scored in any of the genotypes (Table 5.2). Consistently, no thymic, great vessel or outflow tract abnormalities were observed in any of the genotypes at E18.5 (Table 5.3).

[1] All the *Slit2* and *Slit1*;*Slit2* embryos analysed in this study were kindly provided by our collaborator, William Andrews, Department of Anatomy and Developmental Biology, University College London, London, UK. Therefore, there was limitation in the available embryonic stages, while the embryonic heads had been used for his own studies.

Genotype	n	Great vessel defects
WT	1	0
Slit1$^{+/-}$	6	0
Slit2$^{+/-}$	0	0
Slit1$^{-/-}$	1	0
Slit2$^{-/-}$	0	0
Slit1$^{+/-}$;*Slit2*$^{+/-}$	0	0
Slit1$^{-/-}$;*Slit2*$^{+/-}$	6	0
Slit1$^{+/-}$;*Slit2*$^{-/-}$	1	0
Slit1$^{-/-}$;*Slit2*$^{-/-}$	1	0
Total	**16**	

Table 5. 2. Great vessel defects observed in the *Slit1*;*Slit2* double mutant embryos at E14.5. WT, wild type.

Genotype	n	Thymic hypo/aplasia	Great vessel defects
WT	0	0	0
Slit1$^{+/-}$	4	0	0
Slit2$^{+/-}$	1	0	0
Slit1$^{-/-}$	2	0	0
Slit2$^{-/-}$	0	0	0
Slit1$^{+/-}$;*Slit2*$^{+/-}$	6	0	0
Slit1$^{-/-}$;*Slit2*$^{+/-}$	12	0	0
Slit1$^{+/-}$;*Slit2*$^{-/-}$	1	0	0
Slit1$^{-/-}$;*Slit2*$^{-/-}$	4	0	0
Total	**30**		

Table 5. 3. Thymic and great vessel defects observed in the *Slit1*;*Slit2* double mutant embryos at E18.5. WT, wild type.

3.2. *Tbx1-Slit2* genetic interaction

Slit2 was originally identified as a potential Tbx1 downstream effector (van Bueren et al., 2010). Moreover, the *Slit2* expression pattern has overlapping domains with *Tbx1* in the pharyngeal apparatus at E9.5 (Calmont et al., 2009; this thesis), and *Slit2* is detected downregulated in these tissues in *Tbx1* null embryos (Calmont et al., 2009). The potential genetic interaction between *Tbx1* and *Slit2* was therefore examined as part of this thesis. Two different *Tbx1* null alleles (Lindsay et al., 2001; Xu et al., 2004) were used for this purpose, due to lack of available animals.

3.2.1. *Tbx1* and *Slit2* double heterozygosity

Double heterozygous animals were generated for *Tbx1* and *Slit2* and were examined for 22q11DS-like features. The embryos were assessed at E15.5, a stage by which the great vessels (Hiruma et al., 2002), ventricular septum (Webb et al., 1998) and secondary palate (Gritli-Linde, 2007; Meng et al., 2009) have formed completely and the thymic lobes have assumed their final position as a pair above the heart (Grevellec and Tucker, 2010). One out of five (20%) $Slit2^{+/-}$;$Tbx1^{+/lacZ}$ embryos exhibited cervical origin of the RSCA (Figure 5.2.B) as compared to one out of seven (14%) $Tbx1^{+/lacZ}$ embryos that displayed the same phenotype. Four out of five (80%) $Slit2^{+/-}$;$Tbx1^{+/lacZ}$ embryos had a cleft palate (Figure 5.2.C), against three out of three (100%) of the $Slit2^{+/-}$ embryos and four out of seven (57%) of the $Tbx1^{+/lacZ}$ embryos. Moreover, two out of five (40%) *Tbx1*;*Slit2* double heterozygotes had a VSD (Figure 5.2.D), which was in one case accompanied by an overriding aorta (Figure 5.2.E). Two out of seven (29%) $Tbx1^{+/lacZ}$ embryos also displayed a VSD. None of these phenotypes were scored in any of the three wild type controls. Although a trend of increased frequency in all the $Slit2^{+/-}$;$Tbx1^{+/lacZ}$ phenotypes is apparent, in the current sample size none of these values reaches statistical significance (Table 5.4). No outflow tract defects were observed in any of the genotypes.

Genotype	n	Thymic hypo/aplasia	Great vessel defects	Palatal defects	Intracardiac septation
WT	3	0	0	0	0
$Tbx1^{+/lacZ}$	7	1 (14%)	1 (14%)	4 (57%)	2 (29%)
$Slit2^{+/-}$	3	0	0	3 (100%)	0
$Slit2^{+/-}$;$Tbx1^{+/lacZ}$	5	0	1 (20%)	4 (80%)	2 (40%)
Total	**18**				

Table 5. 4. Thymic cardiovascular and palate defects observed in the *Tbx1*;*Slit2* double heterozygous embryos at E15.5. WT, wild type.

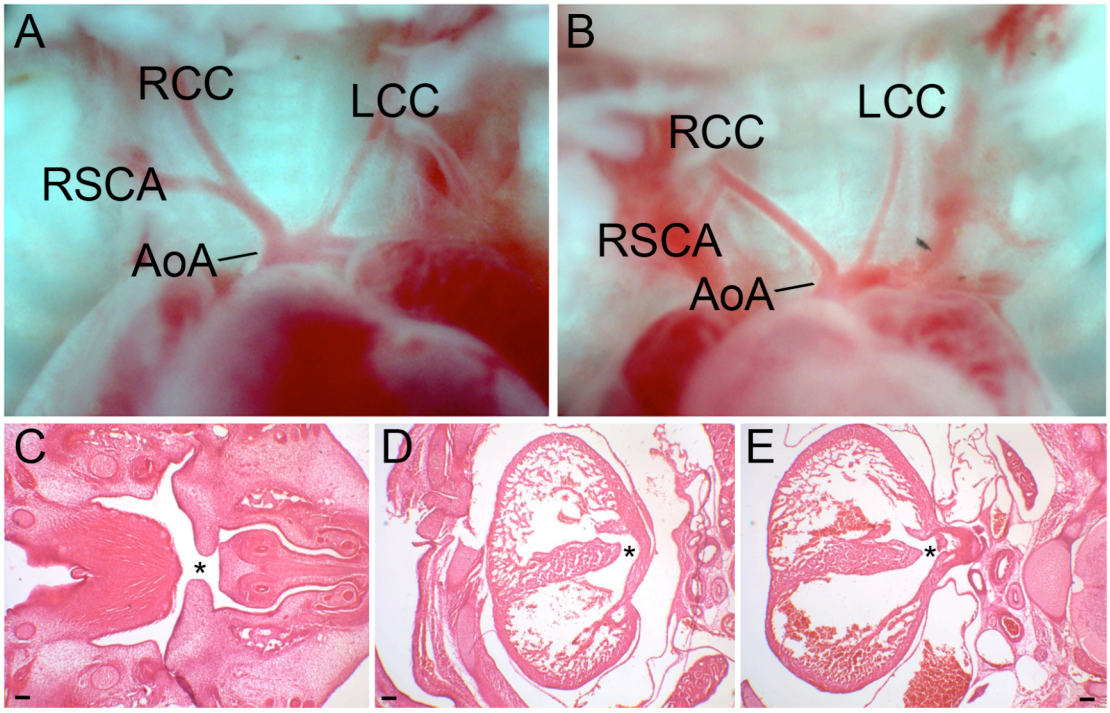

Figure 5. 2. Great vessel, palate and intracardiac defects observed in the *Tbx1*;*Slit2* double heterozygous embryos at E15.5. (A-B) Great vessel defects. Wild type configuration (A) and a *Slit2*$^{+/-}$;*Tbx1*$^{+/lacZ}$ embryo displaying cervical RSCA (B). Cleft palate (C), VSD (D) and VSD with OA (E) observed in *Slit2*$^{+/-}$;*Tbx1*$^{+/lacZ}$ embryos. Asterisks denote missing segments. AoA, aortic arch; RCC/LCC, right/left common carotid artery; RSCA/LSCA, right/left subclavian artery.

3.2.2. *Tbx1* heterozygosity on a *Slit2* null background

To examine whether complete lack of *Slit2* might influence the *Tbx1* haploinsufficient phenotype, double heterozygous animals for *Tbx1* and *Slit2* were intercrossed with *Slit2* heterozygotes, and the progeny was assessed at E15.5 for 22q11DS-like phenotypes. One out of six (17%) *Slit2*$^{-/-}$;*Tbx1*$^{+/mcm}$ embryos displayed thymic hypoplasia (Figure 5.3.D), while two out of seven (29%) *Slit2*$^{+/-}$;*Tbx1*$^{+/mcm}$ embryos (Figure 5.3.C) and two out of six (33%) *Tbx1*$^{+/mcm}$ embryos (Figure 5.3.B) exhibited the same phenotype. In terms of great vessel defects, four out of six (67%) *Slit2*$^{-/-}$;*Tbx1*$^{+/mcm}$ embryos (Figure 5.3.D'), three out of seven (43%) *Slit2*$^{+/-}$;*Tbx1*$^{+/mcm}$ embryos (Figure 5.3.C'), three out of six (50%) *Tbx1*$^{+/mcm}$ embryos (Figure 5.3.B') and one out of eight (13%) *Slit2*$^{+/-}$ embryos displayed a phenotype. The great vessel phenotype ranged from cervical or retro-oesophageal RSCA to IAA-B in all affected

groups, denoting fourth arch artery-derived defects. None of these values reached statistical significance in the current sample size (Table 5.5). No outflow tract defects were observed in any of the genotypes.

Genotype	n	Thymic hypoplasia	Great vessel defects
WT	2	0	0
Tbx1$^{+/mcm}$	6	2 (33%)	3 (50%)
Slit2$^{+/-}$	8	0	1 (13%)
Slit2$^{-/-}$	3	0	0
Slit2$^{+/-}$;*Tbx1*$^{+/mcm}$	7	2 (29%)	3 (43%)
Slit2$^{-/-}$;*Tbx1*$^{+/mcm}$	6	1 (17%)	4 (67%)
Total	**32**		

Table 5. 5. Thymic and great vessel defects observed in the *Tbx1*;*Slit2* double mutant embryos at E15.5. WT, wild type.

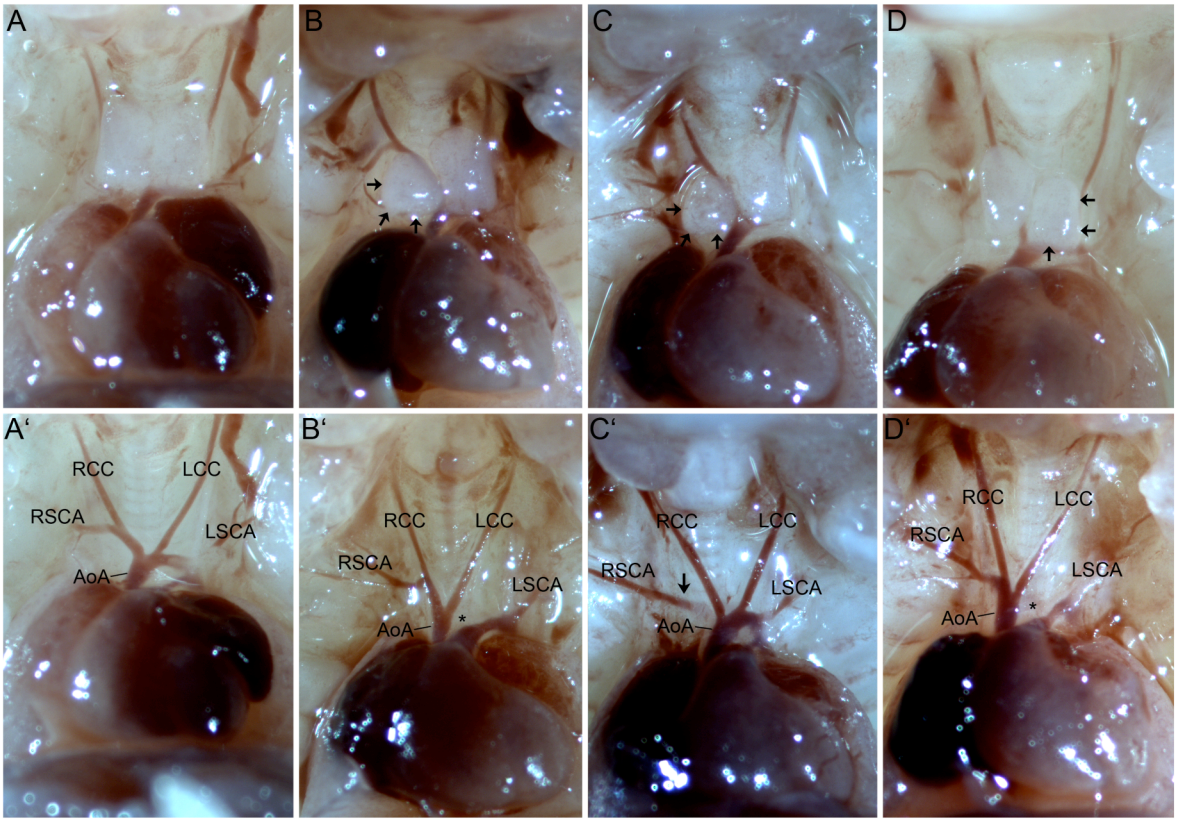

Figure 5. 3. Thymic and great vessel defects observed in the *Tbx1*;*Slit2* double mutant embryos at E15.5. (A-D) Thymic defects. Wild type thymus (A) and hypoplastic phenotypes in *Tbx1*$^{+/mcm}$ (B), *Slit2*$^{+/-}$;*Tbx1*$^{+/mcm}$ (C) and *Slit2*$^{-/-}$;*Tbx1*$^{+/mcm}$ (D) embryos. (A'-D') Great vessel defects. Wild type configuration (A') and IAA-B (B'), retro-oesophageal RSCA (C') and IAA-B (D') in *Tbx1*$^{+/mcm}$ (B), *Slit2*$^{+/-}$;*Tbx1*$^{+/mcm}$ (C)

and *Slit2*$^{-/-}$;*Tbx1*$^{+/mcm}$ (D) embryos. Asterisks denote missing segments. Black arrow, abnormal structure; AoA, aortic arch; RCC/LCC, right/left common carotid artery; RSCA/LSCA, right/left subclavian artery.

4. Discussion - Future directions

4.1. *Slit1* and *Slit2* share expression domains with *Tbx1*

Slit2 was originally identified as a putative Tbx1 downstream effector in our microarray screen comparing *Tbx1*-expressing heterozygous and null cells at E9.5 (van Bueren et al., 2010). Further work conducted in our lab demonstrated that *Slit2* is expressed in an overlapping fashion with *Tbx1* in the surface ectoderm at E8.75, while the receptor *Robo1* is expressed in the migrating neural crest at E9.0 (Calmont et al., 2009). Both genes appeared downregulated or misspatterned in *Tbx1* null embryos (Calmont et al., 2009). Previous studies have shown that the Slit/Robo pathway is involved in trunk neural crest migration in chicken embryos (De Bellard et al., 2003; Jia et al., 2005). These data combined support a role for Slit/Robo signalling in cardiac crest migration, potentially regulated by *Tbx1*.

The Slit genes are expressed in similar patterns in the mouse pharyngeal apparatus (Yuan et al., 1999), and may therefore display functional redundancy. Moreover, synergistic actions between *Slit1* and *Slit2* have been proven in the developing CNS in retinal axon guidance (Plump et al., 2002). The expression pattern of both *Slit1* and *Slit2* was studied in this thesis. *Slit3* is shown to share expression domains with *Slit2* during early embryogenesis (Yuan et al., 1999) but it was not studied due to probe unavailability. Through this thesis, and verifying the previous studies, both *Slit1* and *Slit2* were found expressed in pharyngeal tissues at E9.5, in an overlapping fashion with *Tbx1* but not between them. Although this is further evidence that *Slit2* might be regulated by Tbx1, compensatory roles between Slit1-Slit2 are rather unlikely, while a Slit2-Slit3 compensation appears more possible.

4.2. *Slit2* or *Slit1*;*Slit2* deficiency does not induce cardiovascular defects

The expression pattern of *Slit1* and *Slit2*, as described in this thesis, leads to some predictions as to what might have been expected, if these genes had a role in cardiovascular development. *Slit1*, similarly to *Tbx1* (Zhang et al., 2006), via mesodermal expression could have been required in the developing outflow tract. By contrast, *Slit2* would be expected to regulate the pharyngeal arch arteries through

ectodermal signalling, like *Tbx1* (Calmont et al., 2009). Moreover, targeted mutation for *Slit2* induces prenatal or perinatal lethality (Plump et al., 2002), which has not been justified to date, leaving cardiovascular deficiency as a possible explanation. However, none of the *Slit2* null embryos examined displayed any cardiovascular defects, apart from one embryo that had VSD. Since there is potential redundancy among the *Slit* family genes, double homozygous mutants for *Slit1* and *Slit2* were assessed for cardiovascular defects. Lack of both copies of *Slit1* and *Slit2* did not induce a heart phenotype either. This is also in accordance with the fact that *Slit1* null animals are viable and fertile (Plump et al., 2002). Taken together, these results do not suggest any redundant actions between *Slit1* and *Slit2* or any involvement of either of the genes in heart development, at least in the current sample size.

4.3. *Slit2* or *Slit1*;*Slit2* deficiency does not induce thymic defects

Following the original hypothesis, that *Slit2* might be a Tbx1 downstream effector and hence may be mediating some of its actions, the thymic phenotype was also examined in *Slit2* null and *Slit1*;*Slit2* null embryos. However, neither the *Slit2* null mutation nor the combined *Slit1*;*Slit2* null mutation induced any thymic defects. Therefore, these genes are more likely not involved in thymic development.

4.4. *Tbx1* and *Slit2* probably do not genetically interact

To further investigate a potential relationship between *Tbx1* and *Slit2*, the genetic interaction between the two genes was examined by studying the phenotype of $Slit2^{+/-}$;$Tbx1^{+/-}$ or $Slit2^{-/-}$;$Tbx1^{+/-}$ embryos at E15.5. Due to lack of available animals, two different *Tbx1* null alleles (Lindsay et al., 2001; Xu et al., 2004) were used. Combined heterozygosity for *Slit2* and *Tbx1* when using the $Tbx1^{lacZ}$ allele (Lindsay et al., 2001), showed a trend towards greater frequency in the defects scored. However, the sample size is too small to deduce safe conclusions. In contrast, combined heterozygosity for *Slit2* and *Tbx1* with the use of the $Tbx1^{mcm}$ allele (Xu et al., 2004) produced defect frequencies similar to that induced by single heterozygosity for *Tbx1*. Moreover, the $Slit2^{-/-}$;$Tbx1^{+/-}$ embryos did not differ significantly in terms of great vessel or thymic defects with the *Tbx1* heterozygotes. These results suggest that, in the current sample size, *Tbx1* does not interact with *Slit2* towards cardiovascular or thymic development.

It should be noted that the initial cross, between *Tbx1*$^{+/lacZ}$ and *Slit2*$^{+/-}$ animals did not produce the expected frequency of great vessel defects for *Tbx1* heterozygosity in the *Tbx1*$^{+/lacZ}$ progeny (Calmont et al., 2009; Lindsay et al., 2001; Vitelli et al., 2002b Vitelli et al., 2006; Zhang and Baldini, 2008). The *Tbx1*$^{+/mcm}$ embryos examined from the second cross, however, which was between *Slit2*$^{+/-}$;*Tbx1*$^{+/mcm}$ and *Slit2*$^{+/-}$ animals, displayed the expected frequency of great vessel defects for *Tbx1* haploinsufficiency. This difference is probably due to the small sample size of the first cross. Nonetheless, allele-specific or background-specific modifiers potentially influencing the phenotype between the two different experiments cannot be excluded. Therefore, the results between the experiments cannot be combined, but should rather be discussed independently.

One other aspect that should be discussed here is the cleft palate phenotype identified in the *Slit2*$^{+/-}$ and *Slit2*$^{+/-}$;*Tbx1*$^{+/lacZ}$ embryos. *Tbx1* is required for palatal shelf elongation and elevation (Goudy et al., 2010). Palatal clefting has been reported in *Tbx1* null mutants but not heterozygous embryos (Hu et al., 2004; Jerome and Papaioannou, 2001). Although a proportion of the *Tbx1* heterozygotes examined here displayed cleft palate, both *Slit2*$^{+/-}$ and *Slit2*$^{+/-}$;*Tbx1*$^{+/lacZ}$ groups displayed higher frequency of palatal defects, as compared to the wild type controls or the *Tbx1* heterozygotes. The facial primordia consist of a mesenchymal core that is predominantly of cranial neural crest origin, and of an outer epithelial covering deriving from the embryonic ectoderm (Gritli-Linde, 2007). Overall these results may be an indication of a *Tbx1*-*Slit2* pathway involved in cranial neural crest patterning towards the morphogenesis of craniofacial structures.

4.5. Conclusion and future directions

Through this last chapter, I examined the phenotype caused by *Slit2* or *Slit1*;*Slit2* deficiency, but found no evidence of a role for either of this genes in the development of structures affected in 22q11DS. Moreover, I addressed the possible genetic interaction between *Tbx1* and *Slit2* and also found no evidence of such a relationship. The sample size is small, so an interaction between the two genes cannot be excluded either. Increasing the sample size and using the same *Tbx1* allele consistently may elucidate this. Additionally, it might be worth examining the *Slit2*;*Slit3* mutation for a cardiovascular phenotype and further to that, in combination with *Tbx1*. *Slit3* mutants

display right ventricular hypertrophy (Liu et al., 2003), which is not a *Tbx1* related phenotype. However, *Slit2* and *Slit3* have similar expression patterns during embryogenesis (Yuan et al., 1999) and compensatory actions between them may be masking a *Tbx1* regulatory role on *Slit2*. Multiple gene mutations, for example triple mutants for the *Robo1-3* receptors or the *Slit1-3* ligands are probably the way forward due to the redundancy in the system. Alternatively dominant negative constructs for elements of the pathway can be used on avian models, according to Shiau *et al.* (Shiau and Bronner-Fraser, 2009). In light of the palatal shelf defects identified in $Slit2^{+/-}$ and $Slit2^{+/-}$;$Tbx1^{+/lacZ}$ embryos, further study can involve examining cranial neural crest patterning in *Slit2* and/or *Tbx1*;*Slit2* deficient embryos. Moreover, phenotyping of $Slit2^{-/-}$ animals can address whether palatal clefting contributes to the perinatal lethality observed, since it is a severe defect, incompatible with life in rodents (Gu et al., 2008).

VI. CONCLUSIONS AND SUMMARY

1. Conclusions

1.1. General overview: "From disease to gene and back"

Three decades have passed since subcloning of mammalian genes into prokaryotic plasmids first became possible (Flotte, 2007). This opened the way for gene engineering, while further technical progress, the sequencing of the human genome and the characterisation of animal models contributed to the identification of a multitude of genes in human disease. Currently, over 12,000 genes are linked to at least one mendelian human disease (OMIM website, http://www.ncbi.nlm.nih.gov/omim). The research questions, however, have not changed over the years, and still centre around understanding and modifying the pathogenesis of human disease.

The discovery of the cystic fibrosis gene (Kerem et al., 1989; Riordan et al., 1989) was considered the first successful linkage mapping (Botstein and Risch, 2003). Nevertheless, and despite all the scientific and technical progress since, cystic fibrosis remains one of the most common life-threatening inherited diseases (World Health Organization website, http://www.who.int/en/). This is just one example of how the illusion of single gene disorder simplicity has come and gone. Monogenic diseases are now considered extremely complex syndromes, often involving many different genes together with equally numerous poorly understood effects of the environment (Weatherall, 2000). Variable expressivity, environmental influences, genetic interactions, pleiotropy and genotypic and phenotypic heterogeneity are phenomena that lead to lack of one to one correspondence between genotype and phenotype (Merikangas et al., 2006), which render polygenic disorders even more complex. The environmental contribution is increasingly gaining substantial research interest, as it has been cleverly summarised by the phrase "nature versus nurture" (McClearn, 2004).

It has therefore become apparent that linking one gene to a disease is no longer sufficient. The challenge of our time is now the effort to link the events occurring at a molecular level with the clinical findings of human disorders (Weatherall, 2000). Establishing genetic networks, rather than genes, in the context of but not limited to a human disease can aid the understanding of disease mechanisms, complications and possibly prognosis. From a clinical point of view, identifying such networks can also improve genetic screening, predictive genetic tests as well as genetic counseling.

1.2. Dealing with Tbx1 targets and complex interactions

Cardiovascular disease is the most common cause of mortality worldwide (World Health Organization website, http://www.who.int/en/), while 22q11DS, the most frequent microdeletion syndrome in humans (Emanuel, 2008; Wurdak et al., 2006; Yagi et al., 2003), affects the cardiovasculature in 70% of the cases (Shprintzen, 2008; Wurdak et al., 2006). To date, 22q11DS has a sole major determinant gene, the T-box transcription factor *TBX1* (Paylor et al., 2006; Stoller and Epstein, 2005a; Torres-Juan et al., 2007; Yagi et al., 2003; Zweier et al., 2007).

Since its discovery, *TBX1* has been shown to be an important regulator in the development of several embryonic structures (Arnold et al., 2006; Lindsay et al., 2001; Merscher et al., 2001; Xu et al., 2004; Zhang et al., 2005). During mouse development *Tbx1* is required in a tissue-specific, time and dosage-dependent fashion (Arnold et al., 2006; Vitelli et al., 2009; Xu et al., 2004; Xu et al., 2005; Zhang and Baldini, 2008; Zhang et al., 2005; Zhang et al., 2006). Nevertheless, and although it has been the focus of research for over a decade, the genetic pathways *Tbx1* is involved in as well as its downstream effectors are poorly characterised. Several studies have discussed potential *Tbx1* interactors, including *Fgf8* (Vitelli and Baldini, 2003; Vitelli et al., 2010; Vitelli et al., 2006), *Raldh2* (Ivins et al., 2005; Ryckebusch et al., 2010), *Chordin* (Choi and Klingensmith, 2009), *Prdm1* (Vincent et al., 2010), Wnt-β-catenin signalling (Huh and Ornitz, 2010), *Vegf* (Chen et al., 2010; Stalmans et al., 2003) and *Sprouty 1a* and *2* (Albert Basson, pers. comm.). Each of these appears to interact with *Tbx1* in discrete pathways towards the development of different embryonic structures. Direct interaction between Tbx1 and target promoter sequences has also been proved difficult to identify. Although multiple interactors have been proposed, to date, the only confirmed interactions are between TBX1 and *VEGFR3* (Chen et al., 2010) or *Pitxc2* (Nowotschin et al., 2006). The number of studies as well as the number of different genes suggested to act downstream of *Tbx1* indicate the complexity of the *Tbx1* related networks and the multitude of its downstream effectors. In that respect, *Tbx1* may act as a global modifier gene in mammalian organisms. Systematic mapping of genetic interactions in *Saccharomyces cerevisiae* (Tong et al., 2001; Segre et al., 2005), *Caenorhabditis elegans* (Lehner et al., 2006) and *Arabidopsis thaliana* (Perez-Perez et al., 2009) has identified genes that have wide patterns of interaction across multiple pathways, the so

called "hub" genes (Hartman et al., 2001; Lehner et al., 2006). These can buffer the effects of genetic variation in many functionally diverse loci (Lehner et al., 2006), so that their inactivation can enhance the phenotypic outcome of mutations in functionally unrelated genes and in otherwise unlinked pathways (Lehner et al., 2006). *Tbx1* may, likewise, function as a mammalian hub gene, required to buffer pharyngeal and cardiovascular development. Consequently, dissecting the *Tbx1* networks is not a straightforward process and requires refined approaches.

1.2.1. Microarray screens, outcomes and limitations

Microarray chips became a breakthrough by providing the opportunity of simultaneous expression analysis of tens of thousands of genes (Eszlinger et al., 2007), leading many laboratories to follow this transcriptomics approach. The power of such studies relies on both the experimental design and the statistical analysis of the data produced (Eszlinger et al., 2007). In that respect, limitations exist, which should be considered when discussing the outcomes of microarray screens. Decreased sensitivity in the detection of genes with low expression levels and tissue/cell heterogeneity that may influence the microarray sensitivity by masking changes in gene expression (dilution effects) are some of these limitations (Bunney et al., 2003). The real weakness in microarray studies, however, lies in the statistical treatment of the results. Multiple tests are performed in each array allowing for several incorrect inferences by chance alone, since for each statistical test performed there is some probability that an incorrect assumption will be made (Pounds, 2006). In microarray studies the error rate is commonly measured with the false discovery rate (FDR) that describes the expected proportion of significant findings that are false positives (Pounds, 2006).

Undoubtedly, microarray techniques provide great insight into the transcriptomic regulation of tissues, cells, organs or even organisms, allowing for the comparison between normal and disease, treated and untreated groups or other types of experimental designs. Nevertheless, further *in vitro* and *in vivo* validation is required to prove functional changes in gene expression, while subsequent analysis can determine the biological significance of the initial findings.

We recently undertook a refined microarray approach towards identifying Tbx1 target genes on a cell autonomous setting (van Bueren et al., 2010). Following statistical analysis, quantitative real time PCR validation (van Bueren et al., 2010) and literature

review, *Smad7*, *Hes1* and *Slit2* were selected for further study. Their potential developmental roles, interaction with Tbx1 and relation with the 22q11DS-like phenotypes were the project of this thesis. The aims were to characterise the putative *Tbx1* downstream effectors and to associate the genetic networks with the pathogenesis of the different 22q11DS-like phenotypes. Different approaches were followed to that end.

1.2.2. Characterisation of mutant phenotypes - an invaluable tool for linking genes to developmental processes

Genetically engineered animal models have revolutionised biomedical research (Eisener-Dorman et al., 2009). Mice in particular, by providing an *in vivo*, mammalian system that is easy to handle, can be used effectively for understanding the genetic elements of human disease (Gama Sosa et al., 2010; Claij and Peters, 2006). A plethora of systems are available, including transgenics, standard knock-outs, inducibles, tissue-specifics, multiple gene knock-outs and other, more elaborate designs (Castrop, 2010; Gama Sosa et al., 2010). More commonly a gene's role in a process is studied through its absence, through null mutations of the gene being studied. Without disregarding the genetic background contribution, in many cases an observed phenotype is indeed the result of ablation of a single gene (Eisener-Dorman et al., 2009), which can reveal important information about gene functions (Claij and Peters, 2006).

Throughout this project, I used a gene-trap model to establish the *Smad7* requirements during embryogenesis. I have shown that the *Smad7* gene-trap mutation induces a range of 22q11DS-like phenotypes, including, cardiovascular, thymic and with low penetrance, VSD and secondary palate defects. I also discussed the potential roles for *Smad7* in pharyngeal arch artery remodelling. By contrast, when I examined the phenotype caused by *Slit2* or *Slit1*;*Slit2* deficiency I found no evidence of a role for either of the genes in the development of structures affected in 22q11DS, although there was an indication that *Slit2* may be involved in palatogenesis.

1.2.3. Conditional deletion - a tool for dissecting tissue and/or time-specific gene requirements

More complex systems, like the *Cre*/*lox*, provide the opportunity of controlled gene inactivation, allowing for the study of gene functions in restricted tissues, organs

or at defined time points (Claij and Peters, 2006). Analysis of the effects of such gene ablation strategies can provide useful information about a gene's roles through distinct expression domains (Claij and Peters, 2006).

Using a conditional mutagenesis approach I demonstrated that *Hes1* functions non cell autonomously in the ectoderm affecting great vessel and eye development, while it is essential in both the ectodermal and neural crest lineages for thymus morphogenesis.

1.2.4. Genetic interaction - a tool for dissecting genetic pathways

Given the complexity of biological systems the focus of research has lately turned from individual genes to the interactions between genes (Hartman et al., 2001; Wang et al., 2010). Different types of genetic interactions exist, which are usually identified by the discrepancy between mendelian segregation ratios based on the action of individual genes and the actual outcome of a dihybrid cross (Phillips, 2008). Synergy between mutations is assumed when the phenotype of a double mutation is significantly different to the phenotype of either single mutation alone or the additive effects of the individual mutations (Perez-Perez et al., 2009; Wong et al., 2004). Synergy can be the result of redundant actions among paralogous genes but can also be observed when converging pathways are disrupted, or when a mutation enhances the sensitivity to the effects of another mutation (Perez-Perez et al., 2009). Other types of genetic interaction exist, like epistasis, when the phenotype of the double mutation is reminiscent of the phenotype of one of the single mutants, but not the other, or suppression, when the double mutant phenotype is closer to the wild type condition than either of the single mutants (Perez-Perez et al., 2009). Assessing such functional relationships can be a useful tool in understanding the basic principles of the underlying genetic networks (Wong et al., 2004). Genetic interactions are involved in many complex phenotypes and are the defining basis of human multigenic genetic disease (Wong et al., 2004).

In that respect, the possible interactions between *Tbx1* and the putative downstream effector genes were assessed as part of this thesis. I demonstrated that *Smad7* acts synergistically with *Tbx1* in the development of the great vessels. The mechanism probably requires tissue-specific Tbx1-dependent activation of *Smad7* at an early developmental stage, whilst affecting great vessel remodelling at a much later stage. In addition, I addressed the possible genetic interaction between *Tbx1* and *Slit2*

but found no evidence of such a relationship. However, the sample size was small, so an interaction between the two genes cannot be completely excluded.

1.2.5. Bioinformatics - probably a weak tool in establishing direct interactions

Computational approaches have been widely employed to identify TBEs on regulatory regions of genes being studied. Nevertheless, although most human genes have been successfully annotated, the regulatory elements controlling these genes in different cell types, at various time points and under different environmental influences are largely unknown (Narlikar and Ovcharenko, 2009). This is due to the fact that in eukaryotic organisms a single transcription factor - DNA binding event rarely controls the transcription of the target genes (Narlikar and Ovcharenko, 2009). Rather, different combinations of cell type-specific factors act in co-operation, so that transcriptional regulation requires a complex set of protein-DNA and protein-protein interactions (Narlikar and Ovcharenko, 2009). Apart from the DNA-binding proteins, other trans regulatory factors are non-DNA-binding proteins (co-factors), while the transcription factors utilise cis regulatory elements like promoters, enhancers, silencers, insulators or other elements to promote gene transcription (Narlikar and Ovcharenko, 2009). A common approach in identifying cis regulatory elements is to feed the binding sequence of a protein into a bioinformatics software and examine the conservation of the site among species (phylogenetic footprinting, Hannenhalli, 2008). If the binding sequence of the protein is not known, binding sequences of other family members, or putative sites suggested from the literature can be used instead. Predictions based solely on sequence conservation have been shown to achieve remarkable success (Narlikar and Ovcharenko, 2009). A different approach employs the search for clusters of transcription factor sites, which are more likely to regulate transcription in co-operation (Hannenhalli, 2008; Narlikar and Ovcharenko, 2009).

To date no binding site has been established for Tbx1, so different studies have used either the Tbx5 binding sequence (Ng et al., 2002), or the putative T-half site (Conlon et al., 2001; Wilson and Conlon, 2002), known to be recognised by T-box family members, including TBX1 (Sinha et al., 2000). Putative Tbx1 binding elements have been identified in regulatory regions of the *VEGFR3* (Chen et al., 2010), *Pitx2c* (Nowotschin, 2006), *Fgf8* (Hu et al., 2004) and *Fgf10* (Xu et al., 2004) genes, but only the *VEGFR3* (Chen et al., 2010) and *Pitxc2* (Nowotschin et al., 2006) elements have

been verified. Ablating putative T-box binding elements from the *Mef2c* (Antonio Baldini, pers. comm.) or *Pax9* (Rumiko Matsuoka, pers. comm.) promoters did not affect Tbx1 activation at these promoters. This is an indication that elements other than canonical TBEs must be important for Tbx1 driven transcription. Moreover, a recent study identified by ChIP-Seq active tissue-specific enhancers in the mouse genome, recognised by the ubiquitously expressed coactivator protein p300 (Blow et al., 2010). An enhancer was detected 136 kb from *Smad7*, and in no closer proximity to any other known cardiac gene (Blow et al., 2010). Reporter gene expression of this enhancer appeared reminiscent of *Smad7* expression in the cardiac outflow tract but did not recapitulate all the *Smad7* expression domains. The distance the site was identified at and the restricted expression pattern of the reporter denote that enhancer elements are not necessarily located close to the transcription initiation site of a gene and that different enhancers may regulate tissue-specific expression of a gene. Collectively, these data suggest that the presence or absence of putative binding elements in the immediate regulatory region of a gene does not conclusively answer whether there is direct interaction between the genes of interest. Bioinformatic approaches are essentially indicative but not necessarily conclusive, in terms of establishing direct relationships, unless accompanied by high throughput analyses like ChIP assays (*in vitro*), or reporter gene assays (*in vivo*) (Narlikar and Ovcharenko, 2009).

Through this project I undertook a similar approach and examined T-half site conservation in the *Smad7* regulatory region, among four mammalian species, but found no conclusive evidence of the presence of such an element. *In vitro* binding assays were performed by a member of our lab, which also provided no definitive positive evidence of Tbx1 binding onto the *Smad7* regulatory region. In light of the above, *Smad7* may be controlled by Tbx1 through elements not yet identified or it may be an indirect Tbx1 target.

2. Thesis summary

In the course of this thesis I have employed different means of evaluating *in vivo* and *in vitro* potential Tbx1 downstream effectors, as these were established by microarray screens. I showed that *Smad7* is a Tbx1 target, although more likely indirect, acting synergistically with *Tbx1* in great vessel development. To date there is no evidence supporting a *Hes1-Tbx1* interaction in a mammalian system; however, I demonstrated that *Hes1* plays important roles in great vessel and thymus development through ectodermal and neural crest expression. Finally, by examining *Slit2*, I concluded that it does not appear to be regulated by Tbx1 or have a contribution to the development of structures affected in 22q11DS. Nevertheless, it is part of a redundant system, therefore, complex interactions and compensatory roles from other members of the Slit family cannot be excluded.

At the conclusion of this work, it remains to be decided which studies will be carried forward and in what direction. *Smad7* presents an important regulator of vascular remodelling. Addressing the molecular mechanisms *Smad7* is involved in by means of *in vivo* or *in vitro* examination of endothelial and/or VSM cell behaviours in different *Smad7* genetic settings could be an initial approach. Identifying the TGFβ/BMP pathway branch Smad7 acts on and possible Smad7 interactors are also future directions. Furthermore, a *Cre*/*lox* system can be employed to study the tissue and time-specific requirements for *Smad7* during embryogenesis. *Smad7* deletion in the *Tbx1* expression domains can decisively answer the genetic synergy hypothesis.

Overall, this thesis has described a novel *Tbx1* regulated pathway in pharyngeal arch artery remodelling, as characterised in an *in vivo* mammalian system, which has the potential to be further dissected into its fine elements in future work.

PUBLICATIONS/CONTRIBUTIONS

Developmental Biology 340 (2010) 369–380

Contents lists available at ScienceDirect

Developmental Biology

journal homepage: www.elsevier.com/developmentalbiology

Hes1 expression is reduced in *Tbx1* null cells and is required for the development of structures affected in 22q11 deletion syndrome

Kelly Lammerts van Bueren [a,1], Irinna Papangeli [a,1], Francesca Rochais [b], Kerra Pearce [a], Catherine Roberts [a], Amelie Calmont [a], Dorota Szumska [c], Robert G. Kelly [b], Shoumo Bhattacharya [c], Peter J. Scambler [a,*]

[a] Molecular Medicine Unit, Institute of Child Health, 30 Guilford Street, London WC1N 1EH, UK
[b] Developmental Biology Institute of Marseilles-Luminy, UMR, 6216 CNRS-Université de la Méditerranée, Campus de Luminy, Case 907, 13288, Marseille Cedex 9, France
[c] Department of Cardiovascular Medicine and Wellcome Trust Centre for Human Genetics, University of Oxford, Oxford OX3 7BN, UK

ARTICLE INFO

Article history:
Received for publication 13 July 2009
Revised 13 January 2010
Accepted 19 January 2010
Available online 1 February 2010

Keywords:
Tbx1
Hes1
22q11
Pharyngeal arch artery
Thymus
Mouse
Microarray
FACS

ABSTRACT

22q11 deletion syndrome (22q11DS) is characterised by aberrant development of the pharyngeal apparatus and the heart with haploinsufficiency of the transcription factor *TBX1* being considered the major underlying cause of the disease. *Tbx1* mutations in mouse phenocopy the disorder. In order to identify the transcriptional dysregulation in *Tbx1*-expressing lineages we optimised fluorescent-activated cell sorting of β-galactosidase expressing cells (FACS-Gal) to compare the expression profile of *Df1/Tbx1*^{lacZ} (effectively *Tbx1* null) and *Tbx1* heterozygous cells isolated from mouse embryos. *Hes1*, a major effector of Notch signalling, was identified as downregulated in *Tbx1*$^{-/-}$ mutants. *Hes1* mutant mice exhibited a partially penetrant range of 22q11DS-like defects including pharyngeal arch artery (PAA), outflow tract, craniofacial and thymic abnormalities. Similar to *Tbx1* mice, conditional mutagenesis revealed that *Hes1* expression in embryonic pharyngeal ectoderm contributes to thymus and pharyngeal arch artery development. These results suggest that *Hes1* acts downstream of *Tbx1* in the morphogenesis of pharyngeal-derived structures.

Introduction

22q11 deletion syndrome (22q11DS) has an incidence of approximately 1 in 4000 live births and classically comprises malformations of the cardiovascular system, thymus gland, parathyroid gland and craniofacial structures (Scambler, 2000). Haploinsufficiency of the transcription factor *TBX1* is considered to be the major underlying cause of the disorder. While the penetrance and expression of the deletion phenotype is very varied the cardinal features can be recapitulated by *TBX1* mutations in humans (Paylor et al., 2006; Stoller and Epstein, 2005; Yagi et al., 2003; Zweier et al., 2007), mouse (Jerome and Papaioannou, 2001; Lindsay et al., 2001; Merscher et al., 2001), and zebrafish (Piotrowski et al., 2003; Piotrowski and Nusslein-Volhard, 2000). In order to understand the role of *Tbx1* in development efforts have been made to identify *Tbx1* target genes using "candidate gene" or transcriptomics approaches.

Our previous work has examined the downstream transcriptional events of loss of *Tbx1* in dissected pharyngeal tissues (Ivins et al., 2005; Prescott et al., 2005). Several genes were identified and validated as differentially expressed in *Tbx1* mutants. In particular we were able to show a dysregulation of genes in the retinoic acid metabolism pathway that are likely to contribute to the phenotype (Ivins et al., 2005; Roberts et al., 2006). However, in these experiments the dissection includes cell types that do not express *Tbx1* and thus will either dilute some tissue specific expression changes, or add noise where tissue loss leads to a secondary expression change. We therefore aimed to repeat our analysis using only cells actively expressing from the *Tbx1* promoter. One of the *Tbx1* null alleles was created with a knock in of ß-galactosidase (Lindsay et al., 2001). We investigated whether a fluorogenic substrate for ß-galactosidase could be used to isolate *Tbx1* expressing cells, firstly to further our target identification program, and secondly to demonstrate the general utility of this procedure in light of the thousands of such knock-ins available via the mouse gene trap program. FACS-Gal has been used previously on cultured cells (Laugwitz et al., 2005) but involves preparative procedures that could introduce noise into microarray analyses, and reduce cell viability especially when using early embryos. We therefore examined whether the FACS-Gal procedure could produce good quality microarray data from the material available from mid gestation embryos.

We utilized the *Tbx1*$^{+/lacZ}$ × *Df1*/+ cross to obtain *Tbx1* null mutants to ensure equivalent fluorescence intensity from the *Tbx1*^{lacZ} allele in both genotypes. Df1 is a heterozygous deletion of 20 genes including *Tbx1* (Lindsay et al., 2001), thus the hemizygously deleted *Df1* genes could be used as internal controls to assess the quality of the

* Corresponding author. Fax: +44 20 7905 2609.
E-mail address: p.scambler@ich.ucl.ac.uk (P.J. Scambler).
[1] These investigators made an equal contribution to the work.

0012-1606/$ – see front matter © 2010 Elsevier Inc. All rights reserved.
doi:10.1016/j.ydbio.2010.01.020

Development 136, 3173-3183 (2009) doi:10.1242/dev.028902

Tbx1 controls cardiac neural crest cell migration during arch artery development by regulating *Gbx2* expression in the pharyngeal ectoderm

Amélie Calmont[1], Sarah Ivins[1], Kelly Lammerts Van Bueren[1], Irinna Papangeli[1], Vanessa Kyriakopoulou[1], William D. Andrews[2], James F. Martin[3], Anne M. Moon[4], Elizabeth A. Illingworth[5], M. Albert Basson[6] and Peter J. Scambler[1,*]

Elucidating the gene regulatory networks that govern pharyngeal arch artery (PAA) development is an important goal, as such knowledge can help to identify new genes involved in cardiovascular disease. The transcription factor Tbx1 plays a vital role in PAA development and is a major contributor to cardiovascular disease associated with DiGeorge syndrome. In this report, we used various genetic approaches to reveal part of a signalling network by which Tbx1 controls PAA development in mice. We investigated the crucial role played by the homeobox-containing transcription factor Gbx2 downstream of Tbx1. We found that PAA formation requires the pharyngeal surface ectoderm as a key signalling centre from which Gbx2, in response to Tbx1, triggers essential directional cues to the adjacent cardiac neural crest cells (cNCCs) en route to the caudal PAAs. Abrogation of this signal generates cNCC patterning defects leading to PAA abnormalities. Finally, we showed that the Slit/Robo signalling pathway is activated during cNCC migration and that components of this pathway are affected in *Gbx2* and *Tbx1* mutant embryos at the time of PAA development. We propose that the spatiotemporal control of this tightly orchestrated network of genes participates in crucial aspects of PAA development.

KEY WORDS: Pharyngeal arch arteries, Cardiac neural crest, Slit/Robo, Mouse

INTRODUCTION

The pharyngeal apparatus is a transient embryonic structure present during vertebrate development. It forms gradually as the pharynx segments into a series of arches and pouches in a cranial-to-caudal order. Each pharyngeal arch (PA) possesses an outer pharyngeal surface ectoderm (PSE) layer and an inner pharyngeal endodermal (P.endo) layer. In the centre of each PA, the pharyngeal arch artery (PAA) is encircled by a mesodermal core structure surrounded by a layer of neural crest cells (NCCs). The bi-lateral PAA system develops sequentially as the pharynx segments and allows blood to flow from the heart tube to the dorsal aortae (DeRuiter et al., 1993). At E10.5, five PAAs have formed, and whereas PAAs 1 and 2 have regressed into capillary beds, PAAs 3, 4 and 6 persist in their respective PAs. Starting from E11.5, these caudal PAAs undergo an extensive asymmetrical remodelling and persist later as parts of the great vessels arising from the aorta (Srivastava and Olson, 2000). Defective development of the fourth PAAs is responsible for severe vascular anomalies, such as interrupted aortic arch type B, which is postnatally lethal (Vitelli et al., 2002a). Perturbation of normal pharyngeal development is a feature of congenital diseases, such as DiGeorge syndrome, in which the main cause of death is congenital heart defects (CHDs) (Lindsay, 2001).

[1]Molecular Medicine Unit, Institute of Child Health, 30 Guilford Street, London WC1N 1EH, UK. [2]Department of Cell and Developmental Biology, University College London, London WC1E 6BT, UK. [3]Institute of Biosciences and Technology, Texas A&M Health Science Center, Houston, TX 77030, USA. [4]Departments of Pediatrics, Neurobiology and Anatomy and Human Genetics, University of Utah, Salt Lake City, UT 84112, USA. [5]Dulbecco Telethon Institute, c/o Telethon Institute of Genetics and Medicine, Via Pietro Castellino 111, 80131 Napoli, Italy. [6]Department of Craniofacial Development, King's College London, Floor 27, Guy's Tower, London SE1 9RT, UK.

*Author for correspondence (p.scambler@ich.ucl.ac.uk)

Accepted 16 July 2009

Haploinsufficiency of the T-box transcription factor *TBX1* is responsible for many features of DiGeorge syndrome (Paylor et al., 2006; Stoller and Epstein, 2005; Yagi et al., 2003). *Tbx1* is expressed dynamically in the developing pharyngeal apparatus in the mouse embryo and *Tbx1* homozygous mutants display severe cardiovascular, craniofacial, thymic, parathyroid and ear defects (Jerome and Papaioannou, 2001; Lindsay et al., 1999; Merscher et al., 2001). In particular, CHDs found in *Tbx1* mutant embryos consist of great vessel disruptions arising from defective fourth PAA development (Jerome and Papaioannou, 2001; Lindsay et al., 2001), and/or septation and alignment defects of the outflow tract (OFT) of the heart (Jerome and Papaioannou, 2001; Merscher et al., 2001). The essential role of Tbx1 in pharynx organogenesis relies on its ability to interact with crucial signalling pathways during development, such as the fibroblast growth factor (Fgf) (Hu et al., 2004; Vitelli et al., 2002b; Xu et al., 2004), hedgehog (Yamagishi et al., 2003) and retinoic acid (Guris et al., 2006; Roberts et al., 2006) signalling pathways. Furthermore, Tbx1 is required at different times (Xu et al., 2005), in different tissues (Arnold et al., 2006; Xu et al., 2005; Zhang et al., 2005; Zhang et al., 2006) and at different levels (Liao et al., 2004; Zhang and Baldini, 2008) to pattern all pharyngeal-derived structures. Thus, the analysis of Tbx1 effectors during embryonic development should advance our understanding of how the pharyngeal apparatus develops and, furthermore, aid in the identification of essential genes implicated in CHDs.

The special predisposition of the fourth PAA system toward interruption and/or hypoplasia is linked to the unique vascular morphology of these arteries (Bergwerff et al., 1999). Lineage-tracing in the mouse combined with morphological analysis of specific arterial segments has shown that muscular and non-muscular components of the fourth PAA system originate from cNCCs (Bergwerff et al., 1999; Jiang et al., 2000). cNCCs are pluripotent embryonic cells derived from the neuroepithelium (Le Douarin and Kalcheim, 1999). They originate from the neural folds in a region

BIBLIOGRAPHY

Adachi, I., Uemura, H., McCarthy, K. P. and Ho, S. Y. (2008). Surgical anatomy of atrioventricular septal defect. *Asian Cardiovasc Thorac Ann* **16**, 497-502.

Aggarwal, V. S., Liao, J., Bondarev, A., Schimmang, T., Lewandoski, M., Locker, J., Shanske, A., Campione, M. and Morrow, B. E. (2006). Dissection of Tbx1 and Fgf interactions in mouse models of 22q11DS suggests functional redundancy. *Hum Mol Genet* **15**, 3219-28.

Aggarwal, V. S. and Morrow, B. E. (2008). Genetic modifiers of the physical malformations in velo-cardio-facial syndrome/DiGeorge syndrome. *Dev Disabil Res Rev* **14**, 19-25.

Aman, A. and Piotrowski, T. (2010). Cell migration during morphogenesis. *Dev Biol* **341**, 20-33.

Anderson, R. H. (2000). Clinical anatomy of the aortic root. *Heart* **84**, 670-3.

Anderson, R. H., Webb, S., Brown, N. A., Lamers, W. and Moorman, A. (2003b). Development of the heart: (2) Septation of the atriums and ventricles. *Heart* **89**, 949-58.

Anderson, W. J., Zhou, Q., Alcalde, V., Kaneko, O. F., Blank, L. J., Sherwood, R. I., Guseh, J. S., Rajagopal, J. and Melton, D. A. (2008). Genetic targeting of the endoderm with claudin-6CreER. *Dev Dyn* **237**, 504-12.

Andersson, M., Karlsson, L., Svensson, P. A., Ulfhammer, E., Ekman, M., Jernas, M., Carlsson, L. M. and Jern, S. (2005). Differential global gene expression response patterns of human endothelium exposed to shear stress and intraluminal pressure. *J Vasc Res* **42**, 441-52.

Ando, J. and Yamamoto, K. (2009). Vascular mechanobiology: endothelial cell responses to fluid shear stress. *Circ J* **73**, 1983-92.

Ando, J. and Yamamoto, K. (2010). Effects of Shear Stress and Stretch on Endothelial Function. *Antioxid Redox Signal*.

Andrews, W., Barber, M., Hernadez-Miranda, L. R., Xian, J., Rakic, S., Sundaresan, V., Rabbitts, T. H., Pannell, R., Rabbitts, P., Thompson, H. et al. (2008). The role of Slit-Robo signalling in the generation, migration and morphological differentiation of cortical interneurons. *Dev Biol* **313**, 648-58.

Andrews, W., Liapi, A., Plachez, C., Camurri, L., Zhang, J., Mori, S., Murakami, F., Parnavelas, J. G., Sundaresan, V. and Richards, L. J. (2006). Robo1 regulates

the development of major axon tracts and interneuron migration in the forebrain. *Development* **133**, 2243-52.

Andrews, W. D., Barber, M. and Parnavelas, J. G. (2007). Slit-Robo interactions during cortical development. *J Anat* **211**, 188-98.

Arnold, J. S., Werling, U., Braunstein, E. M., Liao, J., Nowotschin, S., Edelmann, W., Hebert, J. M. and Morrow, B. E. (2006). Inactivation of Tbx1 in the pharyngeal endoderm results in 22q11DS malformations. *Development* **133**, 977-87.

Artavanis-Tsakonas, S., Rand, M. D. and Lake, R. J. (1999). Notch signalling: cell fate control and signal integration in development. *Science* **284**, 770-6.

Ataliotis, P., Ivins, S., Mohun, T. J. and Scambler, P. J. (2005). XTbx1 is a transcriptional activator involved in head and pharyngeal arch development in Xenopus laevis. *Dev Dyn* **232**, 979-91.

Baek, J. H., Hatakeyama, J., Sakamoto, S., Ohtsuka, T. and Kageyama, R. (2006). Persistent and high levels of Hes1 expression regulate boundary formation in the developing central nervous system. *Development* **133**, 2467-76.

Bailliard, F. and Anderson, R. H. (2009). Tetralogy of Fallot. *Orphanet J Rare Dis* **4**, 2.

Bajolle, F., Zaffran, S., Kelly, R. G., Hadchouel, J., Bonnet, D., Brown, N. A. and Buckingham, M. E. (2006). Rotation of the myocardial wall of the outflow tract is implicated in the normal positioning of the great arteries. *Circ Res* **98**, 421-8.

Baldini, A. (2002). DiGeorge syndrome: the use of model organisms to dissect complex genetics. *Hum Mol Genet* **11**, 2363-9.

Baldini, A. (2003). DiGeorge's syndrome: a gene at last. *Lancet* **362**, 1342-3.

Baldini, A. (2004). DiGeorge syndrome: an update. *Curr Opin Cardiol* **19**, 201-4.

Barsi, J. C., Rajendra, R., Wu, J. I. and Artzt, K. (2005). Mind bomb1 is a ubiquitin ligase essential for mouse embryonic development and Notch signalling. *Mech Dev* **122**, 1106-17.

Bartram, U., Molin, D. G., Wisse, L. J., Mohamad, A., Sanford, L. P., Doetschman, T., Speer, C. P., Poelmann, R. E. and Gittenberger-de Groot, A. C. (2001). Double-outlet right ventricle and overriding tricuspid valve reflect disturbances of looping, myocardialization, endocardial cushion differentiation, and apoptosis in TGF-beta(2)-knock-out mice. *Circulation* **103**, 2745-52.

Bialowas, J., Hreczecha, J. and Grzybiak, M. (2000). Right-sided aortic arch. *Folia Morphol (Warsz)* **59**, 211-6.

Blow, M. J., McCulley, D. J., Li, Z., Zhang, T., Akiyama, J. A., Holt, A., Plajzer-Frick, I., Shoukry, M., Wright, C., Chen, F. et al. (2010). ChIP-Seq identification of weakly conserved heart enhancers. *Nat Genet* **42**, 806-10.

Boehm, T. (2008). Thymus development and function. *Curr Opin Immunol* **20**, 178-84.

Bookout, A. L. and Mangelsdorf, D. J. (2003). Quantitative real-time PCR protocol for analysis of nuclear receptor signalling pathways. *Nucl Recept Signal* **1**, e012.

Botstein, D. and Risch, N. (2003). Discovering genotypes underlying human phenotypes: past successes for mendelian disease, future approaches for complex disease. *Nat Genet* **33 Suppl**, 228-37.

Bray, S. J. (2006). Notch : a simple pathway becomes complex. *Nat Rev Mol Cell Biol* **7**, 678-89.

Bujak, M. and Frangogiannis, N. G. (2007). The role of TGF-beta signalling in myocardial infarction and cardiac remodelling. *Cardiovasc Res* **74**, 184-95.

Bunney, W. E., Bunney, B. G., Vawter, M. P., Tomita, H., Li, J., Evans, S. J., Choudary, P. V., Myers, R. M., Jones, E. G., Watson, S. J. et al. (2003). Microarray technology: a review of new strategies to discover candidate vulnerability genes in psychiatric disorders. *Am J Psychiatry* **160**, 657-66.

Calmont, A., Ivins, S., Van Bueren, K. L., Papangeli, I., Kyriakopoulou, V., Andrews, W. D., Martin, J. F., Moon, A. M., Illingworth, E. A., Basson, M. A. et al. (2009). Tbx1 controls cardiac neural crest cell migration during arch artery development by regulating Gbx2 expression in the pharyngeal ectoderm. *Development* **136**, 3173-83.

Carotti, A., Digilio, M. C., Piacentini, G., Saffirio, C., Di Donato, R. M. and Marino, B. (2008). Cardiac defects and results of cardiac surgery in 22q11.2 deletion syndrome. *Dev Disabil Res Rev* **14**, 35-42.

Castrop, H. (2010). Genetically modified mice-successes and failures of a widely used technology. *Pflugers Arch* **459**, 557-67.

Caterino, M., Ruoppolo, M., Fulcoli, G., Huynth, T., Orru, S., Baldini, A. and Salvatore, F. (2009). Transcription factor TBX1 overexpression induces downregulation of proteins involved in retinoic acid metabolism: a comparative proteomic analysis. *J Proteome Res* **8**, 1515-26.

Cau, E., Gradwohl, G., Casarosa, S., Kageyama, R. and Guillemot, F. (2000). Hes genes regulate sequential stages of neurogenesis in the olfactory epithelium. *Development* **127**, 2323-32.

Chapman, D. L., Garvey, N., Hancock, S., Alexiou, M., Agulnik, S. I., Gibson-Brown, J. J., Cebra-Thomas, J., Bollag, R. J., Silver, L. M. and Papaioannou, V. E. (1996). Expression of the T-box family genes, Tbx1-Tbx5, during early mouse development. *Dev Dyn* **206**, 379-90.

Chen, H., Shi, S., Acosta, L., Li, W., Lu, J., Bao, S., Chen, Z., Yang, Z., Schneider, M. D., Chien, K. R. et al. (2004). BMP10 is essential for maintaining cardiac growth during murine cardiogenesis. *Development* **131**, 2219-31.

Chen, L., Fulcoli, F. G., Tang, S. and Baldini, A. (2009a). Tbx1 regulates proliferation and differentiation of multipotent heart progenitors. *Circ Res* **105**, 842-51.

Chen, L., Mupo, A., Huynh, T., Cioffi, S., Woods, M., Jin, C., McKeehan, W., Thompson-Snipes, L., Baldini, A. and Illingworth, E. (2010). Tbx1 regulates Vegfr3 and is required for lymphatic vessel development. *J Cell Biol* **189**, 417-24.

Chen, Q., Chen, H., Zheng, D., Kuang, C., Fang, H., Zou, B., Zhu, W., Bu, G., Jin, T., Wang, Z. et al. (2009b). Smad7 is required for the development and function of the heart. *J Biol Chem* **284**, 292-300.

Chieffo, C., Garvey, N., Gong, W., Roe, B., Zhang, G., Silver, L., Emanuel, B. S. and Budarf, M. L. (1997). Isolation and characterization of a gene from the DiGeorge chromosomal region homologous to the mouse Tbx1 gene. *Genomics* **43**, 267-77.

Choi, M. and Klingensmith, J. (2009). Chordin is a modifier of tbx1 for the craniofacial malformations of 22q11 deletion syndrome phenotypes in mouse. *PLoS Genet* **5**, e1000395.

Choudhary, B., Ito, Y., Makita, T., Sasaki, T., Chai, Y. and Sucov, H. M. (2006). Cardiovascular malformations with normal smooth muscle differentiation in neural crest-specific type II TGFbeta receptor (Tgfbr2) mutant mice. *Dev Biol* **289**, 420-9.

Christiansen, J. H., Coles, E. G. and Wilkinson, D. G. (2000). Molecular control of neural crest formation, migration and differentiation. *Curr Opin Cell Biol* **12**, 719-24.

Claij, N. and Peters, D. J. (2006). Teaching molecular genetics: chapter 2- Transgenesis and gene targeting: mouse models to study gene function and expression. *Pediatr Nephrol* **21**, 318-23.

Conlon, F. L., Fairclough, L., Price, B. M., Casey, E. S. and Smith, J. C. (2001). Determinants of T box protein specificity. *Development* **128**, 3749-58.

Copp, A. J. (2005). Neurulation in the cranial region--normal and abnormal. *J Anat* **207**, 623-35.

Danielian, P. S., Muccino, D., Rowitch, D. H., Michael, S. K. and McMahon, A. P. (1998). Modification of gene activity in mouse embryos in utero by a tamoxifen-inducible form of Cre recombinase. *Curr Biol* **8**, 1323-6.

Davies, M. and Guest, P. J. (2003). Developmental abnormalities of the great vessels of the thorax and their embryological basis. *Br J Radiol* **76**, 491-502.

De Bellard, M. E., Rao, Y. and Bronner-Fraser, M. (2003). Dual function of Slit2 in repulsion and enhanced migration of trunk, but not vagal, neural crest cells. *J Cell Biol* **162**, 269-79.

Dickinson, R. E. and Duncan, W. C. (2010). The SLIT-ROBO pathway: a regulator of cell function with implications for the reproductive system. *Reproduction* **139**, 697-704.

Dillman, J. R., Yarram, S. G., D'Amico, A. R. and Hernandez, R. J. (2008). Interrupted aortic arch: spectrum of MRI findings. *AJR Am J Roentgenol* **190**, 1467-74.

Dodou, E., Xu, S. M. and Black, B. L. (2003). mef2c is activated directly by myogenic basic helix-loop-helix proteins during skeletal muscle development *in vivo*. *Mech Dev* **120**, 1021-32.

Dunwoodie, S. L. (2007). Combinatorial signalling in the heart orchestrates cardiac induction, lineage specification and chamber formation. *Semin Cell Dev Biol* **18**, 54-66.

Echelard, Y., Vassileva, G. and McMahon, A. P. (1994). Cis-acting regulatory sequences governing Wnt-1 expression in the developing mouse CNS. *Development* **120**, 2213-24.

Edlund, S., Lee, S. Y., Grimsby, S., Zhang, S., Aspenstrom, P., Heldin, C. H. and Landstrom, M. (2005). Interaction between Smad7 and beta-catenin: importance for transforming growth factor beta-induced apoptosis. *Mol Cell Biol* **25**, 1475-88.

Eisener-Dorman, A. F., Lawrence, D. A. and Bolivar, V. J. (2009). Cautionary insights on knock-out mouse studies: the gene or not the gene? *Brain Behav Immun* **23**, 318-24.

Emanuel, B. S. (2008). Molecular mechanisms and diagnosis of chromosome 22q11.2 rearrangements. *Dev Disabil Res Rev* **14**, 11-8.

Engert, S., Liao, W. P., Burtscher, I. and Lickert, H. (2009). Sox17-2A-iCre: a knock-in mouse line expressing Cre recombinase in endoderm and vascular endothelial cells. *Genesis* **47**, 603-10.

Epstein, J. A. (2001). Developing models of DiGeorge syndrome. *Trends Genet* **17**, S13-7.

Epstein, J. A., Li, J., Lang, D., Chen, F., Brown, C. B., Jin, F., Lu, M. M., Thomas, M., Liu, E., Wessels, A. et al. (2000). Migration of cardiac neural crest cells in Splotch embryos. *Development* **127**, 1869-78.

Eszlinger, M., Krohn, K., Kukulska, A., Jarzab, B. and Paschke, R. (2007). Perspectives and limitations of microarray-based gene expression profiling of thyroid tumors. *Endocr Rev* **28**, 322-38.

Fischer, A. and Gessler, M. (2007). Delta-Notch--and then? Protein interactions and proposed modes of repression by Hes and Hey bHLH factors. *Nucleic Acids Res* **35**, 4583-96.

Fischer, A., Steidl, C., Wagner, T. U., Lang, E., Jakob, P. M., Friedl, P., Knobeloch, K. P. and Gessler, M. (2007). Combined loss of Hey1 and HeyL causes congenital heart defects because of impaired epithelial to mesenchymal transition. *Circ Res* **100**, 856-63.

Flotte, T. R. (2007). Gene therapy: the first two decades and the current state-of-the-art. *J Cell Physiol* **213**, 301-5.

Frank, D. U., Fotheringham, L. K., Brewer, J. A., Muglia, L. J., Tristani-Firouzi, M., Capecchi, M. R. and Moon, A. M. (2002). An Fgf8 mouse mutant phenocopies human 22q11 deletion syndrome. *Development* **129**, 4591-603.

Fulcoli, F. G., Huynh, T., Scambler, P. J. and Baldini, A. (2009). Tbx1 regulates the BMP-Smad1 pathway in a transcription independent manner. *PLoS One* **4**, e6049.

Galvin, K. M., Donovan, M. J., Lynch, C. A., Meyer, R. I., Paul, R. J., Lorenz, J. N., Fairchild-Huntress, V., Dixon, K. L., Dunmore, J. H., Gimbrone, M. A., Jr.

et al. (2000). A role for smad6 in development and homeostasis of the cardiovascular system. *Nat Genet* **24**, 171-4.

Gama Sosa, M. A., De Gasperi, R. and Elder, G. A. (2010). Animal transgenesis: an overview. *Brain Struct Funct* **214**, 91-109.

Garg, V., Muth, A. N., Ransom, J. F., Schluterman, M. K., Barnes, R., King, I. N., Grossfeld, P. D. and Srivastava, D. (2005). Mutations in NOTCH1 cause aortic valve disease. *Nature* **437**, 270-4.

Gaussin, V., Morley, G. E., Cox, L., Zwijsen, A., Vance, K. M., Emile, L., Tian, Y., Liu, J., Hong, C., Myers, D. et al. (2005). Alk3/Bmpr1a receptor is required for development of the atrioventricular canal into valves and annulus fibrosus. *Circ Res* **97**, 219-26.

Gaussin, V., Van de Putte, T., Mishina, Y., Hanks, M. C., Zwijsen, A., Huylebroeck, D., Behringer, R. R. and Schneider, M. D. (2002). Endocardial cushion and myocardial defects after cardiac myocyte-specific conditional deletion of the bone morphogenetic protein receptor ALK3. *Proc Natl Acad Sci U S A* **99**, 2878-83.

Gill, J., Malin, M., Sutherland, J., Gray, D., Hollander, G. and Boyd, R. (2003). Thymic generation and regeneration. *Immunol Rev* **195**, 28-50.

Gittenberger-de Groot, A. C., Azhar, M. and Molin, D. G. (2006). Transforming growth factor beta-SMAD2 signalling and aortic arch development. *Trends Cardiovasc Med* **16**, 1-6.

Gittenberger-de Groot, A. C., Bartelings, M. M., Deruiter, M. C. and Poelmann, R. E. (2005). Basics of cardiac development for the understanding of congenital heart malformations. *Pediatr Res* **57**, 169-76.

Gong, W., Gottlieb, S., Collins, J., Blescia, A., Dietz, H., Goldmuntz, E., McDonald-McGinn, D. M., Zackai, E. H., Emanuel, B. S., Driscoll, D. A. et al. (2001). Mutation analysis of TBX1 in non-deleted patients with features of DGS/VCFS or isolated cardiovascular defects. *J Med Genet* **38**, E45.

Gordon, J., Wilson, V. A., Blair, N. F., Sheridan, J., Farley, A., Wilson, L., Manley, N. R. and Blackburn, C. C. (2004). Functional evidence for a single endodermal origin for the thymic epithelium. *Nat Immunol* **5**, 546-53.

Goudy, S., Law, A., Sanchez, G., Baldwin, H. S. and Brown, C. (2010). Tbx1 is necessary for palatal elongation and elevation. *Mech Dev* **127**, 292-300.

Graham, A. (2001). The development and evolution of the pharyngeal arches. *J Anat* **199**, 133-41.

Graham, A. (2003). Development of the pharyngeal arches. *Am J Med Genet A* **119A**, 251-6.

Graham, A. (2008). Deconstructing the pharyngeal metamere. *J Exp Zool B Mol Dev Evol* **310**, 336-44.

Grevellec, A. and Tucker, A. S. (2010). The pharyngeal pouches and clefts: Development, evolution, structure and derivatives. *Semin Cell Dev Biol* **21**, 325-32.

Gridley, T. (2003). Notch signalling and inherited disease syndromes. *Hum Mol Genet* **12 Spec No 1**, R9-13.

Grieshammer, U., Le, M., Plump, A. S., Wang, F., Tessier-Lavigne, M. and Martin, G. R. (2004). SLIT2-mediated ROBO2 signalling restricts kidney induction to a single site. *Dev Cell* **6**, 709-17.

Gritli-Linde, A. (2007). Molecular control of secondary palate development. *Dev Biol* **301**, 309-26.

Gu, S., Wei, N., Yu, X., Jiang, Y., Fei, J. and Chen, Y. (2008). Mice with an anterior cleft of the palate survive neonatal lethality. *Dev Dyn* **237**, 1509-16.

Guo, X. and Wang, X. F. (2009). Signaling cross-talk between TGF-beta/BMP and other pathways. *Cell Res* **19**, 71-88.

Guris, D. L., Duester, G., Papaioannou, V. E. and Imamoto, A. (2006). Dose-dependent interaction of Tbx1 and Crkl and locally aberrant RA signalling in a model of del22q11 syndrome. *Dev Cell* **10**, 81-92.

Guris, D. L., Fantes, J., Tara, D., Druker, B. J. and Imamoto, A. (2001). Mice lacking the homologue of the human 22q11.2 gene CRKL phenocopy neurocristopathies of DiGeorge syndrome. *Nat Genet* **27**, 293-8.

Han, G., Li, A. G., Liang, Y. Y., Owens, P., He, W., Lu, S., Yoshimatsu, Y., Wang, D., Ten Dijke, P., Lin, X. et al. (2006). Smad7-induced beta-catenin degradation alters epidermal appendage development. *Dev Cell* **11**, 301-12.

Hannenhalli, S. (2008). Eukaryotic transcription factor binding sites--modeling and integrative search methods. *Bioinformatics* **24**, 1325-31.

Hartman, J. L. t., Garvik, B. and Hartwell, L. (2001). Principles for the buffering of genetic variation. *Science* **291**, 1001-4.

Hatakeyama, J., Bessho, Y., Katoh, K., Ookawara, S., Fujioka, M., Guillemot, F. and Kageyama, R. (2004). Hes genes regulate size, shape and histogenesis of the nervous system by control of the timing of neural stem cell differentiation. *Development* **131**, 5539-50.

Hayashi, S. and McMahon, A. P. (2002). Efficient recombination in diverse tissues by a tamoxifen-inducible form of Cre: a tool for temporally regulated gene activation/inactivation in the mouse. *Dev Biol* **244**, 305-18.

He, W., Li, A. G., Wang, D., Han, S., Zheng, B., Goumans, M. J., Ten Dijke, P. and Wang, X. J. (2002). Overexpression of Smad7 results in severe pathological alterations in multiple epithelial tissues. *Embo J* **21**, 2580-90.

Hein, R., Buscheck, F., Fischer, E., Leetz, M., Bayard, M. T., Ostermayer, S., Reschke, M., Lang, K., Romer, A., Wilson, N. et al. (2005). Atrial and ventricular septal defects can safely be closed by percutaneous intervention. *J Interv Cardiol* **18**, 515-22.

High, F. A. and Epstein, J. A. (2008). The multifaceted role of Notch in cardiac development and disease. *Nat Rev Genet* **9**, 49-61.

High, F. A., Jain, R., Stoller, J. Z., Antonucci, N. B., Lu, M. M., Loomes, K. M., Kaestner, K. H., Pear, W. S. and Epstein, J. A. (2009). Murine Jagged1/Notch signalling in the second heart field orchestrates Fgf8 expression and tissue-tissue interactions during outflow tract development. *J Clin Invest* **119**, 1986-96.

High, F. A., Zhang, M., Proweller, A., Tu, L., Parmacek, M. S., Pear, W. S. and Epstein, J. A. (2007). An essential role for Notch in neural crest during cardiovascular development and smooth muscle differentiation. *J Clin Invest* **117**, 353-63.

Hirata, H., Bessho, Y., Kokubu, H., Masamizu, Y., Yamada, S., Lewis, J. and Kageyama, R. (2004). Instability of Hes7 protein is crucial for the somite segmentation clock. *Nat Genet* **36**, 750-4.

Hirata, H., Tomita, K., Bessho, Y. and Kageyama, R. (2001). Hes1 and Hes3 regulate maintenance of the isthmic organizer and development of the mid/hindbrain. *Embo J* **20**, 4454-66.

Hirata, H., Yoshiura, S., Ohtsuka, T., Bessho, Y., Harada, T., Yoshikawa, K. and Kageyama, R. (2002). Oscillatory expression of the bHLH factor Hes1 regulated by a negative feedback loop. *Science* **298**, 840-3.

Hiruma, T., Nakajima, Y. and Nakamura, H. (2002). Development of pharyngeal arch arteries in early mouse embryo. *J Anat* **201**, 15-29.

Hogers, B., DeRuiter, M. C., Gittenberger-de Groot, A. C. and Poelmann, R. E. (1997). Unilateral vitelline vein ligation alters intracardiac blood flow patterns and morphogenesis in the chick embryo. *Circ Res* **80**, 473-81.

Hogers, B., DeRuiter, M. C., Gittenberger-de Groot, A. C. and Poelmann, R. E. (1999). Extraembryonic venous obstructions lead to cardiovascular malformations and can be embryolethal. *Cardiovasc Res* **41**, 87-99.

Hohenester, E. (2008). Structural insight into Slit-Robo . *Biochem Soc Trans* **36**, 251-6.

Hollander, G., Gill, J., Zuklys, S., Iwanami, N., Liu, C. and Takahama, Y. (2006). Cellular and molecular events during early thymus development. *Immunol Rev* **209**, 28-46.

Hoogaars, W. M., Barnett, P., Moorman, A. F. and Christoffels, V. M. (2007). T-box factors determine cardiac design. *Cell Mol Life Sci* **64**, 646-60.

Hu, T., Yamagishi, H., Maeda, J., McAnally, J., Yamagishi, C. and Srivastava, D. (2004). Tbx1 regulates fibroblast growth factors in the anterior heart field through a reinforcing autoregulatory loop involving forkhead transcription factors. *Development* **131**, 5491-502.

Huh, S. H. and Ornitz, D. M. (2010). Beta-catenin deficiency causes DiGeorge syndrome-like phenotypes through regulation of Tbx1. *Development* **137**, 1137-47.

Hutson, M. R. and Kirby, M. L. (2007). Model systems for the study of heart development and disease. Cardiac neural crest and conotruncal malformations. *Semin Cell Dev Biol* **18**, 101-10.

Hutson, M. R., Sackey, F. N., Lunney, K. and Kirby, M. L. (2009). Blocking hedgehog signalling after ablation of the dorsal neural tube allows regeneration of the cardiac neural crest and rescue of outflow tract septation. *Dev Biol* **335**, 367-73.

Huynh, T., Chen, L., Terrell, P. and Baldini, A. (2007). A fate map of Tbx1 expressing cells reveals heterogeneity in the second cardiac field. *Genesis* **45**, 470-5.

Ikushima, H. and Miyazono, K. (2010). Cellular context-dependent "colors" of transforming growth factor-beta signalling. *Cancer Sci* **101**, 306-12.

Imayoshi, I., Shimogori, T., Ohtsuka, T. and Kageyama, R. (2008). Hes genes and neurogenin regulate non-neural versus neural fate specification in the dorsal telencephalic midline. *Development* **135**, 2531-41.

Ishibashi, M., Ang, S. L., Shiota, K., Nakanishi, S., Kageyama, R. and Guillemot, F. (1995). Targeted disruption of mammalian hairy and Enhancer of split homolog-1 (HES-1) leads to up-regulation of neural helix-loop-helix factors, premature neurogenesis, and severe neural tube defects. *Genes Dev* **9**, 3136-48.

Iso, T., Kedes, L. and Hamamori, Y. (2003). HES and HERP families: multiple effectors of the Notch signalling pathway. *J Cell Physiol* **194**, 237-55.

Ito, T., Udaka, N., Yazawa, T., Okudela, K., Hayashi, H., Sudo, T., Guillemot, F., Kageyama, R. and Kitamura, H. (2000). Basic helix-loop-helix transcription factors regulate the neuroendocrine differentiation of fetal mouse pulmonary epithelium. *Development* **127**, 3913-21.

Ivins, S., Lammerts van Beuren, K., Roberts, C., James, C., Lindsay, E., Baldini, A., Ataliotis, P. and Scambler, P. J. (2005). Microarray analysis detects differentially expressed genes in the pharyngeal region of mice lacking Tbx1. *Dev Biol* **285**, 554-69.

Jain, R., Rentschler, S. and Epstein, J. A. (2010). Notch and cardiac outflow tract development. *Ann N Y Acad Sci* **1188**, 184-90.

Jarriault, S., Brou, C., Logeat, F., Schroeter, E. H., Kopan, R. and Israel, A. (1995). downstream of activated mammalian Notch. *Nature* **377**, 355-8.

Javelaud, D. and Mauviel, A. (2004). Mammalian transforming growth factor-betas: Smad signalling and physio-pathological roles. *Int J Biochem Cell Biol* **36**, 1161-5.

JAX®, N. (2006). The Importance of Genetic Background in Mouse-based Biomedical Research. *JAX® NOTES.*

Jensen, J., Pedersen, E. E., Galante, P., Hald, J., Heller, R. S., Ishibashi, M., Kageyama, R., Guillemot, F., Serup, P. and Madsen, O. D. (2000). Control of endodermal endocrine development by Hes-1. *Nat Genet* **24**, 36-44.

Jerome, L. A. and Papaioannou, V. E. (2001). DiGeorge syndrome phenotype in mice mutant for the T-box gene, Tbx1. *Nat Genet* **27**, 286-91.

Jia, L., Cheng, L. and Raper, J. (2005). Slit/Robo signalling is necessary to confine early neural crest cells to the ventral migratory pathway in the trunk. *Dev Biol* **282**, 411-21.

Jia, Q., McDill, B. W., Li, S. Z., Deng, C., Chang, C. P. and Chen, F. (2007). Smad signalling in the neural crest regulates cardiac outflow tract remodelling through cell autonomous and non-cell autonomous effects. *Dev Biol* **311**, 172-84.

Jiang, X., Rowitch, D. H., Soriano, P., McMahon, A. P. and Sucov, H. M. (2000). Fate of the mammalian cardiac neural crest. *Development* **127**, 1607-16.

Jiao, K., Kulessa, H., Tompkins, K., Zhou, Y., Batts, L., Baldwin, H. S. and Hogan, B. L. (2003). An essential role of Bmp4 in the atrioventricular septation of the mouse heart. *Genes Dev* **17**, 2362-7.

Johnson, T. R. (2010). Conotruncal cardiac defects: a clinical imaging perspective. *Pediatr Cardiol* **31**, 430-7.

Jones, C. A., London, N. R., Chen, H., Park, K. W., Sauvaget, D., Stockton, R. A., Wythe, J. D., Suh, W., Larrieu-Lahargue, F., Mukouyama, Y. S. et al. (2008). Robo4 stabilizes the vascular network by inhibiting pathologic angiogenesis and endothelial hyperpermeability. *Nat Med* **14**, 448-53.

Jones, N. C. and Trainor, P. A. (2005). Role of morphogens in neural crest cell determination. *J Neurobiol* **64**, 388-404.

Jugessur, A., Farlie, P. G. and Kilpatrick, N. (2009). The genetics of isolated orofacial clefts: from genotypes to subphenotypes. *Oral Dis* **15**, 437-53.

Kaartinen, V., Dudas, M., Nagy, A., Sridurongrit, S., Lu, M. M. and Epstein, J. A. (2004). Cardiac outflow tract defects in mice lacking ALK2 in neural crest cells. *Development* **131**, 3481-90.

Kageyama, R., Ohtsuka, T., Hatakeyama, J. and Ohsawa, R. (2005). Roles of bHLH genes in neural stem cell differentiation. *Exp Cell Res* **306**, 343-8.

Kageyama, R., Ohtsuka, T. and Tomita, K. (2000). The bHLH gene Hes1 regulates differentiation of multiple cell types. *Mol Cells* **10**, 1-7.

Kalcheim, C. and Burstyn-Cohen, T. (2005). Early stages of neural crest ontogeny: formation and regulation of cell delamination. *Int J Dev Biol* **49**, 105-16.

Kameda, Y. (2009). Hoxa3 and signalling molecules involved in aortic arch patterning and remodelling. *Cell Tissue Res* **336**, 165-78.

Kamiya, Y., Miyazono, K. and Miyazawa, K. (2010). Smad7 inhibits transforming growth factor-beta family type i receptors through two distinct modes of interaction. *J Biol Chem* **285**, 30804-13.

Kaneta, M., Osawa, M., Sudo, K., Nakauchi, H., Farr, A. G. and Takahama, Y. (2000). A role for pref-1 and HES-1 in thymocyte development. *J Immunol* **164**, 256-64.

Kellenberger, C. J. (2010). Aortic arch malformations. *Pediatr Radiol* **40**, 876-84.

Kelly, R. G., Jerome-Majewska, L. A. and Papaioannou, V. E. (2004). The del22q11.2 candidate gene Tbx1 regulates branchiomeric myogenesis. *Hum Mol Genet* **13**, 2829-40.

Kerem, B., Rommens, J. M., Buchanan, J. A., Markiewicz, D., Cox, T. K., Chakravarti, A., Buchwald, M. and Tsui, L. C. (1989). Identification of the cystic fibrosis gene: genetic analysis. *Science* **245**, 1073-80.

Kim, J., Lo, L., Dormand, E. and Anderson, D. J. (2003). SOX10 maintains multipotency and inhibits neuronal differentiation of neural crest stem cells. *Neuron* **38**, 17-31.

Kim, R. Y., Robertson, E. J. and Solloway, M. J. (2001). Bmp6 and Bmp7 are required for cushion formation and septation in the developing mouse heart. *Dev Biol* **235**, 449-66.

Kimber, W. L., Hsieh, P., Hirotsune, S., Yuva-Paylor, L., Sutherland, H. F., Chen, A., Ruiz-Lozano, P., Hoogstraten-Miller, S. L., Chien, K. R., Paylor, R. et al. (1999). Deletion of 150 kb in the minimal DiGeorge/velocardiofacial syndrome critical region in mouse. *Hum Mol Genet* **8**, 2229-37.

Kirby, M. L. (2002). Molecular embryogenesis of the heart. *Pediatr Dev Pathol* **5**, 516-43.

Kobayashi, T., Mizuno, H., Imayoshi, I., Furusawa, C., Shirahige, K. and Kageyama, R. (2009). The cyclic gene Hes1 contributes to diverse differentiation responses of embryonic stem cells. *Genes Dev* **23**, 1870-5.

Kochilas, L., Merscher-Gomez, S., Lu, M. M., Potluri, V., Liao, J., Kucherlapati, R., Morrow, B. and Epstein, J. A. (2002). The role of neural crest during cardiac development in a mouse model of DiGeorge syndrome. *Dev Biol* **251**, 157-66.

Kolesova, H., Roelink, H. and Grim, M. (2008). Sonic hedgehog is required for the assembly and remodelling of branchial arch blood vessels. *Dev Dyn* **237**, 1923-34.

Kuhlbrodt, K., Herbarth, B., Sock, E., Hermans-Borgmeyer, I. and Wegner, M. (1998). Sox10, a novel transcriptional modulator in glial cells. *J Neurosci* **18**, 237-50.

Kulesa, P., Ellies, D. L. and Trainor, P. A. (2004). Comparative analysis of neural crest cell death, migration, and function during vertebrate embryogenesis. *Dev Dyn* **229**, 14-29.

Kulesa, P. M., Bailey, C. M., Kasemeier-Kulesa, J. C. and McLennan, R. (2010). Cranial neural crest migration: new rules for an old road. *Dev Biol* **344**, 543-54.

Kulesa, P. M. and Gammill, L. S. (2010). Neural crest migration: patterns, phases and signals. *Dev Biol* **344**, 566-8.

Kumar, M. S. and Owens, G. K. (2003). Combinatorial control of smooth muscle-specific gene expression. *Arterioscler Thromb Vasc Biol* **23**, 737-47.

Kuriyama, S. and Mayor, R. (2008). Molecular analysis of neural crest migration. *Philos Trans R Soc Lond B Biol Sci* **363**, 1349-62.

Kutsche, L. M. and Van Mierop, L. H. (1984). Cervical origin of the right subclavian artery in aortic arch interruption: pathogenesis and significance. *Am J Cardiol* **53**, 892-5.

Lallier, T., Leblanc, G., Artinger, K. B. and Bronner-Fraser, M. (1992). Cranial and trunk neural crest cells use different mechanisms for attachment to extracellular matrices. *Development* **116**, 531-41.

Lamb, T. D., Collin, S. P. and Pugh, E. N., Jr. (2007). Evolution of the vertebrate eye: opsins, photoreceptors, retina and eye cup. *Nat Rev Neurosci* **8**, 960-76.

Lamers, W. H. and Moorman, A. F. (2002). Cardiac septation: a late contribution of the embryonic primary myocardium to heart morphogenesis. *Circ Res* **91**, 93-103.

Le Douarin, N. M. and Dupin, E. (2003). Multipotentiality of the neural crest. *Curr Opin Genet Dev* **13**, 529-36.

Lee, H. Y., Wroblewski, E., Philips, G. T., Stair, C. N., Conley, K., Reedy, M., Mastick, G. S. and Brown, N. L. (2005). Multiple requirements for Hes 1 during early eye formation. *Dev Biol* **284**, 464-78.

Lehner, B., Crombie, C., Tischler, J., Fortunato, A. and Fraser, A. G. (2006). Systematic mapping of genetic interactions in Caenorhabditis elegans identifies common modifiers of diverse signalling pathways. *Nat Genet* **38**, 896-903.

Li, R., Rosendahl, A., Brodin, G., Cheng, A. M., Ahgren, A., Sundquist, C., Kulkarni, S., Pawson, T., Heldin, C. H. and Heuchel, R. L. (2006). Deletion of exon I of SMAD7 in mice results in altered B cell responses. *J Immunol* **176**, 6777-84.

Liao, J., Aggarwal, V. S., Nowotschin, S., Bondarev, A., Lipner, S. and Morrow, B. E. (2008). Identification of downstream genetic pathways of Tbx1 in the second heart field. *Dev Biol* **316**, 524-37.

Lindsay, E. A. (2001). Chromosomal microdeletions: dissecting del22q11 syndrome. *Nat Rev Genet* **2**, 858-68.

Lindsay, E. A. and Baldini, A. (2001). Recovery from arterial growth delay reduces penetrance of cardiovascular defects in mice deleted for the DiGeorge syndrome region. *Hum Mol Genet* **10**, 997-1002.

Lindsay, E. A., Botta, A., Jurecic, V., Carattini-Rivera, S., Cheah, Y. C., Rosenblatt, H. M., Bradley, A. and Baldini, A. (1999). Congenital heart disease in mice deficient for the DiGeorge syndrome region. *Nature* **401**, 379-83.

Lindsay, E. A., Vitelli, F., Su, H., Morishima, M., Huynh, T., Pramparo, T., Jurecic, V., Ogunrinu, G., Sutherland, H. F., Scambler, P. J. et al. (2001). Tbx1 haploinsufficieny in the DiGeorge syndrome region causes aortic arch defects in mice. *Nature* **410**, 97-101.

Liu, J., Zhang, L., Wang, D., Shen, H., Jiang, M., Mei, P., Hayden, P. S., Sedor, J. R. and Hu, H. (2003). Congenital diaphragmatic hernia, kidney agenesis and cardiac defects associated with Slit3-deficiency in mice. *Mech Dev* **120**, 1059-70.

Liu, W., Selever, J., Wang, D., Lu, M. F., Moses, K. A., Schwartz, R. J. and Martin, J. F. (2004). Bmp4 signalling is required for outflow-tract septation and branchial-arch artery remodelling. *Proc Natl Acad Sci U S A* **101**, 4489-94.

Liu, X., Chen, Q., Kuang, C., Zhang, M., Ruan, Y., Xu, Z. C., Wang, Z. and Chen, Y. (2007). A 4.3 kb Smad7 promoter is able to specify gene expression during mouse development. *Biochim Biophys Acta* **1769**, 149-52.

Long, H., Sabatier, C., Ma, L., Plump, A., Yuan, W., Ornitz, D. M., Tamada, A., Murakami, F., Goodman, C. S. and Tessier-Lavigne, M. (2004). Conserved roles for Slit and Robo proteins in midline commissural axon guidance. *Neuron* **42**, 213-23.

Lu, W., van Eerde, A. M., Fan, X., Quintero-Rivera, F., Kulkarni, S., Ferguson, H., Kim, H. G., Fan, Y., Xi, Q., Li, Q. G. et al. (2007). Disruption of ROBO2 is associated with urinary tract anomalies and confers risk of vesicoureteral reflux. *Am J Hum Genet* **80**, 616-32.

Luukko, K., Ylikorkala, A. and Makela, T. P. (2001). Developmentally regulated expression of Smad3, Smad4, Smad6, and Smad7 involved in TGF-beta signalling. *Mech Dev* **101**, 209-12.

Ma, L., Lu, M. F., Schwartz, R. J. and Martin, J. F. (2005). Bmp2 is essential for cardiac cushion epithelial-mesenchymal transition and myocardial patterning. *Development* **132**, 5601-11.

Macatee, T. L., Hammond, B. P., Arenkiel, B. R., Francis, L., Frank, D. U. and Moon, A. M. (2003). Ablation of specific expression domains reveals discrete functions of ectoderm- and endoderm-derived FGF8 during cardiovascular and pharyngeal development. *Development* **130**, 6361-74.

MacMullin, A. and Jacobs, J. R. (2006). Slit coordinates cardiac morphogenesis in Drosophila. *Dev Biol* **293**, 154-64.

Maden, M., Hunt, P., Eriksson, U., Kuroiwa, A., Krumlauf, R. and Summerbell, D. (1991). Retinoic acid-binding protein, rhombomeres and the neural crest. *Development* **111**, 35-43.

Manley, N. R. (2000). Thymus organogenesis and molecular mechanisms of thymic epithelial cell differentiation. *Semin Immunol* **12**, 421-8.

Manley, N. R. and Capecchi, M. R. (1998). Hox group 3 paralogs regulate the development and migration of the thymus, thyroid, and parathyroid glands. *Dev Biol* **195**, 1-15.

Mao, J., McGlinn, E., Huang, P., Tabin, C. J. and McMahon, A. P. (2009). Fgf-dependent Etv4/5 activity is required for posterior restriction of Sonic Hedgehog and promoting outgrowth of the vertebrate limb. *Dev Cell* **16**, 600-6.

McClearn, G. E. (2004). Nature and nurture: interaction and coaction. *Am J Med Genet B Neuropsychiatr Genet* **124B**, 124-30.

McElhinney, D. B., Tworetzky, W., Hanley, F. L. and Rudolph, A. M. (1999). Congenital obstructive lesions of the right aortic arch. *Ann Thorac Surg* **67**, 1194-202.

Medioni, C., Astier, M., Zmojdzian, M., Jagla, K. and Semeriva, M. (2008). Genetic control of cell morphogenesis during Drosophila melanogaster cardiac tube formation. *J Cell Biol* **182**, 249-61.

Meng, L., Bian, Z., Torensma, R. and Von den Hoff, J. W. (2009). Biological mechanisms in palatogenesis and cleft palate. *J Dent Res* **88**, 22-33.

Merikangas, K. R., Low, N. C. and Hardy, J. (2006). Commentary: understanding sources of complexity in chronic diseases--the importance of integration of genetics and epidemiology. *Int J Epidemiol* **35**, 590-2; discussion 593-6.

Merscher, S., Funke, B., Epstein, J. A., Heyer, J., Puech, A., Lu, M. M., Xavier, R. J., Demay, M. B., Russell, R. G., Factor, S. et al. (2001). TBX1 is responsible for cardiovascular defects in velo-cardio-facial/DiGeorge syndrome. *Cell* **104**, 619-29.

Meyer, D., Yamaai, T., Garratt, A., Riethmacher-Sonnenberg, E., Kane, D., Theill, L. E. and Birchmeier, C. (1997). Isoform-specific expression and function of neuregulin. *Development* **124**, 3575-86.

Minette, M. S. and Sahn, D. J. (2006). Ventricular septal defects. *Circulation* **114**, 2190-7.

Minoux, M., Antonarakis, G. S., Kmita, M., Duboule, D. and Rijli, F. M. (2009). Rostral and caudal pharyngeal arches share a common neural crest ground pattern. *Development* **136**, 637-45.

Mishra, P. K. (2009). Management strategies for interrupted aortic arch with associated anomalies. *Eur J Cardiothorac Surg* **35**, 569-76.

Mitchell, P. J., Timmons, P. M., Hebert, J. M., Rigby, P. W. and Tjian, R. (1991). Transcription factor AP-2 is expressed in neural crest cell lineages during mouse embryogenesis. *Genes Dev* **5**, 105-19.

Molin, D. G., DeRuiter, M. C., Wisse, L. J., Azhar, M., Doetschman, T., Poelmann, R. E. and Gittenberger-de Groot, A. C. (2002). Altered apoptosis pattern during pharyngeal arch artery remodelling is associated with aortic arch malformations in Tgfbeta2 knock-out mice. *Cardiovasc Res* **56**, 312-22.

Molin, D. G., Poelmann, R. E., DeRuiter, M. C., Azhar, M., Doetschman, T. and Gittenberger-de Groot, A. C. (2004). Transforming growth factor beta-SMAD2 signalling regulates aortic arch innervation and development. *Circ Res* **95**, 1109-17.

Momma, K. (2010). Cardiovascular anomalies associated with chromosome 22q11.2 deletion syndrome. *Am J Cardiol* **105**, 1617-24.

Mommersteeg, M. T., Dominguez, J. N., Wiese, C., Norden, J., de Gier-de Vries, C., Burch, J. B., Kispert, A., Brown, N. A., Moorman, A. F. and Christoffels, V. M. (2010). The sinus venosus progenitors separate and diversify from the first and second heart fields early in development. *Cardiovasc Res* **87**, 92-101.

Moncada, R., Shannon, M., Miller, R., White, H., Friedman, J. and Shuford, W. H. (1975). The cervical aortic arch. *Am J Roentgenol Radium Ther Nucl Med* **125**, 591-601.

Montagutelli, X. (2000). Effect of the genetic background on the phenotype of mouse mutations. *J Am Soc Nephrol* **11 Suppl 16**, S101-5.

Monteleone, G., Kumberova, A., Croft, N. M., McKenzie, C., Steer, H. W. and MacDonald, T. T. (2001). Blocking Smad7 restores TGF-beta1 signalling in chronic inflammatory bowel disease. *J Clin Invest* **108**, 601-9.

Moon, A. M., Guris, D. L., Seo, J. H., Li, L., Hammond, J., Talbot, A. and Imamoto, A. (2006). Crkl deficiency disrupts Fgf8 signalling in a mouse model of 22q11 deletion syndromes. *Dev Cell* **10**, 71-80.

Moorman, A., Webb, S., Brown, N. A., Lamers, W. and Anderson, R. H. (2003). Development of the heart: (1) formation of the cardiac chambers and arterial trunks. *Heart* **89**, 806-14.

Moraes, F., Novoa, A., Jerome-Majewska, L. A., Papaioannou, V. E. and Mallo, M. (2005). Tbx1 is required for proper neural crest migration and to stabilize spatial patterns during middle and inner ear development. *Mech Dev* **122**, 199-212.

Morishima, M., Yanagisawa, H., Yanagisawa, M. and Baldini, A. (2003). Ece1 and Tbx1 define distinct pathways to aortic arch morphogenesis. *Dev Dyn* **228**, 95-104.

Moustakas, A. and Heldin, C. H. (2009). The regulation of TGFbeta signal transduction. *Development* **136**, 3699-714.

Muller, S. M., Stolt, C. C., Terszowski, G., Blum, C., Amagai, T., Kessaris, N., Iannarelli, P., Richardson, W. D., Wegner, M. and Rodewald, H. R. (2008). Neural crest origin of perivascular mesenchyme in the adult thymus. *J Immunol* **180**, 5344-51.

Nadeau, J. H. (2001). Modifier genes in mice and humans. *Nat Rev Genet* **2**, 165-74.

Nagarajan, R. P., Zhang, J., Li, W. and Chen, Y. (1999). Regulation of Smad7 promoter by direct association with Smad3 and Smad4. *J Biol Chem* **274**, 33412-8.

Naiche, L. A., Harrelson, Z., Kelly, R. G. and Papaioannou, V. E. (2005). T-box genes in vertebrate development. *Annu Rev Genet* **39**, 219-39.

Nakajima, Y. (2010). Second lineage of heart forming region provides new understanding of conotruncal heart defects. *Congenit Anom (Kyoto)* **50**, 8-14.

Nakajima, Y., Yamagishi, T., Hokari, S. and Nakamura, H. (2000). Mechanisms involved in valvuloseptal endocardial cushion formation in early cardiogenesis: roles of transforming growth factor (TGF)-beta and bone morphogenetic protein (BMP). *Anat Rec* **258**, 119-27.

Nakamura, T., Colbert, M. C. and Robbins, J. (2006). Neural crest cells retain multipotential characteristics in the developing valves and label the cardiac conduction system. *Circ Res* **98**, 1547-54.

Narlikar, L. and Ovcharenko, I. (2009). Identifying regulatory elements in eukaryotic genomes. *Brief Funct Genomic Proteomic* **8**, 215-30.

Nawshad, A. and Hay, E. D. (2003). TGFbeta3 signalling activates transcription of the LEF1 gene to induce epithelial mesenchymal transformation during mouse palate development. *J Cell Biol* **163**, 1291-301.

Nemir, M. and Pedrazzini, T. (2008). Functional role of Notch signalling in the developing and postnatal heart. *J Mol Cell Cardiol* **45**, 495-504.

Ng, J. K., Kawakami, Y., Buscher, D., Raya, A., Itoh, T., Koth, C. M., Rodriguez Esteban, C., Rodriguez-Leon, J., Garrity, D. M., Fishman, M. C. et al. (2002). The limb identity gene Tbx5 promotes limb initiation by interacting with Wnt2b and Fgf10. *Development* **129**, 5161-70.

Nie, X., Deng, C. X., Wang, Q. and Jiao, K. (2008). Disruption of Smad4 in neural crest cells leads to mid-gestation death with pharyngeal arch, craniofacial and cardiac defects. *Dev Biol* **316**, 417-30.

Nie, X., Luukko, K. and Kettunen, P. (2006). BMP in craniofacial development. *Int J Dev Biol* **50**, 511-21.

Niederreither, K., Subbarayan, V., Dolle, P. and Chambon, P. (1999). Embryonic retinoic acid synthesis is essential for early mouse post-implantation development. *Nat Genet* **21**, 444-8.

Niessen, K. and Karsan, A. (2008). Notch signalling in cardiac development. *Circ Res* **102**, 1169-81.

Nishimura, M., Isaka, F., Ishibashi, M., Tomita, K., Tsuda, H., Nakanishi, S. and Kageyama, R. (1998). Structure, chromosomal locus, and promoter of mouse Hes2 gene, a homologue of Drosophila hairy and Enhancer of split. *Genomics* **49**, 69-75.

Nowotschin, S., Liao, J., Gage, P. J., Epstein, J. A., Campione, M. and Morrow, B. E. (2006). Tbx1 affects asymmetric cardiac morphogenesis by regulating Pitx2 in the secondary heart field. *Development* **133**, 1565-73.

Okano, J., Suzuki, S. and Shiota, K. (2006). Regional heterogeneity in the developing palate: morphological and molecular evidence for normal and abnormal palatogenesis. *Congenit Anom (Kyoto)* **46**, 49-54.

Park, E. J., Sun, X., Nichol, P., Saijoh, Y., Martin, J. F. and Moon, A. M. (2008). System for tamoxifen-inducible expression of cre-recombinase from the Foxa2 locus in mice. *Dev Dyn* **237**, 447-53.

Park, S. H. (2005). Fine tuning and cross-talking of TGF-beta signal by inhibitory Smads. *J Biochem Mol Biol* **38**, 9-16.

Paylor, R., Glaser, B., Mupo, A., Ataliotis, P., Spencer, C., Sobotka, A., Sparks, C., Choi, C. H., Oghalai, J., Curran, S. et al. (2006). Tbx1 haploinsufficiency is linked to behavioral disorders in mice and humans: implications for 22q11 deletion syndrome. *Proc Natl Acad Sci U S A* **103**, 7729-34.

Paylor, R. and Lindsay, E. (2006). Mouse models of 22q11 deletion syndrome. *Biol Psychiatry* **59**, 1172-9.

Pedrazzini, T. (2007). Control of cardiogenesis by the notch pathway. *Trends Cardiovasc Med* **17**, 83-90.

Pekkan, K., Dasi, L. P., Nourparvar, P., Yerneni, S., Tobita, K., Fogel, M. A., Keller, B. and Yoganathan, A. (2008). *In vitro* hemodynamic investigation of the embryonic aortic arch at late gestation. *J Biomech* **41**, 1697-706.

Perez-Perez, J. M., Candela, H. and Micol, J. L. (2009). Understanding synergy in genetic interactions. *Trends Genet* **25**, 368-76.

Perez-Pomares, J. M., Gonzalez-Rosa, J. M. and Munoz-Chapuli, R. (2009). Building the vertebrate heart - an evolutionary approach to cardiac development. *Int J Dev Biol* **53**, 1427-43.

Person, A. D., Klewer, S. E. and Runyan, R. B. (2005). Cell biology of cardiac cushion development. *Int Rev Cytol* **243**, 287-335.

Phillips, P. C. (2008). Epistasis--the essential role of gene interactions in the structure and evolution of genetic systems. *Nat Rev Genet* **9**, 855-67.

Piotrowski, T., Ahn, D. G., Schilling, T. F., Nair, S., Ruvinsky, I., Geisler, R., Rauch, G. J., Haffter, P., Zon, L. I., Zhou, Y. et al. (2003). The zebrafish van

gogh mutation disrupts tbx1, which is involved in the DiGeorge deletion syndrome in humans. *Development* **130**, 5043-52.

Plageman, T. F., Jr. and Yutzey, K. E. (2005). T-box genes and heart development: putting the "T" in heart. *Dev Dyn* **232**, 11-20.

Plump, A. S., Erskine, L., Sabatier, C., Brose, K., Epstein, C. J., Goodman, C. S., Mason, C. A. and Tessier-Lavigne, M. (2002). Slit1 and Slit2 cooperate to prevent premature midline crossing of retinal axons in the mouse visual system. *Neuron* **33**, 219-32.

Poelmann, R. E., Gittenberger-de Groot, A. C. and Hierck, B. P. (2008). The development of the heart and microcirculation: role of shear stress. *Med Biol Eng Comput* **46**, 479-84.

Pounds, S. B. (2006). Estimation and control of multiple testing error rates for microarray studies. *Brief Bioinform* **7**, 25-36.

Puech, A., Saint-Jore, B., Merscher, S., Russell, R. G., Cherif, D., Sirotkin, H., Xu, H., Factor, S., Kucherlapati, R. and Skoultchi, A. I. (2000). Normal cardiovascular development in mice deficient for 16 genes in 550 kb of the velocardiofacial/DiGeorge syndrome region. *Proc Natl Acad Sci U S A* **97**, 10090-5.

Quinlan, R., Martin, P. and Graham, A. (2004). The role of actin cables in directing the morphogenesis of the pharyngeal pouches. *Development* **131**, 593-9.

Randall, V., McCue, K., Roberts, C., Kyriakopoulou, V., Beddow, S., Barrett, A. N., Vitelli, F., Prescott, K., Shaw-Smith, C., Devriendt, K. et al. (2009). Great vessel development requires biallelic expression of Chd7 and Tbx1 in pharyngeal ectoderm in mice. *J Clin Invest* **119**, 3301-10.

Rauch, A., Devriendt, K., Koch, A., Rauch, R., Gewillig, M., Kraus, C., Weyand, M., Singer, H., Reis, A. and Hofbeck, M. (2004). Assessment of association between variants and haplotypes of the remaining TBX1 gene and manifestations of congenital heart defects in 22q11.2 deletion patients. *J Med Genet* **41**, e40.

Reardon, M. J., Hallman, G. L. and Cooley, D. A. (1984). Interrupted aortic arch: brief review and summary of an eighteen-year experience. *Tex Heart Inst J* **11**, 250-9.

Restivo, A., Piacentini, G., Placidi, S., Saffirio, C. and Marino, B. (2006). Cardiac outflow tract: a review of some embryogenetic aspects of the conotruncal region of the heart. *Anat Rec A Discov Mol Cell Evol Biol* **288**, 936-43.

Richarte, A. M., Mead, H. B. and Tallquist, M. D. (2007). Co-operation between the PDGF receptors in cardiac neural crest cell migration. *Dev Biol* **306**, 785-96.

Riordan, J. R., Rommens, J. M., Kerem, B., Alon, N., Rozmahel, R., Grzelczak, Z., Zielenski, J., Lok, S., Plavsic, N., Chou, J. L. et al. (1989). Identification of the cystic fibrosis gene: cloning and characterization of complementary DNA. *Science* **245**, 1066-73.

Roberts, C., Ivins, S. M., James, C. T. and Scambler, P. J. (2005). Retinoic acid down-regulates Tbx1 expression *in vivo* and *in vitro*. *Dev Dyn* **232**, 928-38.

Rochais, F., Dandonneau, M., Mesbah, K., Jarry, T., Mattei, M. G. and Kelly, R. G. (2009b). Hes1 is expressed in the second heart field and is required for outflow tract development. *PLoS One* **4**, e6267.

Rochais, F., Mesbah, K. and Kelly, R. G. (2009a). Signaling pathways controlling second heart field development. *Circ Res* **104**, 933-42.

Ross, S. and Hill, C. S. (2008). How the Smads regulate transcription. *Int J Biochem Cell Biol* **40**, 383-408.

Rudic, R. D., Shesely, E. G., Maeda, N., Smithies, O., Segal, S. S. and Sessa, W. C. (1998). Direct evidence for the importance of endothelium-derived nitric oxide in vascular remodelling. *J Clin Invest* **101**, 731-6.

Ryckebusch, L., Bertrand, N., Mesbah, K., Bajolle, F., Niederreither, K., Kelly, R. G. and Zaffran, S. (2010). Decreased levels of embryonic retinoic acid synthesis accelerate recovery from arterial growth delay in a mouse model of DiGeorge syndrome. *Circ Res* **106**, 686-94.

Sabatier, C., Plump, A. S., Le, M., Brose, K., Tamada, A., Murakami, F., Lee, E. Y. and Tessier-Lavigne, M. (2004). The divergent Robo family protein rig-1/Robo3 is a negative regulator of slit responsiveness required for midline crossing by commissural axons. *Cell* **117**, 157-69.

Saga, Y., Miyagawa-Tomita, S., Takagi, A., Kitajima, S., Miyazaki, J. and Inoue, T. (1999). MesP1 is expressed in the heart precursor cells and required for the formation of a single heart tube. *Development* **126**, 3437-47.

Saitta, S. C., Harris, S. E., Gaeth, A. P., Driscoll, D. A., McDonald-McGinn, D. M., Maisenbacher, M. K., Yersak, J. M., Chakraborty, P. K., Hacker, A. M., Zackai, E. H. et al. (2004). Aberrant interchromosomal exchanges are the predominant cause of the 22q11.2 deletion. *Hum Mol Genet* **13**, 417-28.

Sanford, L. P., Ormsby, I., Gittenberger-de Groot, A. C., Sariola, H., Friedman, R., Boivin, G. P., Cardell, E. L. and Doetschman, T. (1997). TGFbeta2 knock-out mice have multiple developmental defects that are non-overlapping with other TGFbeta knock-out phenotypes. *Development* **124**, 2659-70.

Santiago-Martinez, E., Soplop, N. H. and Kramer, S. G. (2006). Lateral positioning at the dorsal midline: Slit and Roundabout receptors guide Drosophila heart cell migration. *Proc Natl Acad Sci U S A* **103**, 12441-6.

Santiago-Martinez, E., Soplop, N. H., Patel, R. and Kramer, S. G. (2008). Repulsion by Slit and Roundabout prevents Shotgun/E-cadherin-mediated cell adhesion during Drosophila heart tube lumen formation. *J Cell Biol* **182**, 241-8.

Sauka-Spengler, T. and Bronner-Fraser, M. (2008). Evolution of the neural crest viewed from a gene regulatory perspective. *Genesis* **46**, 673-82.

Scambler, P. J. (2010). 22q11 deletion syndrome: a role for TBX1 in pharyngeal and cardiovascular development. *Pediatr Cardiol* **31**, 378-90.

Schafer, K., Neuhaus, P., Kruse, J. and Braun, T. (2003). The homeobox gene Lbx1 specifies a subpopulation of cardiac neural crest necessary for normal heart development. *Circ Res* **92**, 73-80.

Scholl, A. M. and Kirby, M. L. (2009). Signals controlling neural crest contributions to the heart. *Wiley Interdiscip Rev Syst Biol Med* **1**, 220-7.

Schwarz, Q., Vieira, J. M., Howard, B., Eickholt, B. J. and Ruhrberg, C. (2008). Neuropilin 1 and 2 control cranial gangliogenesis and axon guidance through neural crest cells. *Development* **135**, 1605-13.

Schwinger, E., Devriendt, K., Rauch, A. and Philip, N. (2010). Clinical utility gene card for: DiGeorge syndrome, velocardiofacial syndrome, Shprintzen syndrome, chromosome 22q11.2 deletion syndrome (22q11.2, TBX1). *Eur J Hum Genet* **18**.

Segre, D., Deluna, A., Church, G. M. and Kishony, R. (2005). Modular epistasis in yeast metabolism. *Nat Genet* **37**, 77-83.

Shawber, C. J. and Kitajewski, J. (2004). Notch function in the vasculature: insights from zebrafish, mouse and man. *Bioessays* **26**, 225-34.

Shi, W., Sun, C., He, B., Xiong, W., Shi, X., Yao, D. and Cao, X. (2004). GADD34-PP1c recruited by Smad7 dephosphorylates TGFbeta type I receptor. *J Cell Biol* **164**, 291-300.

Shiau, C. E. and Bronner-Fraser, M. (2009). N-cadherin acts in concert with Slit1-Robo2 signalling in regulating aggregation of placode-derived cranial sensory neurons. *Development* **136**, 4155-64.

Shprintzen, R. J. (2008). Velo-cardio-facial syndrome: 30 Years of study. *Dev Disabil Res Rev* **14**, 3-10.

Sinha, S., Abraham, S., Gronostajski, R. M. and Campbell, C. E. (2000). Differential DNA binding and transcription modulation by three T-box proteins, T, TBX1 and TBX2. *Gene* **258**, 15-29.

Snarr, B. S., Kern, C. B. and Wessels, A. (2008). Origin and fate of cardiac mesenchyme. *Dev Dyn* **237**, 2804-19.

Snider, P., Olaopa, M., Firulli, A. B. and Conway, S. J. (2007). Cardiovascular development and the colonizing cardiac neural crest lineage. *ScientificWorldJournal* **7**, 1090-113.

Snider, P., Tang, S., Lin, G., Wang, J. and Conway, S. J. (2009). Generation of Smad7(-Cre) recombinase mice: A useful tool for the study of epithelial-mesenchymal transformation within the embryonic heart. *Genesis* **47**, 469-75.

Solloway, M. J. and Robertson, E. J. (1999). Early embryonic lethality in Bmp5;Bmp7 double mutant mice suggests functional redundancy within the 60A subgroup. *Development* **126**, 1753-68.

Song, L., Yan, W., Chen, X., Deng, C. X., Wang, Q. and Jiao, K. (2007). Myocardial smad4 is essential for cardiogenesis in mouse embryos. *Circ Res* **101**, 277-85.

Soriano, P. (1999). Generalized lacZ expression with the ROSA26 Cre reporter strain. *Nat Genet* **21**, 70-1.

Spence, J. R., Lange, A. W., Lin, S. C., Kaestner, K. H., Lowy, A. M., Kim, I., Whitsett, J. A. and Wells, J. M. (2009). Sox17 regulates organ lineage segregation of ventral foregut progenitor cells. *Dev Cell* **17**, 62-74.

Stalmans, I., Lambrechts, D., De Smet, F., Jansen, S., Wang, J., Maity, S., Kneer, P., von der Ohe, M., Swillen, A., Maes, C. et al. (2003). VEGF: a modifier of the del22q11 (DiGeorge) syndrome? *Nat Med* **9**, 173-82.

Stauber, M., Sachidanandan, C., Morgenstern, C. and Ish-Horowicz, D. (2009). Differential axial requirements for lunatic fringe and Hes7 transcription during mouse somitogenesis. *PLoS One* **4**, e7996.

Stoller, J. Z. and Epstein, J. A. (2005a). Identification of a novel nuclear localization signal in Tbx1 that is deleted in DiGeorge syndrome patients harboring the 1223delC mutation. *Hum Mol Genet* **14**, 885-92.

Stoller, J. Z. and Epstein, J. A. (2005b). Cardiac neural crest. *Semin Cell Dev Biol* **16**, 704-15.

Stottmann, R. W., Choi, M., Mishina, Y., Meyers, E. N. and Klingensmith, J. (2004). BMP receptor IA is required in mammalian neural crest cells for development of the cardiac outflow tract and ventricular myocardium. *Development* **131**, 2205-18.

Swiatek, P. J., Lindsell, C. E., del Amo, F. F., Weinmaster, G. and Gridley, T. (1994). Notch1 is essential for postimplantation development in mice. *Genes Dev* **8**, 707-19.

Szabo-Rogers, H. L., Smithers, L. E., Yakob, W. and Liu, K. J. (2010). New directions in craniofacial morphogenesis. *Dev Biol* **341**, 84-94.

Taddei, I., Morishima, M., Huynh, T. and Lindsay, E. A. (2001). Genetic factors are major determinants of phenotypic variability in a mouse model of the DiGeorge/del22q11 syndromes. *Proc Natl Acad Sci U S A* **98**, 11428-31.

Takatsuka, K., Hatakeyama, J., Bessho, Y. and Kageyama, R. (2004). Roles of the bHLH gene Hes1 in retinal morphogenesis. *Brain Res* **1004**, 148-55.

Takebayashi, K., Sasai, Y., Sakai, Y., Watanabe, T., Nakanishi, S. and Kageyama, R. (1994). Structure, chromosomal locus, and promoter analysis of the gene encoding the mouse helix-loop-helix factor HES-1. Negative autoregulation through the multiple N box elements. *J Biol Chem* **269**, 5150-6.

Tang, S., Snider, P., Firulli, A. B. and Conway, S. J. (2010). Trigenic neural crest-restricted Smad7 over-expression results in congenital craniofacial and cardiovascular defects. *Dev Biol* **344**, 233-47.

Tang, Y., Liu, Z., Zhao, L., Clemens, T. L. and Cao, X. (2008). Smad7 stabilizes beta-catenin binding to E-cadherin complex and promotes cell-cell adhesion. *J Biol Chem* **283**, 23956-63.

ten Dijke, P. and Hill, C. S. (2004). New insights into TGF-beta-Smad . *Trends Biochem Sci* **29**, 265-73.

Todorovic, V., Frendewey, D., Gutstein, D. E., Chen, Y., Freyer, L., Finnegan, E., Liu, F., Murphy, A., Valenzuela, D., Yancopoulos, G. et al. (2007). Long form of

latent TGF-beta binding protein 1 (Ltbp1L) is essential for cardiac outflow tract septation and remodelling. *Development* **134**, 3723-32.

Tomita, K., Hattori, M., Nakamura, E., Nakanishi, S., Minato, N. and Kageyama, R. (1999). The bHLH gene Hes1 is essential for expansion of early T cell precursors. *Genes Dev* **13**, 1203-10.

Tomita, K., Ishibashi, M., Nakahara, K., Ang, S. L., Nakanishi, S., Guillemot, F. and Kageyama, R. (1996). Mammalian hairy and Enhancer of split homolog 1 regulates differentiation of retinal neurons and is essential for eye morphogenesis. *Neuron* **16**, 723-34.

Tong, A. H., Evangelista, M., Parsons, A. B., Xu, H., Bader, G. D., Page, N., Robinson, M., Raghibizadeh, S., Hogue, C. W., Bussey, H. et al. (2001). Systematic genetic analysis with ordered arrays of yeast deletion mutants. *Science* **294**, 2364-8.

Topper, J. N., Cai, J., Qiu, Y., Anderson, K. R., Xu, Y. Y., Deeds, J. D., Feeley, R., Gimeno, C. J., Woolf, E. A., Tayber, O. et al. (1997). Vascular MADs: two novel MAD-related genes selectively inducible by flow in human vascular endothelium. *Proc Natl Acad Sci U S A* **94**, 9314-9.

Torres-Juan, L., Rosell, J., Morla, M., Vidal-Pou, C., Garcia-Algas, F., de la Fuente, M. A., Juan, M., Tubau, A., Bachiller, D., Bernues, M. et al. (2007). Mutations in TBX1 genocopy the 22q11.2 deletion and duplication syndromes: a new susceptibility factor for mental retardation. *Eur J Hum Genet* **15**, 658-63.

Trainor, P. and Krumlauf, R. (2000). Plasticity in mouse neural crest cells reveals a new patterning role for cranial mesoderm. *Nat Cell Biol* **2**, 96-102.

Trainor, P. A. and Krumlauf, R. (2001). Hox genes, neural crest cells and branchial arch patterning. *Curr Opin Cell Biol* **13**, 698-705.

Tucker, R. P. (2004). Neural crest cells: a model for invasive behavior. *Int J Biochem Cell Biol* **36**, 173-7.

van Bueren, K. L. (2008). Genomic and Transcriptomic Approaches to Pathways affected in DiGeorge Syndrome. *PhD Thesis, UCL - Institute of Child Health*.

van Bueren, K. L., Papangeli, I., Rochais, F., Pearce, K., Roberts, C., Calmont, A., Szumska, D., Kelly, R. G., Bhattacharya, S. and Scambler, P. J. (2010). Hes1 expression is reduced in Tbx1 null cells and is required for the development of structures affected in 22q11 deletion syndrome. *Dev Biol* **340**, 369-80.

Van Mierop, L. H. and Kutsche, L. M. (1984). Interruption of the aortic arch and coarctation of the aorta: pathogenetic relations. *Am J Cardiol* **54**, 829-34.

Van Praagh, R., Bernhard, W. F., Rosenthal, A., Parisi, L. F. and Fyler, D. C. (1971). Interrupted aortic arch: surgical treatment. *Am J Cardiol* **27**, 200-11.

Vargesson, N. and Laufer, E. (2001). Smad7 misexpression during embryonic angiogenesis causes vascular dilation and malformations independently of vascular smooth muscle cell function. *Dev Biol* **240**, 499-516.

Vermot, J., Niederreither, K., Garnier, J. M., Chambon, P. and Dolle, P. (2003). Decreased embryonic retinoic acid synthesis results in a DiGeorge syndrome phenotype in newborn mice. *Proc Natl Acad Sci U S A* **100**, 1763-8.

Verzi, M. P., McCulley, D. J., De Val, S., Dodou, E. and Black, B. L. (2005). The right ventricle, outflow tract, and ventricular septum comprise a restricted expression domain within the secondary/anterior heart field. *Dev Biol* **287**, 134-45.

Vincent, M., Duband, J. L. and Thiery, J. P. (1983). A cell surface determinant expressed early on migrating avian neural crest cells. *Brain Res* **285**, 235-8.

Vincent, S. D., Miyagawa-Tomita, S. and Buckingham, M. (2010). Prdm1, Encoding the Blimp1 Transcriptional Repressor, Genetically Interacts With Tbx1 During Distal Outflow Tract Morphogenesis. *Weinstein Cardiovascular Development Conference.*

Vitelli, F. and Baldini, A. (2003). Generating and modifying DiGeorge syndrome-like phenotypes in model organisms: is there a common genetic pathway? *Trends Genet* **19**, 588-93.

Vitelli, F., Huynh, T. and Baldini, A. (2009). Gain of function of Tbx1 affects pharyngeal and heart development in the mouse. *Genesis* **47**, 188-95.

Vitelli, F., Lania, G., Huynh, T. and Baldini, A. (2010). Partial rescue of the Tbx1 mutant heart phenotype by Fgf8: Genetic evidence of impaired tissue response to Fgf8. *J Mol Cell Cardiol* **49**, 836-40.

Vitelli, F., Morishima, M., Taddei, I., Lindsay, E. A. and Baldini, A. (2002a). Tbx1 mutation causes multiple cardiovascular defects and disrupts neural crest and cranial nerve migratory pathways. *Hum Mol Genet* **11**, 915-22.

Vitelli, F., Taddei, I., Morishima, M., Meyers, E. N., Lindsay, E. A. and Baldini, A. (2002b). A genetic link between Tbx1 and fibroblast growth factor signalling. *Development* **129**, 4605-11.

Vitelli, F., Zhang, Z., Huynh, T., Sobotka, A., Mupo, A. and Baldini, A. (2006). Fgf8 expression in the Tbx1 domain causes skeletal abnormalities and modifies the aortic arch but not the outflow tract phenotype of Tbx1 mutants. *Dev Biol* **295**, 559-70.

Wagner, M. and Siddiqui, M. A. (2007a). Signal transduction in early heart development (I): cardiogenic induction and heart tube formation. *Exp Biol Med (Maywood)* **232**, 852-65.

Wagner, M. and Siddiqui, M. A. (2007b). Signal transduction in early heart development (II): ventricular chamber specification, trabeculation, and heart valve formation. *Exp Biol Med (Maywood)* **232**, 866-80.

Waldo, K. L., Hutson, M. R., Stadt, H. A., Zdanowicz, M., Zdanowicz, J. and Kirby, M. L. (2005). Cardiac neural crest is necessary for normal addition of the myocardium to the arterial pole from the secondary heart field. *Dev Biol* **281**, 66-77.

Wang, H., Li, M., Lin, P. H., Yao, Q. and Chen, C. (2008). Fluid shear stress regulates the expression of TGF-beta1 and its signalling molecules in mouse embryo mesenchymal progenitor cells. *J Surg Res* **150**, 266-70.

Wang, J., Nagy, A., Larsson, J., Dudas, M., Sucov, H. M. and Kaartinen, V. (2006). Defective ALK5 signalling in the neural crest leads to increased postmigratory neural crest cell apoptosis and severe outflow tract defects. *BMC Dev Biol* **6**, 51.

Wang, Y., Dur, O., Patrick, M. J., Tinney, J. P., Tobita, K., Keller, B. B. and Pekkan, K. (2009). Aortic arch morphogenesis and flow modeling in the chick embryo. *Ann Biomed Eng* **37**, 1069-81.

Wang, Y. P., Dakubo, G., Howley, P., Campsall, K. D., Mazarolle, C. J., Shiga, S. A., Lewis, P. M., McMahon, A. P. and Wallace, V. A. (2002). Development of normal retinal organization depends on Sonic hedgehog signalling from ganglion cells. *Nat Neurosci* **5**, 831-2.

Wang, Z., Liu, T., Lin, Z., Hegarty, J., Koltun, W. A. and Wu, R. (2010). A general model for multilocus epistatic interactions in case-control studies. *PLoS One* **5**, e11384.

Warthen, D. M., Moore, E. C., Kamath, B. M., Morrissette, J. J., Sanchez, P., Piccoli, D. A., Krantz, I. D. and Spinner, N. B. (2006). Jagged1 (JAG1) mutations in Alagille syndrome: increasing the mutation detection rate. *Hum Mutat* **27**, 436-43.

Weatherall, D. J. (2000). Single gene disorders or complex traits: lessons from the thalassaemias and other monogenic diseases. *Bmj* **321**, 1117-20.

Webb, S., Anderson, R. H., Lamers, W. H. and Brown, N. A. (1999). Mechanisms of deficient cardiac septation in the mouse with trisomy 16. *Circ Res* **84**, 897-905.

Webb, S., Brown, N. A. and Anderson, R. H. (1998). Formation of the atrioventricular septal structures in the normal mouse. *Circ Res* **82**, 645-56.

Webb, S., Qayyum, S. R., Anderson, R. H., Lamers, W. H. and Richardson, M. K. (2003). Septation and separation within the outflow tract of the developing heart. *J Anat* **202**, 327-42.

Weng, A. P., Ferrando, A. A., Lee, W., Morris, J. P. t., Silverman, L. B., Sanchez-Irizarry, C., Blacklow, S. C., Look, A. T. and Aster, J. C. (2004). Activating mutations of NOTCH1 in human T cell acute lymphoblastic leukemia. *Science* **306**, 269-71.

Wilson, V. and Conlon, F. L. (2002). The T-box family. *Genome Biol* **3**, REVIEWS3008.

Wong, S. L., Zhang, L. V., Tong, A. H., Li, Z., Goldberg, D. S., King, O. D., Lesage, G., Vidal, M., Andrews, B., Bussey, H. et al. (2004). Combining biological networks to predict genetic interactions. *Proc Natl Acad Sci U S A* **101**, 15682-7.

Wrana, J. L. (2000). Crossing Smads. *Sci STKE* **2000**, re1.

Wurdak, H., Ittner, L. M., Lang, K. S., Leveen, P., Suter, U., Fischer, J. A., Karlsson, S., Born, W. and Sommer, L. (2005). Inactivation of TGFbeta signalling in neural crest stem cells leads to multiple defects reminiscent of DiGeorge syndrome. *Genes Dev* **19**, 530-5.

Wurdak, H., Ittner, L. M. and Sommer, L. (2006). DiGeorge syndrome and pharyngeal apparatus development. *Bioessays* **28**, 1078-86.

Xian, J., Clark, K. J., Fordham, R., Pannell, R., Rabbitts, T. H. and Rabbitts, P. H. (2001). Inadequate lung development and bronchial hyperplasia in mice with a targeted deletion in the Dutt1/Robo1 gene. *Proc Natl Acad Sci U S A* **98**, 15062-6.

Xu, H., Cerrato, F. and Baldini, A. (2005). Timed mutation and cell-fate mapping reveal reiterated roles of Tbx1 during embryogenesis, and a crucial function during segmentation of the pharyngeal system via regulation of endoderm expansion. *Development* **132**, 4387-95.

Xu, H., Morishima, M., Wylie, J. N., Schwartz, R. J., Bruneau, B. G., Lindsay, E. A. and Baldini, A. (2004). Tbx1 has a dual role in the morphogenesis of the cardiac outflow tract. *Development* **131**, 3217-27.

Yagi, H., Furutani, Y., Hamada, H., Sasaki, T., Asakawa, S., Minoshima, S., Ichida, F., Joo, K., Kimura, M., Imamura, S. et al. (2003). Role of TBX1 in human del22q11.2 syndrome. *Lancet* **362**, 1366-73.

Yamagishi, H. (2002). The 22q11.2 deletion syndrome. *Keio J Med* **51**, 77-88.

Yamagishi, H. and Srivastava, D. (2003). Unraveling the genetic and developmental mysteries of 22q11 deletion syndrome. *Trends Mol Med* **9**, 383-9.

Yan, X., Liu, Z. and Chen, Y. (2009). Regulation of TGF-beta signalling by Smad7. *Acta Biochim Biophys Sin (Shanghai)* **41**, 263-72.

Yanagisawa, H., Hammer, R. E., Richardson, J. A., Williams, S. C., Clouthier, D. E. and Yanagisawa, M. (1998). Role of Endothelin-1/Endothelin-A receptor-mediated signalling pathway in the aortic arch patterning in mice. *J Clin Invest* **102**, 22-33.

Yang, D. H., Goo, H. W., Seo, D. M., Yun, T. J., Park, J. J., Park, I. S., Ko, J. K. and Kim, Y. H. (2008). Multislice CT angiography of interrupted aortic arch. *Pediatr Radiol* **38**, 89-100.

Yashiro, K., Shiratori, H. and Hamada, H. (2007). Haemodynamics determined by a genetic programme govern asymmetric development of the aortic arch. *Nature* **450**, 285-8.

Yuan, W., Rao, Y., Babiuk, R. P., Greer, J. J., Wu, J. Y. and Ornitz, D. M. (2003). A genetic model for a central (septum transversum) congenital diaphragmatic hernia in mice lacking Slit3. *Proc Natl Acad Sci U S A* **100**, 5217-22.

Yuan, W., Zhou, L., Chen, J. H., Wu, J. Y., Rao, Y. and Ornitz, D. M. (1999). The mouse SLIT family: secreted ligands for ROBO expressed in patterns that suggest a role in morphogenesis and axon guidance. *Dev Biol* **212**, 290-306.

Zhang, H. and Bradley, A. (1996). Mice deficient for BMP2 are nonviable and have defects in amnion/chorion and cardiac development. *Development* **122**, 2977-86.

Zhang, L. F., Gui, Y. H., Wang, Y. X., Jiang, Q. and Song, H. Y. (2010). Effect of Tbx1 knock-down on cardiac performance in zebrafish. *Chin Med J (Engl)* **123**, 1182-9.

Zhang, Z. and Baldini, A. (2008). *In vivo* response to high-resolution variation of Tbx1 mRNA dosage. *Hum Mol Genet* **17**, 150-7.

Zhang, Z., Cerrato, F., Xu, H., Vitelli, F., Morishima, M., Vincentz, J., Furuta, Y., Ma, L., Martin, J. F., Baldini, A. et al. (2005). Tbx1 expression in pharyngeal epithelia is necessary for pharyngeal arch artery development. *Development* **132**, 5307-15.

Zhang, Z., Huynh, T. and Baldini, A. (2006). Mesodermal expression of Tbx1 is necessary and sufficient for pharyngeal arch and cardiac outflow tract development. *Development* **133**, 3587-95.

Zweier, C., Sticht, H., Aydin-Yaylagul, I., Campbell, C. E. and Rauch, A. (2007). Human TBX1 missense mutations cause gain of function resulting in the same phenotype as 22q11.2 deletions. *Am J Hum Genet* **80**, 510-7.

Zwijsen, A., van Rooijen, M. A., Goumans, M. J., Dewulf, N., Bosman, E. A., ten Dijke, P., Mummery, C. L. and Huylebroeck, D. (2000). Expression of the inhibitory Smad7 in early mouse development and upregulation during embryonic vasculogenesis. *Dev Dyn* **218**, 663-70.

APPENDIX I

Stock solutions and Antibodies

1. Stock Solutions

10mM dNTP	10mM dATP, 10mM dCTP, 10mM dGTP, 10mM dTTP
20X SSC	3M NaCl, 0.3M Sodium Citrate pH 7.0
BM Purple staining solution	BM Purple (Roche, UK), 1X Levamisole (Sigma Aldrich), 0.1% Tween-20
Bone and cartilage staining solution	1/20 0.3% alcian blue in 70% EtOH, 1/20 0.1% alizarin red in 95% EtOH, 1/20 acetic acid, 17/20 70% EtOH
DNA ladder	50 ng/µl DNA ladder in 1 X loading buffer
Hybridisation buffer	50% formamide, 5X SSC, 1% SDS, 50µg/ml yeast RNA, 50µg/ml heparin, 0.1% Tween-20, in DEPC H_2O
Laemmli buffer (6X)	125mM Tris-HCl pH 6.8, 6% SDS, 20% glycerol, 0.1% bromophenol blue - 10% 2-mercaptoethanol, added prior to use
LB agar	2% Bactoagar, 1% Bactotryptone, 0.5% Bactoyeast, 1% NaCl
LB broth	1% Bactotryptone, 0.5% Bactoyeast, 1% NaCl
Loading buffer (6X)	10mM Tris-HCl pH 7.5, 50mM EDTA pH 8.0, 10% Ficoll-400, 0.4% Orange G
MAB	100mM maleic acid, 150mM NaCl, 0.001% Tween-20, NaOH pellets
NTMT	100mM Tris-HCl pH 9.5, 100mM NaCl, 50mM $MgCl_2$, 0.1% Tween-20 in DEPC H_2O
PBS (10X) pH 7.4	80g NaCl, 2.0g KCl, 14.4g Na_2HPO_4, 2.4g KH_2PO in 1L water, pH 7.4
RIPA buffer	150mM NaCl, 1% NP-40 or Triton-X, 50mM Tris-HCl pH 8.0
Running buffer	25mM Tris-base, 192 mM Glycine, 0.1% SDS
Solution I	50% formamide, 5X SSC pH 5.0, 1% SDS, in DEPC H_2O
Solution II	50% formamide, 2X SSC pH 5.0, 0.2% SDS, 0.1% Tween-20, in DEPC H_2O
TAE buffer (10X)	0.4M Tris-acetate, 10mM EDTA pH 8.0

Tail lysis buffer	100mM Tris-HCl pH 8.5, 5mM EDTA pH 8.0, 0.2%, SDS, 200mM NaCl, 100 μg/ml proteinase K (added immediately prior to use)
TE pH 8.0	10mM Tris-HCl pH 8.0, 1mM EDTA pH8.0
TBST (10X)	25ml Tris-HCl pH 7.5, 8g NaCl, 0.2g KCl, 11ml Tween-20 in 100ml water
Transfer buffer	0.5X Running buffer, 20% MeOH
X-gal buffer	20mM $K_3Fe(CN)_6$, 20mM $K_4Fe(CN)_6$-$3H_2O$, 5mM EGTA, 2mM $MgCl_2$, 0.02% NP40, 0.01% Deoxycholate, in PBS - 1mg/ml X-gal, added prior to use

Table AI. 1. Stock solutions.

2. Antibodies

Antigen	Source	Application	Acquired from
Tbx1	rabbit	IF	Zymed, Invitrogen
Hes1	guinea pig	IF	Ryoichiro Kageyama
pSmad2/3	rabbit	WB	Cell Signaling Technology
pSmad1/5/8	rabbit	WB	Cell Signaling Technology
Gapdh	mouse	WB	Millipore

Table AI. 2. Antibodies. IF, immunofluorescence; WB, western blotting.

APPENDIX II

Primer Sequences and Cycling conditions

1. Genotyping primer sequences

Reference	Forward	Reverse	Alleles	Tm
Tbx1^{lacZ}	AGTCTGGGGACTCTGGAAGG	AAGGCAGATCCTGCTACACC	wt	65 ^{0}C
		TCGACTAGAGCTTGCGGAAC	mutant	65 ^{0}C
Tbx1^{mcm}	GCTCCACTTCAGCACATTCC	CATAAGCCAGAGAAGGGTCG	-	60 ^{0}C
Tbx1^{Neo2}	GCCAGAGGCCACTTGTGTAG	AGGCTGGGATTCCAAAAGAC	-	60 ^{0}C
Smad7	GCTCCAGATGTTCAGTTGC	CTCCTTTAGAAAGAGTGGTGCC	wt	60 ^{0}C
		CATACAGTCCTCTTCACATCCATGCTG	mutant	60 ^{0}C
Hes1	CCCCTTTGCAGTCATCAAAG	GCATTGCTCACTTACATCTTTC	wt	60 ^{0}C
	GGGAGGATTGGGAAGACAAT	GGCGGAAGTCTGGAAGAAAT	mutant	60 ^{0}C
Hes1^{Flox}	CAGCCAGTGTCAACACGACACCGGACAAAC	TGCCCTTCGCCTCTTCTCCATGATA	-	62 ^{0}C
Cre	GTTCGCAAGAACCTGATGGACA	CTAGAGCCTGTTTTGCACGTTC	-	60 ^{0}C
Sox17-iCre	GTGTATAAGCCCGAGATGG	CTCAACTGTTCAAGTGGCAG	wt	60 ^{0}C
		GATCTATGGTGCCAAGGATGAC	mutant	60 ^{0}C
Slit1	AAGATGCCTCCTCTGACTTC	ACCCTTAGCTTCTACCAACC	wt	55 ^{0}C
	TCTCCTTTGATCTGAGACCG	AGGTTTCTCGAGCGTCATAG	mutant	55 ^{0}C
Slit2	AAGACCTGTCGCTTCTGTCAG	AAACAGGTTTCTACCGCACG	wt	55 ^{0}C
	AAGACCTGTCGCTTCTGTCAG	AAGTCTAGTAGAGTCGAGCG	mutant	55 ^{0}C
R26R/R	AAAGTCGCTCTGAGTTGTTAT	GGAGCGGGAGAAATGGATATG	wt	60 ^{0}C
		GCGAAGAGTTTGTCCTCAACC	mutant	60 ^{0}C
En2	AACAAACTTGGCCTCACCAG	GCCAAGGCCATACAAGTGTT	-	60 ^{0}C
pGT0lxf-SA	GATGCCAGAGACTCAGTGAA	GTTGTAAAACGACGGGATCCTC	-	60 ^{0}C

Table AII. 1. Genotyping PCR primer sequences.

2. Quantitative real time PCR primer sequences

Reference	Forward	Reverse	Tm
Smad7 exon 3-4	GAAACCGGGGGAACGAATTAT	CGCGAGTCTTCTCCTCCCA	60 ^{0}C
Smad7 exon 4	TCTACTGTGTCCAAGAGCCCT	GCGGTTGTAAACCCACACG	60 ^{0}C
Klf2	GGACCTAAACAACGTGTTGGA	CTCCGGGTAGTAGAAGGCAG	60 ^{0}C
Klf4	TGATGGTGCTTGGTGAGTTG	TTGCACATCTGAAACCACAG	60 ^{0}C
Klf10	TTCTCTCCAGCAAGCTTCGGA	TCACTCTGCTCAGCTTTGTCCC	60 ^{0}C
Etv4	CCCACCACCAGGATCAAGAAG	TGTCTGGAGTAAAGGCACTGC	60 ^{0}C
Etv5	TCAGTCTGATAACTTGGTGCTTC	GGCTTCCTATCGTAGGCACAA	60 ^{0}C
GAPDH	TGCACCACCAACTGCTTAGC	GGCATGGACTGTGGTCATGAG	60 ^{0}C

Table AII. 2. Quantitative real time PCR primer sequences.

3. Smad7 luciferase construct primer sequences

Reference	Forward	Reverse	Tm
Smad7.1	CCCCAGCTCTTCCGATTT	GACGAAGAGAGTCTCCGAGG	60 ^{0}C
Smad7.2	GGGATAGCTTTCTCTGGTACC	GGAGGAGGTACCTGTCTGTT	60 ^{0}C
Smad7.3	GGTACCAGGCAGTCCTAGAA	CAGTTGGTACCACCCTCTCC	60 ^{0}C
Smad7.4	GAAGGGGAATGGTACCAGA	GGTACCTGCTTAGGGTCAGA	60 ^{0}C

Table AII. 3. Smad7 luciferase construct PCR primer sequences.

4. Cycling conditions

Reference	PCR	Cycling conditions
General	genotyping	94 °C - 2 minutes 94 °C - 30 seconds 60 °C - 30 seconds (30x cycles) 72 °C - 30 seconds 72 °C - 10 minutes
Tbx1^{lacZ}	genotyping	95 °C - 30 seconds 95 °C - 30 seconds 65 °C - 20 seconds (33x cycles) 72 °C - 20 seconds
Hes1^{Flox}	genotyping	95 °C - 2 minutes 95 °C - 10 seconds 62 °C - 30 seconds (33x cycles) 72 °C - 1 minute 72 °C - 5 minutes
Sox17-iCre	genotyping	95 °C - 5 minutes 95 °C - 30 seconds 60 °C - 30 seconds (35x cycles) 72 °C - 1 minute 72 °C - 10 minutes
Slit1, Slit2	genotyping	95 °C - 5 minutes 95 °C - 30 seconds 60 °C - 30 seconds (30x cycles) 72 °C - 30 seconds
General	quantitative	94 °C - 15 minutes 94 °C - 15 seconds 60 °C - 30 seconds (40x cycles) 72 °C - 30 seconds dissociation stage

Table AII. 4. PCR cycling conditions.

APPENDIX III

Plasmid constructs

1. Whole mount *in situ* hybridisation probe plasmids

Reference	A/S	S	Vector	Acquired from
Tbx1	XhoI, T7	ClaI, T3	pBSKII(-)	Albert Basson
Smad7	EcoRI, T3	NotI, T7	pBSKII	Christine Mummery
Sox10	NcoI, T7	N/A	N/A	Christiana Ruhrberg
Hes1	EcoRI, T7	BamHI, T3	pBSKII(+)	Francois Guillemot
Jag1	EcoRI, T3	NotI, T7	pYX-Asc	imaGenes
RBP-J	SalI, T7	NotI, Sp6	pCMV-SPORT6	imaGenes
HOXD4	PmeI, T7	NotI, T3	pCR4-TOPO	Geneservice Limited
Fgf8	SmaI or XhoI, T7	N/A	pBSK	Gail Martin
Fgf10	BamHI, T3	PstI, T7	pBSKII(+)	Albert Basson
Etv4	ApaI or XbaI, Sp6	BamHI, T7	N/A	N/A
Slit1	BamHI, T7	XhoI, T3	pBSK	Marc Tessier-Lavigne
Slit2	NcoI, Sp6	SpeI, T7	pGEM-T	David Ornitz

Table AIII. 1. Whole mount *in situ* hybridisation probe plasmids. Restriction digests and RNA polymerases for anti-sense (A/S) or sense (S) orientation, and vector backbone information. N/A, not available.

2. Expression and luciferase constructs

Reference	Vector	Description	Acquired from
Smad7.1;TKGL2	pTKGL2	firefly luciferase	in house
Smad7.2;TKGL2	pTKGL2	firefly luciferase	in house
Smad7.3;TKGL2	pTKGL2	firefly luciferase	in house
Smad7.4;TKGL2	pTKGL2	firefly luciferase	in house
pTKGL2	pTKGL2	firefly luciferase	Anita Rauch
p2T-TKGL2	pTKGL2	firefly luciferase	Anita Rauch
TBX1C	CMV	human *TBX1* expression	Anita Rauch
β-galactosidase	pcDNA3	β-galactosidase expression	in house
pRLSV40	SV40	renilla luciferase	Bruno Ferraz de Souza
pcDNA3	pcDNA3	-	Promega

Table AIII. 2. Expression and luciferase constructs.